Treatment of wastewater from textile dyeing by ozonization

(Article begins on next page)

POLITECNICO DI TORINO

Dipartimento di scienza applicata e tecnologia

Dottorato di Ricerca in Ingegneria Chimica
XXVII ciclo (2012-2014)

Treatment of wastewater
from textile dyeing by ozonization

Candidato: **Giuseppe Actis Grande**
Matricola: 189102

Relatori: Controrelatore
Prof. Giorgio Rovero   **Prof.ssa Barbara Bosio**
Prof. Silvio Sicardi

Coordinatore del Corso di Dottorato
Prof. Marco Vanni

Contents

Chapter 1 – Introduction

1.1 Wastewater characteristics

Wet processes for textile production are one of the largest water consuming and polluting sources [1-4]. The production of textiles requires a significant amount of water for preparation, dyeing, washing and finishing stages from five to forty times fibre weight [5]. It depends on machinery type, treatment type and operator care. Consequently, large amounts of wastewater must be treated before restitution to the environment.

The main treatments characterizing a textile production cycle are:
- pre-treatments such as bleaching, desizing and mercerization;
- purgiry, dyeing, wash-off operations and post-dyeing treatment e.g. to increase dye fasteness (wet or dry);
- wet operations to confer peculiar properties to textile goods.

At the end of each treatment, the exhausted liquor must be changed and clean water may be required to rinse the textile. According to the hydrodynamic feature of machinery, the needed water amount is two or three times with respect to the previous treatment.

Following this general considerations, it is quite understandable that textile industry is one of the largest water consuming sector.

Each textile process has peculiar characteristics that lead to a different composition of the resulting wastewater, and consequently different operations and processes in wastewater treatment.

The wastewater produced can be classified as follows [6]:
- process wastewater discharged from different process steps, such as desizing, bleaching, dyeing, printing, … . These wastewaters are characterized by low flow rate and highly pollutant load;
- wash-off water with high flow rate and medium pollutant load;
- utility cooling waters with temperature as sole pollution parameter.

As an example, Fig 1.1 gives the percentages of water used in the different step of the wool chain production from weaving to finishing, passing through spinning and dyeing.
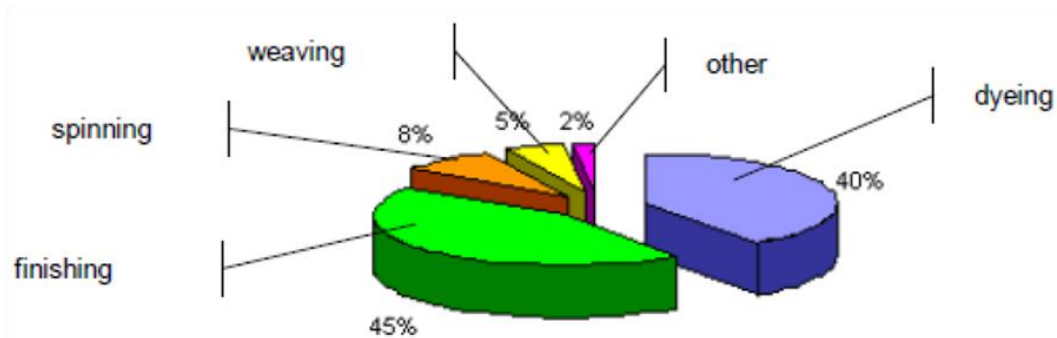
Fig 1.1 – Repartition of water consumption in a wool milling

Textile wastewater characteristics show a great variety depending on the types of inorganic and organic compounds used in each process. Generally, wastewater contains noticeable colour (coming from unfixed dyes on fibre after the dyeing process), high concentration of COD (due to organic molecules such as dyes, surfactants and dyeing auxiliaries) and heavy metals contained typically of some dye structures. Moreover, some chemicals including salts, acids, bases and buffers can be used for pH regulation.

The organic and inorganic contaminant of the textile wastewaters must be removed by appropriate treatments according to environmental rules.

In order to define the optimal wastewater treatment technology, different aspects need definition. First of all, it is essential specifying the final destination of the treated water, i.e. if it can be discharged to the environment or recycled/reused in the process. In the first case, the concentration limit by law have to be considered, while in the second one well defined water characteristics must be reached to preserve product quality.

Considering a sound environment preservation, treated water can be:

- saved by optimizing process in water point of view thanks to, e.g., processes control automation;
- reused: use of water source from civil and/or industrial activities in general, after suitable treatment;
- recycled: the liquid will be reused, after treatment, in the same process.

Considering dyeing processes, dyes and surfactants represent the two classes of compounds that shown some refractoriness during treatment, particularly in biological treatment. In other word, the biological treatments alone do not guarantee the achievement of the limits required by law.

In the following table are reported the Italian law limits (D. Lgs 152/2006) for discharge to surface water and sewage.

Table 1.1 – Colour and surfactant concentration limit by Italian law (D. Lgs. 152/2006)

Parameter	Surface water discharge	Sewage discharge
Colour	Colour is not perceptible with dilution 1:20	Colour is not perceptible with dilution 1:40
Surfactants	≤ 2 mg/L	≤ 4 mg/L
COD*	≤ 160 mg/L	≤ 500 mg/L

* COD: Carbon Oxygen Demand

In literature, there are a few data about dyeing wastewater characterization: Rozzi et al. [7] reported data came from a mixing between textile industry discharge (80%) and civil wastewater (20%), and Rott et al. [8] listed typical values of textile wastewater. In the first case, COD values are in the range of 400 – 490 mg/L and in the second one 400 – 800 mg/L. However, as machinery become more compact, higher values (up to about 2000 mg/L) can be encountered, especially if we consider dyeing of synthetic fibre.

A wide variety of dyes are used, depending on the types of yarn. It is estimated that about $7 \cdot 10^5$ tonnes/year of dyes are produced in the world [1, 2]: azo, anthraquinone, sulphur and indigoid derivatives are mostly employed. The dyes are classified according to their chromophore groups, which are the parts of the molecule conferring colour; it can be an aromatic or a functional typ. The most common chromophore are azo and anthraquinone groups. Azo type constitutes 60-70% of the textile dyestuff produced [9].

Synthetic dyes are toxic for the environment. It was shown that azo dyes in wastewater could produce carcinogenic aromatic amines [10].

Quite usually, at the end of the dyeing process, a noticeable amount of dyes remains in wastewater as is not absorbed by fibres, leading to wastewater colouration. As example, when reactive dyes are used, it is estimated that about 30% of the recipe dyes remains in the exhausted liquor [11].

Dyes show resistance to degradation in the environment, since their peculiarity is chemical stability. Besides visual problems, the effect of residual dyes is negative on aquatic life because they inhibit sunlight transmission and may enter in the food chain.

Typical characteristics of dyeing wastewater are summarized in the following table.

Table 1.1 – Typical data of dyeing wastewater

Composition	Characteristics	Typical values	
dyes	highly coloured	BOD*	400 mg/L
acetic acid	high COD concentration	COD	< 1000 mg/L
reducing agents	high salts concentration	pH	$6 \div 8$
salts	probable heavy metals	Surfactants	20 mg/L
surfactants		SO_4^-	800 mg/L
		Cl^-	400 mg/L

* BOD: Biochemical Oxygen Demand

1.2 Treatment technologies in textile wastewater

As mentioned before, one of the main problems in textile industry is represented by the large amount of water used, so to treat, and colour, particularly in dyeing industry.

Considering a typical textile district (Biella - Italy), water need has been estimated in about $30 \cdot 10^6$ m^3/year. About 88% of the total goes to collection system, while the remaining part represents evaporation loss by drying the wet textile material and other minor uses. The water amount used in the dyeing process has been estimated in about 15 to $20 \cdot 10^6$ m^3/year [11]. This massive flow rate may compete against the domestic uses, especially during dry period. It is important to outline that civil and industrial uses are in the same magnitude order in densely industrialized areas.

Closely related to this consideration is the environmental impact. Pollution of the superficial water from textile industry have both aesthetic problem and toxic and carcinogenic problems for fauna and flora. Pollution is caused by all that products used in the different textile processes and in particular by dyes. Many studies have demonstrated the biological ability to degrade biodegradable matter, but dyes are recalcitrant to these processes.

According to the update view point, considering also climate changes, water must be increasingly considered an indispensable resource for the human life, as well as for industry.

Considering the above reasons, wastewater must be treated to restore water to the environment and save fresh water and reuse treated water in the industrial processes.

Ahead of designing a wastewater treatment system is important to take into account what the goal are:

- preliminary simplified treatment to reach threshold values of the parameters and discharge wastewater in a sewage collector upstream of a consortium final process;
- complete treatment to reach the minimum requirements given by law to discharge treated water into surface aquatic system;
- advanced treatment to generate process water characteristics given by an assisted method and address clear water to any production step.

1.2.1 The modular wastewater platform

A pilot wastewater treatment platform was design and built by Politecnico di Torino within the framework of a collaborative research project (FILIDEA International settlement by Regione Piemonte). In this project several technologies are considered to identify the optimal operational sequence and obtain minimum water specifications for standard and technical fibre dyeing.

This platform includes primary (physical), secondary (biological) and tertiary (refinement) operations.

Primary operations are chosen to remove floating and settleable pollutants in wastewater to minimize problems in downstream steps. Additionally, an in-line wastewater basin balances hydraulic and chemical features of wastewater originated by dyeing batch production.

In secondary treatment, complex biological processes are carried out to remove most of soluble organic matter and suspended sludge here originated. Moreover, disinfection is also typically included in this section.

Finally, tertiary systems are used to polish the treated water from the previous sections in order to reach water quality specifications.

The process structure of the platform built in FILIDEA is modular (Fig 1.2), in order to offer several configurations and remove any treatment which is of no interest for the specific case considered. The concept of modularity is a strong feature of the system. In this way, it is possible to define the optimal treatment process referred to given incoming wastewater.
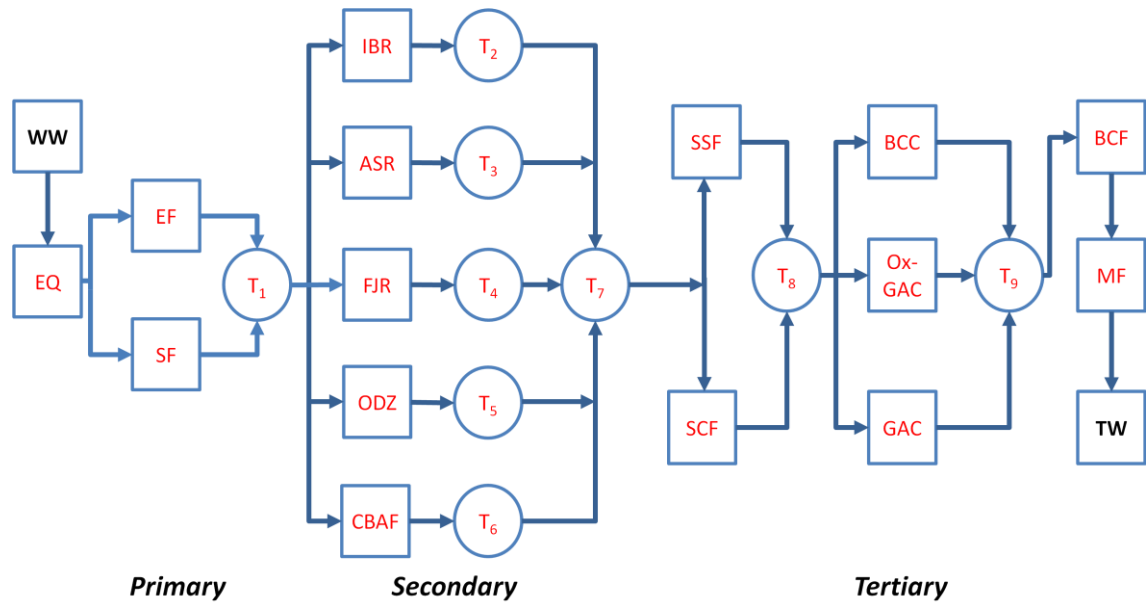
Fig 1.2 – Modular treatment platform scheme (symbol are given in the below description)

Primary Treatments

An equalization vessel (*EQ*) collects the wastewater from the dye-house discharge (*WW*). A suitable flow rate of air is fed at the bottom of the vessel by a perforated pipe to avoid anaerobic conditions and exert adequate mixing.

An electroflotation unit (*EF*) is placed in-line to remove emulsified oil from the wastewater. It is widely demonstrated that fibre lubricating oils cause efficiency problems to both biological units and tertiary treatments. As alternative a simplified fine screen filter (*SF*) protects downstream equipment from carried-over suspended short fibres.

Secondary Treatments

Five oxidation units are placed in parallel. All of them have been designed to have identical wastewater residence times (in the range of 8 to 24 hrs) and are interconnected by a heat exchanger network to control the operating temperature. The goal is to

compare treatment efficiency by analysing COD removal, surfactant content, O_2 transfer efficiency from each air dispersion device and sludge production. Each of them is provided of a settler to recycle the required sludge rate (*T2-T6*), when required.

- Activated sludge reactor (*ASR*) is considered the standard reference for all the units.
- Immobilized biomass reactor (*IBR*): here a polypropylene packing supports the biomass to guarantee longer sludge residence time, prolonged mineralization and optimal aeration.
- Bioflotation® (*ODZ*): here wastewater is continuously recycled in the system by a high pressure pump, which thoroughly mix it with air by means of four small ejectors. The extremely fine bubbles float the pollutants to the vessel surface, form an active biological foam layer and carry on the removal of biodegradable matter.
- Continuous Backwash Biological Aerated Filter (*CBAF*): this unit works by percolating the wastewater through a slowly downward moving bed of GAC (Granulated Activated Carbon), counter-current with air from a bottom distributor. This operation intensifies the treatment by adsorbing pollutants and microorganisms on the carbon surface. The reactor is provided of an air-lift system to separate sludge from GAC by recirculation.
- Flow-Jet aerated Reactor (*FJR*): this system offers an alternative to the aeration carried out by a bottom gas disperser.

Tertiary Treatments

Tertiary treatments are carried out to reach a specific water quality specifications which depend on whether water requires some additional treatment (surfactant and colour removal) to meet the limit imposed by law, or is addressed to specific uses.

Referring to the mentioned platform case, two filters in parallel, *SSF* (Static Sand Filter) and/or *SCF* (Static expanded Clay Filter), are used to protect the subsequent tertiary treatments.

The equipment designed for the tertiary processing are:

- Granular Activated Carbon treatment (*GAC*). This operation is planned to remove the colour and the other non-polar substances present dissolved in the wastewater.
- Oxygenated Granular Activated Carbon treatment (*Ox-GAC*). In this technology the partially treated water is saturated with O_2 to complete the biological degradation of pollutants on GAC, since it catalyzes organic pollutant degradations thanks to adsorption and biomass immobilization.
- Ozone treatment in a bubble column (*BCC*). This oxidative process is specific to demolish the chromophoric bonds or groups of dye molecules: it generates a very high decolouration, though there is a modest COD decrease. Ozone, being a gaseous unstable reactant, is produced on line from a dehydrated O_2 stream and transferred to the liquid system by bubbling the gas at the bottom of a suitable height column or, alternatively, through an ejector by adopting a reactor provided of a recirculation loop.
- Bag Cartridge Filters (*BCF*) are used to remove fine suspended solid and protect from fouling the membrane filtration system.

- Membrane Filtration (*MF*). Nanofiltration (NF) and reverse osmosis (RO) can remove both organic molecules and inorganic ions at very high efficiency. No other technology exists (if we exclude distillation), able to separate the ions generated in wet textile processes by acids, bases and salts. Removing them is a necessary step to successfully recycle process water without accumulating these substances in the water system. NF and RO differ in terms of rejection capacity as a function of molecular weight.

T1, T7, T8 and *T9* are equalization tanks used to collect the water generated by the previous operations. In this way water parameters for the following operation are the same if the systems are used in parallel.

1.2.2 Previous studies and researches on some platform equipments

As demonstrated by experimental study [12], biological treatment described more suitable in dyeing wastewater treatment. Experimental data have demonstrated that the above biological reactors can reach, after optimization, discharge limit imposed by Italian law (D. Lgs 152/2006) in terms of COD. Similar evaluation can be drown by analysing the outputs of several wastewater treatment system in the Biella textile district.

Table 1.2 – COD, TC and surfactants influent wastewater content [12]

Influent	
Pollutant content [ppm]	
COD	$200 \div 450$
TC*	$110 \div 280$
surfactant	$6 \div 15$

*TC: Total Carbon

Table 1.3 – COD, TC and surfactants evaluation after biological treatments [12]

	Effluent					
	COD		**TC**		**surfactant**	
Reactor type	value [ppm]	removal [%]	value [ppm]	removal [%]	value [ppm]	removal [%]
Bioflotation®	$30 \div 13$	$85 \div 70$	$25 \div 100$	$75 \div 65$	$1.5 \div 2.5$	$75 \div 85$
FBBR	$30 \div 160$	$85 \div 65$	$25 \div 115$	$75 \div 60$	$2 \div 3$	$70 \div 80$
Activated sludge	$50 \div 225$	$75 \div 50$	$40 \div 155$	$65 \div 45$	$2.5 \div 4.5$	$60 \div 70$
Flow-jet	$60 \div 225$	$70 \div 50$	$45 \div 155$	$60 \div 45$	$2 \div 2.5$	$70 \div 85$

Bioflotation® and FBBR seem to be the optimal reactors in dyeing treatment both for COD (85÷65% reduction) and surfactants reduction (85÷70% reduction). In addition, the final concentration of COD approaches very close to the value indicated as the limit to be a safe overall figure for a chemical reducing activity (< 25 mg/L COD) for recycling treated water in dyeing system [11]. TC (Total Carbon content) is a parameter

which can be measures by on-line instrumentation, as an alternative to COD discontinuous sampling.

Considering the complex pollution existing in textile wastewater, conventional biological treatment alone cannot guarantee adequate characteristics to allow the discharge into the environment or reuse in other processes. A high salt content and residual colour are still present in the treated water after secondary treatments.

It is worthwhile noting that wastewater from dyeing has high salt content, as salts (Na_2SO_4 and $NaCl$) are typically used to control process kinetics. Membrane filtration is probably the only technology which can be suggested to remove ionic substances.

Salts can be removed by membrane filtration in order to reach the desired concentration. A correlation between water being recycled and the brine reused in the dyeing process has been demonstrated [11], unless a specific brine removal disposal is considered.

1.3 Aim and scope of the study

Colour removal deserves a particular attention in the treatment scheme. Dyes are quite recalcitrant to biological processes and remain in the water without altering in their structure. They cause environmental and visual problems also at relatively low concentration. A mass balance takes into account dye liquor exhaustion and wash-off step can easily demonstrate that the concentration of residual dyestuff accounts to few mg/L only in the raw wastewater.

Additionally, many sources (see Chapter 2) comparatively identify processes able to remove colour efficiently from water. Coagulation-flocculation, adsorption, membrane filtration, activated sludge and oxidation approach to dye removal. Except for the last mentioned operation most technologies have to consider the final destination of the separated matter, namely land filling or incineration. On the contrary, oxidation steps demolish this contaminant at molecular scale, even though not necessary the oxidation is complete. Ozonization has been demonstrated at various operation scales to be very effective at a reasonable cost.

Ozone, being an oxidant agent, has a high oxidation potential (even at a low concentration), high efficiency in decomposition of organic matter, adds oxygen to water and has process low sensitivity to changes in temperature [13]. Ozone destroyed the conjugated bonds of organic matter thanks to a direct reaction between ozone and the organic compound or indirectly through the generation of hydroxyl radicals.

In principle, ozone can be used ahead or after the biological treatments for its high reactivity with organic molecules. It is able to break refractory molecule to be treated in a biological system and therefore makes for biological attack easier. For this reason it can be used as a pre-treatment before the biological reactors. Unfortunately, ozone provided non selective reactions and so a large amount of ozone may be used. On the other hand, a downstream treatment required a much lower ozone supply.

Many studies [13-15] are reported in literature and show the effectiveness of ozone in decolouration.

The degradation of dyes with O_3 is a typical two phase reaction where an effective transfer of ozone from gas to liquid is a critical point. On the other hand, the kinetics of decolouration is usually fast. Therefore, the mass transfer is the rate limiting step. To achieve the best mass transfer condition, several gas diffusers and gas–liquid contactors have been proposed, such as turbines, ejectors, gas diffusers, etc [16].

In this work cavitation was considered as the mean to increase mass transfer of ozone in liquid medium. For this reason, a pilot equipment was designed and built. Two types of cavitation were considered: hydrodynamic cavitation by ejector and ultrasound cavitation. The two types of cavitations were used separately or simultaneously in order to clean wastewater from different dyes typology.

In addition, hydrodynamic and ultrasonic cavitation alone produce hydroxyl radicals which can be used to attack dye cromophores groups of dye molecule.

Moreover, a bubble column reactor was designed and built. Bubble column was used in order to study dye transport mechanisms along the reactor and as a benchmark process to compare the decolourisation results obtained in the cavitation rigs.

References

[1] M.T. Yagub, T.K. Sen, S. Afroze, H.M. Ang, Dye and its removal from aqueous solution by adsorption: A review, *Advances in Colloid and Interface Science,* **209**, 2014, 172-184.

[2] M.F.R. Pereira, S.F. Soares, J.J.M. Órfão, J.L. Figueiredo, Adsorption of dyes on activates carbons: influence of surface chemical group, *Carbon*, **41**, 2003, 811-821.

[3] N. Tüfekci, N. Sivri, İ. Toroz, Pollutants of textile industry wastewater and assessment of its discharge limits by water quality standards, *Turkish Journal of Fisheries and Aquatic Sciences*, **7**, 2007, 97-103.

[4] R. Kant, Textile dyeing industry an environmental hazard, *Natural Science*, **4**, 2012, 22-26.

[5] Meso-level eco-efficiency indicators to assess technologies and their uptake in water use sectors, Ecowater, report 7th Frame Work European Program, Deliverable 4.1, December 2012.

[6] R. Gori, Impianti di trattamento di reflui da industria tessile, 2008, 1-19.

[7] A. Rozzi, F. Malpei, R. Bianchi, D. Mattioli, Pilot-scale membrane bioreactor and reverse osmosis studies for direst reuse of secondary textile effluents, *Water Science Technology*, **41**, 2000, 189-195.

[8] U. Rott, R. Minke, Overview of wastewater treatment and recycling in the textile processing industry, *Water Science Technology*, **40**, 1999, 137-144.

[9] S. Padmavathy, S. Sandhya, K. Swaminathan, Y.V. Subrahmanyam, T. Chakrabarti, S.N. Kaul, Aerobic Decolourization of Reactive Azo Dyes in Presence of Various Cosubstrates, *National Environmental Engineering Research Institute*, **17**, 2003, 147-151.

[10] S.K. Vishwakarma, M.P. Singh, A.K. Srivastava, V.K. Pandey, Azo dye (direct blue 14) decolourization by immobilized extracellular enzymes of pleurotus species, *Cellular and Molecular Biology*, **58**, 2012, 21-25.

[11] G. Rovero, M. Percivale, C. Beltramo, Water recycling for wet textile productions: an example of collective research between SMEs and University, 2nd National Conf. CIWEM, Wakefield, 13-15/09/2004.

[12] S. Papadia, G. Rovero, F. Fava, D. Di Gioia, Comparison of different pilot scale bioreactors for the treatment of a real wastewater from the textile industry, *International Biodeterioration & Biodegradation*, **65**, 2011, 369-403.

[13] S.M. Souza, K.A. Bonilla, A.A. de Souza, Removal of COD and colour from hydrolyzed textile azo dye by combined ozonation and biological treatment, *Journal of hazardous materials*, **179**, 2010, 35-42.

[14] K. Turhan, I. Durukan, S.A. Ozturkan, Z. Turgut, Decolouration of textile basic dye in aqueous solution by ozone, *Dyes and Pigments*, **92**, 2012, 897-901.

[15] C. Tizaoui, N. Grima, Kinetics of the ozone oxidation of Reactive Orange 16 azo-dye in aqueous solution, *Chemical Engineering Journal*, **173**, 2011, 463-473.

[16] EPA, Ozone for industrial water and wastewater treatment, 1980.

Chapter 2 – Dyes removal methods to textile wastewater effluent

2.1 Introduction

One of the main problems of textile wastewater treatment is colour removal [1]. Today, most of the existing treatment processes include an initial step of biological treatment, aimed at removing organic matter, followed by an oxidation one able to reduce the colour content. A large variety of dyestuff is available because they are used according to their compatibility with the textile substrate, therefore the difficulties to improve a system able to reduce colour content increase.

Generally, dyes are described as chemical complex organic molecules that can connect themselves with surfaces or fabrics to confer colour. They are used in different fields such as various kinds of textile, paper, leather tanning, food processing, plastics, cosmetics, rubber, printing and dye manufacturing industries.

It has been estimated that the world annual production of dyestuff is about $7 \cdot 10^5$ tonnes/year and an estimate of about 5% of the total amount is discharged in wastewater by textile industries [2, 3]. Obviously, the exact amount of dyes discharged in the environment is unknown.

Their discharge into hydrosphere is a significant source of pollution due to their same nature, difficult to treat. This will give undesired colour to the water, and this will reduce sunlight penetration and resist photochemical and biological attacks towards aquatic life. Several dyes and their degradation products are toxic and/or mutagenic to life. Sporadic and excessive exposure to colour effluents to human body could drastically reduce immune defences. Moreover, such coloured allergens may undergo chemical and biological assimilations, cause eutrophication, consume dissolved oxygen, prevent re-oxygenation in receiving streams and tend to sequester metal ions, accelerating genotoxicity and microtoxicity [4]. In Table 2.1 the main direct/indirect effects of textile wastewater into the environment are reported schematically.

Table 2.1 – Schematic representation of textile wastewater effects to the environment

Textile wastewater effluent to the environment	
Direct effects	*Indirect effects*
- Aesthetic problems - Decreasing sunlight penetration: damage of flora and fauna ecosystem - Suppression of the re-oxygenation capacity of the system - Ground water pollution	- Eutrophication - Coloured allergen accelerates genotoxicity and microtoxicity - Suppression of immune system of human beings - Killing aquatic life

Without an adequate treatment, dyes are stable and remain in the environment for a long period of time, for example Reactive Blue 19 has a hydrolysis half-time, at 25°C and pH 7, of 46 years [1].

In this chapter some methods, present in literature, used in wastewater treatments industry to refine textile water for reducing dyes concentration and, consequently, able to confer the water to reservoir, are described.

2.2 Dyestuff, general characterisation

As just introduced before, dyes are macro-molecules used to give colour to materials. They are characterized by some particular groups that give colour: chromophore and auxochrome groups.

Chromophore groups are responsible of the colour because they absorb a fraction of the visible light. Typically, chromophore groups are –C=C– (ethenyl), –C=O (carbonyl), –C=N– (imino), –CH=S (thio-carbonyl), –N=N– (azo), –N=O (nitroso), –NO$_2$ (nitro). The intensity of colour depends on the number of the previous groups. Compounds of benzene containing chromophore radicals are called chromogens.

The auxochrome groups are essential for defining a macro-molecule as dye. They are able to fix the dye to a substrate, increasing the absorbed radiating light wavelength (thus bringing in the visible range a molecule that first absorbed in the field of UV) and finally intensifying the colour given by chromophores. The auxochromes are electron withdrawing or donating substituent and they are responsible for imparting the property of electron dissociation and forming salts with either acid or alkali. Some auxochrome groups are –COOH (carboxilic), –NH$_2$ (amino), –SO$_3$H (sulphonyl) and –OH (hydroxyl). The colours given by only these compounds are not dyes because they do not have the affinity or the ability to make the substrate adhere to colour.

Following, some dyestuff structures are reported showing chromophore (red rectangles) and auxochrome (yellow rings) groups (Figg. 2.1, 2.2, 2.3)
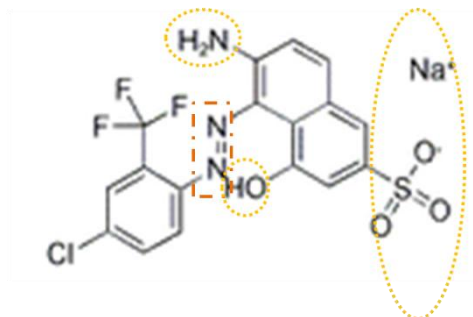
Fig 2.1 - Acid red 266
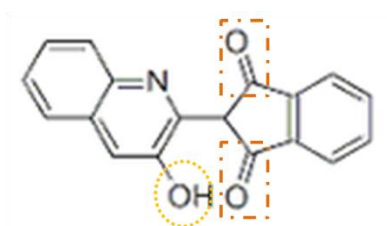
Fig 2.2 - Disperse Yellow 54
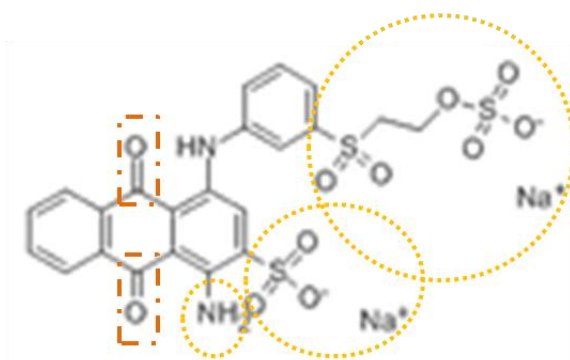
Fig 2.3 - Reactive Black 5

Generally, dyes can be classified using two methods: either according to the charge that they assume in water or by their characteristic chemical groups.
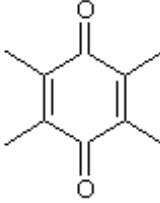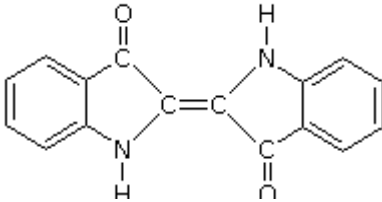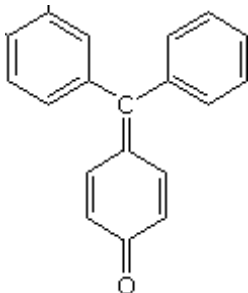
If dyes are classified according to their particular charge in aqueous medium, and therefore their chemical nature, they may classified in cationic (basic dye), anionic (direct, acid, reactive dye) and non-ionic (disperse). Table 2.2 shows this subdivision, including more information about substrate (fibres) and method of application, and types of interaction dye-fibre.

Table 2.2 – Dye classification on their chemical nature [2, 3]

Class	Characteristics	Fibre	Dye-fibre interaction	Method of application
Acid	Anionic Water soluble	Wool Silk Nylon	Electrostatic Hydrogen bonding	From neutral to acid bath
Basic	Cationic Water soluble	Polyester Treated nylon	Electrostatic	Acid bath
Direct	Anionic Water soluble	Nylon Rayon Cotton	Intermolecular forces	From neutral to slightly alkaline bath containing additional electrolyte
Disperse	Low water solubility	Polyamide Polyester Acetate	Solid state mechanism	Fine aqueous dispersion often applying high temperature/pressure or lower temperature carriers method
Reactive	Anionic water soluble	Cotton Wool Silk Nylon	Covalent bonding	Reactive site on dye reacts with functional group on fibre to bind dye covalently, under influence of heat and pH
Sulphur	Colloidal insoluble	Cotton Rayon	Covalent bonding	Aromatic substrate vatted with sodium sulphite and re-oxidised to insoluble sulphur-containing products on fibre
Vat	Colloidal, insoluble	Wool Cotton	Impregnation and oxidation	Water-insoluble dyes solubilised by dropping in sodium hydrogen sulphite, then oxidation on fibre

The other classification is based on their chemical structure: dyes are divided according to a particular characteristic group that composes them (Table 2.3).

Table 2.3 – Dye classification on their chemical structure [2]

Class	Characteristic group
Azo dyes	–N=N–
Anthraquinone dyes	(quinone structure)
Indigo dyes	(indigo structure)
Nitroso dyes	–N=O
Nitro dyes	–NO$_2$
Triarylmethane dyes	(triarylmethane structure)

About 70% of the total amount of dyestuff produced in the world are azo dyes. Azo dyes are characterized by reactive groups (–OH, –NH or –SH) that form covalent bonds with fibres. This type of dyes are used for yellow, orange and red. The second class of colour mostly used in textile manufacturing are anthraquinone dyes, especially for violet, blue and green colour.

2.3 Decolourisation methods

In literature there are lots of methods used to decrease dye content from water. Each of these have advantages and disadvantages: in the following paragraphs both most important methods studied and new developed technologies are exposed.

2.3.1 Biological treatment

Biological treatments to remove colour using biomass have been investigated. They can imply an aerobic or anaerobic process. In aerobic conditions, a total mineralization could be achieved, instead in anaerobic conditions toxic aromatic amines are produced. In general, this kind of process removes not only colour but they have a great

effectiveness on COD (carbon oxygen demand), AOX (adsorbate organo-halogen) and toxicity (via aerobic process) removal. Unfortunately, not all the dyestuffs are reduced by biomass, some of them are difficult to treat with biological reaction [5].

Some studies demonstrated that biological treatments are environmental friendly, they produce less sludge than physical and chemical methods, and are relatively inexpensive, because their running cost is low [6].

Biological decolourisation methods can occur via biosorption, enzymatic degradation or a combination of both.

Biosorption is a technology used to remove dye molecule from dilute aqueous media thanks to inactive or dead biomass. This techniques is often much more selective than traditional ion-exchange resins and activated carbons.

Usually, algae, yeast, filamentous fungi and bacteria has been used to remove colour by enzymatic degradation. Biomass is able to absorb colour thanks to the structure on its cellular wall: it contains different functional groups (such as amino, carboxyl, phosphate, and other charged groups) which create attractive forces with the azo dyes groups.

Living microbial biomasses are used to remove acid, reactive and direct dyes. Moreover, they have the potential to remove metal ions such as copper and chromium, which are integrated in the molecules of some dyes (metal-complex dyes).

Some pre-treatments to biological treatment have the capacity to modify the removal activity of biomass changing the wall characteristics; in this way, it is possible to increase or decrease the adsorption. For example, high temperature, acid condition, using formaldehyde, NaOH, $CaCl_2$, $NaHCO_3$, modify the functional groups of the biomass and therefore the adsorption capacity. Neutral conditions are considered the best ones to use biomass.

Also died biomass plays a specific role on biosorption: they do not require nutrients, can be stored and used for long period and can be regenerated using organic solvents or surfactants [1].

The microbial biomass mentioned above, in addition to absorb the dyes, creates some enzymes capable of reducing particular dye groups. Azo linkage (–N=N–) and sulphuric group (–SO_3), for example, are resistant to aerobic bacteria, but in the presence of specific oxygen-catalyzed enzymes (called azo reductases) they are able to react producing aromatic amines. The enzyme mono- and di-oxygenase catalyzes the incorporation of O_2 in the aromatic ring with the consequent ring fission.

The main advantage of fungi over single cell biomass is the fungal mycelia [5, 7]: they are able to solubilize the insoluble substrates by producing extracellular enzymes. Using fungi in decolourization process is an attractive alternative due to its low cost and the possibility of the total mineralization of the dye itself. The mechanism of fungi dye degradation can be divided in biosorption, biodegradation and bioaccumulation [7]. The first mechanism occurs when the fungal mycelia creates a link with the solutes: energy and transport are not involved. Then, biodegradation consists on the demolition of the dye in by products using enzymes. This is an energy dependent process. In the end, by-products are accumulated (bioaccumulation) and used as metabolites in the growing fungi phase.

The regeneration of the fungal biomass plays an important role: recovery of biosorbent and dye makes treatment process more economical.

In the case of anaerobic condition, a low redox potential is necessary for the decolourization of dyes. The breaking of double azo bond (–N=N–) involves a transfer of four electrons. Following, the two stage reactions involved to remove the azo bond in anaerobic conditions are shown:

$$R_1\text{-}N\text{=}N\text{-}R_2 + 2e^- + 2H^+ \rightarrow R_1\text{-}NH\text{-}NH\text{-}R_2 \text{ (Hydroazo intermediate)}$$
$$R_1\text{-}NH\text{-}NH\text{-}R_2 + 2e^- + 2H^+ \rightarrow R_1\text{-}NH_2 + R_2\text{-}NH_2$$
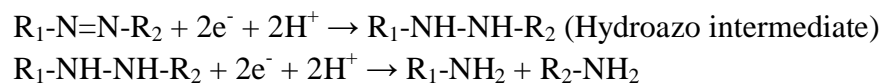
where R_1 and R_2 are radical groups specific for a particular dye.

No information is available about the influence of bacteria on decolourization at high salt concentration: it is possible to suppose that a large amount of salt would be toxic [1].

The biological treatment can be the union of anaerobic and aerobic process. Anaerobic treatment is a strong process with high colour and COD removal. It is not necessary adaptation to a specific dye, anaerobic biomass withstands high dye concentration and short retention time. It is necessary, though, a second aerobic stage where the aromatic and the remaining resistant dye are removed [8].

A promising technology that combines wastewater treatment and electricity generation is the use of Microbial Fuel Cells (MFCs) [6]. In particular, the main goal using this method is the azo dye removal from wastewater. Electricity is produced during the co-metabolism of azo dye and other carbon sources (such as glucose).

The main advantages are:
-   reduction of azo dye content using the electron produced by MFC, in situ;
-   reduction in the use of noble metal as catalyst to assist electron transfer thanks to biocathode;
-   the electricity produced by MFCs could be used for biocathode aeration or for other uses: if combined, many MFCs have higher voltage outputs;
-   increase reduction of azo dye adding redox mediators.

Unfortunately, during the breaking of the azo bond, toxic amines can be produced.

Biological treatment is also used with AOPs (Advanced Oxidation Processes) technologies (see paragraph 2.3.5.6) to remove azo dyes. The main aim of the AOPs is to convert the recalcitrant compounds into smaller molecules that are easy to eliminate by microorganisms. The goal of AOPs/biological treatments is to allow partial degradation of the dyestuff by minimal costly AOP and after that using inexpensive microbiological processes [1].

2.3.2 Coagulation-flocculation process

In physical-chemical treatments, coagulant agents to form flocs with dyes are used; therefore separation or sedimentation techniques are needed in order to remove them from the liquid media. Typical coagulants are aluminium, aluminium polychloride

(PACl), MgCl$_2$ and anionic coagulants. To create steady flocs, polyelectrolytes can be used during flocculation [9].

The coagulation-flocculation treatment can be used in primary or tertiary treatments. It is successfully used to remove sulphur, disperse and reactive dyes, it presents low capacity to form flocs with the other categories of dyestuffs. The main disadvantages are the large demand of chemical input and so high volume of sludge.

In literature, there are some studies where the researchers used natural (vegetal or animal) coagulants to remove dyes. The main advantages are their non-toxicity to the environment and their biodegradability. For these reason, the effluent after natural coagulation process can be treated with biological means, if required [10].

2.3.3 Adsorption and adsorbents

The term adsorption refers to the accumulation of a "substance" on the surface of solid matter (adsorbent). The "substance", called adsorbate, can generally be in liquid or in gas phase. Adsorption can be classified in chemical sorption and physical sorption.

Chemical sorption is characterized by the formation of strong chemical bonds between adsorbate and adsorbent surface, which is generally due to the exchange of electrons. It is an irreversible reaction. On the contrary, physical adsorption is characterized by van der Waals forces, hydrogen bonds, dipole-dipole interaction, polarity between adsorbate and adsorbent. Thanks to the low energy interactions, the reactions are, in most cases, reversible [11, 12].

The main factors affecting dye adsorption are solution pH, temperature, initial dye concentration, adsorbent surface, particle size and contact time.

The main criteria for the selection of an adsorbent should be based on characteristics such as high affinity and capacity for target compounds. In order to improve economical efficiency, the adsorbent should have the quality of adsorbent regeneration.

2.3.3.1 Activated carbon

Activated carbon is commonly used to adsorb pollutants from wastewater: it removes a large variety of dyestuff in a wide range of pH. Only for vat and disperse dyes is quite ineffective. Pereira et al. [4] carried out a study about surface treatment to modify activated carbon surface. They noted that surface chemical groups on the surface of activated carbon play an important role in dye adsorption. Using appropriate physical, chemical or thermal treatments to modify carbon surface, without changing significantly its textural properties, they observe a different dye removal capacity. According to the authors, the best treatment is the thermal one, under H$_2$ flow at 700 °C.

Unfortunately, activated carbons are non-selective, so the dye adsorption competes with the other organic pollutants in water [2]. The regeneration of activated carbon is possible via thermal or solvent treatments. In addition, the losses during activated carbon regeneration are estimated in about 10% [5]. Only in the case of carbon regeneration of smaller particle size adsorbents with H$_2$O$_2$/O$_3$ process the virgin capacity is recovered, but consuming more oxidants [1].

2.3.3.2 Low cost adsorbents

In recent years, low cost adsorbents in dye removal from wastewater have started being used in order to increase economy in treatment processes. With the term "low cost adsorbents", we mean all the materials that:

- require little processing to be optimum for the process;
- are abundant in nature;
- are solid wastes from agricultural, industry or by-products.

Thanks to these characteristics, low cost adsorbents have a dual role: on one hand a waste is used to treat and on the other one there is a waste management.
In the next table (Table 2.4) some low cost adsorbent are listed, together with their origin and what type of dyestuff they are intended to remove from wastewater.
q_m is the maximum adsorption capacity in Langmuir isotherm.

Table 2.4 – Examples of low cost adsorbents

Low cost adsorbent		Maximum adsorption capacity q_m [mg/g] - Dyestuff		Characteristics
Agricultural solid wastes				
Row agricultural by-products	Coffee residues	90.1	M Basic Red 13	Economic
	Tree fern	408	Methylene Blue	Environmental
	Pine Sawdust	398.8	Acid Yellow 132	friendly
Activated carbon from biomass solid waste	Pinewood	1176	Acid Blue 264	Replacement for
	Pinewood	1119	Basic Blue 69	non-renewable
	Pine fruit shell-carbon	529	Methylene Blue	coal
		42.2	Malachite Green	Better adsorption
	Bagasse fly ash			efficiency
Industrial by-products				
Metal hydroxide sludge (from electroplating industry)		45.9	Reactive Red 120	pH played an
		61.7	Reactive Red 2	important role on
		270.8	Remazol Brilliant Blue	adsorption and metal-complexes formation
Red mud (from bauxite processing residue from alumina production)		75	Methylene Blue	Basic pH
		27.8	Remazol Brilliant Blue	

Inorganic materials				
Clay minerals	Clay	58.2	Methylene Blue	Sorption capacity strongly depend on pH
	Raw ball clay	34.7	Methylene Blue	
	Modified montmorillonite	24	Methyl orange	
		322.6	Methylene Blue	Improves flocculation of organic impurities
				Strong affinity with cationic and anionic dyes
				Contain exchange ions
Siliceous materials	Modified silica	45.8	Acid Blue 25	Abundance
	Charred dolomite	950	Dye E-4BA	High sorption
	Glass fibres	2.2	Methylene Blue	Mechanical stability
				High surface area
Zeolites	Zeolite	55.8	Basic blue	Highly porous
				High specific surface area
				High ion-exchange capacity

In the case of agricultural residues adsorbents, some researchers showed that the dye removal from textile effluent is possible [30].

Moreover, the dye-adsorbed substrate can be biodegraded in solid state fermentation, with the possibility of using the fermented product as solid conditioner [13].

2.3.3.3 Ion-exchange resins

In a previous paragraph (2.2) dyes are been classified, most of them are either cationic (basic) and anionic (acid, reactive, direct and complex). Whereby, the previous dyes and ion-exchange resins form complexes together, like flocs, which can be separated by filtration. Although ion-exchange resins provided good results in adsorption but the regeneration is quite difficult.

The main disadvantage of ion-exchange resins is low hydrodynamic properties and production of high amount of sludge. Compared to activated carbon, the resin doesn't tolerate high pressures, required to force large volumes of liquid through the bed at high liquid flow rate. The sludge produced required further treatments, such as incineration or dumping, with subsequent air pollution or expensive posing in landfill.

2.3.4 Separation techniques

Separations techniques are normally used in textile water treatments: ultrafiltration, nanofiltration and reverse osmosis have been used for water reuse and chemical recovery. Reverse osmosis, for example, is especially used to separate salts from water. Ultrafiltration and nanofiltration techniques are effective on dyestuff removal but with some inconveniences. The membrane technology has high investment costs, rapid membrane fouling and production of a concentrated bath which needs to be treated.

2.3.5 Oxidation treatments

Oxidation treatments are the most common techniques used in wastewater decolouration. In addition, some oxidant agents (such as chlorine and ozone) are commonly used in potable water treatment as disinfectants.

Oxidation, in general terms, is used to oxidize and decompose dyestuff molecules to lower molecular weight species (aldehydes, carboxylates, sulphates and nitrogen). The ultimate goal is the mineralization of the all oxidative species to carbon dioxide and water.

2.3.5.1 Chlorine

Chlorine is used in gaseous form (Cl_2) or, mostly common, in liquid form (sodium hypochlorite).

Water soluble dyes (reactive, acid, direct and metal complex) are readily decolourized with hypochlorite, instead water non-soluble dyes (disperse and vat) are more resistant. Non-soluble dyes require a long treatment time and metal complex dyes bath remains partially coloured for a long time of treatment.

Toxic compounds (such as trihalomethane) and heavy metals (such as copper, iron, nickel, chromium by metal complex dyes) are by-products formed from dyestuff decomposition.

2.3.5.2 Fenton's reaction

The reactions that involve Fenton's reagent with any organic compound (RH) are shown below:

$$H_2O_2 + Fe^{2+} \rightarrow Fe^{3+} + OH^- + OH\cdot$$
$$RH + OH\cdot \rightarrow H_2O + R\cdot$$
$$R\cdot + Fe^{3+} \rightarrow R^+ + Fe^{2+}$$
$$R^+ + H_2O \rightarrow ROH + H^+$$
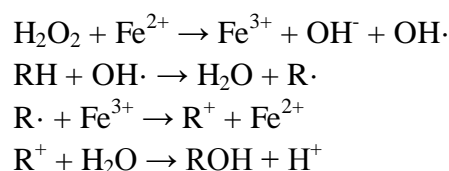
Hydrogen peroxide alone is not effective in dye decolourisation at normal conditions. Using hydrogen peroxide and in presence of iron ions, though, hydroxyl radicals (OH·) are generated [1]. Hydroxyl radicals are much stronger than hydrogen peroxide and they react with organic molecules, mineralizing the compounds. In presence of unsaturated dye molecules, the reaction eliminates the colour.

The reaction must be done in acid condition: dye removal efficiency by Fenton oxidation is not affected by pH changes in the range of pH 2÷7; when pH > 8, Fe^{2+} ion

begins to form floc and precipitates. Furthermore, H_2O_2 is also unstable in alkali condition and may decompose to give oxygen and water, in this way it loses its oxidation capacity. In conclusion, most studies show that pH around 3 is the most effective for decolouration [14-16].

The so-called Fenton's reagent is iron sulphate, but it is possible to use other reagents such as peroxomonosulphuric acid, manganese dioxide, ferrous sulphate, ferric sulphate, ferrous chloride [1].

In the reaction also OH^- ions are produced; they react with ferric ions and produce ferric hydroxo complex. This complex is capable to capture decomposed dye molecule or other dye by-products and precipitate them. Therefore the dye decolouration is promoted by chromophoric bonds distruption and metal complex formation.

In this process, both colour, COD, TOC (Total Organic Carbon) and toxicity decrease. It is suitable for acid, reactive, direct and metal-complex dyestuff. Unfortunately, the sludge produced contains toxic degraded organic compounds.

Continuous Fenton's treatments were also investigated: some researchers used steel swarf as catalyst and iron source (modified Fenton's process) [16]. The main disadvantage is the long processing time.

2.3.5.3 Ultrasound and hydrodynamic cavitation

An innovative method to oxidize dyestuff is cavitation. Cavitation can be described as the formation of nuclei, growth and collapse of bubbles in liquid, producing a large amount of energy [33, 34]. So, localized supercritical conditions (pressure and temperature values near few thousands atmospheric pressure and few thousand Kelvin temperature, respectively) are formed by bubbles implosion. Locally, free radicals formation (particularly $OH\cdot$) is promoted and so favourable environmental is created in order to oxidize pollutant. In addition, supercritical condition may favour pyrolysis reactions.

Cavitation can be promoted by ultrasound or in hydrodynamic way. In ultrasound cavitation, sound waves are propagated in a liquid media, where they induce pressure variations. Only in particular conditions the formation and implosion of bubble is possible. Usually, ultrasound frequencies are in the range 16 kHz – 1 MHk. In the case of hydrodynamic cavitation, bubbles formation are promoted by pressure variations obtained using a device that, changing the geometry, induces velocity variations.

Gogate et al. [35] performed their experiments using Orange Acid-II and Malachite Green (cationic dye). They investigated both ultrasound and hydrodynamic cavitation. They affirm that acidic conditions (pH = 2), low temperature (T = 20 °C) and optimal inlet pressure for hydrodynamic cavitation (5 bar) or high ultrasound potential (80 W, 20 kHz) are the best conditions to reach colour degradation in the range of 50-60% after 120 min. Here, hydrodynamic cavitation was performed using an orifice (2 mm diameter).

Saharan et al. [36] worked using Reactive Red 120 dye in the case of hydrodynamic cavitation performed by ejector (throat section 2 mm diameter): at neutral pH and ejector inlet pressure 3 bar, they reached about 94% of dyestuff decolouration.

Wang et al. [37] used an ultrasonic reactor (20 kHz, 150 W) to degrade reactive Brilliant Red K-BP. After 240 min of treatment at 25 °C and pH 5.5, colour removed is about 20%. Moreover, they affirmed that the best pH to oxidize dye under examination is 12.

In the previous research works, ultrasound cavitation is performed using ultrasound horn and treating small volumes of solution (maximum volume 400 ml). Hydrodynamic cavitation, instead, uses larger volume but with a capacity lower than 4 L.

In conclusion, in literature there are not many articles about dye cavitation decolouration and, apparently, they could seem in contrast: dyes are different, so different degradation kinetics could be involved in the reaction bath.

2.3.5.4 Electrocoagulation

The electrochemical process consists in the formation of the coagulant, generated as a result of the oxidation of the anode material by passing electrical current in an electrochemical cell [1]. Usually, the anode is made of iron and the oxidation forms $Fe(OH)_2$ or $Fe(OH)_3$: they create flocs in acidic solution conditions. When the amount of iron in the solution exceeds the solubility of the metal hydroxide, amorphous metal hydroxide precipitates are formed, which causes sweep-floc coagulation, therefore the colour is removed by adsorption. This method is especially suitable for acid dyes and the maximum colour removal takes place in acid conditions.

Two reaction mechanisms at the anode and cathode are shown below [17]:

1) Anode $\qquad Fe_{(s)} \rightarrow Fe^{2+}_{(aq)} + 2e^-$

$\qquad\qquad\qquad Fe^{2+}_{(aq)} + 2OH^-_{(aq)} \rightarrow Fe(OH)_{2(s)}$

$\quad$ Cathode $\qquad 2H_2O_{(l)} + 2e^- \rightarrow H_{2(g)} + 2OH^-_{(aq)}$

$\quad$ Overall reaction $\quad Fe_{(s)} + 2H_2O_{(l)} \rightarrow Fe(OH)_{2(s)} + H_{2(g)}$

2) Anode $\qquad 4Fe_{(s)} \rightarrow 4Fe^{2+}_{(aq)} + 8e^-$

$\qquad\qquad\qquad 4Fe^{2+}_{(aq)} + 10H_2O_{(l)} + O_{2(g)} \rightarrow 4Fe(OH)_{3(s)} + 8H^+_{(aq)}$

$\quad$ Cathode $\qquad 8H^+_{(aq)} + 8e^- \rightarrow 4H_2(g)$

$\quad$ Overall reaction $\quad 4Fe_{(s)} + 10H_2O_{(l)} + O_{2(g)} \rightarrow 4Fe(OH)_{3(s)} + 4H_{2(g)}$
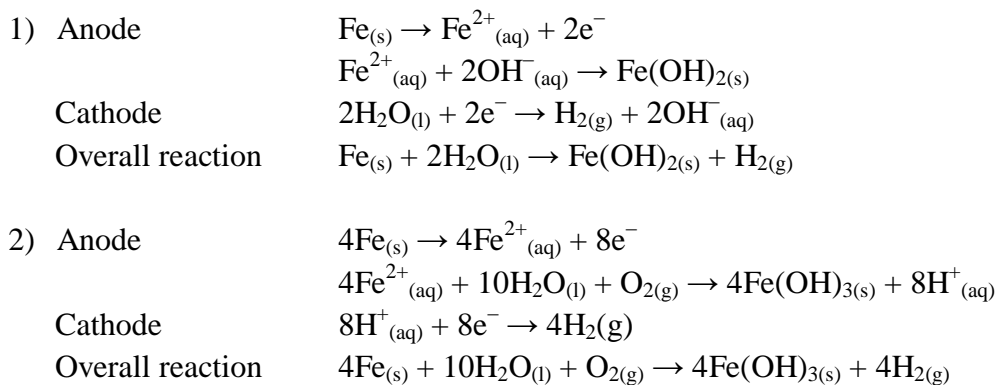
2.3.5.5 Ozone

Ozone is a very powerful oxidizing agent, and it is able to participate in a great number of reactions with organic and inorganic compounds.

The ozonation process could be considered an AOP (Advanced Oxidation Process) itself: at particular pH conditions, hydroxyl radicals are generated from the decomposition of ozone, which is catalyzed by the hydroxyl ion or initiated by the presence of traces of other substances.

In an ozonation process, two possible reactions have to be considered in function of pH:
- direct pathway – pH <4
  reaction between molecular ozone and dissolved compound in water media;
- indirect pathway – pH > 10

reaction between the hydroxyl radicals generated by ozone decomposition in water and the dissolved compounds.

Increasing pH, also the decomposition rate of ozone in water increases. In ground and surface water (pH ≈ 7) both pathways can be important.

In textile wastewater treatment, ozone removes colour and turbidity by oxidation.

Ozone could be used also such as pre-treatment for biological process. Chemical-biological treatment is a potential process for enhanced colour removal and biodegradability of wastewater containing dyes [29].

More information about ozone are presented in Chapter 4.

2.3.5.6 Advanced oxidation processes (AOPs)

AOPs is an acronym that indicates all the methods used in wastewater decolourisation that have common principles in terms of generation of oxidizing species, such as hydroxyl radicals (OH·) [18]. Moreover, this term is used only when there is the simultaneous application of more than one oxidation process. In most cases, a single oxidation system is not enough for the total decomposition of dyes into carbon dioxide and water, and so AOPs are used to reach total mineralization. As an example, some AOPs are listed: H_2O_2/UV, O_3/UV, $H_2O_2/O_3/UV$, TiO_2/UV, H_2O_2/Fe^{2+}, $UV/H_2O_2/Fe^{2+}$, H_2O_2/Fe^{3+}, $Fe^{2+}/oxalate/UV$, $H_2O_2/Fe^{3+}/oxalate$, $H_2O_2/Fe^{3+}/oxalate/UV$, $Mn^{2+}/oxalic$ $acid/O_3$ and $H_2O_2/Fe^{2+}/Fe^{3+}/UV$ [20]. These processes involve a complex set of reactions, with the formation of radical species at high oxidation potential, able to degrade a large variety of organic water contaminants.

OH· is the major reactive intermediate responsible for organic substrate oxidation. Due to the instability of OH·, it must be generated continuously ''in situ'' through chemical or photochemical reactions.

2.3.5.6.1 H_2O_2/UV

The generation of hydroxyl radicals can be done by the activation of H_2O_2 by ultraviolet (UV) light [1]:

$$H_2O_2 + UV \rightarrow 2OH\cdot$$

The UV radiation is ineffective when the water contains high quantities of solids, i.e. in presence of turbidity. In some cases, chemicals that cause turbidity adsorb UV light. Usually, UV is used in potable water to destroy bacteria. The main parameters that influence treatment efficiency are: treatment time, hydrogen peroxide concentration, UV light intensity, dyes chemical structure, surfactants and pH. Generally, the best pH is neutral.

The use of H_2O_2/UV, in comparison to other AOPs, is a considerably safe and easy operation.

This process is more effective with direct, disperse, reactive, metal-complex, vat dyes. Unfortunately, a high reaction time is necessary: to reach colour removal of about 95%, about 90 min at pH 7 are needed [19, 20].

2.3.5.6.2 Photo Fenton process

In this process, UV radiation and Fenton's reaction are used to improve colour and organic compound removal.

Photo Fenton oxidation can be homogeneous or heterogeneous, depending on the type of catalyst: in the first case, iron is in the form of ions Fe^{2+} and Fe^{3+}, in the other case zero iron valence is used [21, 22].

The mechanism involved in dye degradation can be described in three stages [22]:

1st – dissolution of iron (iron salt or swarf - most economic) and release of Fe^{2+} ions in the media;

2nd – solar/UV irradiation to photo Fenton reaction, consequently formation of hydroxyl radicals;

3th – oxidation of textile dyeing wastewater.

Considering real dye effluents, pH 3, 1 g/L catalyst concentration and 15 g/L H_2O_2 concentration are the best doses to have about 90% decolouration in 15 min [1]. Another study showed that only 40% colour removal is achieved in 25 min of photo-Fenton exposure at neutral condition [22].

2.3.5.6.3 Photocatalytic oxidation

In photocatalytic oxidation, heterogeneous catalysts made of metal oxide semiconductor are used. Examples of semiconductors usually used in wastewater treatment are TiO_2, ZnO, CdS, WO_3 and SnO_2 [1].

The basic principle of heterogeneous photocatalysis using semiconductor oxide is well known and can be briefly summarized in the following simplified processes. The photo-excitation of semiconductor particles promotes an electron from the valence band to the conduction band (e_{CB}^-). In this way, an electron deficiency or a so-called positive hole (h_{VB}^+) in the valence band is created. Therefore, electron/hole pairs are generated. Both reductive and oxidative processes can occur at/or near the surface of the photo excited semiconductor particle [26].

The whole process can end in complete mineralization of organic compounds.

According to this, the relevant reactions at the semiconductor surface causing the degradation of dyes can be expressed as follows:

$$TiO_2 + h\nu(UV) \rightarrow TiO_2(e_{CB}^- + h_{VB}^+)$$
$$TiO_2 (h_{VB}^+) + H_2O \rightarrow TiO_2 + H^+ + OH\cdot$$
$$TiO_2 (h_{VB}^+) + OH- \rightarrow TiO_2 + OH\cdot$$
$$TiO_2 (e_{CB}^-) + O2 \rightarrow TiO_2 + O_2\cdot^-$$
$$O_2\cdot^- + H^+ \rightarrow HO_2\cdot$$
$$Dye + OH\cdot \rightarrow degradation\ products$$
$$Dye + h_{VB}^+ \rightarrow oxidation\ products$$
$$Dye + e_{CB}^- \rightarrow reduction\ products$$
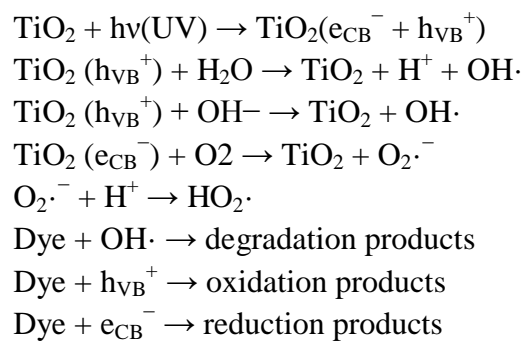
Furthermore, the addition of H_2O_2 to this heterogeneous system increases the concentration of OH· radicals. In this way, it inhibits electron hole recombination process and consequently dramatically increases the degradation rate.

Photocatalytic processes are suitable for a wide range of dyes, including direct, vat and disperse. Usually the colour removal occurs at acidic conditions (best pH is 3), but it depends on the chemical structure of the dye. Degradation kinetics is influenced by electrical nature of the catalyst, number of azo groups and radicals attached to them. Photocatalytic process is effective also for COD and TOC removal, although there is an increase in BOD [23-26].

2.3.5.6.4 O_3- based AOPs

As it was mentioned, it is possible to consider ozone as an AOP itself, because it can generate hydroxyl radical in water solution. Nonetheless, it is possible to increase colour and organic matter removal using O_3 together with other technologies such as UV, H_2O_2, ultrasound (US) and a combination of them.

The O_3/UV process is an effective method for the oxidation and destruction of toxic and refractory organics in water. In detail, this technology was found to be effective in wastewater decolouration. The addition of H_2O_2 to the O_3/UV process accelerates decomposition of ozone and consequently increases OH· radicals generation.

Another method used in O_3-based AOPs are ultrasounds: pressure waves are propagated in the liquid, producing bubbles cavitation. The waves have frequencies higher than 20 kHz. When ozone is introduced into a sonolysis reactor, the ultrasonic irradiation enhances the mass transfer, dispersion and solubility of ozone and production of hydroxyl radical [28].

When dissolved ozone is into a cavitational field, the thermal decomposition of ozone leads to an increase of OH· concentration in the liquid media:

$$O_3 +))) \rightarrow O_2 + O·$$
$$O· + H_2O \rightarrow 2\ OH·$$
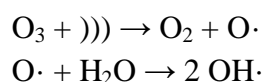
where))) is US iradiation.

References

[1] R.M. Chriestie, Environmental Aspects of textile dyeing, *The textile Institute*, chap. 7, 151-160, 2007

[2] M.T. Yagub, T.K. Sen, S. Afroze, H.M. Ang, Dye and its removal from aqueous solution by adsorption: A review, *Advances in Colloid and Interface Science*, **209**, 2014, 172-184.

[3] M.F.R. Pereira, S.F. Soares, J.J.M. Órfão, J.L. Figueiredo, Adsorption of dyes on activates carbons: influence of surface chemical group, *Carbon*, **41**, 2003, 811-821.

[4] A.K. Verma, R.R Dash, P. Bhunia, A review on chemical coagulation/flocculation technologies for removal of colour from textile wastewater, *Journal of Environmental Management*, **93**, 2012, 154-168.

[5] A.B. dos Santos, F.J. Cervantes, J.B. van Lier, Review paper on current technologies for decolourisation of textile wastewater: Perspectives for anaerobic biotechnology, *Bioresource Technology*, **98**, 2007, 2369-2385.

[6] M. Solís, A. Solís, H.I. Pérez, N. Manjarrez, M. Flores, Microbial decolouration of azo dyes: A review, *Process Biochemistry*, **47**, 2012, 1723-1748.

[7] P. Kaushik, A. Malik, Fungal dye decolourisation: Recent advances and future potential, *Environmental International*, **35**, 2009, 127-141.

[8] M. Jonstrup, N. Kumar, M. Murto, B. Mattiasson, Sequential anaerobic–aerobic treatment of azo dyes: Decolourisation and amine degradability, *Desalination*, **280**, 2011, 339–346.

[9] P.W. Wong, T.T. Teng, N.A.R.N. Norulaini, Efficiency of the Coagulation-Flocculation Method for the Treatment of Dye Mixtures Containing Disperse and Reactive Dye, *Water Quality Resource Journal Canada*, **42**, 2007, 54-62.

[10] H. Patel, R.T. Vash, Comparison of naturally prepared coagulants for removal of COD and colour from textile wastewater, *Global NEST Journal*, **15**, 2013, 522-528.

[11] Ingegneria delle acque reflue, trattamento e riuso, 4th edition, *Metcalf & Eddy*, 2006, p. 1098.

[12] G. De Feo, S. De Gisi, M. Galasso, Acque reflue, progettazione e gestione di impianti per il trattamento e lo smaltimento, 1st edition, p. 574.

[13] P. Nigam, G. Aemour, I.M. Banat, D. Singh, R. Marchant, Physical removal of textile dyes from effluents and solid-state fermentation of dye-adsorbed agricultural residues, *Bioresource Technology*, **72**, 2000, 219-226.

[14] T.R. Sundararaman, V. Ramamurthi, N. Partha, Decolourization and COD Removal of Reactive Yellow 16 by Fenton Oxidation and Comparison of Dye Removal with Photo Fenton and Sono Fenton Process, *Modern applied science*, **8**, 2009, 15-22.

[15] K. Barbusiński, The Modified Fenton Process for Decolourization of Dye Wastewater, *Polish Journal of Environmental Studies*, **14**, 2005, 281-285.

[16] M.E. Haddad1, A. Regti, M.R. Laamari1, R. Mamouni, N. Saffaj, Use of Fenton reagent as advanced oxidative process for removing textile dyes from aqueous solutions, *Journal Material Environment Science*, **5**, 2014, 667-674.

[17] G.O. El-Sayed1, M.S. Awad1, Z.A. Ayad1, Electrochemical Decolourization of Maxilon Red GRL Textile Dye, *International Research Journal of Pure & Applied Chemistry*, **4**, 2014, 402-416.

[18] M.P.G. De Sousa Lucas, Application of advanced oxidation processes to wastewater treatment, Utad 2009.

[19] M. Dinarvand, Decolourized of Textile dye waste waters by Hydrogen peroxide, UV and Sunlight, *International Journal of ChemTech Resource*, **6**, 2014, 985-990.

[20] J. Mitrović, M. Radović, D. Bojić, T. Nđelković, M. Purenović, A. Bojić, Decolourization of the textile azo dye Reactive Orange 16 by the UV/H_2O_2 process, *Journal of Serbian Chemical Society,* **77**, 2012, 465–481.

[21] M. Punzi, B. Mattiasson, M. Jonstrup, Treatment of synthetic textile wastewater by homogeneous and heterogeneous photo-Fenton oxidation, *Journal of Photochemistry and Photobiology A: Chemistry*, **248**, 2012, 30–35.

[22] R. Ganesan, K. Thanasekaran, Decolourisation of textile dyeing Wastewater by modified solar PhotoFenton Oxidation, *International Journal of Environmental Sciences*, **1**, 2011, 1168-1176.

[23] I.K. Konstantinou, T.A. Albanis, TiO_2-assisted photocatalytic degradation of azo dyes in aqueous solution: kinetic and mechanistic investigations A review, *Applied Catalysis B: Environmental*, **49**, 2004, 1–14.

[24] C. Singaravadivela, M. Vanithab, N. Balasubramanianb, Photo and Electrocatalytic Treatment of Textile Wastewater and Its Comparison, *Journal of Electrochemical Science and Technology*, **3**, 2012, 44-49.

[25] E. Chatzisymeon, C. Petrou, D. Mantzavinos, Photocatalytic treatment of textile dyehouse effluents with simulated and natural solar light, *Global NEST Journal*, **15**, 2013, 21-28.

[26] M. Kulkarni1, P. Thakur, Photocatalytic Degradation and Mineralization of Reactive Textile Azo Dye Using Semiconductor Metal Oxide Nano Particles, *International Journal of Engineering Research and General Science*, **2**, 2014, 245-254.

[27] A. Muhammad, A. Shafeeq, M.A. Butt, Z.H. Rizvi, M.A. Chughtai and S. Rehman, Decolourization and removal of COD and BOD from raw and biotreated textile dye bath effluent through advanced oxidation processes (AOPs), *Brazilian Journal of Chemical Engineering*, **25**, 2008, 453-459.

[28] Z. He, L. Lin, S. Song, M. Xia, L. Xu, H. Ying, J. Chen, Mineralization of C.I. Reactive Blue 19 by ozonation combined with sonolysis: Performance optimization and degradation mechanism, *Separation and Purification Technology*, **62**, 2008, 376–381.

[29] S.M.d.A.G.U.de Souza, K.A.S. Bonilla, A.A.U. de Souza, Removal of COD and colour from hydrolyzed textile azo dye by combined ozonation and biological treatment, *Journal of hazardous Materials*, **179**, 2010, 35-42.

[30] S.M. Kanawade, R.W. Gaikwad, S.A. Misal, Low cost Sugarcane Bagasse Ash as an Adsorbent for Dye Removal from Dye Effluent, *International Journal of Chemical Engineering and Applications*, **1**, 2010, 309-318.

[31] A.S. Raymundo, R. Zanarotto, M.B.M. de Godoi Pereira, J.N. Ribeiro, A.V.F.N. Ribeiro, Evaluation of sugar-cane bagasse as bioadsorbent in the textile wastewater

treatment contaminated with carcinogenic congo red dye, *Brazilian archives biology Technology*, **53**, 2010, 931-938.

[32] S. Karcher, A. Kornmüller, M. Jekel, Anion exchange resins for removal of reactive dyes from textile wastewaters, 36, 2002, 4717-4724.

[33] P.R, Gogate, A.B. Pandit, A review of imperative technologies for wastewater treatment I. Oxidation technologies at ambient conditions, *Advances in environmental research*, **8**, 2004, 501-551.

[34] Y.G. Adewuyi, Sonochemistry, environmental science and engineering applications, *Industrial and Engineering Chemistry Research*, **40**, 2001, 4681-4715.

[35] P.R. Gogate, G.S. Bhosale, Comparison of effectiveness of acoustic and hydrodynamic cavitation in combined treatment schemes for degradation of dye wastewater, *Chemical Engineering Process*, 2013, http://dx.doi.org/10.1016/j.cep.2013.03.001.

[36] V.K. Saharan, M.P. Badve, A.B. Pandit, Degradation of Reactive Red 120 dye using hydrodynamic cavitation, *Chemical Engineering Journal*, **178**, 2011, 100-107.

[37] X. Wang, Z. Yao, J. Wang, W. Guo, G. Li, Degradation of reactive brilliant red in aqueous solution by ultrasonic cavitation, *Ultrasonic Sonochemistry*, **15**, 2008, 43-48.

Chapter 3 – Ozone and ozone contactors

3.1 Introduction - Ozone brief history

The history of ozone started in 1785 when Van Marum [1, 2] smelled a characteristic odour coming from his electrostatic machine when a series of electric sparks formed through air [3]. The same odour was observed by Cruickshank in 1801 during his water electrolysis experiments at the anode [6]. Only forty years after, Christian Friedrich Schönbein identified the "odour" as a distinct chemical compound and he gave it the name of ozone, from the Greek *ozein* (to smell). On March 13, 1839, he reported to the local Naturforschung Gesellschaft in Bessel that the electrolysis of sulphuric acid produced an odour at the positive electrode which is the same odour produced by an arc between electrodes in oxygen or air atmosphere [1]. Moreover, Schönbein was the first scientist that suggested the natural presence of ozone in atmosphere.

Mariniak and Delarive showed that ozone is an allotropic modification of oxygen and in 1863 Jacques-Louis Soret, thanks to his studies, proposed the relationship between oxygen and ozone: three volumes of oxygen produce two volumes of ozone.

In 1845, Schönbein reported some results about reaction between ozone and organic substances. First of all, he noted that the ozone odour disappears in the presence of straw, humus, egg white, flour, cyanine dye, etc, and secondly he discovered that organic substances were not converted to the highest oxidation state of carbon (CO_2) but to aldehydes and carboxylic acids.

Probably, the first well documented reaction between an organic compound and ozone is the reaction of indigo dye with ozone by Schönbein in 1851. Probably this is the first documented experiment of decolouration.

In the last fifteen years of the 19th century, lots of scientists studied ozone in term of reaction and improving ozone generation.

Many oxidations of inorganic and organic materials were conducted in order to understand the reactivity of the ozone with materials. In many cases scientists did not know neither the reaction paths nor the final products. Only at the beginning of the 20th century they had the possibility to understand the ozone's behaviour with organic

compounds. In the same period, scientist started to develop innovative methods for ozone analysis, and commercial equipment for ozone production was developed.

Ozone could be used in water treatments in different fields, thanks its high reactivity as oxidant agents:

- disinfection;
- oxidation of inorganic compounds;
- oxidation of organic compounds (including colour and odour removing);
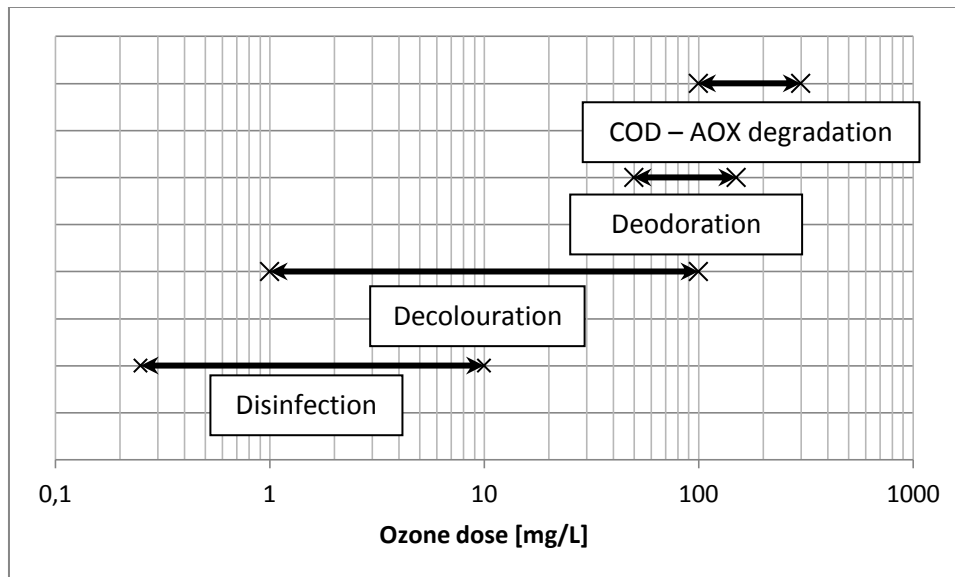- particle removal.

Fig 3.1 – Characteristic ozone dose according to ozonation fields (Feretra et al. modified [10])

The early ozone studies reported in literature are about water disinfection. The earliest experiments were conducted in France by de Meritens (1886): he used ozone as a germicide agent to treat water. He showed that using ozonated air in polluted water, the final effect was water sterilization. Five years later, the bacterial properties of ozone are reported by Frölich from pilot test conducted in a German water treatment plant. In 1893 in Ousdshoorn, Holland, the first water treatment plant was built, where an ozone reactor was employed after settling and filtration. This plant was built to treat the Rhine River water. Thanks to this example, in 1906 in Nice (France), a water treatment plant in which the ozone was used continuously to disinfect water was developed. For this reason Nice was called "the birthplace of ozonation for drinking water".

In the years prior to World War I, there was an increase in the use of ozone installations in various countries. Around 1916, 49 ozone installations were in use throughout Europe (26 of which were located in France). Between the World Wars, the increase in ozone application started to falter due to new researches on toxic gas, especially the development of chlorine. This gas appeared to be a suitable alternative to ozone, thanks to low applicative guarantee and low yield of ozone generation.

In the period between the end of the World War II and the end of the 70s, the number of ozone plants increased to 1043 installations worldwide. Today, chlorine is still preferred over ozone for water disinfection. However, in the last decade the application of ozone

started to increase again. This was caused by the discovery of harmful by-products of chlorine disinfection (trihalomethanes) [4]. Another problem was an increase in disturbing, difficultly removable organic micro-pollutants in surface waters. These compounds appear to be oxidized by ozone faster than by chlorine and chlorine compounds. Finally, there has been a progress in the abolishment of shortcomings in ozone management.

Ozone, today, is not only used in drinking disinfections: multiple uses for ozonation have been developed. Ozone is applied for colour and odour removal at the end of the treatment process, and obviously a significant amount of disinfection is obtained.

Ozone decolouration is more important in wastewater come from dye manufacturing and textile dyeing plants. Generally, this type of wastewaters are very coloured, containing dyestuff, sizing agents (organic and inorganic), surface active agents, organic acid and inorganic acid salts.

The first study in which ozone is employed to eliminate colour from water is of the early 1970s.

Ozone presents some advantages for its use in water treatment, but also some disadvantages:

Advantages
- ozone is easy to produce from air or oxygen by electric discharge;
- ozone reacts with organic and inorganic matters thanks to its high reduction potential and reactivity;
- it does not produce more toxic compounds than the removed ones, neither introduces foreign substances in the medium;
- it does not produce sludge;
- ozone reduces COD, colour, odour and turbidity of the water treated.

Disadvantages
- the effectiveness of the generator is low and ozone concentration is low as well;
- the ozone must be generated in situ;
- gas-liquid mass transfer may be increased to increase reaction kinetics.

3.2 Ozone physical properties

Ozone, at room temperature, is a blue gas with a pungent odour, highly corrosive, toxic and explosive when the concentration is higher than 240 g/m^3 (20% in air). The ozone is detectable at very low concentration from $2 \cdot 10^{-5}$ to $1 \cdot 10^{-4}$ g/m^3 (from 0.01 to 0.05 ppm by volume).

Through electron diffraction study, ozone, in gas phase, is composed of three atoms that form a isosceles triangle with a vertex angle of 127° ± 3°, the length of the equal sides being 0.126 ± 0.002 nm and the base being about 0.224 nm.
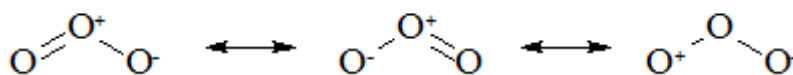

Fig. 3.2 – Ozone resonance formulas

The reaction that leads to the formation of ozone is

$$3O_2 \leftrightarrow 2O_3 \quad \Delta H°_f \text{ at } 25°C = +142.67 \text{ kJ/mol}$$

The molecule of ozone is unstable and spontaneously goes back into oxygen.

In aqueous solution, ozone is relatively unstable: in distilled water at 20 °C, the ozone half-life is about 20 to 30 min. If oxidant-demanding materials are present in solution, the ozone half-life decreases. The presence of ozone in water is also depending on pH and temperature.

In air, ozone is much more stable than in water and the half-life is in the order of 12 hours, at ambient condition [6]. For this reason and because its reactivity and instability, ozone cannot be stored and transported, so it has to be produced in situ.

Ozone is a strong oxidizing agent with an oxidation potential of 2.07 V, which means to be one of the most powerful oxidant agents.

Table 3.1 – Standard redox potential of some oxidant species

Oxidant species		Potential (V)	Relative potential of ozone
Fluorine	F	2.87	1.48
Hydroxyl radical	OH·	2.86	1.35
Atomic oxygen	O	2.42	1.17
Ozone	O_3	2.07	1.00
Hydrogen peroxide	H_2O_2	1.78	0.85
Oxygen	O_2	1.23	0.59

Thanks its great reactivity, it is capable to react with inorganic and organic matters, including human body tissues. For this reason, ozone is considered a dangerous material.

Ozone is soluble in many substances, forming either stable or metastable solutions. In water it produces metastable solutions. Its stability is influenced by the environment conditions and the presence of impurities in water, such as heavy metal cations and metal complex.

Ozone is more soluble in water than oxygen. At 20 °C, the solubility of 100% ozone is 570 mg/L.

Table 3.2 – Ozone solubility in water

Temperature [°C]	Solubility [mg/L]
0	1090
10	780
20	570
30	400
40	270
50	190
60	140

The determination of ozone solubility in pure water is complicated by the fact that ozone decomposes irreversibly in water. Some researchers [8] found an equation to determinate the Henry's law constant (K_H) in pure water to best represent their data:

$$K_H = 3.842 \cdot 10^7 \, [OH^-]^{0.035} \exp\left(-\frac{2428}{T}\right)$$

where [OH⁻] is the hydroxide ion concentration (mol/L) and T the temperature (K). In Table 3.3 are reported the main physical characteristics of ozone

Table 3.3 – Ozone physical characteristics [5]

Physical property	**Value**		
Melting point	-251	°C	
Fusion point	-193	°C	
Boiling point	-112	°C	
Critical pressure	5532	kPa	
Critical temperature	-12.1	°C	
Specific gravity	1.658	g/cm^3	higher than air
	1.71	g/cm^3	at -183 °C
Critical density	436	kg/m^3	
Heat of vaporization	14.9	kJ/kg	at boiling point temperature
Heat of formation	33.88	kcal/mol	at 25°C and 1 atm
Free energy of formation	38.86	kcal/mol	
Vapour tension	11.0	kPa	at -183 °C

3.3 Ozone generation methods

Ozone is an unstable molecule that decomposes in a very short time after generation. For this reason, it should be generated in the area of application. Generally, ozone involves the intermediate formation of atomic oxygen radicals, which react with molecular oxygen:

$$O_2 + e^- \rightarrow 2O\cdot + e^-$$
$$O\cdot + O_2 \rightarrow O_3$$
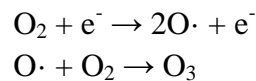
This set of reactions require a large amount of energy.
The following simplified scheme shows the process for the decomposition of ozone in the generating flow.

$$O\cdot + O_3 \rightarrow 2O_2$$
$$e^- + O_3 \rightarrow O\cdot + O_2 + e^-$$
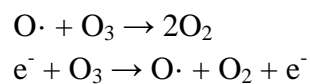
Ozone is produced from oxygen or air (as air enriched of oxygen): obviously, at same gas flow, the concentration of ozone produced increases with the increase of oxygen concentration in the inlet feed.

When oxygen is used, higher ozone concentrations are achieved (about from 3 to 10% in weight).

If air is used, a pre-treatment system will be important to prevent ozone generator damage. The air supplied in the generator should be dry and clean with a maximum dew point of -60 °C. Ozone content is lower than pure oxygen, and corresponds to 1-3% in weight.

Generally, air treatment system is composed of air compressor, filters, dryers and pressure regulator.

Considering that the energy required for ozone generation is high, the energy source that can perform it are electrons or photoquantum energy.

Ozone can be produced by electrolysis (such as Schönbein in 19th century), by UV radiation or radiochemical treatment of a gas containing oxygen. However, in the ozone generation industry corona discharge generation method predominates.

In the second half of the 19th century Wern von Siemens (German), Brodie (England) and Berthellot (France) designed ozone generators using corona discharge [6]. The generators were composed of two coaxial glass tubes where air feed gas passes through the annular space. The main difference of the three equipments consisted in the dielectric material: Siemens coated the glass tube with tin foil, Brodie used water in place of tin foil and Berthellot used sulphuric acid. All operate with the same general principle: they use corona discharge which requires high voltage.

Nowadays, the industrial ozone generator use the technology developed by Siemens: glass tubes are coated internally with a dielectric metal and the single tubes are cooled by water.

Corona discharge, also known as silent electrical discharge, consists in passing gas flux, containing oxygen, through two electrodes separated by a dielectric and a discharge gap. Applying voltage to the electrodes, it causes an electron flow across the discharge gap. Thanks to these electrons, the energy to dissociate the oxygen molecules is provided.

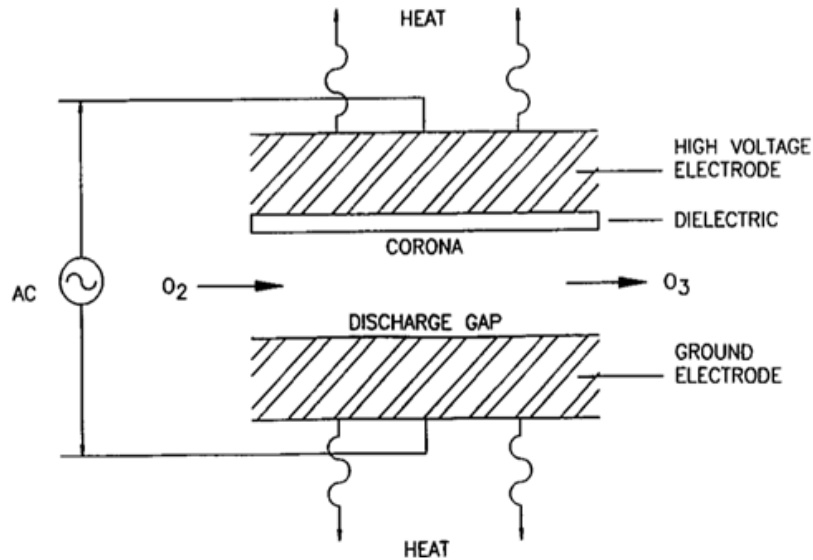In Fig 3.3 the basic corona discharge generator is schematized.

Fig 3.3 – Corona discharge ozone generator layout

The commercial ozone generation has two electrodes geometry configurations: concentric cylinders (Fig 3.4) and parallel plates. Usually parallel plates are used for small ozone generators.

About 85% of the total input energy in an ozone generator is lost as heat. For this reason, adequate cooling should be provided in order to maintain the global efficiency of the generator. Usually, the excess heat is removed using water flowing around the stainless steel ground electrodes.
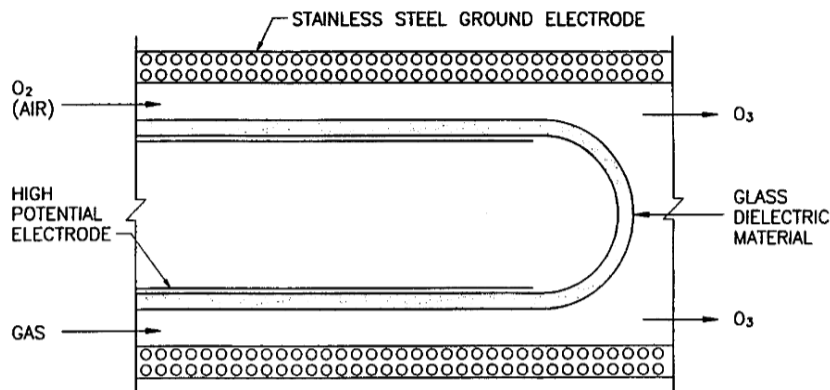
Fig 3.4 – Cylindrical electrode [6]

3.4 Ozone reactions

Ozone involves different reactions in water solutions; they can be classified in two categories: direct and indirect reactions. In the first case, ozone reacts directly with the chemical species, instead in the second one the reaction is between free radicals (the most stable is hydroxyl radical) and compounds present in water. Free radicals are more reactive with organic and some inorganic matters in water solutions and they are formed from ozone decomposition or from others direct ozone reactions with water.

It can be said that direct ozone reaction is the initiation step leading to radical reaction [4].

Fig 3.5 – Ozone reaction types in water solution

The two oxidation paths compete with each other: direct water oxidation is relatively slow but the ozone concentration is relatively high. On the other hand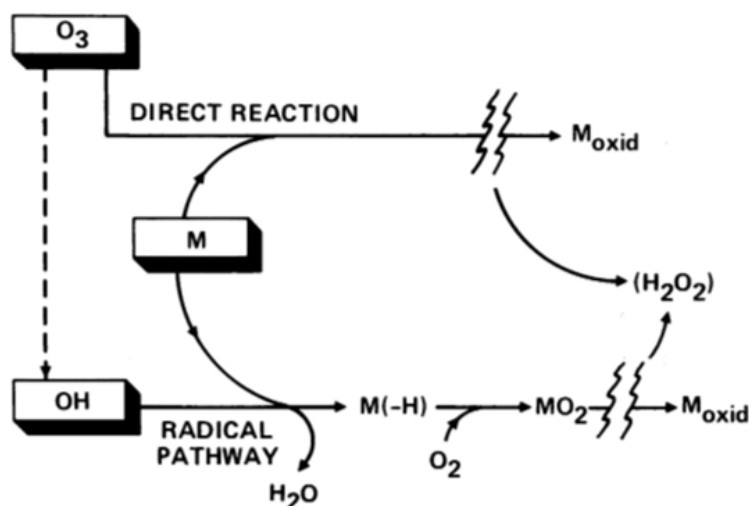, the reaction with hydroxyl free radicals is fast but the concentration of the radical species in normal ozonation conditions is small (it never reaches levels above 10^{-12} M) [5]. Ozone is highly selective in the reactions with organic compounds, but hydroxyl radicals are highly reactive and, consequently, their reaction with organics is not selective [4].

Usually, pH is used to understand how the ozone reacts with the component in solution:
- pH < 4   direct reaction is the predominant reaction path;
- pH > 10   ozone leads to the formation of hydroxyl radicals that react with the compounds in solution;
- 4 < pH < 10   coexistence of both reaction paths.

The decomposition of ozone in water leads to the formation of unstable radicals: not only hydroxyl radicals but also peroxide ion, superoxide anion, singlet oxygen and oxygen radical anion.
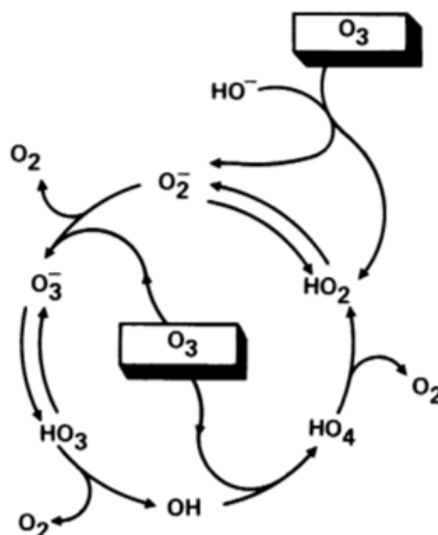

Fig 3.6 – Ozone decomposition in water initiated by hydroxyl ions [3]

In normal condition, as mention before, the half-life of the ozone is in the order of 20 to 30 min in comparison with hydroxyl radical that is in the magnitude of microseconds [5, 6]. The final product coming from the ozone decomposition is environment friendly oxygen.

The direct ozone reaction in water can be divided in:
- Dipolar cycloaddition reactions;
- Electrophilic substitution reactions;
- Nucleophilic reactions.

3.4.1 Direct ozone reaction

3.4.1.1 Dipolar cycloaddition reactions

In general terms, addition reaction results from the combination of two molecules, one of these having unsaturated bonds and the other one having an electrophilic character. The following scheme corresponds to an addition reaction where the second reagent has electrophilic character:

$$-C=C- + XY \rightarrow -XC-CY-$$
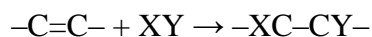
Comparing addition and cycloaddition, the addition reaction involves only π bonds, opposite to cycloaddition where π and σ lead to the reaction.

Compounds with other double bonds (C=O or C=N) do not react with ozone using cycloaddition reaction. In the cases of aromatic compounds, ozone could react through 1,3-cycloaddition reactions breaking the aromatic ring. But the possibility of 1.3-cycloaddition reaction is less probable than electrophilic attack because of the stability of the aromatic rings.

The mechanism of Criegge constitutes an example of cycloaddition reaction. The mechanism is composed of three steps (see Figg 3.6 to 3.9 [4]). In the first one, a very unstable five elements ring is formed: it is named as primary ozonide (I). In the second step, the primary ozonide breaks up forming a carbonyl compound (aldehyde or keton) and a zwitterion (II). The zwitterion, depending on the solvent where the reaction develops, experimental conditions and nature of the olefinic compounds, decomposes in different way in the last step (III a to c).

In a neutral solvent, zwitterions could decompose to yield another ozonide, a peroxide or ketone. In the case in which the reaction is in a participating solvent, some oxy-hydroperoxide species are generated. Finally, abnormal ozonolysis could develop both in participating and non-participating solvents. The final product of this reaction paths are keton, aldehyde or carboxylic acids.
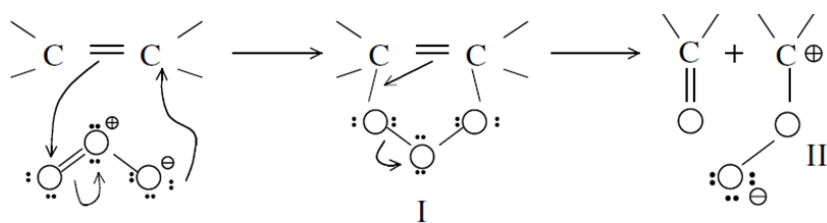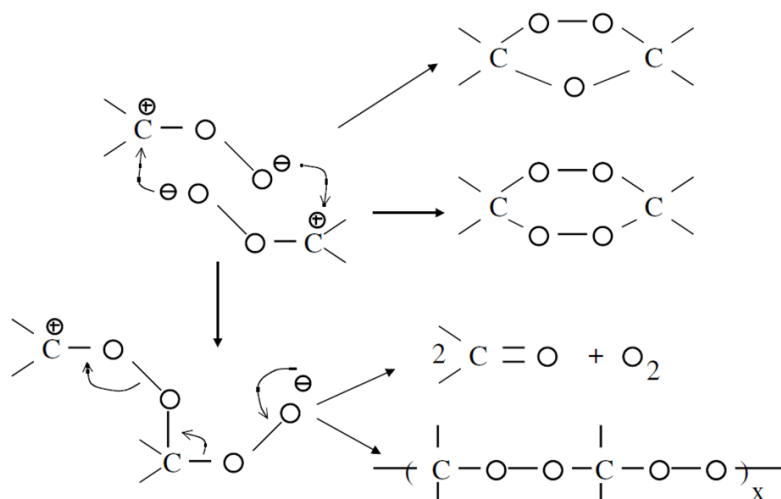
Fig. 3.7 – Criegee mechanism

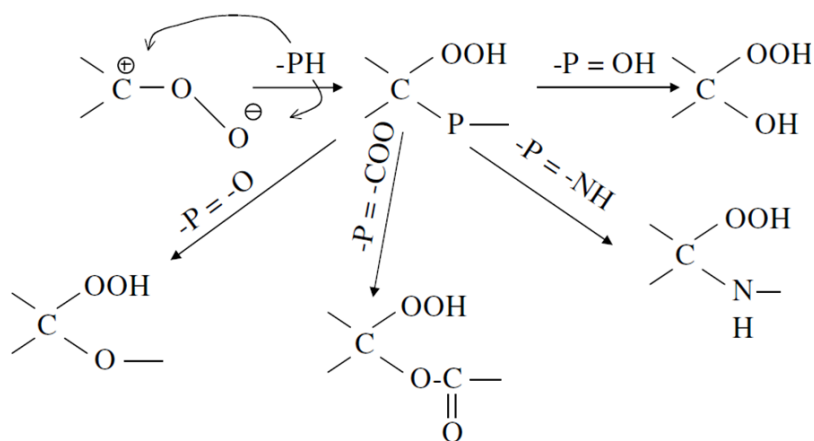Fig 3.8 – Step IIIa decomposition in an inertial solvent

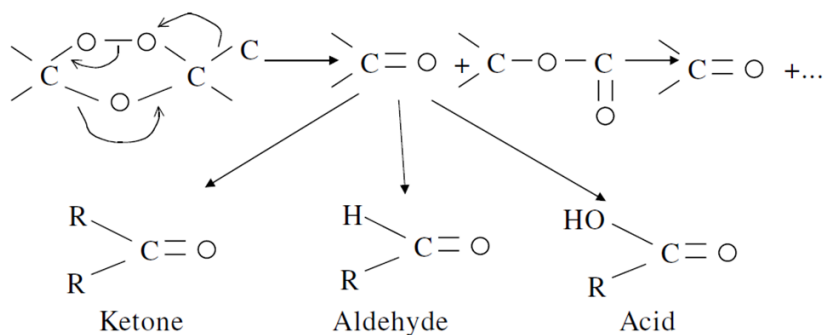Fig 3.9 – Step IIIb decomposition in a participating solvent

Fig 3.10 – Step IIIc Abnormal ozonolysis

3.4.1.2 Electrophilic substitution reactions

In this reaction, one electrophilic agent (ozone) attacks one nucleophilic position of the organic molecule (aromatic compound), resulting in the substitution of one part of the molecule. The electrophilic reaction is restricted only to the molecule that has a strong electronic density, such as special aromatic compounds. Aromatic substituted with electron donor groups (–OH, –NH$_2$) shows high electronic densities on carbon located in orto and para positions, in this way there is high reactivity with ozone in this positions. On the other hand, electron-withdrawing groups (–COOH, –NO$_2$) on aromatic molecule are less reactive. In Table 3.4 aromatic groups which allow/don't allow electrophilic substitution are reported.

Table 3.4 – Aromatic groups associate to their electrophilic reaction

Aromatic groups	Electrophilic reaction
–OH⁻, –O⁻, –NH$_2$, –NHR, –NR$_2$	Ok
–OR, –NHCOR	Ok
–C$_6$H$_6$, –Alkyl	Ok
–NO$_2$, –NR$_3{}^+$	No
–C≡N, –CHO, –COOH	No
–F, –Cl, –Br, –I	No
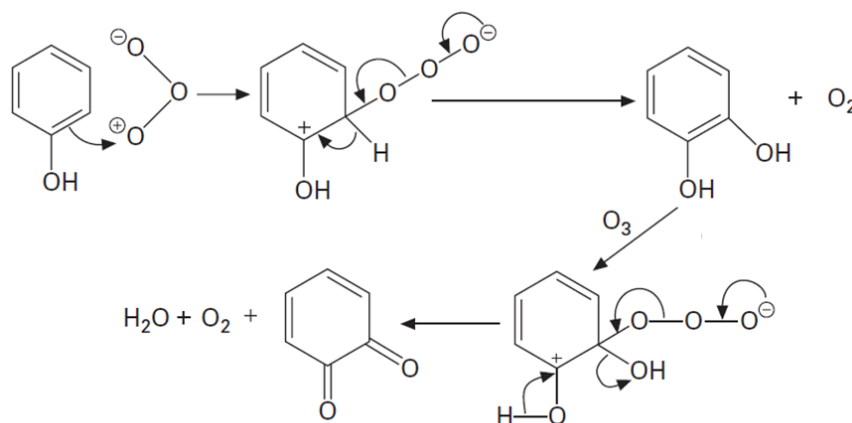
Fig. 3.11 - Electrophilic reaction between phenol and ozone [10]

The reactivity of the donor group in orto and para positions is strong and so the aromatic compounds react quickly with the ozone. In this way the hydroxylated compounds are highly susceptible to further ozonation. The intermediate compounds take the name of quinoids. In conclusion this mechanism leads to the opening of the aromatic ring and the formation of aliphatic products with carbonyl and carboxyl functions.

3.4.1.3 Nucleophilic reactions

Because of the resonance structures of the ozone, there is a negative charge on one of the oxygen atoms. This charge gives a nucleophic character to the ozone molecule.

Therefore, the ozone could react with molecules that have electrophilic positions, such as molecules with double and triple bounds between atoms with different electronegativity (such as double or triple carbon nitrogen bounds).

3.4.2 Indirect reaction

As mentioned in the early part of this chapter, ozone could be indirectly oxidized by organic/inorganic substances in the water medium. Indeed, it could be also decomposed in water, forming free radical species: in the ozone decomposition mechanism, the hydroxyl radical is the main responsible of oxidation of the pollutant present in water. Generally, free radicals are not selective.

The two most representative, generally accepted, mechanisms of ozone decomposition are the mechanism SHB (Staehelin, Hoigné, Buhler) and TFG (Tomiyasu, Fukutomi, Gordon). The second model is used at high pH. Each model describes ozone decomposition mechanism using three reaction steps: initiation, propagation and termination. In the first step, initiators are all the components able to involve the formation of superoxide radical ion ($O_2^-\cdot$) from ozone molecule. This substance is the key for propagating free radical species because it rapidly reacts with ozone and consequently contributes to the formation of ozonide ion radical ($O_3^-\cdot$) and hydroxyl radical ($OH\cdot$). Initiators are hydroxyl ions (OH^-), hydroperoxide ions (HO_2^-), some cations, organic compounds (such as humic substances, glyoxylic acid, formic acid) and UV radiation. Successively, in the propagation step the regeneration of the superoxide radical ion is important. It is produced by the reaction between the species in the medium and the hydroxyl radical. As proposed by TFG mechanism, hydrogen peroxide is considered a reaction promoter. Finally, the radical chain is terminated by the so called hydroxyl-free radical scavengers (such as carbonates) because their presence limits or inhibits the action of the free radicals on the target pollutants and, consequently, superoxide generation.

Table 3.5 – SHB ozone decomposition mechanism in pure water [4]

| Reaction	Rate constant	
Initiation reactions		
$O_3 + HO_2^- \rightarrow HO_2\cdot + O_2^-\cdot$	70	$M^{-1}\,s^{-1}$
Propagation reactions		
$HO_2\cdot \rightarrow O_2^-\cdot + H^+$	$7.9\cdot10^5$	s^{-1}
$O_2^-\cdot + H^+ \rightarrow HO_2\cdot$	$5\cdot10^{10}$	$M^{-1}\,s^{-1}$
$O_3 + O_2^-\cdot \rightarrow O_3^-\cdot + O_2$	$1.6\cdot10^9$	$M^{-1}\,s^{-1}$
$O_3^-\cdot + H^+ \rightarrow HO_3\cdot$	$5.2\cdot10^{10}$	$M^{-1}\,s^{-1}$
$HO_3\cdot \rightarrow O_3^-\cdot + H^+$	$3.3\cdot10^2$	s^{-1}
$HO_3\cdot \rightarrow HO\cdot + O_2$	$1.1\cdot10^5$	s^{-1}
$O_3 + HO\cdot \rightarrow HO_4\cdot$	$2\cdot10^9$	$M^{-1}\,s^{-1}$
$HO_4\cdot \rightarrow HO_2\cdot + O_2$	$2.8\cdot10^4$	s^{-1}
Termination reactions		
$HO_4\cdot + HO_4\cdot \rightarrow H_2O_2\cdot + 2O_3$ [1]	$5\cdot10^9$	$M^{-1}\,s^{-1}$
$HO_4\cdot + HO_3\cdot \rightarrow H_2O_2\cdot + O_2 + O_3$ [1]	$5\cdot10^9$	$M^{-1}\,s^{-1}$

[1] The reaction products are not confirmed

Table 3.6 – TFG ozone decomposition mechanism in pure water at alkaline condition [4]

Reaction		Rate constant	
Initiation reactions			
$O_3 + OH^- \rightarrow HO_2^- + O_2$	(1)	40	$M^{-1} s^{-1}$
$O_3 + HO_2^- \rightarrow HO_2\cdot + O_3^-\cdot$		2.2	$M^{-1} s^{-1}$
Propagation reactions			
$HO_2\cdot \rightarrow O_2^-\cdot + H^+$		$7.9\cdot10^5$	s^{-1}
$O_2^-\cdot + H^+ \rightarrow HO_2\cdot$		$5\cdot10^{10}$	$M^{-1} s^{-1}$
$O_3 + O_2^-\cdot \rightarrow O_3^-\cdot + O_2$		$1.6\cdot10^9$	$M^{-1} s^{-1}$
$O_3^-\cdot + H_2O \rightarrow HO\cdot + O_2 + OH^-$		20-30	$M^{-1} s^{-1}$
$O_3^-\cdot + HO\cdot \rightarrow HO_2 + O_2^-\cdot$		$6\cdot10^9$	$M^{-1} s^{-1}$
$O_3 + HO\cdot \rightarrow HO_2\cdot + O$		$3\cdot10^9$	$M^{-1} s^{-1}$
$HO_2^- + H^+ \rightarrow H_2O_2$		$5\cdot10^{10}$	$M^{-1} s^{-1}$
$H_2O_2 \rightarrow HO_2^- + H^+$		0.25	s^{-1}
Termination reactions			
$O_3 + HO\cdot \rightarrow O_3 + OH^-$		$2.5\cdot10^9$	$M^{-1} s^{-1}$
$HO\cdot + CO_3^= \rightarrow OH^- + CO_3^-\cdot$	(1)	$4.2\cdot10^8$	$M^{-1} s^{-1}$
$CO_3^-\cdot + O_3 \rightarrow O_2 + CO_2 + O_2^-\cdot$	(1)(2)	No data given	
$HO\cdot + H_2O_2 \rightarrow HO_2\cdot + H_2O$		$2.7\cdot10^7$	$M^{-1} s^{-1}$
$HO\cdot + HO_2^- \rightarrow HO_2\cdot + OH^-$		$7.5\cdot10^9$	$M^{-1} s^{-1}$

[1] Carbonates were assumed to be present because of alkaline condition
[2] Not confirmed

In presence of natural organic matter (NOM), other reactions are usually included in the decomposition ozone mechanism: organic matter could act as promoters or inhibitors of ozone decomposition.

$$NOM + HO\cdot \rightarrow \alpha\, O_2^-\cdot + P$$
$$NOM + \alpha\, HO\cdot \rightarrow O_2^-\cdot + P$$
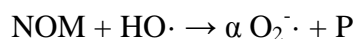
In this way, part of the hydroxyl radical reacts with NOM, producing superoxide and therefore NOM is a promoter. On the other hand, NOM reacting with hydroxyl radical could be considered as inhibitor because it reduces their concentration.

3.5 Ozone contactors

In the previous paragraph it is written that the ozone concentration, generated in a gas flux, is very small: the maximum concentration is about 10% (oxygen gas flow). For this reason the mass transfer efficiency has a great important in ozone transfer from gas to liquid phase. Also, increasing ozone transfer is significant for the economy of the ozonation process. Transfer efficiency greater than 80% is required in an ozonation process.

Common ozone methods used in wastewater treatments are:

- bubble diffuser contactor;
- ejector;
- turbine mixer.

Usually the reactors are closed to vent the end-gases in appropriate suppression systems. The off-gas coming from the ozonation reactors must be destroyed because the ozone is a toxic and irritating gas. Usually, the off-gas has ozone concentration well above the fatal concentration, if the reactor is well designed. Ozone is readily destroyed at high temperature (> 350 °C or via catalytic operation above 100 °C) or it could be absorbed on activated carbon. The final product is an oxygen flux that could be re-used in the same process, for example to aerate the wastewater to treat before biological treatment.

Table 3.7 – Advantages and disadvantages of the main ozone contacting technologies

Contacting system	Advantages	Disadvantages
Bubble diffuser	No moving parts Operational simplicity Low hydraulic headloss Effective ozone transfer	Vertical channelling of bubbles Maintenance of gaskets and piping
Ejector	No moving parts Effective ozone transfer Contactor depth less than bubble diffusion	Additional headloss due to static mixers Complex operation
Turbine mixer	Ozone transfer is enhanced by high turbulence and very small bubbles Aspirating turbines can draw off-gas from other chambers for reuse Eliminate diffuser clogging Contactor depth less than bubble diffusion	Energy input Constant gas flow rate should be maintained, Maintenance requirements for turbine and motor

In Fig 3.12 typical schemes of bubble contactor reactors are presented. Usually a three stages configuration is implemented in bubble contactor (generally, the number of stages can vary from two to six). The gas is introduced in the reactor in the first stage thanks to the diffuser in the bottom of the tank. Here the reactions are fast. In the second room, the ozone is introduced in the same way of the previous one, but here the reactions are slower. Usually, the reactions of disinfection take place in this stage. The last stage is used to increase residence time and to increase ozone decomposition.
There are three possible configurations: counter-current flow configuration (liquid and gas flowing in opposite directions), an alternating concurrent/counter-current arrangement and, finally, concurrent flow configuration where the two flows have the same directions.

Typically, bubble diffuser contactors are constructed with about 3 m water depths to achieve from 85 to 95% ozone transfer efficiency.

Bubble diffuser contactors are made of ceramics or stainless steel and they are either rod-type or disc-type. The configuration provides plug flow hydraulics.
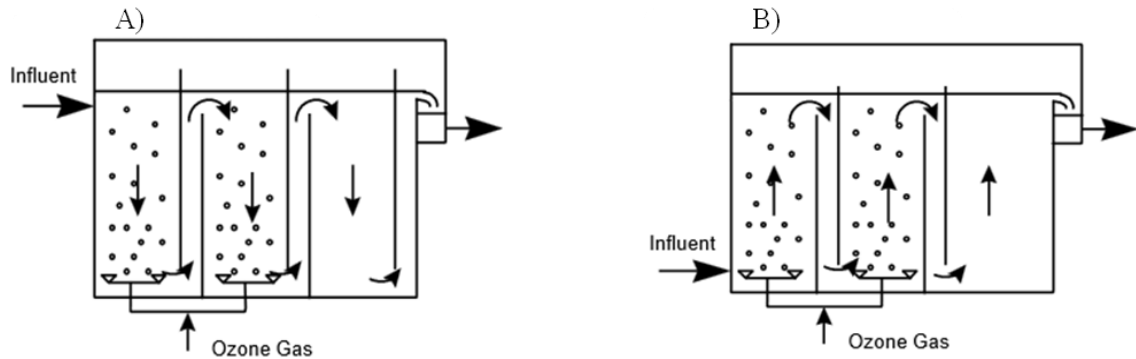
Fig 3.12 – Bubble diffuser contactor typical schemes: A) counter-current and B) co-current

In the case of ejector, ozone is introduced in the liquid flow under negative pressure, which is generated in a Venturi section. Two configurations are possible: in-line configuration, where the ejector is directly placed on the liquid flow, and side-stream configuration, where a part of the total amount of the liquid to treat is pumped to a higher pressure to increase the available vacuum for ozone ejector.
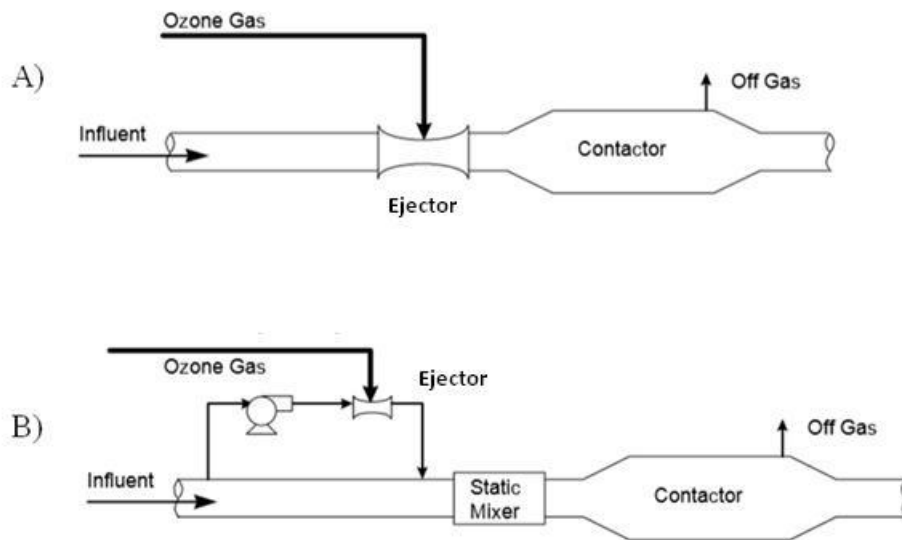
Fig 3.13 – Ejectors configurations: A) In-line and B) Side-stream injector contactors

Finally, turbine mixers are used to create an intimate contact between gas and liquid. The transfer efficiency can be higher than 90% and in order to reach this value, the power required is in the order of 5 kWh per gram of transfer ozone. As in ejector contacting, both in disinfection and in decolouration processes, the contact time in the turbine mixer is not sufficient, therefore an extra contacting volume is needed.
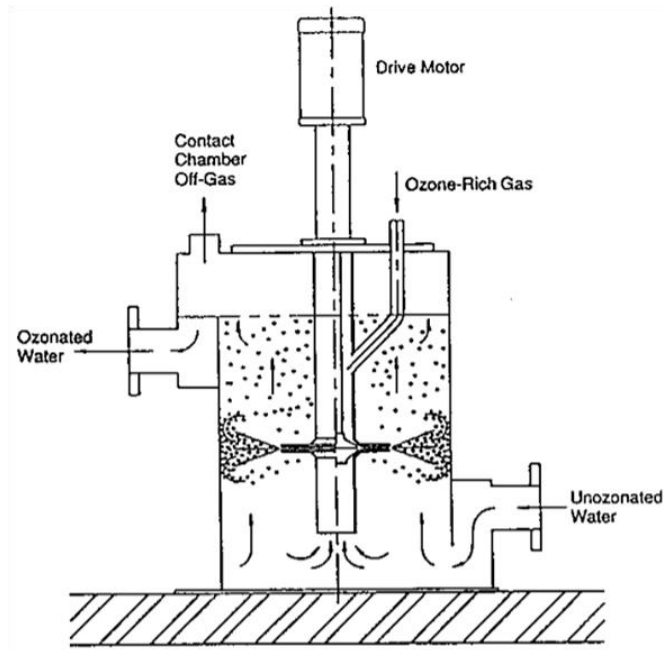
Fig 3.14 – Turbine mixer contactor

References

[1] M.B. Rubin, The history of ozone. The Schönbein period, 1839-1869, *Bulletin For the History of Chemistry,* **26**, 2001, 40-56.

[2] M.B. Rubin, The history of ozone. II. 1869-1899, *Bulletin For the History of Chemistry,* **27**, 2002, 81-106.

[3] S.D. Razumovskii, G.E. Zaikov, Ozone and its reactions with organic compounds, *Elsevier*, 1984.

[4] F.J. Beltran, Ozone reaction kinetics for water and wastewater system, *Lewis Publishers*, Florida 2004.

[5] EPA Guidance Manual Alternative Disinfectants and Oxidants, 1999.

[6] EPA Ozone for industrial water and wastewater treatment, 1980.

[7] Ingegneria delle acque reflue, trattamento e riuso, 4th edition, *Metcalf & Eddy*, 2006.

[8] R. Battino, T.R. Rettich, T. Tominaga, The solubilità of oxygen and ozone in water, *Journal of Physical and Chemical Reference Data*, **12**, 1983, 163-178.

[9] G. Faretra, G. Scaramuzzi, M.D. Ricci, UV e Ozono, Tecnologie per la depurazione senza additivi chimici, *Acqua & Aria*, 2009.

[10] R.M. Chriestie, Environmental Aspects of textile dyeing, *The textile Institute*, chap. 7, *2007*, 151-160.

Chapter 4 – Ozone in textile wastewater decolouration

4.1 Introduction

In the previous chapters, ozone reaction and its properties are described. Ozone has been used in wastewater treatment with the main purpose of disinfection. In the last twenty years though, it was also used to decolourise effluents: its effectiveness to oxidize organic molecule such as dyes, has been proven wastewater colouration being one of the main problem in textile effluent. Ozone is suitable for decolourising textile effluents thanks to its high oxidation potential and due to the fact it produces, in alkaline condition, hydroxyl radicals which have higher oxidation potential than ozone.

Ozone has appeared an optimal alternative in comparison to the other systems (see Chapter 2) as it minimize the production of sludge or toxic reaction products as secondary contaminants in the liquid medium. As gaseous residual, it decomposes to environmental friendly oxygen. The other decolouration systems such as adsorption, Fenton's reaction, electrochemical oxidation are effective in decolouration because they separate in an efficient way the dye molecules from the liquid media, but they shift the pollutants from liquid to solid. Consequently, final incineration or land filling are needed. Biological treatment takes long reaction time to eliminate colour and some dyes are preferably adsorbed than decomposed.

Ozone provides a noticeable contribution in reducing COD (Chemical Oxygen Demand), BOD (Biological Oxygen Demand) and TOC (Total Organic Carbon). Dyestuff usually gives a little contribution to COD values as in textile effluent other additives (surfactants and dyeing auxiliaries in particular) are predominant.

The overall attack of ozone often proceeds through the formation of intermediate low molecular weight products such as acetic acid, aldeydes, ketones, which are not completely mineralized under oxidant conditions [2, 29]. In particular, if COD is measured during reaction, its value may increase, since the intermediate products are more easily to oxidize.

In some conditions, dyestuff oxidation promoted by ozone can release metal atoms into water. This event occurs when ozone reacts with metal-complex dyes. For example, the

ozonation of chromium-complex dye releases this metal as a cation form Cr^{6+}, then toxicity increases to a great deal.

Ozone is not effective for all dye classes: for example, reactive dyes are easier to be degraded than water-insoluble disperse dyes.

Dye molecule degradation efficiency with ozone is affected by many parameters: temperature, pH, dyebath auxiliaries, dye chemical structure, initial concentration of the organic matter and gas diffuser (it affects ozone mass transfer efficiency from the gas to the liquid phase).

4.1.1 Effect of pH

Quite a number of contrasting hypotheses on the pH effect on decolouration promoted by ozone are given in the literature. It is known (see Chapter 3) that ozone reacts in two different forms according to the pH: at pH greater than 10 it forms hydroxyl radicals; if the pH is lower than 4, it reacts directly with molecules and in the range from 4 to 10 both reactions may occur.

Consequently, a well defined boundary on the optimal pH for decolouration has not been defined. OH· radicals are preferred as they are stronger oxidants than molecular ozone. It has also claimed that pH has no effects on decolouration. Kusvuran et al. [5] show that an increase of pH (from 3 to 10) results in a reduction of decolouration degree (from 90% to 50%) of Basic Yellow 28. Therefore, the ozone direct reaction is more effective than the one promoted by OH· radicals. Reactive Orange RO16 was used, in the experiments of Tizaoui et al. [6]. In these experiments, decolouration kinetics appeared very similar in the range from pH 2 to 7, but increased when the pH has set at 11. The author interpreted the data arguing that, at a high pH, hydroxyl radicals concentration is greater than at the other pH investigated and the molecules had a greater number of sites for electrophilic attack by ozone. Souza et al. [2] used in their experiments a different initial pH (5, 7, 9 and 11) with Remazol Black B dye, while they noted that the final pH was around 4 in non buffered solution. They inferred that the degradation of azo-dyes generates acid products. In addition, they claim that pH did not have effect on dye removal in the aforementioned range. Alvarez et al. [3] and Soares et al. [4] observed that the decolouration is favoured by direct ozone attack to dyes, therefore at a low pH. Also, the ozone molecule reacts selectively with chromophore groups. Contrarily, an acidic condition leads to the formation of hydroxyl radicals, which are less selective than the ozone molecule. According to this route, decolouration rate decreases and mineralization increases.

The possibility that pH affects positively the decolouration degree depends on the type of dyes to be ozonated. Some dyes require alkaline pH to outset radical reactions, but the same dyes in acid condition, direct ozone reactions undergoes a scarce decolouration.

The regulation of pH in an aqueous system is therefore important in relation to decolouration efficiency.

Different results could be obtained using salts in buffered solutions. For example, sodium hydroxide increases efficiency because it is considered as radical initiator, forming OH· and O_2^-·, and propagator in chain reactions. Contrarily, sodium carbonate

decreases efficiency: the CO_3^{2-} ion acts as an inhibitor for the free-radical reactions. It reacts with OH· without generating other radicals useful in the decolouration [1].

As a conclusion, it is possible to affirm that different results can be due to different methodologies used by researchers: some use buffered solution to control pH and other adjusted the initial pH with an acid or basic substances.

4.1.2 Effect of temperature and ozone gas mixture solubility

The temperature has a double effect on decolouration by ozone. Increasing temperature, ozone mass transfer from gas to liquid phase decreases, as well as solubility. Sotelo et al. [31] found that the dissolved ozone concentration at 10 °C was 11.52 mg/L, but at 35 °C it reduced to 4.8 mg/L. On the other hand, by increasing the temperature, the decolouration kinetic increases [1]. Therefore, this may indicate that an increase in temperature balances the decrease of the ozone solubility during the global reaction.

In Chapter 3 a table, where solubility values of pure ozone at different temperature are reported, is present. In water treatment we need to consider the solubility of ozone according to the gas used in its production. In the case of ozone from pure oxygen, the solubility is much lower than the value reported in Chapter 3.

Table 4.1 – Solubility of ozone in water at different ozone/oxygen mixture concentration and temperature [19]

Temperature [°C]	Ozone concentration in gas phase (% v/v)			
	1 %	1.5 %	2%	3 %
	Ozone concentration in water [mg/L]			
5	7.39	11.09	14.79	22.18
25	3.53	5.29	7.05	10.58
30	2.70	4.04	5.39	8.09

4.1.3 Effect of textile wastewater characteristics

Generally, wastewater coming from a dye house is contaminated by residual dyestuff and additional auxiliaries required in dyeing. All this components react with ozone and consequently increase its consumption.

It is demonstrated that surfactants at low concentrations enhance dye degradation, reducing surface tension of the solution [20]. This phenomena is due to increasing ozone solubilisation in the liquid medium.

Foaming agents increase decolouration time and ozone consumption [21]. Moreover, auxiliary agents react more easily with ozone compared to dyes.

In textile industry, salts are extensively used as exhausting and retarding agents. Particularly, sulphate sodium and chloride sodium are the most used. Salt type and quantity have different effects on decolouration time.

Sodium sulphate does not have effects on decolouration in acid conditions, on the contrary, at alkaline pH it depletes the action of hydroxyl radicals [22, 11]. Sodium chloride brings some improvement to decolouration. The mechanism existing between

ozone and NaCl is not clear: probably the reaction of hypochlorous ions (OCl⁻) has effect on dyes decolouration [1].

4.1.4 Effect of ozone dosage

Dye degradation depends on the solubilisation of ozone in the liquid phase. According to Sevimli et al. [9], when the ozone concentration is increased in the gas phase, the driving force will increase. Consequently, the ozone concentration in liquid phase becomes higher and so gives better decolouration degree.

These results indicate that dye degradation depends on ozone solubilisation, which determines the concentration of radicals and ozone concentration. Being ozonation a gas to liquid reaction, the limiting step that affects the process is the mass transfer between phases.

Obviously, the optimum ozone concentration should defined as a compromise between energy consumption to generate ozone and the amount of ozone in the gas exhaust.

When the ozone dose is higher than the appropriate value, mineralization phenomena can occur [10].

4.1.5 Effect of initial dye concentration

More than one study [12-14] reports the effect of the initial dye concentration on the decolouration kinetics. Increasing the initial dye concentration leads to a decrease on decolouration rate.

Two possible interpretations can be given:
- hydroxyl radicals generated in the solution approach saturation, at steady state, gradually with the increase of initial dye concentration;
- the competition between the free radicals generated by the oxidation reaction and the original pollutants (carbonaceous substances) with the hydroxyl radicals became intense because of the non selective reactivity of hydroxyl radicals themselves.

The direct consequence is an increase in decolouration time.

4.2 Ozonation products and toxicology

According to a dye structure, a large variety of intermediates and products can be formed upon ozonation. In the degradation of aromatic structure of any molecule, aromatic rings are opened by oxidation with ozone and intermediates containing –C=C– bonds are formed. During ozonation, the breakage of a long complicated dye molecule is achieved by the oxidation of other groups, such as azo or sulfonate group, beside aromatic groups.

The main products that can be detected after ozonation are carboxylic acids.

The ozonation of Acid Black 1 [15] brings to the formation of formic, oxalic and acetic acid. Formic acid is the most abundant one, followed by oxalic and acetic acid. Since in the structure of dye also nitrogen and sulphur atoms, sulphur and sulphuric groups exist, they are converted to several intermediates and end-products. Part of nitrogen atoms may be converted to amino or even to nitro-compounds, more resistant to ozone attack.

Song et al. [12] proposed a probable degradation pathway for Direct Red 23. They detected products at different reaction time. They suggested that the final product of ozonization after 80 min (they did not reach complete oxidation) are urea and carboxylic acids (acetic, oxalic and formic). They also detected inorganic salts such as Na_2SO_4.

He et al. [14] analyzed the end-products by ozonolisis of Reactive Yellow 84 to give buten diacid, urea and acetic, oxalis and maleic acid.

Other authors [23, 24] argued that the aldehydes were primarily seen as products of many dyes. In detail, formaldehyde and acetaldehyde constituted about 80% of the main compounds.

As a conclusion, the studies described above provide different results only in appearance: carboxylic acids derive from aldehyde oxidation at high ozone dosage [25].

As mentioned in the introductive chapter of this thesis nowadays and increasingly in the future recycling and reusing wastewater in textile processes is needed as an environmental concern. Moreover, industry takes also into account the recycling economic view point.

Therefore, for economic reasons it was not intended to mineralise the organic and dye substances completely, but only cleaving the chromophores bond. When mineralization is reached, the final products are CO_2 and H_2O. At intermediate oxidation conditions many compounds are generated with possible risks for the environmental. Then, toxicity evaluations are needed.

In literature there are some studies about toxicology on textile wastewater after ozonation [16-19]. The main results are reported below:

- phyto-toxicity test were done on bean plants with ozonated water containing Congo Red dye. The results demonstrated no significant change in the shape and in the morphology of the grown plants compared to that irrigated with distilled water;
- ozonated solution showed no toxic effect on the bacterial species tested;
- toxic products were generated by ozonation process when dyestuff containing metals were used. Possible toxic effects can be avoided if the metal realised can be precipitated or flocculated;
- ozone is effective for removing acute toxicity from textile wastewater;
- the first products have the highest toxic potential, while long ozonation time decrease toxicity.

4.3 Mass transfer effect in ozonation chemical reaction

The main target of the initial studies about ozone was determining the kinetics of ozone decomposition in water and the chemical reaction between the organic pollutant and ozone. But also mass transfer from the gas phase to liquid one is extremely important.

Generally, in a gas-liquid process, gas diffuses towards the liquid phase through bubble interface as a first step. Therefore, the design and modelling of ozone reactors are mainly based on the accurate contribution of mass transfer for the process and the determination of gas-liquid mass transfer coefficient ($k_L a$). The transfer rate of ozone from gas to liquid phase is described according to the film theory [28]. The film theory

assumes a plane interfacial surface when the bubble radius is much higher than the film thickness, δ, a situation that occurs in most of the gas–liquid systems. The film is between the gas and liquid surfaces. The bulk liquid is kept uniform in composition by agitation. The concentration at the gas-liquid interface changes linearly in the film according to the following equation:

$$j = k_L a (C_{O_3}^* - C_{O_3,L})$$

where j is the transfer rate, $k_L a$ is the gas-liquid volumetric mass transfer coefficient, $C_{O_3}^*$ is the equilibrium concentration of O_3 at the gas-liquid interface and $C_{O_3,L}$ is the concentration of ozone in the bulk liquid.

The concentration of ozone at the gas-liquid interface is related to the ozone concentration in the gas phase according to the Henry's Law as follows:

$$C_{O_3}^* = \frac{C_{O_3,G}}{He}$$

where He is the Henry's Law constant and $C_{O_3,G}$ is the O_3 concentration in the phase gas.

In literature there are correlations [26, 27] used to determinate the Henry's Law constant in function of pH [M] and temperature [K]. The most used correlation is reported below:

$$He = 3.842 \; 10^7 \; [OH^-]^{0.035} exp\left(-\frac{2428}{T}\right)$$

Commonly, ozone mass transfer coefficient, in a given reactor, is generally found from the determination of oxygen mass transfer coefficient, $(k_L a)_{O_2}$, at the unsteady-state condition:

$$j_{O_2,L} = (k_L a)_{O_2} (C_{O_2}^* - C_{O_2,L})$$

where $C_{O_2}^*$ and $C_{O_2,L}$ are the oxygen concentrations in the gas-liquid interface and in the bulk liquid, respectively.

According to Dankwerts theory [30] ozone mass transfer coefficient, $(k_L a)_{O_3}$ is given by the following expression:

$$(k_L a)_{O_3} = (k_L a)_{O_2} \sqrt{\frac{D_{O_3}}{D_{O_2}}}$$

where D_{O_3} and D_{O_2} are the ozone and oxygen diffusivity.

When a chemical reaction takes place in a gas-liquid system, the gas is adsorbed in the liquid phase and the reaction can occur in the liquid film, in the bulk of the liquid or in both zones at the same time according to the relative rates of the chemical reaction and mass transfer. For slow and very slow reactions, the reaction develops in the bulk being the rate limiting step. Compounds undergo a reaction in the liquid film when fast or instantaneous reactions are considered; in that case, mass transfer phenomenon is the rate limiting step. In intermediate rate reactions, the reaction may develop both in the liquid film and in the bulk liquid [28].
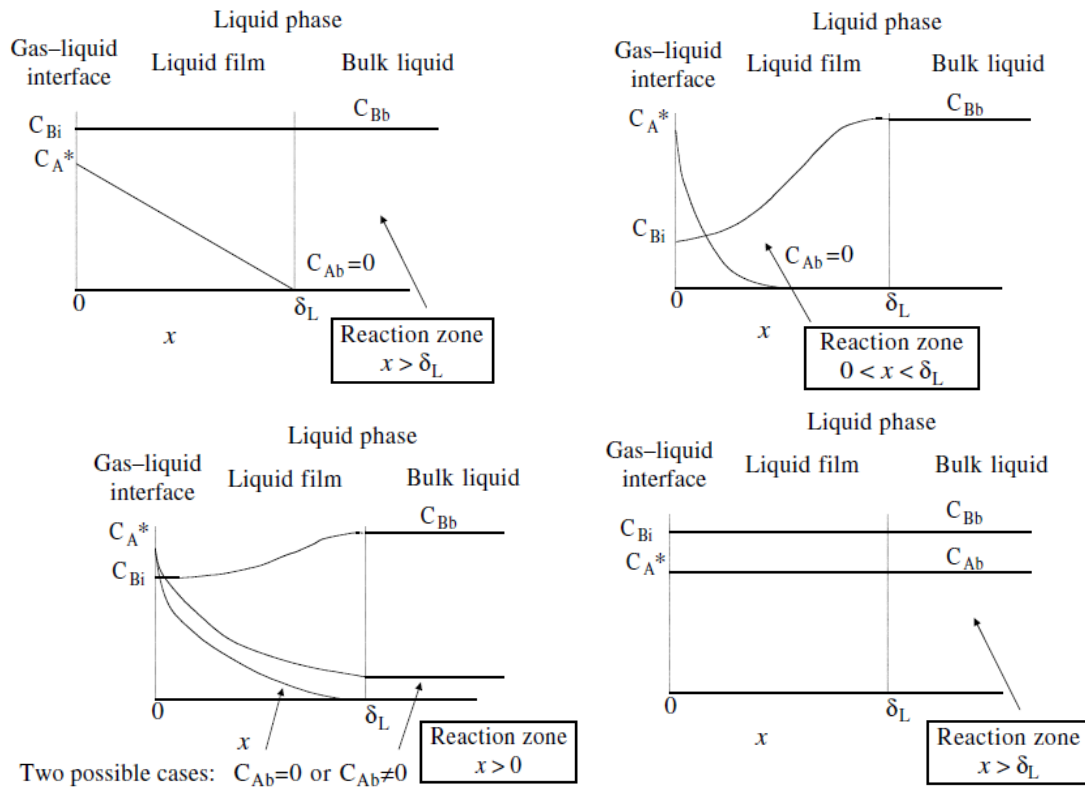

Fig 4.1 – Kinetic regimes in a gas-liquid reaction

As being a very strong oxidant, ozone reacts very fast with most of the organic pollutants, especially with dyes in the liquid phase. Also, since ozone is known as a sparingly soluble gas in water, mass transfer of ozone into the liquid phase is the rate-limiting step in most of its reactions.

In order to enhance mass transfer in liquid, either hydrodynamic or ultrasonic cavitation are used. Some studies showed a decrease in time reaction thanks to cavitation.

Fast reactions of ozone in a liquid lead to a significant enhancement of mass transfer. The driving force for mass transfer increases, due to the fast chemical reaction of O_3 with the organic matter. The criterion showing the enhancement of mass transfer coefficient is shown by Hatta number (Ha) and Enhancement Factor (E) [28].

Hatta number is a dimensionless parameter that compares the maximum possible reaction rate in the gas-liquid film to the maximum rate of physical absorption. Assuming that the gas-phase resistance is negligible, Hatta number is:

$$Ha = \frac{\sqrt{k\, C_D D_{O_3}}}{k_L}$$

where k [M^{-1}s^{-1}] is the reaction rate constant between dye and ozone, C_D [M] is the dye concentration, D_{O_3} [m^2/s] is the ozone diffusivity and k_L [m/s] is the mass transfer coefficient.

Enhance factor is defined as [28]:

$$E = \frac{amount\ of\ adsorbed\ reactant\ in\ a\ given\ time\ in\ a\ reacting\ liqud}{amount\ of\ absorbed\ reactant\ if\ there\ were\ no\ reaction}$$

$$E = \frac{Ha\sqrt{\dfrac{E_i - E}{E_i - 1}}}{\tanh\left[Ha\sqrt{\dfrac{E_i - E}{E_i - 1}}\right]}$$

where E$_i$ is the enhancement factor for an infinitely fast reaction and it is defined as

$$E_i = 1 + \frac{D_D C_D}{r_s D_{O_3} C_{O_3}^*}$$

where r_s is the mole ratio between dye and ozone, D_D and C_D are respectively dye diffusivity and concentration.

As it has been noted in the above equation, enhancement factor of mass transfer is affected by Ha and E_i

The magnitude of Hatta number provides a general idea about the reaction zone in the system. In the following table are reported the correspondence between Ha and kinetics regime.

Table 4.1 – kinetic regime corresponding to Hatta number [28]

Kinetic regime	Condition	Reaction zone	E
Very slow	Ha < 0.02	Liquid bulk	1
Slow	0.02 < Ha < 0.3	Liquid bulk	1
Moderate	0.3 < Ha < 3	Both bulk and film	E > 1
Very fast	3 < Ha	Film	E > 1
Pseudo first order	3 < Ha and Ha < E$_i^2$	C$_D$ is constant	E = Ha
Instantaneous	3 < Ha and Ha > 10E$_i$	Mass transfer control	E = E$_i$

References

[1] R.M. Chriestie Environmental Aspects of textile dyeing, chap. 7, 162-166, *The textile Institute*, 2007.

[2] S.M d.A.G.U. de Souza, K.A.S. Bonilla, A.A.U de Souza, Removal of COD and colour from hydrolyzed textile azo dye by combined ozonation and biological treatment, *Journal of Hazardous Material*, **179**, 2010 35-42.

[3] A.B.C. Alvares, C. Diaper, S.A. Parsons, Partial oxidation of hydrolyzed and unhydrolysed textile dyes by ozone and the effect on biodegradability, *Process Safety and Environmental Protection*, **79 Part B**, 2001, 103-108.

[4] O. Soares, J. Orfão, D. Portela, A. Vieira, M. Pereira, Ozonation of textile effluents and dye solutions under continuous operation: influence of operating parameters, *Journal of Hazardous Material*, *B,* **137**, 2006, 1664-1673.

[5] E. Kusvuran, O. Gulnaz, A. Samil, M. Erbil, Detection of double bond-ozone stoichiometry by an iodometric method during ozonation processes, *Journal of Hazardous Material,* **175**, 2010, 410-416.

[9] M.F. Sevimli, H.Z. Sarikaya, Ozone treatment of textile effluents and dyes: effect of applied ozone dose, pH and dye concentration, *Journal of Chemical Technology and Biotechnology,* **77**, 2002, 842-850.

[10] G. Xu, S. Chen, J. Shi, S. Wang, G. Zhu, Combination treatment of ultrasound and ozone for improving solubilisation and anaerobic biodegradability of waste activated sludge, *Journal of Hazardous Material*, **180**, 2010, 340-346.

[11] P. Colindres, H. Yee-Mandeira, E. Reguera, Removal of reactive black 5 from aqueous solution by ozone for water reuse in textile dyeing processes, *Desalination*, **258**, 2010, 154-158.

[12] S. Song, H. Ying, Z. He, J. Chen, Mechanism of decolouration and degradation of CI Direct Red 23 by ozonation combined with sonolysis, *Chemosphere*, **66**, 2007, 1782-1788.

[13] Z. He, L. Lin, S. Song, M. Xia, L. Xu, H. Ying, J. Chen, ,Mineralization of C.I. Reactive Blue 19 by ozonation combined with sonolysis: performance optimization and degradation mechanism, *Separation and Purification Technology*, **62**, 2008, 376-381.

[14] Z. He, S. Song, M, Xia, J. Qiu, H. Ying, B. Lu, Y. Jiang, J. Chen, Mineralization of CI Reactive Yellow 84 in aqueous solution by sonolytic ozonation, *Chemosphere*, **69**, 2007, 191-199.

[15] J.A. Paprocki, H.S. dos Santos, M.E. Hammerschitt, M. Pires, C.M.N. Azevedo, Ozonation of azo dye acid black 1 under the suppression effect by chloride ion, Journal of the Brazilian Chemical Society, **21**, 2010, 193-201.

[16] G. Eremektar, H. Selcuk, S. Meric, Investigation of the relation between COD fractions and the toxicity in a textile finishing industry wastewater: Effect of preozonation, *Desalination*, **211**, 2007, 314–320.

[17] M. Khadhraoui, H. Trabelsi, M. Ksibi, S. Bouguerra, B. Elleuch, Discolouration and detoxicification of a Congo red dye solution by means of ozone treatment for a possible water reuse, *Journal of Hazardous Material*, **161**, 2009, 974-981.

[18] E. Boschke, U. Böhmer, J. Lange, M Constapel, M. Schellenträger, T. Bley, The use of respirometric measurements to determine the toxicity of textile dyes in aqueous solution and after oxidative decolourisation processes, *Chemosphere*, **67**, 2007, 2163–2168.

[19] R.G. Rice, Chemistries of ozone for municipal pool and spa water treatment, *The journal of the swimming pool and spa industries*, **1**, 1995, 25-44.

[20] W. Chu, K.H. Chan, N.J.D. Graham, Enhancement of ozone oxidation and its associated processes in the presence of surfactant: degradation of Atrazine, *Chemosphere*, **64**, 2006, 931-936.

[21] C.G. Namboodri, W.S. Perkins, W.K. Walsh, Decolourizating dyes with chlorine and ozone: Part I, *American Dyestuff Reporter*, **34**, 1994, 18-22.

[22] M. Muthukumar, N. Selvakumar, Studies on the Effect of Inorganic Salts on Decolourization of Acid Dye Effluents by Ozonation, *Dyes and Pigments*, **62**, 2004, 221-228.

[23] A. Lopez, G. Ricco, G. Tiravanti, Biodegradability Enhancement of Refractory Pollutants by Ozonation: A Laboratory Investigation on an Azo-dyes Intermediate, Water Science Technology, **38**, 1998, 239-245.

[24] A. Dabrowska, B. Kaspryzk-Hordern, Aldehydes formation during water disinfection by ozonation and chlorination process, Journal Global NEST, **7**, 2005, 61-71.

[25] G. Mascolo, A. Lopez, H. James, M. Fielding, By-products formation during degradation of isoproturan in aqueous solution, *Ozonation Water Resource*, **35**, 2001, 1695-1704.

[26] R. Battino, T.R. Rettich, T. Tominaga, The solubility of oxygen and ozone in liquids, *Journal Of Physical and Chemical Reference Data,* **12**, 1983, 163-178.

[27] C. Tizaoui, N. Grima, Kinetic of the ozone oxidation of Reactive Orange 16 azo-dye in aqueous solution, *Chemical Engineering Journal*, **173**, 2011, 463-473.

[28] F.J. Beltran, Ozone reaction kinetics for water and wastewater system, *Lewis Publishers*, Florida 2004.

[29] G. Actis Grande, G. Rovero, S. Sicardi, Comparative ozone decolouration in bubble column and in ejector mixer units, XXIII IFATCC International Congress, Budapest, 8-10 May 2013.

[30] F.J. Beltran, L.A. Fernández, P. Álvarez, E. Rodriguez, Comparison of ozonation kinetic data from film and Danckwerts theories, *Ozone science and engineering*, **20**, 1998, 403-420.

[31] J.L. Sotelo, J. Beltran, J. Beltran-Heredia, Henry's Law Constant for the ozone water system, *Water Research*, **23**, 1989, 1239–1246.

Chapter 5 – Pilot plants description

5.1 Bubble column pilot plant design

In the previous Chapter, some ozone contactors have been presented, and among these the most widespread is bubble contactor. There are lots of configurations depending on liquid and gas flowing: counter current, co-current and alternating co-current/counter current.

Usually, the reactor is composed of two sections: the first one where the ozone is introduced (liquid residence time of about 30 min) and the second one, called deaeration section, where the solubilised ozone is removed.

Ozone diffusers are placed in the bottom of the reactor, as it is shown in Fig 5.1.

Fig 5.1 – Typical ozone diffuser arrangement in an industrial bottom reactor

The reactors are closed in order to carry out the exhausted gas to a suppression system.

In this work, a bubble column was built in order to simulate only a portion of real ozone contactor reactor. In particular, the studied region is above a gas diffuser. Bubble column was used like a benchmark for decolouration tests: the results were compared with the tests performed using a multi-task reactor (see the following paragraph), at the same conditions.

Taking into account the previous considerations, a counter-current bubble column reaction was designed. The liquid is introduced from the top and the gas from the bottom of the column.

The bubble column reactor used in this work is a cylindrical PVC column with an internal diameter of 0.10 m and a total height of 3.50 m. At the ends, PVC tube is connected with cylindrical glass tubes: they are used to detect column behaviour both in terms of colour and bubbles coalescence.

The liquid height was chosen equal to 3.2 m because it is the average liquid height in an industrial ozone reactor. In this way, the liquid total volume was 25 L and, in order to have a residence time similar to industrial plant one, liquid flow rate was imposes equal to 50 L/h.

The liquid storage tank has a capacity of 120 L and it is pumped into the column by Milton Roy gear pump (maximum flow rate 160 L/h, maximum pressure 3.5 bar). At the exit of the pump, a flow meter is placed to control the liquid flow. In order to eliminate pulse flow generated by gear pump, an expansion tank is installed before flow meter. Liquid is introduced through a tube (internal diameter 27 mm) at the top of the reactor. At the bottom, the liquid came out from a siphon system used to keep the liquid level in the column constant.

The gas diffuser device installed was a porous sinterized glass disc with a diameter of 6 mm and pore size of 45-60 μm. Ozone is produced from pure oxygen using an ozone generator (MCP1V-O model) by Ozono Elettronica Internazionale. The ozone is produced by the so-called corona effect, in which the high energy potential generated between the electrodes break the oxygen molecule to form ozone. To maintain the global efficiency of the generator, the heat produced by reaction was removed by a water cooling system.

Gas flow rate was defined using the following procedure. First of all, the dimension of the bubbles is of fundamental importance even in terms of surface area to enhance ozone mass transfer than in energy consumption to form bubbles of a define diameter. Onofrio et al. [1] demonstrated that a correlation between the ozone quantity transfer in the time unit (N) and the mean diameter of bubble (d_b) exists:

$$N \propto d_b^{-2.5}$$

Consequently, if N is the ozone quantity in the exhausted gas, theoretically a mean bubbles diameter that reach the result will exist. From the above relation, decreasing mean bubbles diameter, surface area between ozone and water increases, and therefore mass transfer is improved. Moreover, gas residence time increases because bubble rising velocity is lower, being gas bubbles smaller.

Although the quantity of ozone is improved by smaller bubble diameter, also economics must be evaluated. Energy per gas volume unit needed for bubbles formation is given by the following relation [2]:

$$E = 6 \frac{\sigma}{d_b}$$

where σ is liquid surface tension.

Considering water as liquid media, the following values can be calculated:

Table 5.1 – Energy consumption to produce bubbles at different diameter

d_b [mm]	E [kWh/m³$_{ozonated\ air}$]
2.5	0.8
1	2
0.1	20

Therefore, bubbles diameter and energy consumption compromise is needed. For this reason, the maximum bubble surface area was verified by a mean bubbles diameter of 3-4 mm [2]. These bubbles dimension can be obtained using porous sinterized glass diffuser.

In order to have a homogeneous flow condition in the bubble column, bubbles rise velocity required may be in the range from 0.03 to 0.22 m/s [3]. If the velocity is greater, coalescence will be the most probable consequence.

Using Mendelson correlation [3], the final bubble rising velocity may be calculated:

$$u_b^* = \sqrt{\frac{2\sigma}{d_b\rho_L} + 0.5d_bg}$$

where ρ_L is liquid density. Considering water as liquid and a bubble diameter of 4 mm, final bubble rise velocity is in the order of 0.24 m/s.
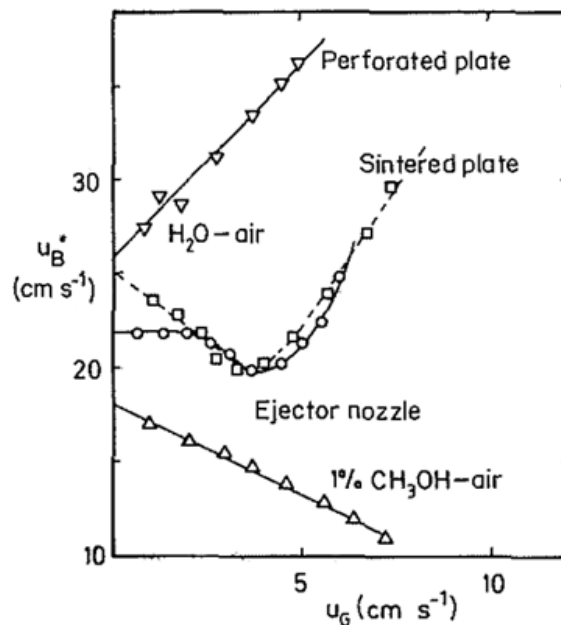

Fig 5.2 – Mean bubble rise velocity in swarm as a function of gas velocity [3]

Using the graph of Fig 5.2, bubbles mean velocity (bubbles formation by sintered plate) is defined and it is estimated in about 100 L/h.

Mixture oxygen/ozone is supplied in the column with a pressure of 1 barg.

Fig 5.3 – Bubble column reactor

Fig 5.4 – Bubbles formation by
sinterized glass diffuser (Q_g = 100 L/h)

Fig 5.5 – Sinterized glass distributor

Along the column height, there are four ports for sampling gas and liquid phases. Each port is connected with a T-tube phase separator (Fig. 5.6a). Adjusting valves V2 and V3, regular liquid and gas flow rates could be obtained. Inside the column, mixture passes through an inverted funnel of 20 mm diameter.

The sample ports are at the same distance (760 mm) and the lower one is positioned at 520 mm from gas distributor.
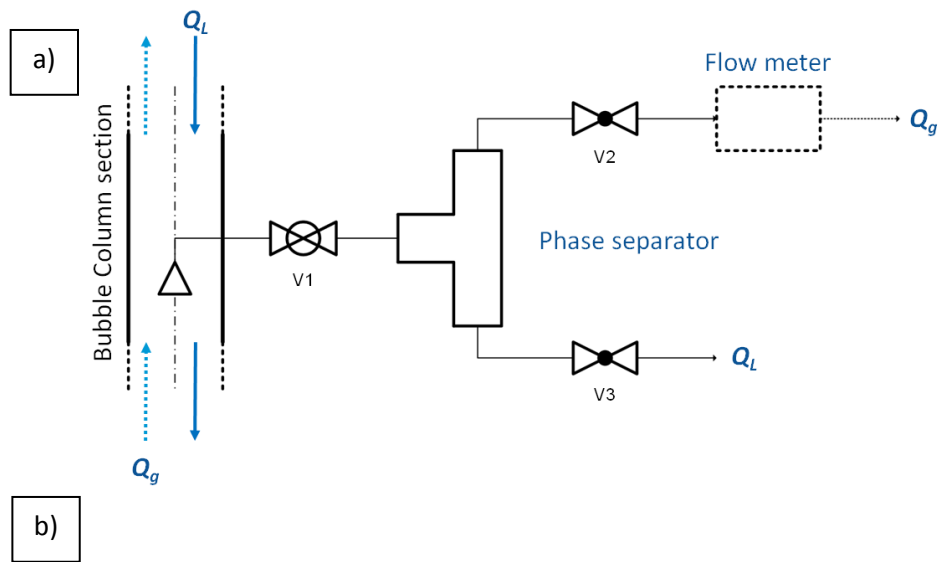

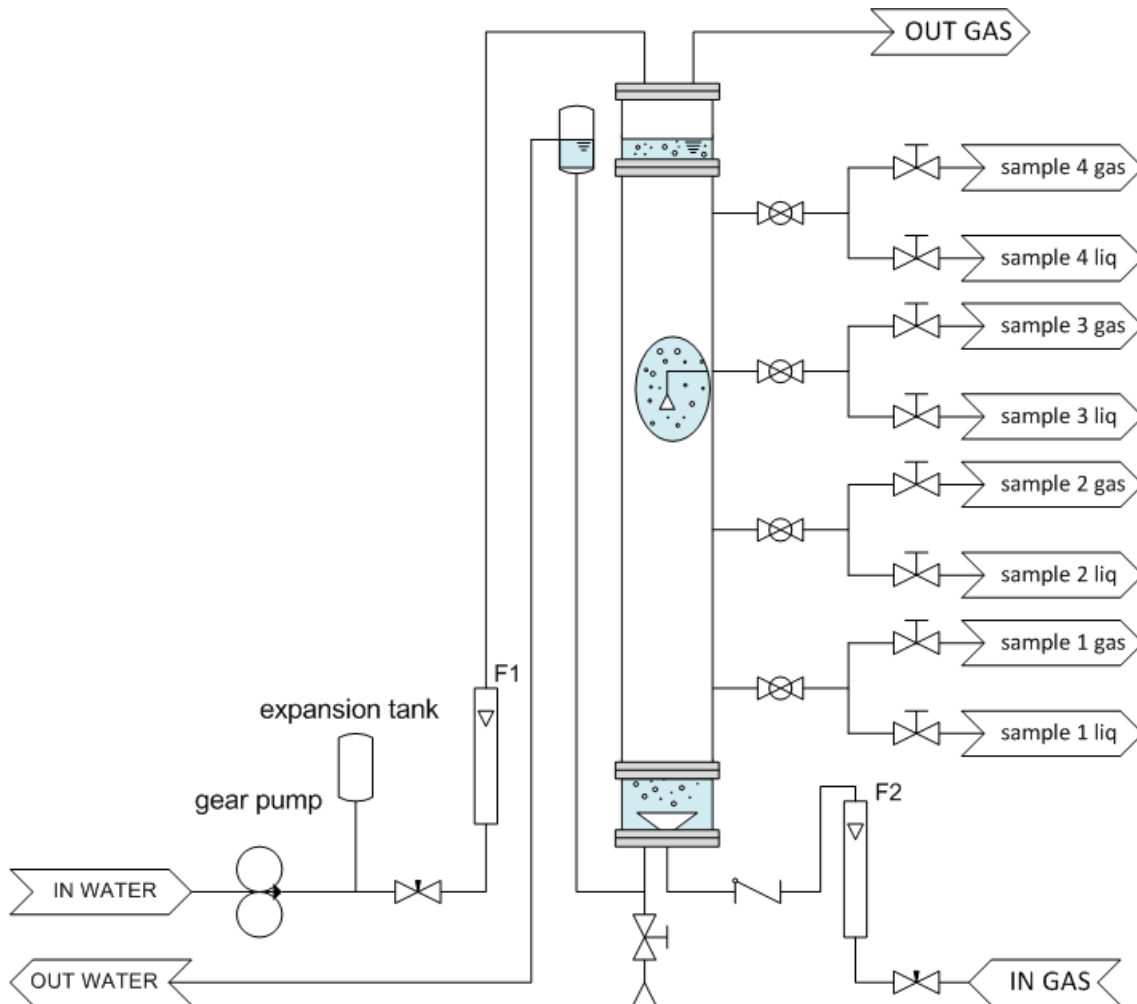Fig 5.6 – a) Phase separator scheme and b) sample port along the column.

Fig 5.7 – Bubble column schematic representation

5. 2 Multi-task cavitational reactor pilot plant

Multi-task cavitational reactor pilot plant was build with the main purpose to incorporate in the same plant different devices, in order to improve decolouration kinetic. The plant is able to operate using different configurations: it worked only with ozone or using ultrasonic and hydrodynamic device, or a combination of the previous decolouration techniques. Ozone was introduced using two different inlet ports: the first directly in the pipe and the second using an ejector to increase gas-liquid phase mixing. Fig. 5.8 shows a schematic representation of the pilot plant.

First of all, the plant was designed to have a total capacity of 25 L. The liquid volume is the same as the bubble column one, therefore the experimental data obtained in the pilot plant can be immediately compared with the data of the benchmark at the same conditions.

To reach the desired volume, a cylindrical tank (T1) is used (diameter 200 mm, height 770 mm). T1 is made of glass, because the transparency help bubbles dispersion and decolouration progress visual examination. Moreover, it is used to separate gas from liquid phase in order to prevent gas flow into the pump. The inlet liquid tube is positioned at the bottom of the tank and the outlet takes the liquid to a height of 600

mm. If ozone is used to oxidize pollutants, the reactor inlet will be a gas/liquid mixture. Around the outlet, a metallic fine grid is positioned to prevent little gas bubbles from being sucked in the pump.
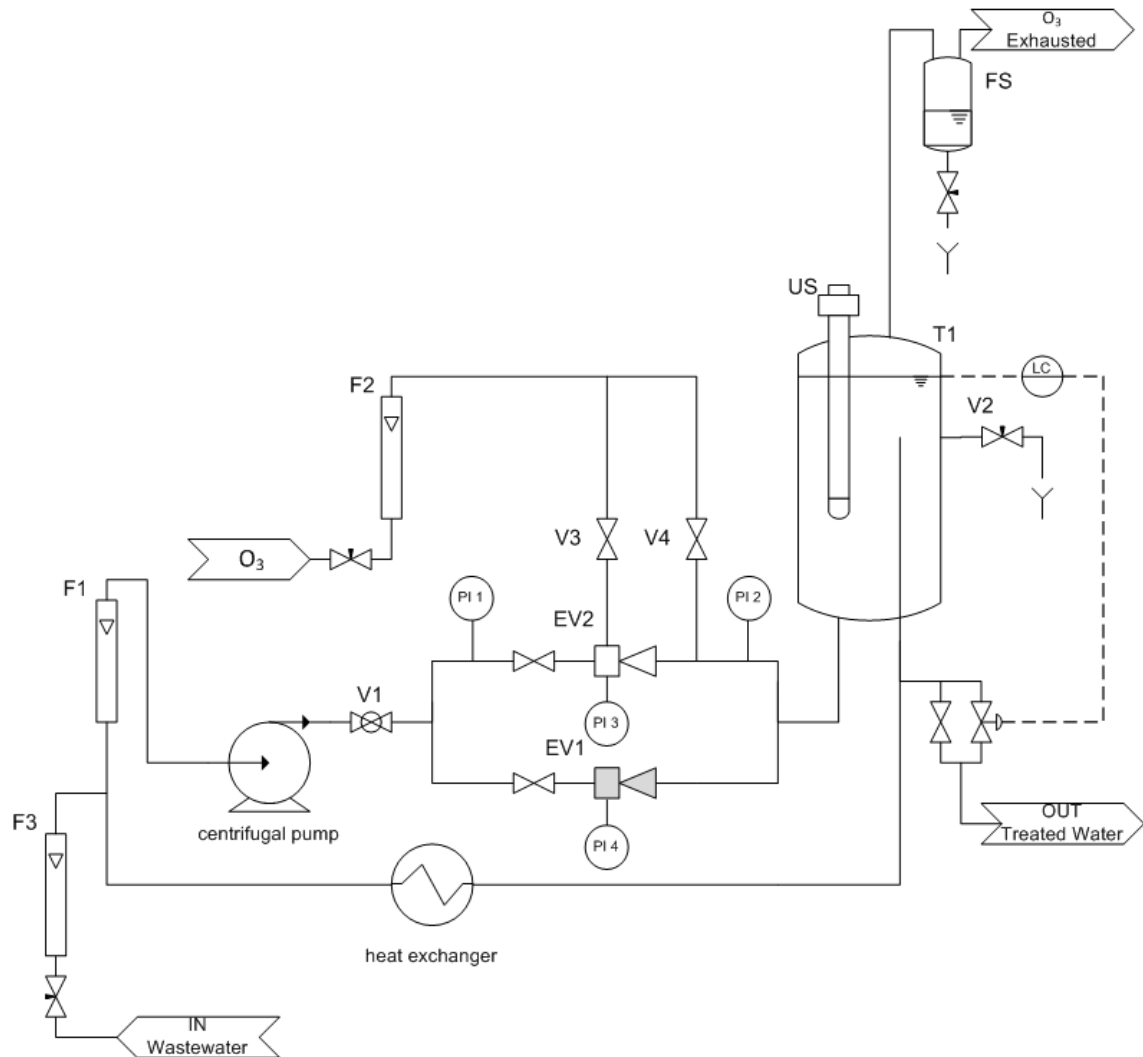

Fig 5.8 – Multi task pilot plan scheme

The exhausted gas came out the reactor from a port on the flange. The outlet is connected to a phase separator tank (FS): it is used in the case in which gas drags liquid or possibly foam along the tube.

From the flange at the top of the tank, an ultrasound transducer (US) is placed. The device is cylindrical and radiates waves homogeneously around it.

Along the tank vertical wall, there is a sample port used to inspect water samples.

Considering that ozonation reaction and also ultrasound waves propagation (then molecular fluid vibration) are exothermic processes, a heat exchanger is needed. A coaxial tube heat exchanger is positioned between the tank and the pump inlet.

The liquid is circulated in the plant using a vertical multistage centrifugal pump by Lowara (model 3SV, 8 stages).

Finally, two ejectors are positioned in the plant (EV1 and EV2). The ejectors have different geometry and uses. Ejector EV2 (Fig 5.9) is used to enhance gas/liquid mixing thanks to the mixing chamber between the throat section and the divergent part. Instead,

ejector EV1 (Fig 5.13) is a Herschel-type Venturi and it is designed to generate a high vacuum degree and hydrodynamic cavitation. Both ejectors are made of PVC.
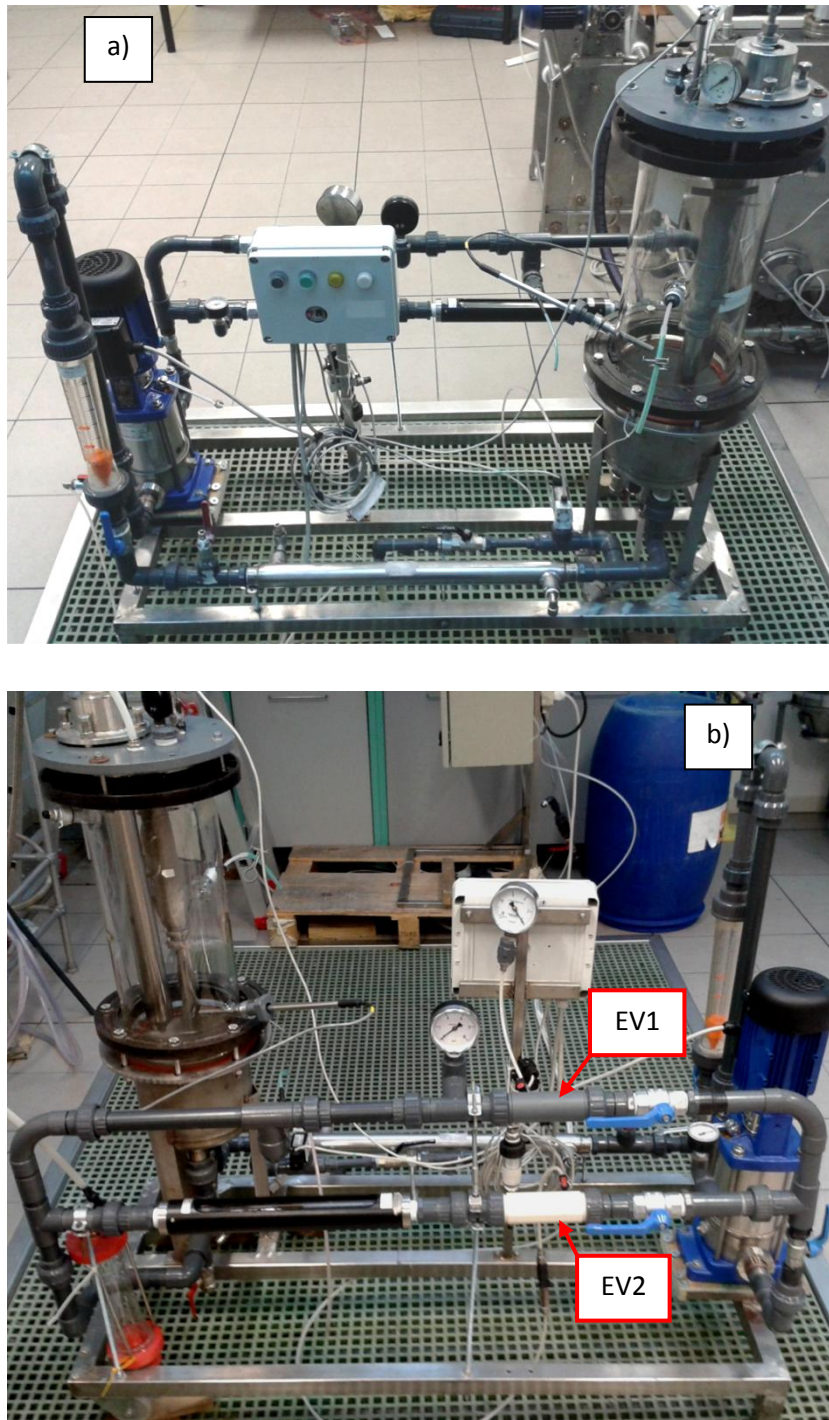

Fig 5.9 – Multi-task reactor pilot plant: a) front view and b) rear view

EV2 ejector is already used in wastewater biological treatment reactor [9]. The ejector was designed to operate at high pressure (in the order of 6 - 7 barg) and it was used as air diffuser in the reactor. The ejector is composed of two parts: the main body and the insert. The insert (Fig 5.10 a) has converged and restricted sections. Different inserts are

built changing their throat section diameter: 2, 2.5, 3, 4, and 4.25 mm. The main body (Fig 5.10 b), instead, have a threaded opening used to accommodate the inserts and the divergent section of the ejector. Convergent and divergent angles are 8°, respectively. The union between the two parts (Fig 5.10 c) creates a room inside the ejector, called mixing room. Vacuum gauge or flow-meter could be connected to this room.
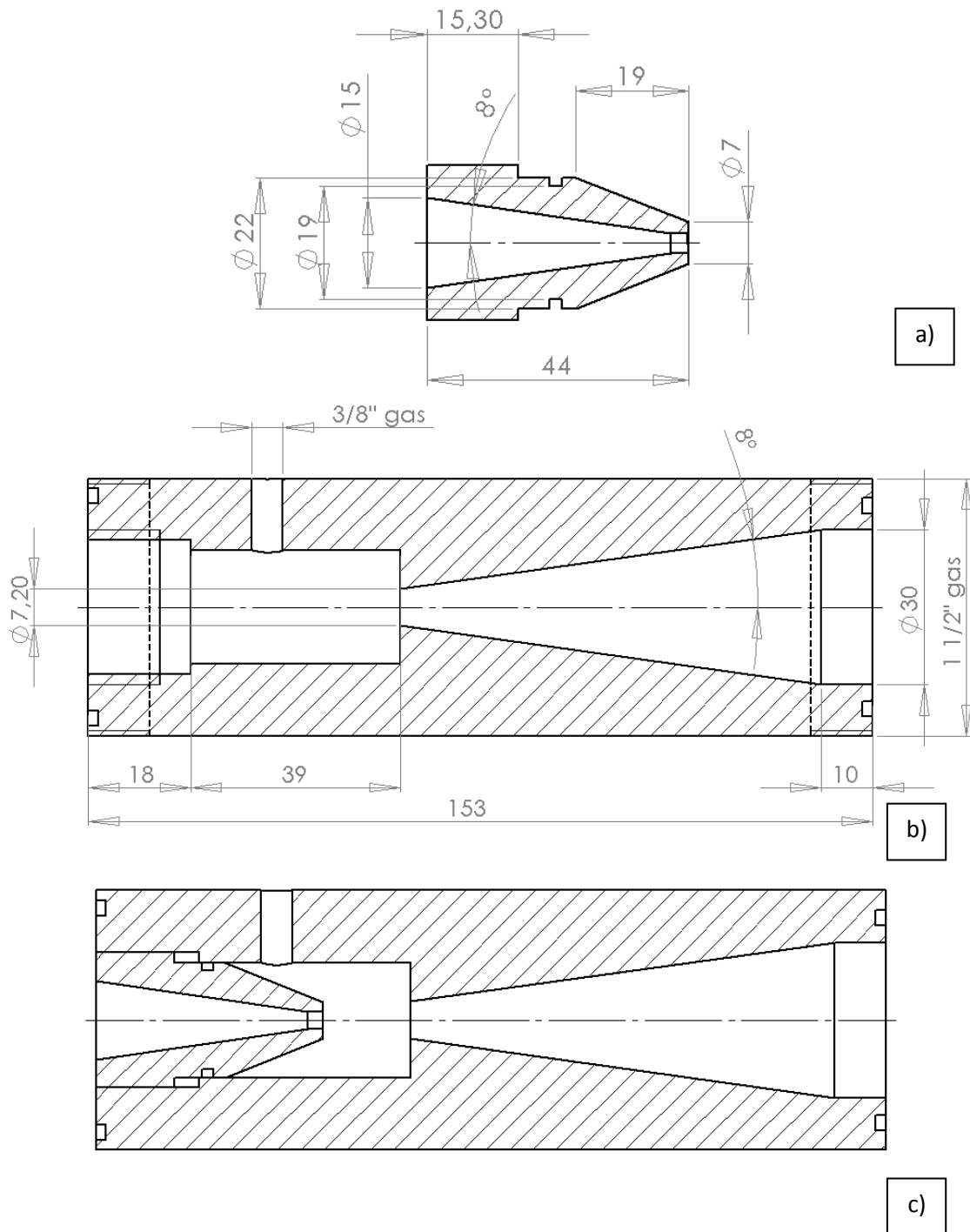

Fig 5.10 – EV2 Mixed Venturi ejector: a) insert, b) main body and c) assembled

EV1 is a Herschel-type Venturi. It consists of a short tapered pipe section which ends in a throat; a second conical section is designed with a smaller angle. Recommended

proportion to minimize the net pressure drop are inlet angle $\alpha_1 = 21° \pm 2°$ and outlet one $\alpha_2 = 5°$ to 15° [10]. Convergent and divergent parts are connected with a small cylindrical tube (length of 10 mm). In this place, the lowest pressure can be reached. While EV2 was only designed, as written above, EV1 was designed and built during this research work.
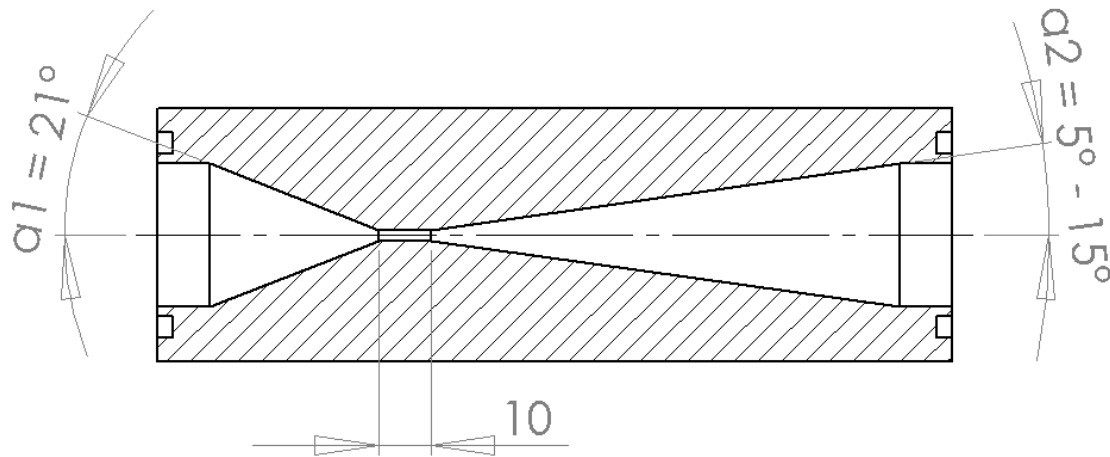

Fig 5.11 – Schematic Herschel-type Venturi ejector

The main design problem was the definition of flow rate and pressure optimal values needed to guarantee ultrasound and hydrodynamic cavitation effects together. In particular, the design focus was on type of pump and ejector EV1 geometrical characteristics (throat section diameter and divergent angle α_2).

From previous work [4], ultrasounds cavitation intensity depends on liquid flow rate, especially by its flow regime. In turbulence conditions, the cavitation intensity decreases until it disappears due to high Reynolds number, instead in laminar regime the cavitation intensity remains almost constant. After Reynolds number evaluation in the tank, the optimum liquid flow rate able to guarantee ultrasound cavitation is evaluated below 1500 L/h.

On the other hand, inlet pressure of ejector and flow rate through it are important to reach hydrodynamic cavitation state. The hydrodynamic cavitation exists only if the pressure decreases above the liquid vapour pressure. In this condition, the liquid is subjected to rapid changes of pressure that cause the formation of cavities where the pressure is above vapour liquid pressure. When subjected to higher pressure, the voids implode and can generate an intense shockwave of vapour bubbles. In the ejector throat section, low pressure could occur and then bubbles formation is possible, successively vapour bubbles implode in the first part of divergent section where pressure increases and velocity decreases.

Some papers in literature [5-8] affirm that an optimal inlet pressure in the ejector that maximizes the kinetic degradation of dyes exist. It is in the range 4÷6 barg.

In conclusion, from the above explanation, the pump must guarantee at least 6 barg prevalence and flow rate 1500 L/h.

To validate pressure and flow rate values define above, and the geometrical characteristic of EV1 (throat section diameter and divergent angle α_2), fluid dynamic simulation was done using COMSOL Multiphysics®.

COMSOL Multiphysics® is a general-purpose software platform, based on advanced numerical methods, for modelling and simulating physics-based problems. It is a finite element analysis and it is able to solve problems where coupled phenomena are present (therefore multiphysics problem).

The simulation aim is to calculate the characteristic curves of the ejector, considering different divergent angles and throat section diameters. After this, identifying the working point through the pump and ejector curves intersection, and the presence of vacuum. For our purpose, the characteristic curve of the chosen pump (Lowara 3SV 8 stages, maximum prevalence 60 mH$_2$O) was used.

A 2D axial symmetric model has been used to simulate the ejector, changing throat diameter from 2 to 4 mm and divergent angle α_2 from 5° to 15°. In the simulation test, convergent angle was set identical to 21°.

The *k-ε* turbulent flow model was set in COMSOL; this allows to use Navier-Stokes equations for conservation of momentum and the continuity equation for conservation of mass. Turbulence effects are modelled using the standard two-equation *k-ε* model with feasibility constraints. Flow close to walls was modelled using wall functions. The liquid (water) was considered incompressible.

As border conditions, the inlet velocity was set in a range of 0.065 to 1.7 m/s (in terms of volume, flow rate is in a range from 0.13 to 3.5 m^3/h) and the outlet was set to atmospheric pressure.

Fig 5.12 shows the ejector EV1 characteristic curves: these are ideal curves because the roughness is not taken into account. In the graph, there are three regions: each region is characterized by a throat section diameter changing the divergent angles according to the recommended proportion by Perry [10]. In all of them, the simulation vacuum pressure is reached.

From the data obtained by simulation, the best working points seem to be 2 mm diameter (each divergent angles) and only $\alpha_2 = 15°$ in the case of 3mm diameter, since they respect the water flow rate and pressure condition declared above. It is important to outline, though that the simulations were carried out considering the ejector material without roughness. Consequently, in a real condition the characteristic curves may be shifted to lower flow liquid rate.

To have comparable results in decolouration experiments between the two types of ejector, the divergent angle was chosen equal to $\alpha_2 = 8°$.
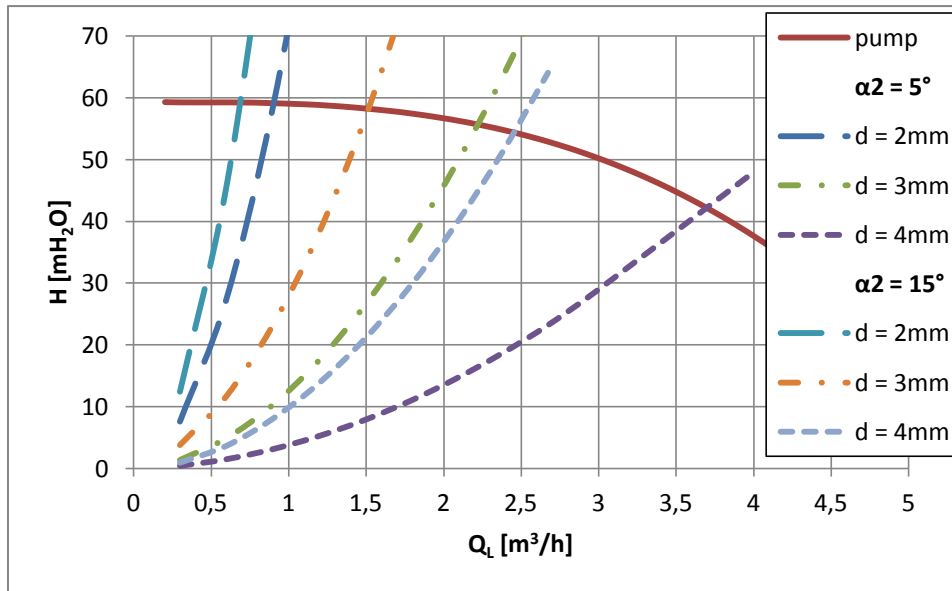
Fig 5.12 – Herschel-type Venturi ejector characteristic curves

Fig 5.13 shows the design picture of ejector EV1. Gauge pressure may be connected to ejector to measure vacuum in the throat section thanks to a sample port.

The plant working point was discovered doing experimental tests, changing ejector diameter (2, 3 and 4mm). As it may be seen in Fig 5.14, the real plant working points (red stars) are quite distant from the ideal ones. So, as presumed before, also ejector with 4 mm diameters can respect the condition to have hydrodynamic and ultrasonic cavitation together.
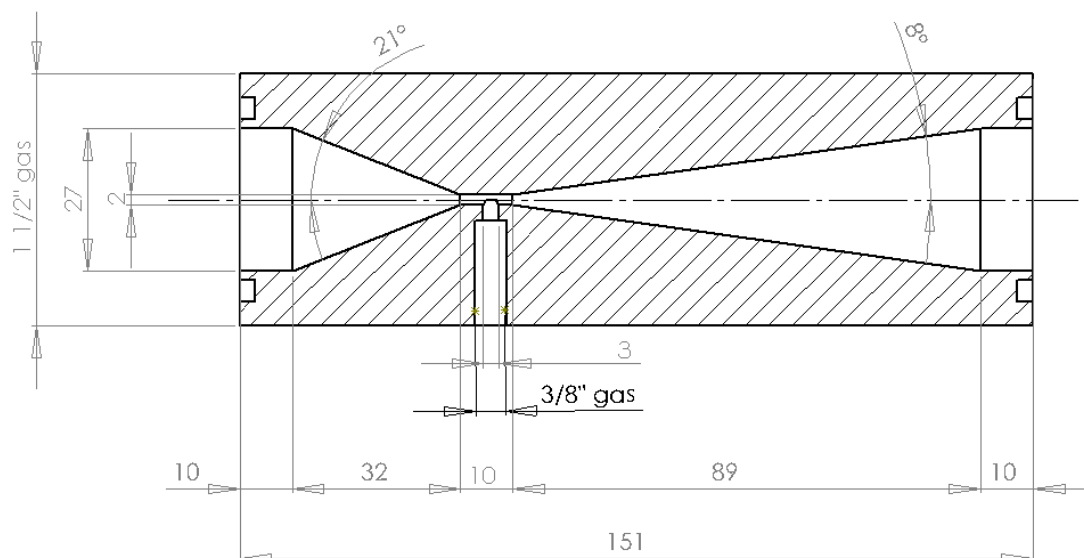
Fig 5.13 – Herschel-type Venturi (EV1)

Furthermore, using experimental data, it is possible to define an average roughness of the wall ejector with COMSOL simulation. The software is able to return $k_{s,eq}$ value (equivalent of sand-grain roughness) according to Nikuradse definition. In our case, sand roughness is evaluated and for the three ejectors the mean value is 2 mm equivalent sand-grain roughness. According to the conversion formula proposed by

Adams et al. [11], the arithmetic average roughness is about 180 μm. In Fig 5.14 are reported the characteristic curves in accordance with roughness and without roughness.
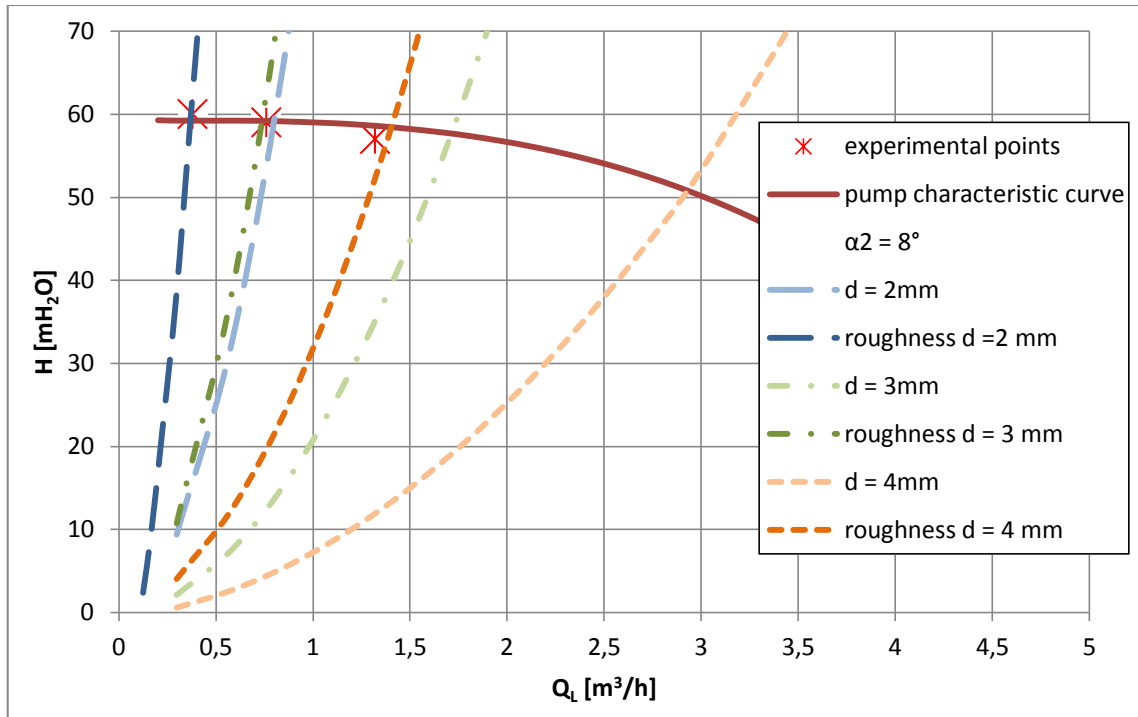

Fig 5.14 – EV1 Ejector ideal and real working points

In conclusion, the design of ejector EV1 was done and flow rate and pressure condition were respected. In the following Chapter, other experiments to verify the effective presence of hydrodynamic cavitation in the same ejector will be described.

References

[1] M. Onofrio, M.P. Prati Gaglia, *ICP*, **47**, 1984.

[2] G. Rovero, Riciclo delle acque nell'industria tessile, *Atti di convegno*, 2000, pag 82.

[3] W. Deckwer, Bubble column reactor, *John Wiley and soon*, 1992.

[4] M. Giansetti, S. Sicardi, G. Rovero, F. Pastorelli, V. Ginevro, Cavitation energy mapping for ultrasound application in dyeing processes, *AUTEX Research Journal*, **1**, 2011, 246-250.

[5] P.R. Gogate, G.S. Bhosale, Comparison of effectiveness of acoustic and hydrodynamic cavitation combined treatment schemes for degradation of dye wastewater, *Chemical Engineering and Processing*, 2013, http://dx.doi.org/10.1016/j.cep.2013.03.001.

[6] V.K. Saharan, M.P. Badve, A.B. Pandit, Degradation of reactive red 120 dye using hydrodynamic cavitation, *Chemical Engineering Journal*, **178**, 2011, 100-107.

[7] V.K. Saharan, M.A. Rizwai, A.A. Malani, A.B. Pandit, Effect of geometry of hydrodynamically cavitating device on degradation of orange-G 2013, *Sonochemistry*, **20**, 2013, 345–353.

[8] P.N. Patil, P.R. Gogate, Degradation of methyl parathion using hydrodynamic cavitation: Effect of operating parameters and intensification using additives, *Separation and Purification Technology*, **95**, 2012, 172-179.

[9] S. Papadia, G. Rovero, F. Fava, D. Di Gioia, Comparison of different pilot scale bioreactors for the treatment of a real wastewater from the textile industry, *International Biodeterioration & Biodegradation*, **65**, 2011, 369-403.

[10] Perry, D. Green, Perry's Chemical Engineers' Handbook, 5th edn., chap 5, 1973.

[11] T. Adams, C. Grant, A simple algorithm to relate measured surface roughness to equivalent sand-grain roughness, *International Journal of Mechanical Engineering and Mechatronics*, **1**, 2012, 66-71.

Chapter 6 – Hydrodynamic and ultrasound cavitation

Cavitation is a particular phenomena that consists in the formation of vapour cavities in a liquid and their consequent implosion. It usually occurs when a liquid is subjected to rapid changes of pressure, which cause the formation of cavities. Collapse of bubbles will begin when the pressure drastically increases in a short time [1, 2].

Cavitation is usually classified in two categories: inertial cavitation and non inertial cavitation [2].

Inertial cavitation occurs when voids or bubbles in a liquid rapidly collapse, producing shock waves. Typically, it takes place spontaneously in control valves, pumps, propellers and impellers. Collapsing bubbles involved close to a surface, cause cyclic stress through repeated implosion that brings to a "corrosion" and after this a possible breaking of the solid. Obviously, bubbles cavitation has no effects on solid surface when the collapse doesn't occur on device.

Also ultrasound systems can produce cavitation in a liquid medium. They propagate ultrasound waves, therefore pressure waves, and in particular conditions they produce bubble implosion.

In the case of ultrasound, both inertial and non inertial cavitation can be produced, depending on the energy power supply of the system. So, when inertial cavitation occurs, bubbles collapse, on the other hand, when non inertial cavitation happens, bubbles in a fluid are forced to oscillate for many cycles before imploding.

Both in hydrodynamic and in ultrasound cavitation, bubbles implosion generates a localized hot spot with high temperature and pressure [5, 7]. In these extreme conditions, water molecules are dissociated into OH· and H· radicals. OH· radicals diffuse in the liquid media and react directly with organic pollutants and oxidize/mineralized them.

Decolouration analysis, assisted by hydrodynamic or ultrasound cavitation, has been developed in the last few years [5, 8]. Generally, in order to remove dye from wastewater, lots of technologies have been developed (see Chapter 2). The main problem, though, is treating the secondary sludge produced by treatment, that may be more dangerous than the water to treat.

Cavitation could be a valid alternative: the "reactants" used in the reaction are built during bubbles implosion, such as hydroxyl peroxide that is one of the highest reduction potential radical. Cavitation is able not only to produce hot spots (i.e. high temperature and pressure), but it is also able to destroy organic pollutants by pyrolytic decomposition.

Moreover, intense turbulence is generated, and consequently liquid circulation currents increase mixing.

6.1 Hydrodynamic Cavitation

A practical definition of hydrodynamic cavitation is the formation and collapse of vapour cavities in a flowing liquid. Vapour cavity can form anywhere in the flowing liquid, especially where the local pressure is reduced to that of the liquid vapour pressure at the temperature of the flowing liquid. At these locations, some liquid vaporizes to form bubbles or cavities of vapour. Low-pressure zones can be produced by local increase in velocity (in accordance with Bernoulli's equation) as in vortices and by an overall reduction in static pressure.

The collapse of bubbles will begin when they are moved into regions where the local pressure is higher than the vapour pressure. Collapse of these cavities may produce noise and vibration, and extensive erosion or pitting of the boundary materials in the region of bubbles collapse.

In pipe systems, cavitation typically occurs either as the result of an increase in the kinetic energy (through an area constriction) or an increase in the pipe elevation.

Generally, hydrodynamic cavitation can be produced by making a liquid pass through a constricted channel at a specific velocity or by mechanical rotation of an object through a liquid.

In the case of a constricted channel, the cavities will be created in the restricted section where the pressure is lower than the vapour pressure. The combination of pressure and kinetic energy can generate high energy cavitation bubbles: when they collapse, they generate very high temperature and pressure, locally. Usually the cavitation bubbles collapse in a few microseconds. The overall liquid medium environment, therefore, remains at ambient conditions.

When uncontrolled, cavitation is damaging: by controlling the flow of the cavitation, however, the power can be harnessed and non-destructive. Controlled cavitation can be used to enhance chemical reactions or propagate certain unexpected reactions, because free radicals are generated in the process, due to disassociation of vapours trapped in the cavitating bubbles.

Cavitation can be performed using orifices and Venturi ejectors. A Venturi ejector has an intrinsic advantage over an orifice thanks to its converging and diverging sections. The converging section generates a higher velocity at the throat section for a given pressure drop across it, and the diverging part is used for pressure recovery. On the other hand, if orifices are used, there isn't pressure recovery but it can accommodate lots of holes in a given cross sectional area of the pipe.

The parameter which describes the condition for cavitation is the cavitation number σ_c:

$$\sigma_c = \frac{p - p_v}{\rho v^2/2}$$

where p is the static pressure (absolute) in undisturbed flow, p_v is liquid vapour pressure (absolute), ρ is the liquid density and v is the liquid free-stream velocity and [9].

The cavitation number expresses the relationship between the difference of a local absolute pressure from the vapour pressure and the kinetic energy per volume. Generally, the cavities are generated when the value of cavitation number is equal or under the unit, in an ideal condition. σ_c in many cases is a value greater than one, due to the presence of dissolved gas and suspended particles which increase the number of nucleation site for the cavities to form [5].

The two main mechanisms of reaction involved during hydrodynamic cavitation for volatile compounds are decomposition/pyrolysis and reaction with the OH· radicals. The first mechanism may occur inside the cavities as they collapse and the second one occur in the interface between cavity and water. In the case of non-volatile pollutant, the main reaction involves hydroxyl radicals in the cavity-water interface and in the bulk fluid medium. Mechanical effects are also important, particularly for large molecule weight compounds: the shock waves, generated by bubbles collapse, may break molecular bonds. Consequently, the molecules react easier with other hydroxyl radicals in the medium or by biological reaction [5].

6.1.1 Venturi ejector devices

A general definition of ejector is given by Alves [3]: "*An ejector is a device in which the kinetic energy of one fluid (primary fluid) is used to pump another fluid (secondary fluid). Generally, the primary fluid may be a liquid or a gas/vapour and the secondary one may be a solid in a liquid emulsion (if it is corrosive), liquid or gas/vapour*".

The ejectors used in this study have double effects: they are used both to introduce ozone in the system and to implement hydrodynamic cavitation. In this way the ejector design has the main purpose to reach a significant vacuum degree in order to obtain bubble implosion, and therefore cavitation.

Generally, ejectors are used in chemical industries in different applications, for example for exhausting fumes, producing vacuum, transporting particles, lifting acids and alkalis, pneumatic conveyor feeding and preventing smoke from stationary plant. Moreover, they are used in chemical and biochemical process industry because they are more efficient in gas-liquid contacting, such as in hydrogenation, chlorination, ozonation and oxygenation. Their fluid-dynamic promotes mass transfer from gas phase to liquid one and mixing [4, 6].

Mixing from two phases is the result of a particular fluid-dynamic condition called Mixing Shock. When the secondary fluid (gas) is sucked by the primary (liquid), they are initially coaxial. Namely, an annular geometry is created between the two fluids: the inside fluid is the primary fluid and the secondary is around it. The jet flow persists for a certain length in the system, after that the jet flow changes into a froth flow, in a

particular position. In this position, the secondary fluid is dispersed in the primary one. Finally, the dispersion separates in two separate fluid phases [4]. The same phenomenon is at the basis of the promotion of mass transfer, because the gas-liquid contact area increases in the portion of fluid where mixing shock persists.

An ejector can be called by different names, depending on its application [3]:

- Syphon: it is a liquid pump using a condensable vapour as motive fluid;
- Exhauster: it is a liquid pump using liquid as motive fluid;
- Jet blower: it is used to pumping gases against very low differential pressures;
- Jet compressor: it is a gas jet pump used to boost pressure of gases.

On the other hand, an ejector is called injector when a condensable gas is used as primary fluid and the discharge pressure is higher than either motive or suction pressure [3].

In any case, the ejector may be classified in two main categories: Venturi type and draft-tube type. The main difference between them is the geometry: Venturi ejector is constituted by convergent and divergent sections connected by a restricted section, instead draft-tube one has no restricted section. In the last case, the secondary fluid is put in motion by the primary one either for velocity or density difference.

Venturi ejector takes advantage of the so-called Venturi effect: it is the reduction in fluid pressure that results when a fluid flows through a constricted section of pipe.

6.1.2 Ejectors behaviour in multi-task reactor

The main purpose in ejector characterization is defining the condition to have cavitation inside the ejector. As mentioned, cavitation has two main purposes: producing hydroxyl radicals by cavitation and increasing mixing.

Experimentally, cavitation can be detected using numerical evaluation (cavitation number) and by determination of changes in auditory noise in experimental conditions.

Moreover, the characterization is important to define:

- vacuum degree in throat section;
- air flow rate sucked by ejector from the environment (atmospheric condition);
- air flow rate sucked by ejector at different inlet air pressure.

The device primary fluid is liquid flow and the gas one is eventually introduced in the throat section.

6.1.2.1 Herschel-type Venturi (EV1)

The first part of EV1 experimentation consists in the evaluation of the cavitation condition.

The scheme reported in Fig 6.1 shows how the tests are performed in the multi-task pilot plant. In this case, valve V1 was completely open.
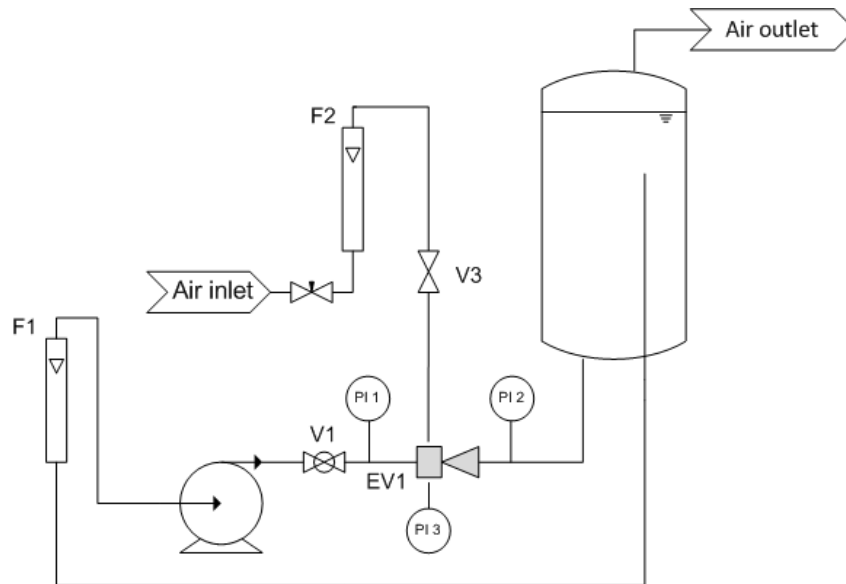
Fig 6.1 – Pilot plant configuration for hydrodynamic cavitational study

The pump worked at the same rpm, for all the experiments: in this way, the pump characteristic curve doesn't change. The experiments were performed with different throat section diameters from 2 to 4 mm each 0.2 mm. Consequently, ejector characteristic curves change, showing different values of flow rate/pressure pair (Fig 6.2) from pump and ejector characteristic curve intersection.

Pressure was measured with the manometer P1 and flow rate with the flow meter F1. The manometer P2 gave atmospheric pressure as result, for all the experiments.

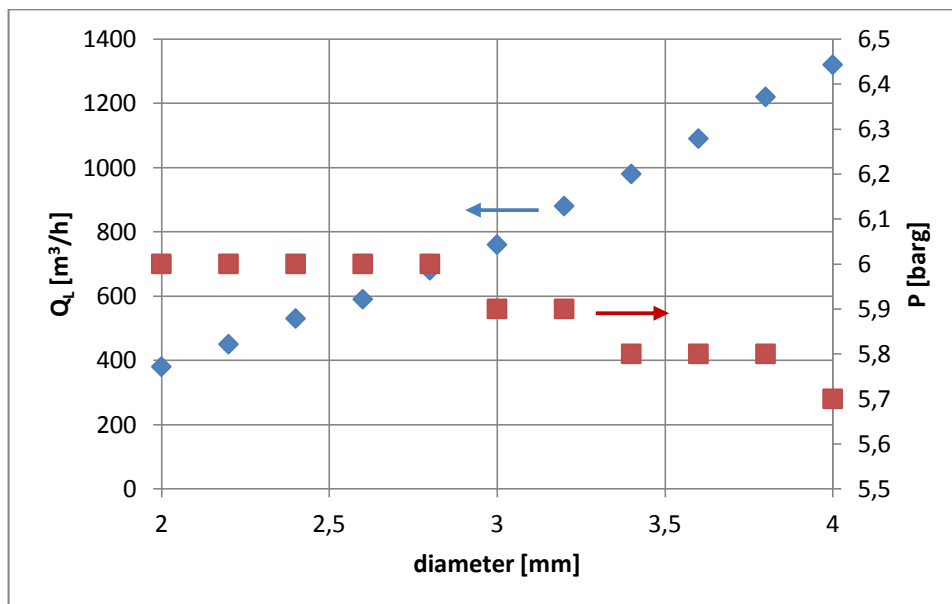Fig 6.2 - Pair values flow rate-pressure of the system, for each throat section diameters.

As mentioned in a previous paragraph, cavitation number σ_c is a dimensionless parameter used to describe the condition of cavitation. When $\sigma_c \leq 1$ [5], it is possible to have cavitation. It is possible to detect cavitation also from the noise produced by the

phenomena. Therefore numerical data and subjective/objective noise considerations can be done. From the data reported in the following graphs (Figg 6.3 and 6.4), it is possible to understand that also a minimum cavitation number value, under which cavitation is absent, exists.

Considering EV1 with 4 mm throat section diameter, cavitation numbers are calculated changing the ejector inlet pressure. In Fig 6.4 the values of vacuum (P3) are reported: 0 mH_2O indicates atmosphere pressure and 10.33 mH_2O absolute vacuum. It is important to underline that moving towards the region of the absolute vacuum the noise increases. The noise represents an evidential signal of bubble implosion, and therefore cavitation.
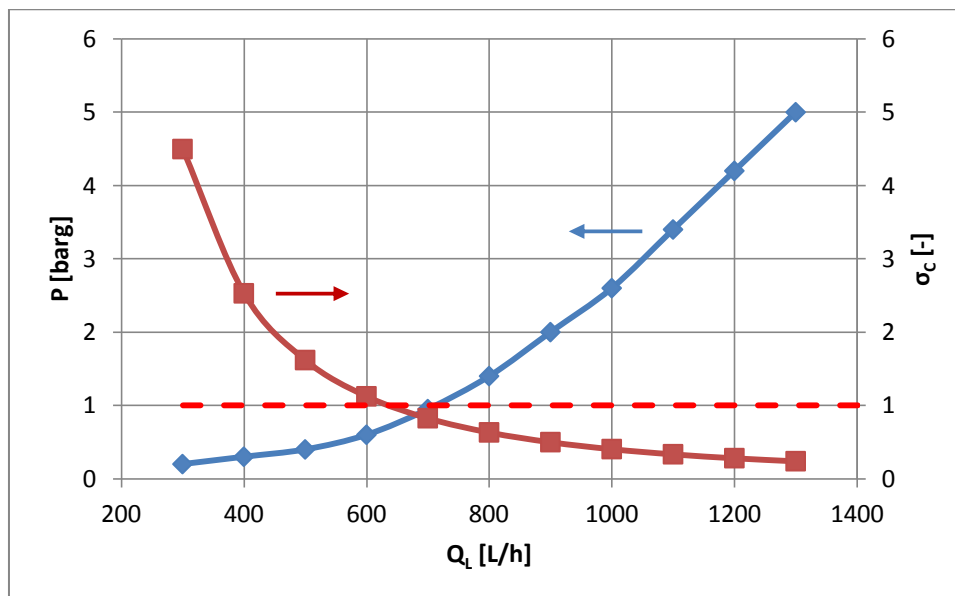

Fig 6.3 – Cavitation number and inlet pressure vs inlet liquid flow rate (d = 4 mm)
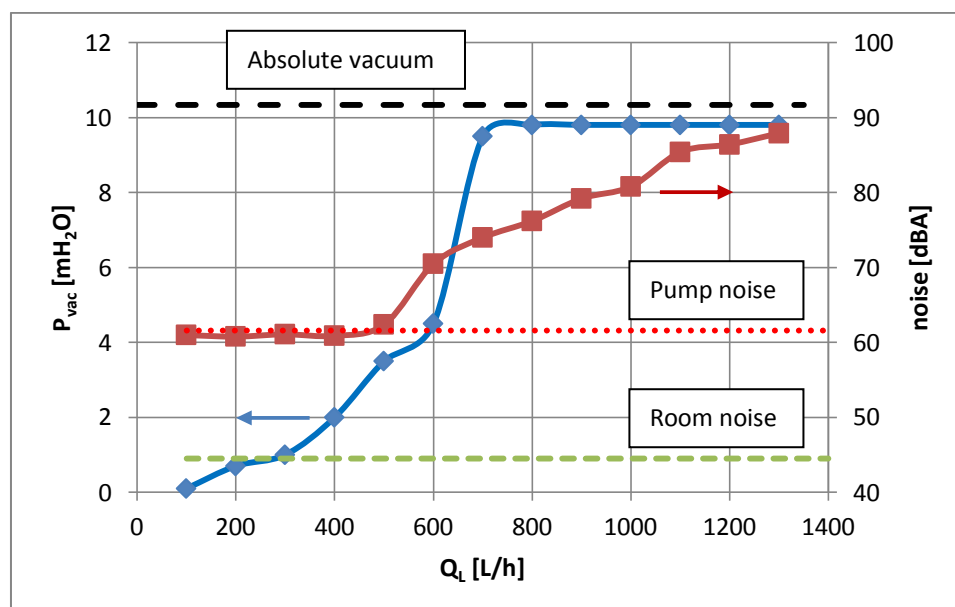

Fig 6.4 – Vacuum degree (d = 4 mm)

Subjective sound listening by researcher put in evidence a sound changing when the fluid flow rate approached 600 L/h and inlet pressure was of about 0.6 barg, which corresponds to σ_c = 1.12 and a vacuum of about 4 mH_2O. Noise increases with the increase in inlet pressure. At the maximum pressure and velocity conditions, cavitation number reaches its minimum value equal to 0.24.

If the sound is measured with a phone-meter, an important increase in noise is remarked when flow rate is in the order of 700 L/h and the inlet pressure is about 1 bar (σ_c = 0.83).

It is important to outline that the noise was measured near to the external surface of the ejector in correspondence of the throat section. Therefore, the noise is the sum of several components such as room noise, pump noise and all the phenomena occurring in the ejector. Obviously, the last noise is given by liquid flow in a constricted channel and cavitation.

Regarding the case in study, the minimal noise corresponding to a cavitation inception correspond to about 74 dBA. Considering a general case, if the relative noise produced by an ejector is greater than 12 dB compared to room noise, cavitation will take place in the device.

Fig 6.5 shows Vacuum pressure and cavitation number by changing the geometry of the ejector EV1, namely the ejector throat section diameter from 2 to 4 mm each 0.2 mm.
When the ejector have a throat section of 2, 2.2 and 2.4, inlet pressure and flow rate are not sufficient to produce a vacuum degree able to trigger cavitation (P < 2 mH_2O). Confirming this affirmation, the noise was at the same level of room noise, as can be seen in Table 6.1.
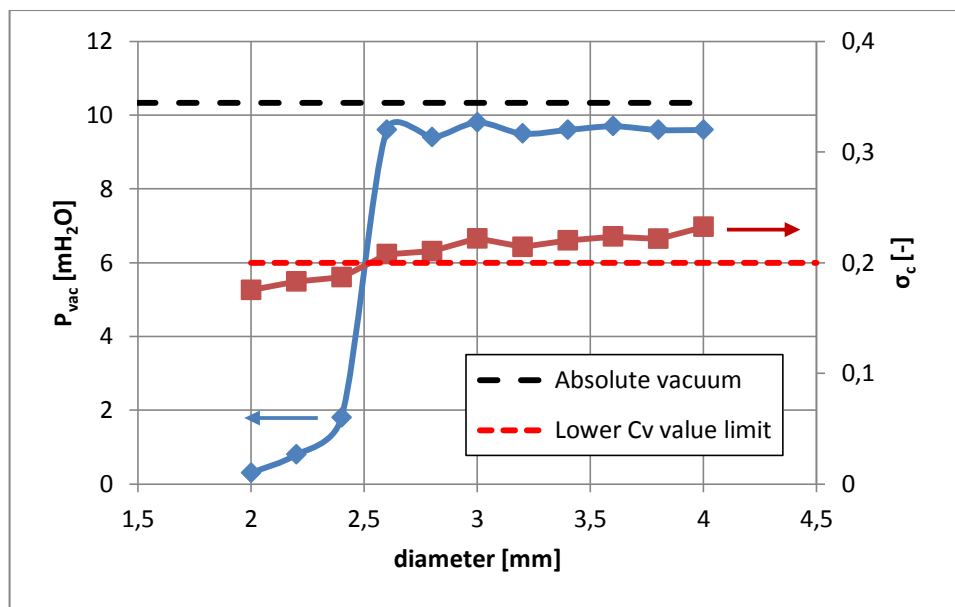

Fig 6.5 – Vacuum and cavitation number changing ejector geometry

Table 6.1 – Data noise considering different ejector diameter (mean room noise 61.6 dBA)

Diameter [mm]	Q_L [L/h]	σ_c [-]	P [barg]	P_{vac} [mH$_2$O]	Noise [dBA]
2	380	0.175	6	0,3	61,2
2,2	450	0.183	6	0,8	61,8
2,4	530	0.187	6	1,8	61,9
2,6	590	0.208	6	9,6	73,1
2,8	680	0.210	6	9,4	79,9
3	760	0.222	5.9	9,8	83,8
3,2	880	0.214	5.9	9,5	85,9
3,4	980	0.220	5.8	9,6	86,4
3,6	1090	0.224	5.8	9,7	87,1
3,8	1220	0.222	5.8	9,6	87,9
4	1350	0.232	5.7	9,6	88,1

Although cavitation number is below one, cavitation does not exist. In these conditions, it is probable that the kinetic energy of the fluid is not sufficient to promote bubble formation.

Instead, σ_c= 0.2 can be considered the lower value beyond which cavitation either do not exist or it is as choked cavitation. Choked cavitation occurs when the density number of cavities increases to such an extent that cavities start coalescing and can form a cavity cloud. The range of cavitation number where cavitation exists is in function of the device [27]. So, σ_c = 0.2 may be considered, in our case, the lower limit for cavitation implosion.

The second part of EV1 experiments consists in evaluating the ejector capacity to suck gas both from atmospheric condition (0 barg) and from a fixed gas pressure (0.5, 1, 1.3, 1.6 barg).

So, in the following experiments valve V1 and V2 was completely opened and gas flow rate ($Q_{g\ suc}$) was measured using the F2 flow-meter (Fig 6.1).

It may be observed that air flow rate increases by increasing the diameter of the throat section, in all pressure conditions. Moreover, from 2 to 2.8 mm, the graphs show an almost constant intake air flow rate. By increasing the diameter, intake air increases faster with increasing gas pressure.

At the lowest pressure (0 and 0.5 barg), from 2 to 2.8 mm, inlet air flow rate is negligible even if the ejector is able to generate vacuum (Fig 6.6). This fact may be due to the ejector geometry: air enters the ejector through a connection channel of 2 mm diameter. Therefore the throat section and the inlet air channel have the same dimension. Considering the high flow velocity of the liquid in the restricted section, the bubbles formation is quite difficult.
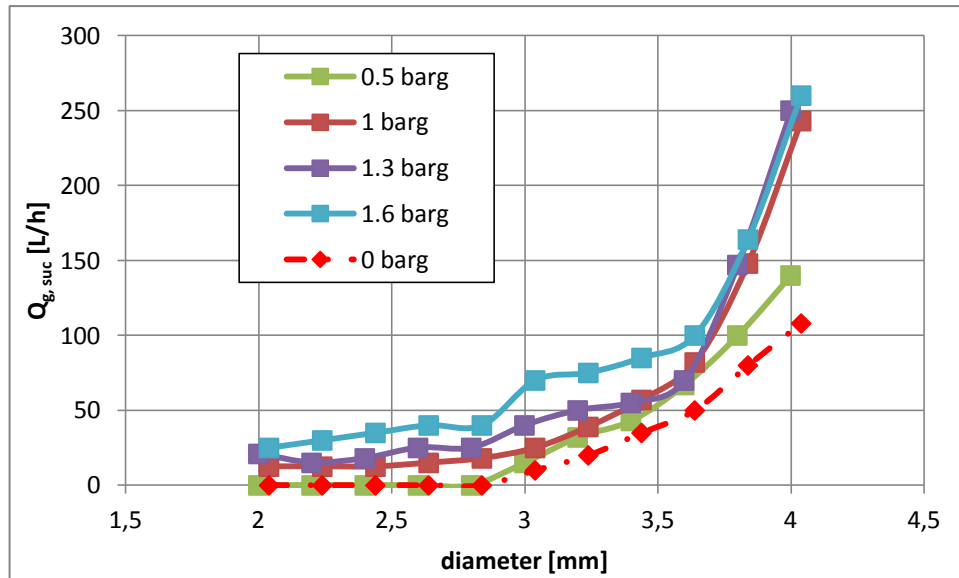
Fig 6.6 – Air flow rate sucked by ejector at different inlet air pressure

Keeping in mind the previous results, it is possible to outline some considerations:
- when noise is greater than 12 dB over the room noise, there is cavitation;
- the range of cavitation number in order to have bubble implosion is $0.2 < \sigma_c < 1$.

6.1.2.2 Mixed Venturi ejector (EV2)

Taking into account the scheme shown in Fig 6.1, the characteristic of Mixed Venturi ejector EV2 were measured in terms of vacuum and sucked air.

Tests using four different inserts having outlet diameter of 2, 2.5, 3, 4, 4.25 mm were performed. Inlet diameter is always the same.

In Fig 6.7 the trends of the cavitation number for the different ejector configurations and the pairs flow rate/pressure are reported. At the same previous conditions, vacuum is measured and it is showed in Fig. 6.8 changing liquid flow rate. Maximum vacuum reached in the experiment is 9.8 mH$_2$O with 4 and 4.25 mm hole diameter. It is evident that decreasing the velocity in the throat section, kinetic energy decreases and the pressure tends to the atmospheric value.

Approaching to absolute vacuum, noise increases. It is particularly evident a change in sound after peculiar flow rate limit. It is possible to assume that this value is the transition between no cavitation and bubbles implosion. Assuming that cavitation is associated to noise, hydrophone is used to evaluate noise numerically. In Fig 6.9 the noise trend for each insert is reported. Red dash line is the noise produced by pump and dark green one represents room noise.
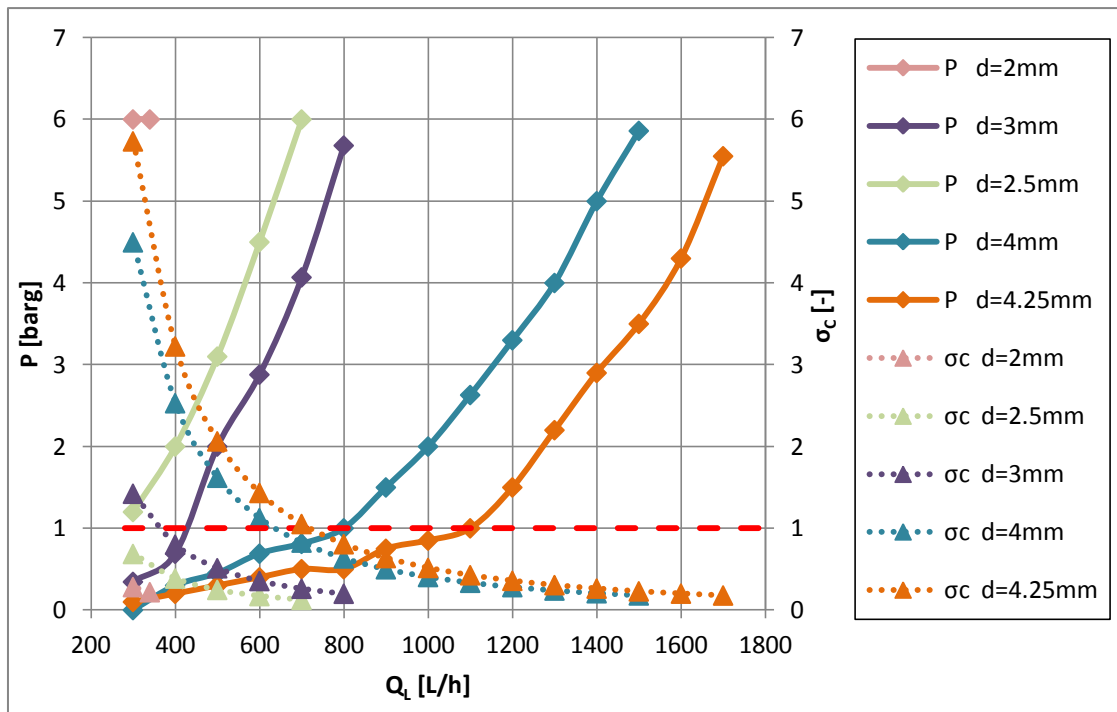
Fig 6.7 – Cavitation number and inlet pressure vs liquid flow rate
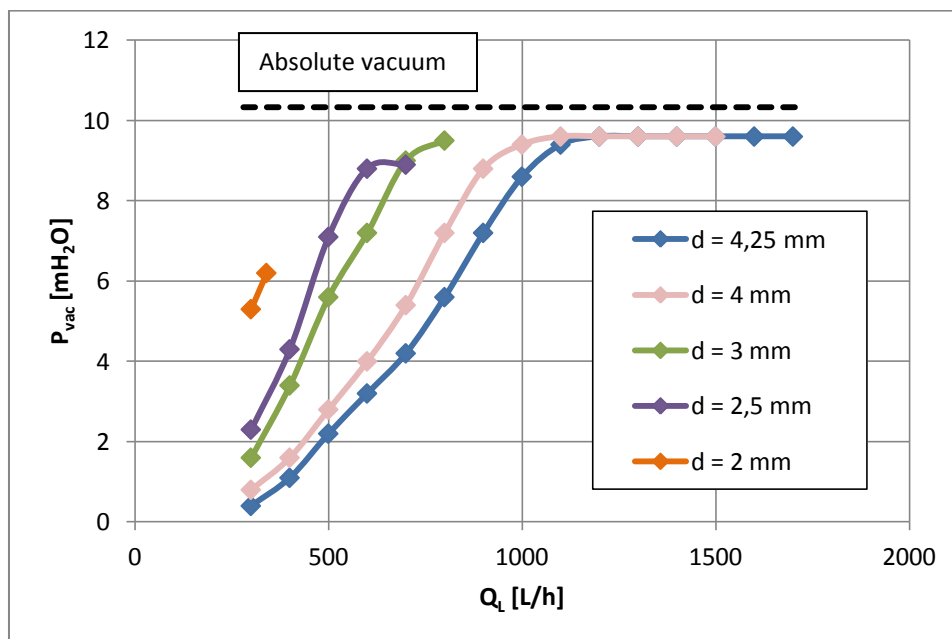
Fig 6.8 – Vacuum evaluation

Unlike the EV1 results, data of Mixed Venturi have partial correlation between cavitation number and subjective/objective noise. As an example, we can take into account the cavitation numbers and vacuum values in the case of insert diameter d = 4.25 mm. There are the same conditions in which cavitation number is below one, but the noise measured is in the order of room noise and vacuum degree is not enough marked to have cavitation. So, these conditions may be considered like inception cavitation, where little bubbles are formed and their implosion is not significant for the environment.

The results discrepancy may be due to the EV2 geometry: in EV1 exist only one throat section, instead in EV2 two restricted section exist. The first one is the end part of the insert and the second one is the inlet of ejector divergent part.

Comparing subjective noise (when the noise changes clearly, according to the researcher) with noise measured by hydrophone and vacuum, noise trend value beyond which cavitation exists is possible to define. The experimental red line in Fig 6.9 describes noise limit above which cavitation occurs: the line has a good agreement for each insert considered, whatever diameter.
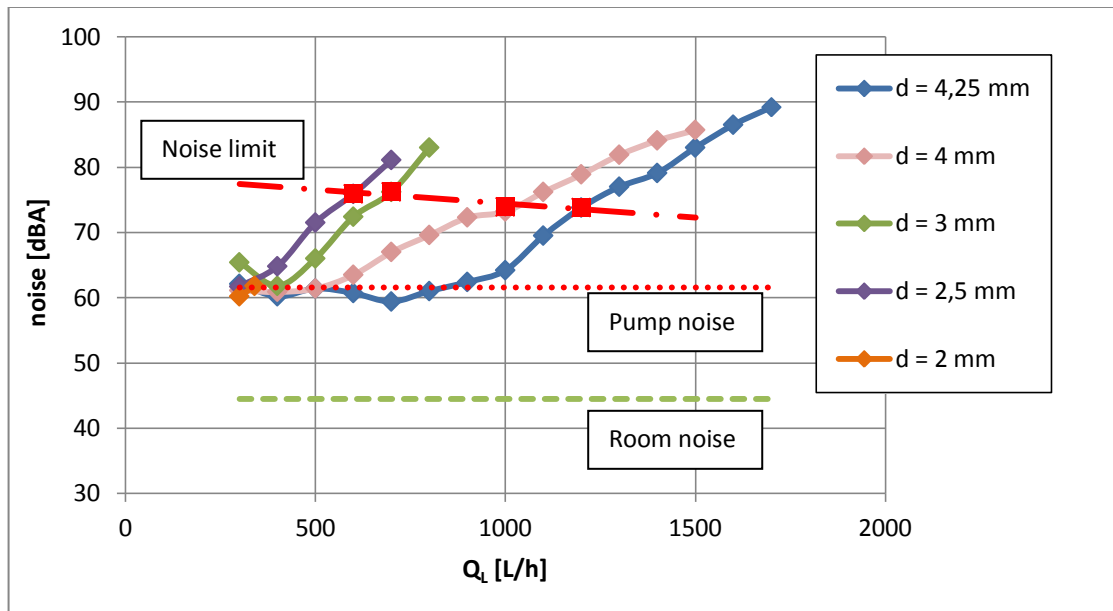
Fig 6.9 – Hydrophone noise evaluation

When the ejector is used to suck air, it is much more efficient compared to EV1. The reason is the mixing room: if EV1 throat section limits the air passage as explained in the previous paragraph, mixing room increases the capacity to attract air from the external environment. For example, let's take into account the restricted section equal to 4 mm for ejectors EV1 and EV2. The maximum air flow rate sucked from the environment (atmospheric pressure) is quite different in the two cases: about 800 L/h for EV2 and little more than 100 L/h for EV1 at the maximum flow rate through the ejectors.

In the following graph (Fig 6.10) the mixing room pressure values compared to different insert diameter are reported. The range of gas flow is restricted to values equal or below 250 L/h.

Fig 6.10 – Vacuum evaluation vs sucked air flow rate
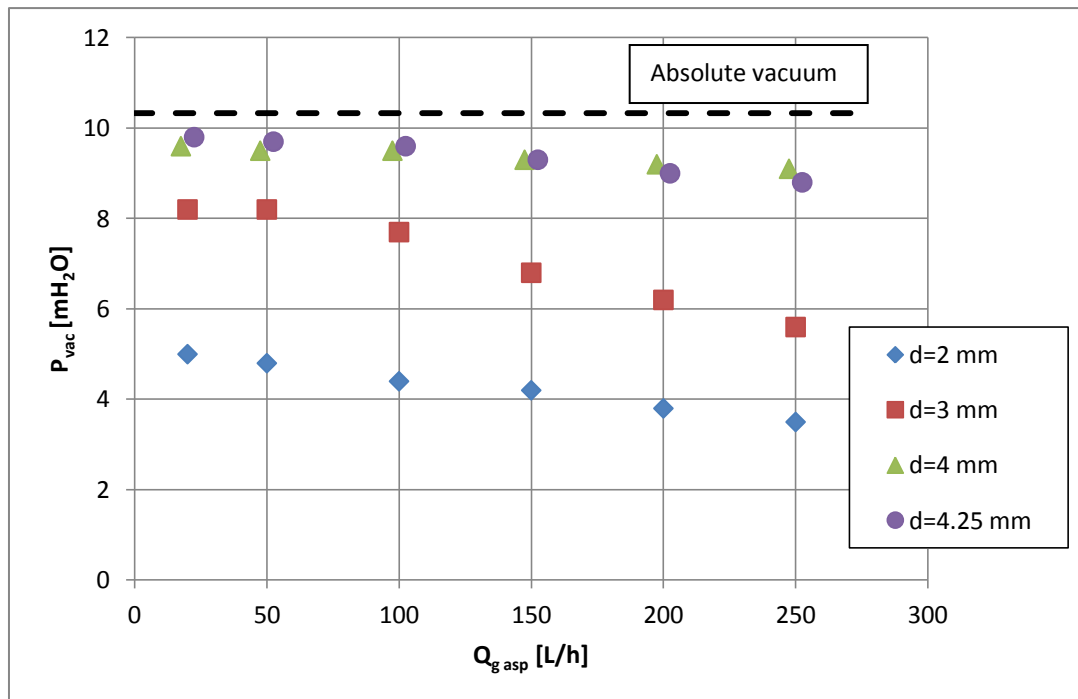
6.2 Ultrasonic cavitation

Ultrasounds (US) are cyclic sound pressure waves with a characteristic frequency higher than 20 kHz. They propagate in liquid and solid media with a sinusoidal dynamics. When these waves propagate in a liquid, they create compression and rarefaction cycles with possible creation of micro-bubbles. The power per unit area required for cavitation depends on the liquid medium and on the content of soluble gases. When superficial power intensity of ultrasounds reaches about 3 W/cm^2, the micro-bubbles can be defined stable; instead, when the superficial power of ultrasounds is higher than 10 W/cm^2 the micro-bubbles have a transient life. These bubbles collapse within one acoustic cycle, while - if the intensity power is lower than the latter value - bubbles will oscillate for several acoustic cycles, almost in unison with the acoustic wave before collapsing; in some instances they never collapse at all [11]. The previous values are related to air-free water; while, if tap water is used in sonication, the power intensity necessary to shift from stable to transient bubble is lower: about 0.34 W/cm^2 [12]. Micro-bubbles implode when they change their condition from stable to transient, which define the cavitation mechanism [1].

Usually, industrial applications require a superficial power in excess of the transition state to reach bubbles collapse. During the implosion status, these bubbles create extreme local physical conditions both in terms of pressure and temperature, as high as 100 MPa and 5000 K, respectively [7].

Sonochemistry is the name used to indicate chemical reaction enhanced by ultrasonic cavitation. When vapour bubbles generated by ultrasound implode, there is generation of hot spots and so high temperature. As result of which, molecular bonds can be broken.

From a reacting point of view, most of the effects of interest regarding sonication are related to cavitation. Cavitation causes solute thermolysis along with the formation of highly reactive radicals and reagents, such as hydroxyl radicals and hydrogen peroxide, which induce drastic reactive conditions in the liquid media. In addition, if a solid is present in solution, the sample size of the particles is diminished by solid disruption, thereby increasing the total solid surface in contact with the solvent.

Luche et al. [16] classified the sonochemistry reaction in two categories: true and false sonochemistry. When the reaction path is influenced by ultrasound cavitation, the sonochemistry is defined true. In this case there is radical formation and the formation of reactive intermediates from the starting compound is possible. If the ultrasound enhanced the reaction by mechanical effects, such as mixing, the sonochemistry in define false.

In the case of water sonication H· and OH· are formed. The radicals produced can be combined with each other to form new bonds or they can also start chain of reactions and so releasing new radicals into the environment [15]. In the case of water system, the following reactions represent the main reaction mechanisms [17]:

$$H_2O \rightarrow H\cdot + OH\cdot$$
$$H\cdot + H\cdot \leftrightarrow H_2$$
$$OH\cdot + OH\cdot \leftrightarrow H_2O_2$$
$$H\cdot + O_2 \leftrightarrow HO_2\cdot$$
$$H\cdot + HO_2\cdot \leftrightarrow H_2O_2$$
$$HO_2\cdot + HO_2\cdot \leftrightarrow H_2O_2 + O_2$$
$$H_2O\cdot + OH\cdot \leftrightarrow H_2O_2 + H\cdot$$
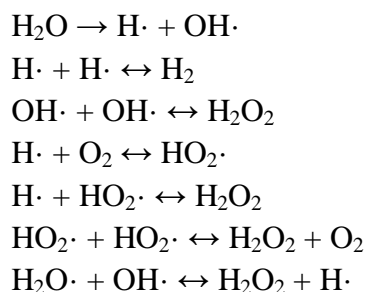
Frequency is an important parameter: as the frequencies increase, the pulsation and collapse of the bubbles occurs more rapidly and more radicals escape from the bubble. However, as the frequency increases the cavitation intensity decreases and this reduces the yield of radicals and consequently the numbers that reach the interface and bulk solution [3].

Nowadays ultrasound are used in different innovative fields; indeed cavitation offers a high potential for intensifying physical, chemical, biological and textile processes (in an energy-efficiency improvement) [13-15].

6.2.1 Parameters that influence ultrasound cavitation

The intensity of bubbles implosion is influenced by some experimental parameters such as temperature, dissolved gas in the liquid, flow rate of the liquid in the reactor, power intensity and ultrasound frequency. Therefore, their effects must be taking into account in reactors design.

- Temperature
Increasing in temperature causes a reduction in the intensity of ultrasound required to the formation of cavity bubbles in liquid medium. The reason is probably due to the

increasing of the vapour pressure of the liquid and also of cohesive forces within the fluid.

Increasing liquid temperature, the nucleation of cavities is favoured, but the presence of liquid and vapour between the bubble leads to a cushioning of the implosion during the compression cycle. In this way, cavitation intensity decreases because the shock wave released on cavity implosion becomes less intense.

In Fig 6.11 the effect of temperature on cavitation in tap water is reported. Here is also shown its hysteric phenomena.
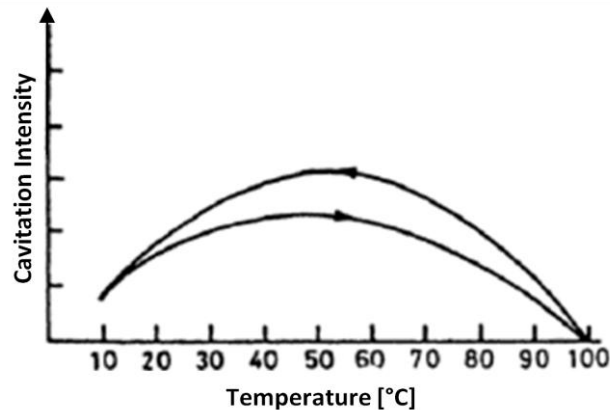

Fig 6.11 – Effect of temperature on intensity cavitation and its hysteric effect [22]

From the graph, it is possible to understand that the optimal value of temperature corresponding to a maximum cavitation intensity exists. This temperature value is in the range 50 - 60°C. After this temperature, an increase in temperature towards water boiling point corresponds to a reduction in cavitation intensity observed, due to the increase in vapour pressure and its associated cushioning effect. Also when the temperature decreases from boiling point to the lowest temperature, the optimum temperature is in the same range. Moreover, the upper curve shows that the intensity of cavitations increased more than the initial optimum, probably due to the degassing of solution after boiling.

- Dissolved gas in the liquid

Ultrasound cavitation is more influenced by the air content of water. Liu et al. [16] have demonstrated, by hydrophone measurements, that there are differences in the cases of tap water and boiled water sound detection. The presence of small bubbles persisting in the liquid for long time after ultrasound propagation is no good for cavitation. Bubbles disturb the acoustic wave propagation and cavitation bubbles generated in high air content medium collapse in a weaker way in comparison to vapour bubbles. But the same authors affirm that traces of gas dissolved in the medium are helpful for cavitation: the initial bubbles content is gas-vapour mixture and they are the precursors that induced the rupture of the liquid.

On the other hand, dissolved gas in a sonicated liquid can enhance chemical reactions. Usually, gas molecule can easily form radicals, such as oxygen, can increase radical production [17, 20].

- Flow rate in the reactor

Generally, the flow rate, and so its fluid-dynamic, influences the propagation of ultrasound in the reactor and so its intensity. From previous study, the cavitation intensity is influenced by the velocity in which the fluid moves in the reactor [9]. An increase in the system turbulence coincides with a decrease in cavitation intensity. Turbulence could facilitate the coalescence of bubbles and consequence a decrease in the bubbles implosion.

- Power intensity

Increasing the power intensity, the collapse pressure rises, causing faster and more violent transient cavitation implosion. Obviously, a limit to irradiation intensity, due to practical and engineering considerations, exist.

Moreover, high intensity corresponds to an increase in the number of cavities for volume unit, with the possibility to form conglomeration and more stable bubbles. Consequently, cavitation intensity decreases.

- Ultrasound frequencies

The ultrasound frequencies are connected with bubble dimension. If the frequency is below a threshold value, the amplitude of the sound field is not able to induce nucleation or bubble growth. Above cavitation threshold value, increasing in frequencies increase the effective size of the zone where cavitation is possible. At the same time, sonochemical reaction rate increases. This phenomena is not infinite: a frequency threshold after which sonochemical effect diminishes exists. The possible explanations are that bubble shroud the sonic device and do not permit to ultrasound wave to pass and the bubbles overgrow.

6.2.2 Transducer device

Experiments were performed using cylindrical transducer SONOPUSH®, which was produced from Weber Ultrasonics GmbH. The transducer was operated at a frequency of 25 kHz with maximum power of 1000 W (minimum power allowed by the instrument is 500 W).

The transducer is made from a special titanium alloy and it radiates sound field waves at 360 degree in homogeneously space. The device have high level of stability, resistance to temperatures up to 95 °C even in continuous operation and vacuum and overpressure resistance up to 10 bar.

The transducer vibrating part is positioned at the head of the device, as can be seen in the X-ray picture in Fig. 6.12.

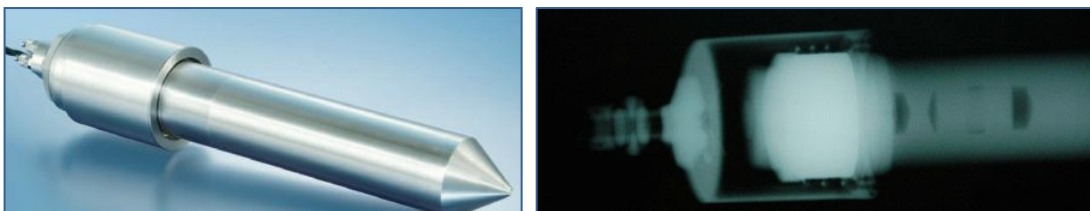The probe is immersed in the tank containing the liquid to sonicate.

Fig. 6.12 – Cylindrical transducer device (on the right X-ray picture)

6.2.3 Cavitation intensity field determination

A schematic representation of the reactor assembly for ultrasound cavitation characterization is shown in Fig 6.13.
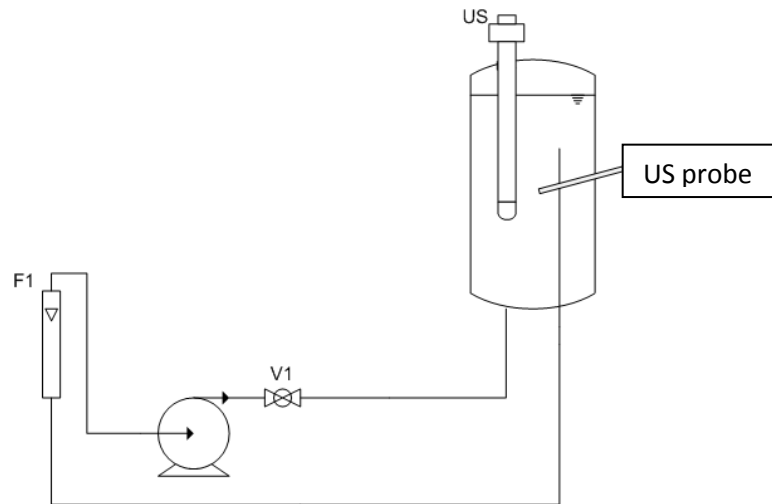

Fig 6.13 - Pilot plant configuration for ultrasound cavitation characterization

An Ultrasonic Energy Meter made by PPB Megasonics was used to measure the cavitation field in the liquid. A BX-408 0.5 inch OD stainless steel probe transducer was connected with the instrument case. The probe was introduced in the reactor through a sampling point along the reactor wall (Fig 6.14). The meter detected the density of the cavitation energy of the imploding bubbles with a frequency of two measurements per second; the output was directly given in W/in^2.
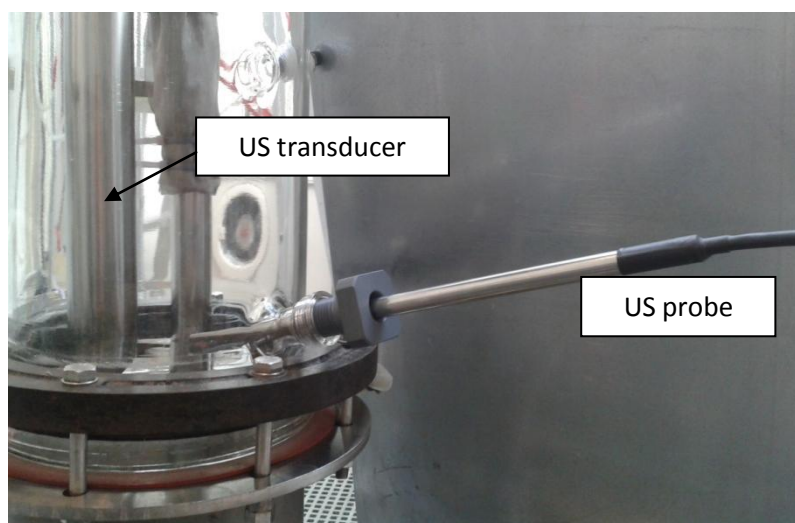

Fig 6.14 – Particular of sampling point to measure cavitation intensity

The Ultrasonic Energy Meter is able to split the ultrasonic field in two components: the sound energy and the cavitation collapse energies. In this way, the acoustic component (due to the compression and rarefaction waves) was removed, thus purging the overall signal given to provide the cavitation implosion energy.

Since the software details are part of the undisclosed instrument know-how, an indirect test was set to verify whether the instrument was really capable to measure the cavitation energy alone. The experiment consisted in carrying out a zero-signal test in silicon oil, according to the suggestion by Moholkar at al. [23]. They measured the cavitation energy by using a hydrophone and they demonstrated that cavitation cannot be measured in this type of fluids. The same result was obtained by using our cavitation measuring device.

According to the analysis of an acoustic field presented by Pierce [21] and to the investigations in mass transfer enhancement in textiles with US done by Moholkar and Warmoeskerken [22], the point where the maximum of pressure occurs is located at a distance of $\lambda/2$ from the emitting device, λ being the wavelength characteristic of a given frequency. That distance, for a 25 kHz wave in water medium at 25°C, corresponds to 30 mm. Moreover, from other mapping experiments, the researchers had identified the best region at a distance of about 15 mm from the transducer [24]. The maximum and minimum pressure peaks repeat themselves in space with a periodicity equal to $\lambda/2$ [22]. Keeping in mind the previous experiments, repeated US measurements at different distance were performed, starting from 15 mm and $\lambda/4$ periodicity until the maximum distance allowed by the reactor geometry: 15, 30, 45, 60, 75, 90, 105, 120 mm. Distances are taken from the US transducer surface to the US probe bottom as in Fig 6.15.
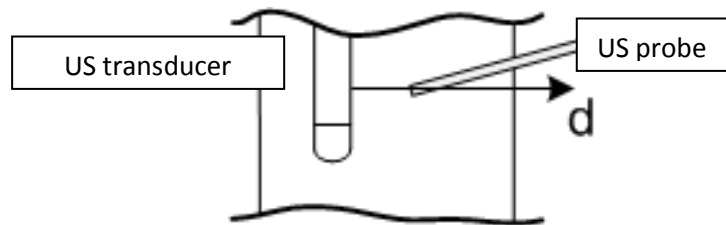
Fig 6.15 – Particular of the multi-task plant enlargement

Water in the vessel was at ambient condition. The fluid was re-circulated by a centrifugal pump to simulate the wastewater treatment hydraulics. The inlet flow come in through the vessel bottom.

Ultrasound power was fixed at two levels: 500 and 1000 W.

In the following graphs are reported relative power ultrasound intensity values (I_r) that are the ratio between the local power intensity values and the maximum value for all the trials (34 W/in^2)

Fig 6.16 shows the superficial intensity of cavitation referring to the liquid flow rate and to the maximum ultrasound power (1000 W).
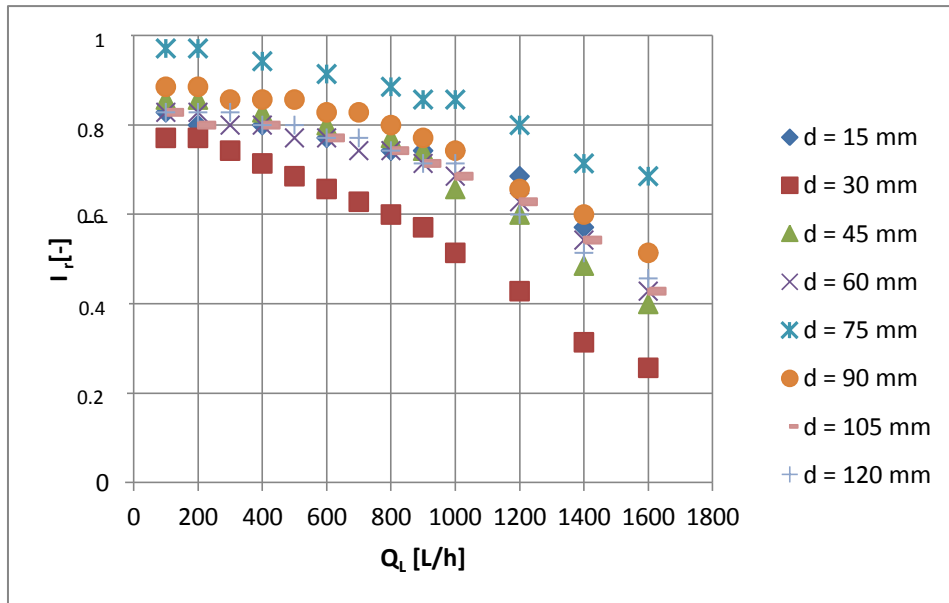
Fig 6.16 – Superficial power intensity vs liquid flow rate (US: P = 1000 W, f = 25 kHz)

Increasing flow rate, the superficial cavitation intensity decreases. In contrast to the conclusion of the previously cited authors, in this work the distance corresponding to maximum intensity is 75 mm. It can be even better observed in Fig 6.17. The data measured at different distances show the same trend with maximum and minimum intensity that repeat in particular positions. They have a sort of "sinusoidal" trend.

Displacement of the peak in comparison to the previous works, corresponding to the maximum intensity, may be due to the moving liquid. Moreover, the distance of 75 mm could be a characteristic of the reactor where the mean turbulent degree is lower than in other regions.
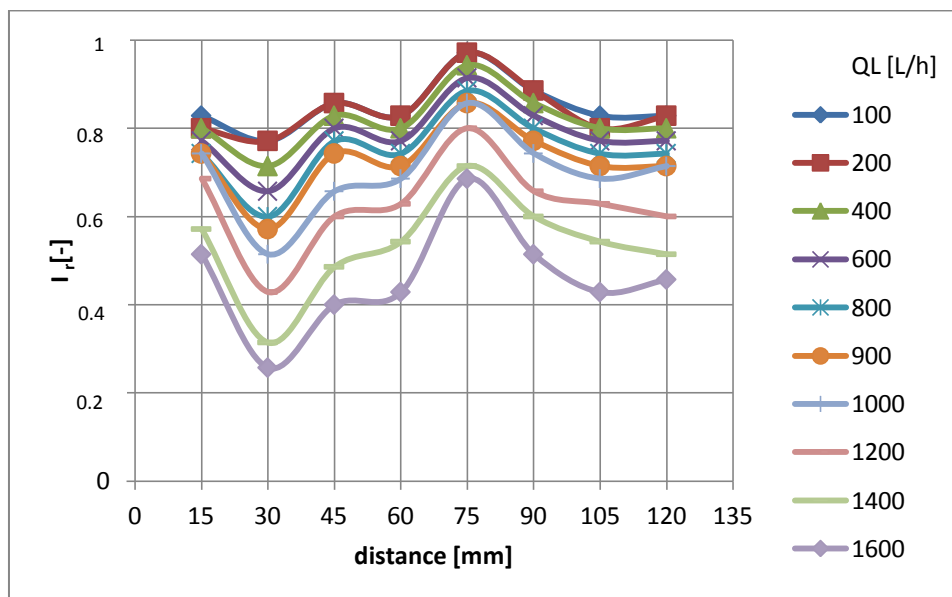
Fig 6.17 - Superficial power intensity vs distance transducer-probe (US: P = 1000 W, f = 25 kHz)

In the case of ultrasound power of 500 W, data are showed in the following graphs. In this case there is a particular flow rate value between 500 and 600 L/h that divided the

reactor space in two regions: high superficial intensity region and the low one region. Generally, a decrease in power supplied to the system corresponds to a lower superficial cavitation intensity.

Distance of 75 mm from the probe is the optimal distance in which the superficial intensity has its maximum value. For each flow rate, the trend of the values is always the same, but opposite of the P = 1000 W, pressure peaks are diminished in the low intensity region.

Fig 6.18 – Superficial power intensity vs liquid flow rate (US: P = 500 W, f = 25 kHz)

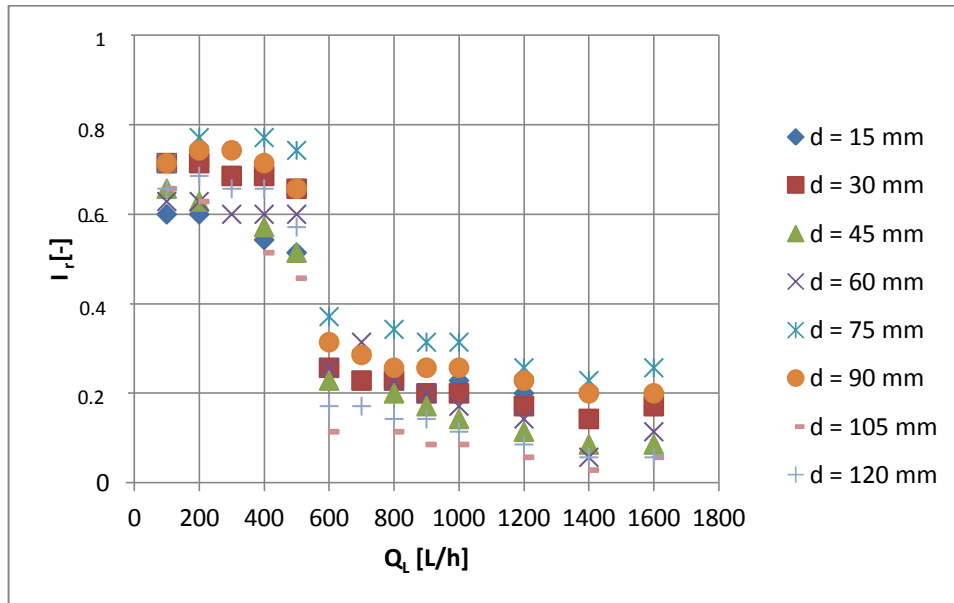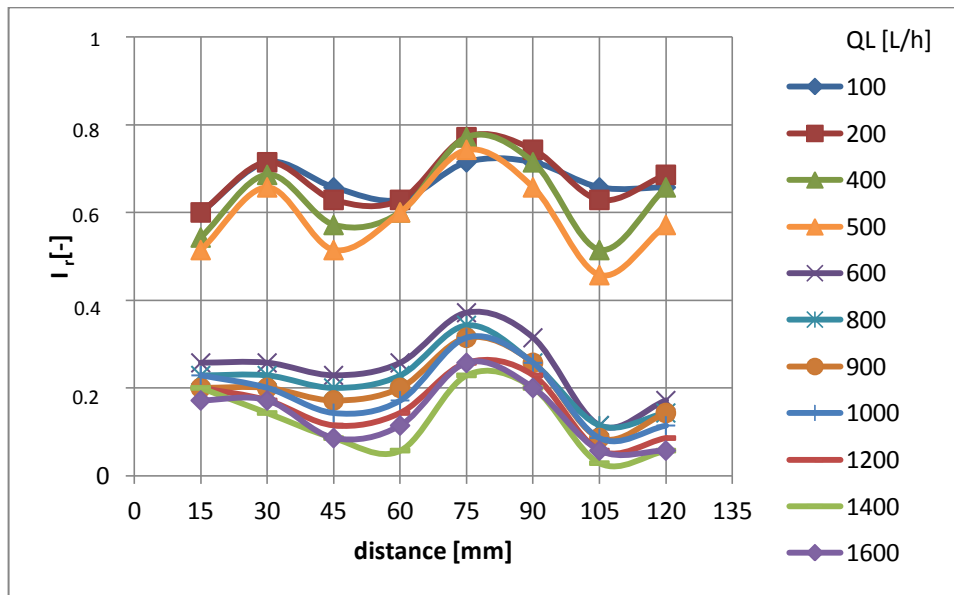Fig 6.19 - Superficial power intensity vs distance transducer-probe (US: P = 500 W, f = 25 kHz)

When air is supplied in the reactor, the cavitational intensity decreases, at the same time increasing mixing. Generally, curves trend are similar to the previous cases, but the intensity decreases of about 50%.

References

[1] C.E Brennen, Cavitation and bubble dynamics, *Oxford University Press*, 1995.

[2] L. Somaglino, G. Bouchoux, J. Mestas, C. Lafon, Validation of an acoustic cavitation dose with hydroxyl radical production generated by inertial cavitation in pulsed mode: Application to in vitro drug release from liposomes, *Ultrasonic sonochemistry*, **18**, 2011, 577-588.

[3] Fluid and particle mechanics, E.C. Lapples, *University of Delaware*, Newark, Delaware, chapter 5, 1951.

[4] M.T. Kandakure, V.G. Gaikar, A.W. Patwardhan, Hydrodynamic aspects of ejectors, *Chemical Engineering Science*, **60**, 2005, 6391-6402.

[5] V.K. Saharan, M.P. Badve, A.B. Pandit, Degradation of reactive red 120 dye using hydrodynamic cavitation, *Chemical Engineering Journal*, **178**, 2011, 100-107.

[6] T. Utomo, Z. Jin, M. Rahman, H. Jeong, H. Chung, Investigation on hydrodynamics and mass transfer characteristics of a gas-liquid ejector using three-dimensional CFD modelling, *Journal of Mechanical Science and Technology*, **22**, 2008, 1821-1829.

[7] N.H. Ince, G. Tazcanli, R.K. Belen, İ.G. Apikyan, Ultrasound as a catalyzer of aqueous reaction systems: the state of the art and environmental applications, *Applied Catalysis B: Environmental*, **29**, 2001, 167–176.

[8] P.R. Gogate, G.S. Bhosale, Comparison of effectiveness of acoustic and hydrodynamic cavitation in combined treatment schemes for degradation of dye wastewater, *Chemical Engineering and Processing*, **71**, 2013, 59-69.

[9] M. Giansetti, S. Sicardi, G. Rovero, F. Pastorelli, V. Ginevro, Cavitation energy mapping for ultrasound application in dyeing processes, *AUTEX Research Journal*, **1**, 2011, 246-250.

[10] Y.T. Shah, A.B. Pandit, V.S. Moholkar, Cavitation Reaction Engeneering, *Spriger*, New York, 1999.

[11] L.K. Doraiswamy, Organic Synthesis Engineering, First ed., *Oxford University Press*, New York, 2001.

[12] Y.T. Shah, A.B. Pandit, V.S. Moholkar, Cavitation Reaction Engeneering, *Spriger*, New York, 1999.

[13] P.R. Gogate, A.M. Kabadi, A review of applications of cavitation in biochemical engineering/biotechnology, *Biochemical Engineering Journal,* **44**, 2009, 60–72.

[14] P.R. Gogate, Application of cavitational reactors for water disinfection: Current status and path forward, *Journal of Environmental Management*, **85**, 2007, 801–815.

[15] S.J. McNeil, R.A. McCall, Ultrasound for wool dyeing and finishing, *Ultrasonic Sonochemistry*, **18**, 2011, 401–406.

[16] L. Liu, Y. Yang, P. Liu, W. Tan, The influence of air content in water on ultrasonic cavitation field, *Ultrasonic Sonochemistry*, **21**, 2014, 566-571.

[17] J. Rooze, E.V. Rebrov, J.C. Schouten, J.T. Keurentjes, Dissolved gas and ultrasonic cavitation - a review, *Ultrasonic Sonochemistry*, **20**, 2013, 1-11.

[18] J.L. Luche, C. Einhorn, J. Einhorn, J.V. Sinis Terra-Gago, Organic sonochemistry: a new interpretation and its consequences, *Tetrahedron Letters*, **31**, 1990, 4125-4128.

[19] C. Gong, D.P. Hart, Ultrasound induced cavitation and sonochemical yields, *Journal of the acoustic society of America*, **104**, 1998, 2675-2691.

[20] P.R. Gogate, A.B. Pandit, Sonophotocatalytic reactors for wastewater treatment: a critical review, *AIChE Journal*, **50**, 2004, 1051-1079.

[21] A.D. Pierce, Acoustics: An Introduction to its Physical Principals and Applications, *Acoustical Society of America*, New York, 1989.

[22] V.S. Moholkar, M.M.C.G. Warmoeskerken, Investigations in mass transfer enhancement in textiles with ultrasound, *Chemical Engineering Science*, **59**, 2004, 299-311.

[23] V.S. Moholkar, S.P. Sable, A.B. Pandit, Mapping the Cavitation Intensity in an Ultrasonic Bath Using The Acoustic Emission, *AIChE Journal*, **46**, 2000, 684-694.

[24] M. Giansetti, S. Sicardi, G. Rovero, F. Pastorelli, V. Ginevro, Cavitation energy mapping for ultrasound application in dyeing processes, *AUTEX2011 - 11th World Textile Conference*, 2011, 246-251.

[25] M. Ashokkumar, T.J. Mason, Encyclopedia of Chemical Technology, Sonochemistry, *John Wiley and Son*, 1998.

[26] R.S. Hiremath, V.M. Bhandari, V.V. Ranade, Hydrodynamic cavitation for degradation of Auramine O dye solution by vortex diode, *Annual Meeting AIChE*, 2013.

Chapter 7 – Bubble column reactor

7.1 Introduction

Bubble columns are mass transfer and reaction devices in which one or several components of a gas phase, in form of bubbles, get in contact and react with the liquid phase itself or with a component dissolved or suspended in it.

A bubble column reactor is a vertical cylinder where, in the bottom, the gas enters through a gas distributor (which may vary in design) and the liquid phase may be supplied in batch form or it may move with or against the flow of the gas phase (co-current or counter-current respectively). The top of the bubble column is often widened to facilitate gas separation [1].

The major advantages in the use of bubble column reactors are:
- very simple structure resulting in low cost;
- absence of moving parts;
- good heat and mass transfer properties;
- low energy input (only gas compression);
- high liquid phase residence time.

On the other hand, the disadvantages are:
- complicated hydrodynamic flow patterns;
- uncertainties in scale-up;
- short residence time of gas (determined by bubble rise velocity);
- volume demand increased due to back-mixing.

The continuous phase in bubble column is normally segregate. Longitudinal concentration differences depend on the mixing of the liquid phase, and the mixing of the liquid phase may require attention during bubble column design.

Longitudinal and radial mixing in bubble column are usually characterized by dispersion coefficients. The dispersion coefficient is the analogous to the diffusion coefficient in Fick's law. If diffusion coefficient is due to diffusive motion, dispersion

coefficient will arise by convective motion. Convective motion in liquid phase may be caused by:

- relative movement of the gas and liquid phase;
- bubble coalescence and break up;
- turbulence generated by the flow of liquid;
- movement of the liquid phase behind the rising bubbles and, consequently, return of the flow generated (back-mixing).

From articles found in literature [2-4], radial dispersion coefficients are normally in the order of 1 to 10% the value of longitudinal coefficient.

7.2 Flow regimes

The main important characteristics of bubble columns, such as phase hold-up, mixing and transport, depend on the flow regime in the column. In addition, bubbles dimension is function of the gas-liquid superficial tension and gas distributor.

Fig 7.1. shows two flow regimes according to the increase in gas flow rate in air-water system.
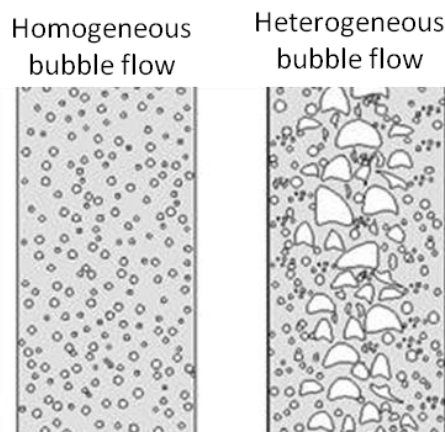
Fig. 7.1 – Operating state in bubble column

Homogeneous flow occurs at low gas flows: bubbles are uniformly distributed in the liquid and the size distribution is relatively well defined. However, this state is not maintained when gas passes more rapidly through the column. Bubbles aggregate and larger bubbles are formed, consequently these ones rise more rapidly than the small bubbles. This type of flow takes the name of churn-turbulent or heterogeneous regime and is quite common as a result of the high gas flow rate commonly adopted in industry. The detection of regime transition from homogeneous to turbulent flow and the investigation of the transition regime are important. As the transition takes place, significant changes can be observed in the hydrodynamic behaviour of the system. In heterogeneous regime, part of the gas is transported through the reactor in the form of large fast-ascending bubbles. The mass transfer coefficient is greater in the case of these larger bubbles, but the interfacial area does not increase and is not proportional to the

gas flow. Hence, the conversion of the gas phase reactant, in the heterogeneous operating range, is almost always below in comparison of the homogeneous zone [5].

The liquid flow patterns in bubble column reactors are complex. It is often assumed that large scale eddies with well defined circulation patterns are formed. The mechanism of liquid circulation is explained via the rising gas bubbles which contain liquid with them, this amount of liquid being considerably greater in bubble column reactors than that corresponding to the input liquid [6]. Continuity ensures that fluid returns down the column, producing a pronounced circulation pattern in which the central liquid is moving upwards and that next to the walls it moves downwards (Fig 7.2). This circulatory flux is depending on gas flow-rate, column diameter, cross-sectional shape, gas hold-up, bubble diameter, bubble rise velocity and liquid viscosity.
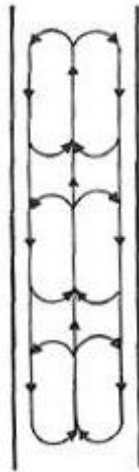
Fig. 7.2 – Example of liquid circulation patterns

7.3. Mixing in bubble column - hydrodynamics

The mechanisms responsible for the mixing in bubble columns are:
- turbulent eddies in the main liquid stream as well as eddies introduced by the movement of the dispersed gas phase related to the continuous liquid phase;
- liquid contained in the wakes of the bubbles combined with mass exchange between these wakes and the liquid phase;
- molecular diffusion.

During experiments, it is difficult to distinguish the contribution from each individual mechanism. Therefore, simplified models, such as the one dimensional axial dispersion model, are often assumed to represent the overall mixing phenomena. Dispersion may be defined as the spreading of fluid particles, as a result of the departure from ideal plug flow conditions. The fluid particles move forward in the direction of overall flow, but at different speeds, thus resulting in different residence times. The dispersion occurring in a direction opposite to the main flow, such as that occurring in bubble columns, is commonly known as back-mixing.

Back-mixing in bubble column reactors is affected both by superficial gas velocity and column diameter. Back-mixing influences the residence time distribution in the reactor and thus influences the reaction yield and selectivity. Liquid back-mixing can be reduced by incorporating partition plates in order to section the column.

The wanted degree of dispersion may be obtained from tracer experiments such as residence time distribution function (RTDF) studies and batch liquid mixing tests.

It is common to use the axial dispersion model (ADM) to describe liquid phase mixing in bubble column reactors. In the ADM a lumped dispersion parameter E_z is used to represent the degree of back-mixing. The higher is the value of E_z, the greater will be the degree of back-mixing in the reactor.

Mathematically, the axial dispersion model in the longitudinal z-direction is given by [3]:

$$\frac{\partial C}{\partial t} = E_z \frac{\partial^2 C}{\partial z^2} - u_L \frac{\partial C}{\partial z}$$

with t as time, u_L the superficial liquid velocity based on an empty reactor volume and E_z the liquid dispersion coefficient.

The assumptions of the ADM are:
- negligible radial dispersion;
- plug flow with constant velocity;
- no stagnant pockets;
- no bypassing or short-circuiting of fluid in the vessel.

7.3.1. Boundary conditions

The analysis and measurement of residence time distribution experiments are subject to many errors:
- experimental errors in the tracer measurements;
- mathematical errors in the analysis of the tracer response measurements;
- application of wrong boundary conditions.

The solution of ADM depends on the applied boundary conditions. The correct boundary conditions depend on the inlet and outlet stream of the investigated system. Two types of boundary condition can be identified in literature [10]: open and close. In the first case, the molecules of the tracer pass the boundary several times in opposite directions, therefore allowing them to spend some time outside the reactor. On the contrary, in the second case, the molecule can pass the boundary only once.

In general, four boundary configurations are possible: open-open, closed-closed, open-closed and close-open boundaries. Such as example, in Fig 7.3 are reported the graphical representation of open-open and closed-closed boundary conditions.

Obviously, wrong dispersion coefficients can be obtained if boundary conditions are wrong.
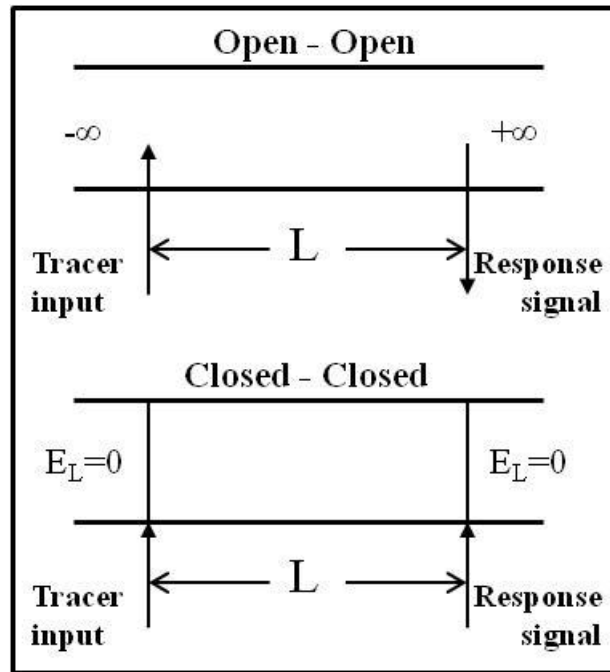
Fig. 7.3 Example of two boundary conditions

7.3.2. Tracers characteristics

Choosing the correct tracers is important in order to understand the real behaviour of the system investigated.

The selection of the tracer must meet the following specification:

- be easily detectable;
- not change the hydrodynamics within the vessel;
- no tracer transfer between phases;
- no reaction between the substances present in the reactor.

The common tracers used in literature are electrolytes, concentrated acids and dyes. They are easy to detect and the changing tracer can be measured, respectively, by simple analyses on conductivity, pH and spectrophotometry.

In literature other tracer techniques, which use heat and radioactive particles as tracer, are described.

7.3.3. Residence time distribution functions (RTDF)

In general, in order to predict the behaviour of a vessel as a chemical reactor, knowledge of the passage of the fluid through the vessel is required. The distribution of molecules residence times within the reactor can be determined by the stimulus-response technique. In this technique, a quantity of tracer is injected into the inlet feed of the reactor and its resulting exit concentration profiles monitored in time.

Analysing the response of tracer injection, information on the behaviour of the system are provided. Each element of the fluid, taking different routes through the reactor, may take at different time to pass through the vessel. The exit age distribution $E(t)$ is the function that describes the distribution times for the stream of fluid leaving the vessel.

$E(t)$ is also called residence time distribution function (RTDF) and has the units of time^{-1}.

E is defined in such a way that $E(t)dt$ is the fraction of material in the exit stream with age between t and $t + dt$.

Related with $E(t)$, there is the function $F(t)$. It is the fraction of the fluid that leaves the reactor with an age time $0 < t < t_1$

$$F(t) = \int_0^{t_1} E(t)dt$$

Both the $E(t)$ and $F(t)$ functions are normalized.

The tracer input signal may be step, pulse or periodic injection. The stimulus-response technique determines the form of the response of the tracer at the reactor exit. To simplify the residence time distribution analysis, step tracer and pulse (Dirac function) inputs are generally preferred.

The advantage of a pulse test is that the output response is identical to the RTDF function $E(t)$. Nevertheless, using pulse it is often difficult to inject tracer rapidly enough so that it is approximates a pulse; moreover, an accurate measurement of the low concentrations in the tail of the concentration curve becomes quite difficult as time increases.

The second common method consists in a step injection of tracer. Compared to the pulse method, it is easy to generate a step change of concentration. However, the residence time distribution function must be obtained by numerical differentiation of the $F(t)$ curve. In this way, inherent error could be added and, consequently, it will be less accurate than with pulse test. Another problem arisen after long times, in the case in which C/C_0 is about 1, is that measurement problems became significant.

In the periodic injection method, the main problems are related to the generation of periodic concentration fluctuations.

The study of RTDF curves is important for different aspects:
- in heterogeneous systems, the RTDF may be used directly for design;
- comparison of RTDF in vessels of the same type but different size gives an indication of the effect of scale-up on flow properties;
- comparison of RTDF determinates a mathematical model of the system, useful to analyse the existence of dead space and bypassing;
- understanding if in the reactor there are dead regions or by-passing.

Dead space region are zones in the vessel in which the fluid resides for a time considerably longer than the overall mean residence time of the fluid actually flowing through the system. If $E(t)$ has a very long tail, this indicates that the fluid entering the dead space leaves only very slowly.

Bypassing refers to a condition in which some fluid elements pass through the vessel much more rapidly than others: this means that there is a fraction of the fluid spending a time considerably shorter than the overall mean residence time of the fluid.

If there is a large dead space or significant bypassing, there is no clear distinction between them.

For a single fluid, under steady-state flow, without reaction and without density change, the mean residence time of the fluid in a vessel of volume V and length L is given by:

$$\tau = \frac{V}{\dot{Q}} = \frac{L}{u}$$

where $\dot{Q}$ is the volumetric flow-rate of the fluid under consideration and u is the mean fluid superficial flow rate.

7.3.4. Determination of characteristics parameter from RTDF curve

From a concentration vs time curve is possible to define some parameters:
- the exit age distribution $E(t)$

$$E_i(t_i) = \frac{C_i}{\sum C_i \Delta t_i}$$

- the first moment of the RTDF curve or mean residence time μ:

$$\mu = M_1 = \frac{\int_0^\infty tE(t)\,dt}{\int_0^\infty E(t)\,dt} = \frac{\sum t_i C_i \Delta t_i}{\sum C_i \Delta t_i}$$

- the second moment of the RTDF curve or variance σ^2 (it measures the spread of the distribution from the mean value)

$$\sigma^2 = M_2 = \frac{\int_0^\infty (t-\mu)^2 E(t)\,dt}{\int_0^\infty E(t)\,dt} = \frac{\sum (t_i - t)^2 C_i \Delta t_i}{\sum C_i \Delta t_i}$$

7.4 Longitudinal mixing parameter estimation – E_z

7.4.1 Batch liquid

Mixing parameter E_z is calculated using non steady state stimulus response. This method has been utilised extensively in literature. Ohki and Inoue [3] is a well cited paper. Mixing time measurements, where the time required to reach a specific level of concentration uniformity, are used to obtain liquid dispersion coefficients. The term mixing is used here to denote movement, distribution or diffusion of a component through a reaction vessel, tending to make a fluid composition thoroughly uniform. In batch mixing experiments, a tracer is injected as a pulse into the batch liquid phase (at the top of the column) and the resulting concentration is measured at different distance from the feed point position (Fig 7.4).
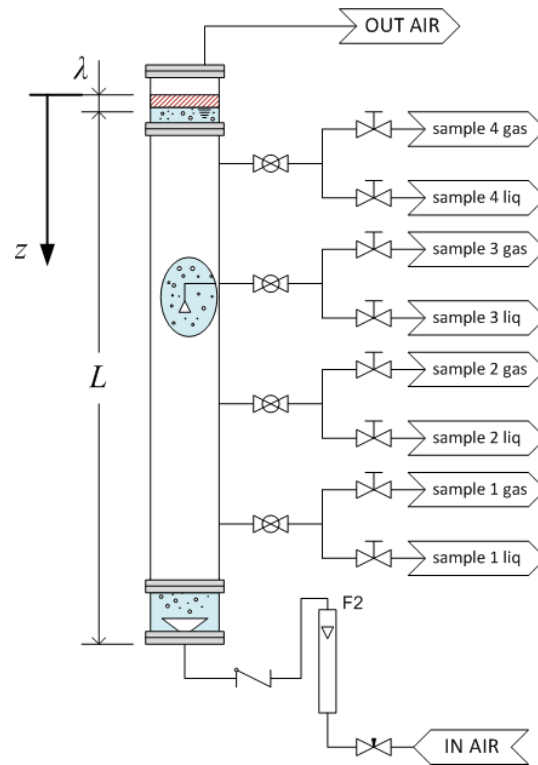
Figure 7.4 – Graphical representation of the model

The one dimensional axial dispersion model (ADM) may be used when the distance between the injection point of tracer and the measuring points are sufficiently long. The longitudinal dispersion coefficient E_z is used to express the characteristics of the liquid mixing in bubble columns. The mathematical description of the spreading of the tracer is described in analogy to Fick's second law, where the convective term $(u_L \, {\partial C}/{\partial z})$ is null because batch liquid:

$$\frac{\partial C}{\partial t} = E_z \frac{\partial^2 C}{\partial z^2} \tag{7.1}$$

with closed-closed boundary conditions:

$$\frac{\partial C}{\partial z} = 0 \text{ at } z = 0 \ \ z = L$$

The initial conditions are:

$$
\begin{aligned}
t = 0 \qquad & C = C_0 \qquad & 0 \leq z < \lambda \\
t = 0 \qquad & C = 0 \qquad & z > \lambda
\end{aligned}
$$

where λ is the height of the column corresponding to the volume of tracer injected at the top of the column (during the experimental test the tracer was introduced by an almost-pulse).

Solution Eq. 7.1, considering initial and boundary conditions, gives:

$$\frac{C}{C_{eq}} = 1 + \frac{2L}{\pi\lambda} \sum_{n=1}^{\infty} \left(\frac{1}{n} \sin\left(\frac{n\pi}{L}\lambda\right) \cos\left(\frac{n\pi}{L}z\right) e^{-\left(\frac{n\pi}{L}\right)^2 E_z t} \right) \qquad (7.2)$$

where

$$C_{eq}L = C_0\lambda$$

for a final uniform distribution of the tracer.

When $n\lambda \ll L$, the Eq. 7.2 gives the following approximate form

$$\frac{C}{C_{eq}} = 1 + 2 \sum_{n=1}^{\infty} \left(\cos\left(\frac{n\pi}{L}z\right) e^{-\left(\frac{n\pi}{L}\right)^2 E_z t} \right)$$

Ohki and Inoue determined that six terms are sufficient to evaluate E_z with an error under one per cent.

The relation between C/C_{eq} and the argument of the exponential term gives the plot shown in Fig. 7.5. The curve parameter is the ratio z/L.

sample	z/L
4	0.20
3	0.44
2	0.67
1	0.91
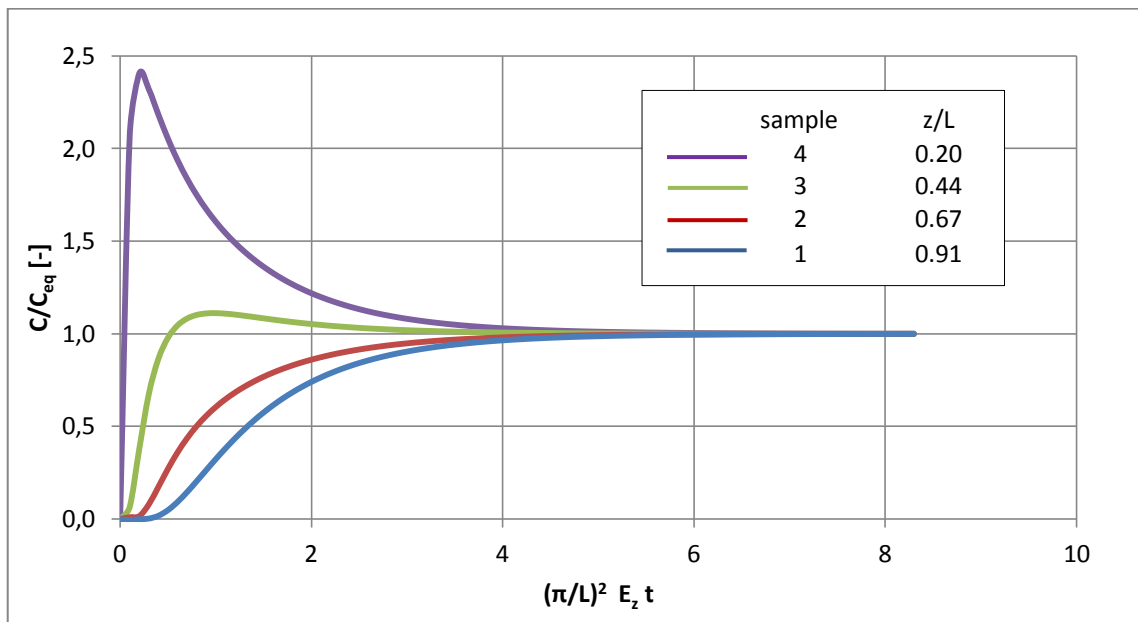
Figure 7.5 – Tracer response curve derived from the dispersion model

7.4.2 Continuous liquid

The residence time distribution can be recorded when the liquid phase passes continuously through the reactor and from this the dispersion coefficient can then be calculated using an appropriate model for the liquid phase.

The one-dimensional axial dispersion equation for the system is [6]:

$$\frac{\partial C}{\partial t} = E_z \frac{\partial^2 C}{\partial z^2} - u_L \frac{\partial C}{\partial z} \qquad (7.3)$$

If dimensionless parameters are introduced, the above Eq. 7.3 becomes

$$\frac{\partial \mathcal{C}}{\partial \theta} = \frac{1}{Bo_L} \frac{\partial^2 \mathcal{C}}{\partial Z^2} - \frac{\partial \mathcal{C}}{\partial Z} \tag{7.4}$$

where

$$\mathcal{C} = C/C_0$$
$$Z = z/L$$
$$\theta = t\, u_L/L$$
$$Bo_L = L\, u_L/E_z$$

When the tracer substance is introduced in the reactor as a Dirac pulse at the inlet, the boundary conditions are:

$$\theta < 0\ (t < 0) \qquad Z \in [0,1] \qquad\qquad \mathcal{C} = 0$$
$$\theta < 0\ (t < 0) \qquad Z = 0 \qquad \delta(\theta) = \mathcal{C} - \frac{1}{Bo_L}\frac{d\mathcal{C}}{dZ}$$
$$\theta > 0\ (t > 0) \qquad Z = 1 \qquad \frac{d\mathcal{C}}{dZ} = 0$$

The axial-dispersion equation with dimensionless parameters and the appropriate boundary condition, is solved by Laplace's transformation and the solution in the Laplace space is:

$$\mathcal{C}(\theta, Z) = e^{(Bo_L/2)Z} \sum_{k=1}^{\infty} R_k e^{s_k \theta}$$

where

$$R_k = \frac{2\phi_k \cos\phi_k (1-Z) + \phi_k Bo_L \sin\phi_k (1-Z)}{\phi_k (2 + Bo_L)\sin\phi_k - [(Bo_L^2/4) + Bo_L - \phi_k^2]\cos\phi_k}$$

$$\tan\phi_k = \frac{4\phi_k Bo_L}{Bo_L^2 - 4\phi_k^2}$$

$$s_k = -(\phi_k^2 + \frac{Bo_L^2}{4})/Bo_L$$

The dispersion coefficient E_z can be calculated using the residence time distribution curves. Van der Lann and Aris have shown that there are correlations between the moments from RTDF curves and transfer function (solution in Laplace space) by the following formulae:

$$M_1 = \mu = -\lim_{s \to 0} \frac{d\mathcal{C}'(s)}{ds}$$

$$M_2 = \sigma^2 = -\lim_{s \to 0} \frac{d^2 \mathcal{C}'(s)}{ds^2} - \mu_1^2$$

where M_1 and M_2 are respectively the first and the second moments of RTDF function, and $\mathcal{C}'(s)$ is the function solution in the Laplace domain.

Following, the Eq. 7.4 that introduces the standardization of some parameters, it follows that

$$\int_0^\infty \mathcal{C} d\theta = 1$$

the first moment (mean value) is given by

$$\mu = \int_0^\infty \mathcal{C} \theta d\theta$$

the variance of the distribution (second moment) is calculated as follows

$$\sigma^2 = \int_0^\infty \mathcal{C} (\theta - \mu)^2 d\theta$$

In conclusion, the first moment of the reactor model close on both sides is

$$\mu = 1$$

and the variance is

$$\sigma^2 = \frac{2}{Bo_L} - \frac{2}{Bo_L^2} (1 - e^{-Bo_L}) \tag{7.5}$$

Bodenstein's number and so E_z can be calculated from the variance of the RTDF curves.

7.5 Experimental measurements of the axial dispersion coefficient E_z

As said in the previous paragraphs of this chapter, longitudinal dispersion coefficient is used as a parameter to evaluate the longitudinal mixing. Two different models are used as a result of the hydrodynamic condition in which the column works. In the case in which mixing is given only by gas flow, Eq. 7.1 is used when both gas and liquid flow are present the model is based on Eq. 7.3.

The experiments were done using dye as tracer. In this work, two dye tracers are used: Methylene Blue and Acid Red CI 249.

Methylene Blue is a pure dye, that means there are no bulking agents mixed with it. Bulking agents are all the chemical substances introduced by the industrial producers to confer to dye specific characteristics in favour of dyeing processes optimisation (e.g. surfactants or inertial materials).

Acid Red CI 249 is an industrial dye and there are bulking agents in it. Acid Red cannot be considered in good agreement with the specification described above (paragraph 7.3.2) because surfactants form foam, especially if aerated. In this way, fluid-dynamic can be influenced by it. On the other hand, the tests with this dye may be useful to understand the real behaviour of the system as occurs in textile wastewater treatment application.

The tracers are introduced from the top of bubble column, simulating a pulse, in agreement with the paragraphs 7.4.1 and 7.4.2.

In all the experiments, 50 ml of dye solution were introduced. They correspond to an equivalent height $\lambda = 6.4$ mm and the ratio between tracer equivalent height and liquid total height is 1:500. The dye concentrations are 0.7 g/L for Methylene Blue and 5 g/L for Acid Red. These values are in agreement with a good spectrophotometric analysis.
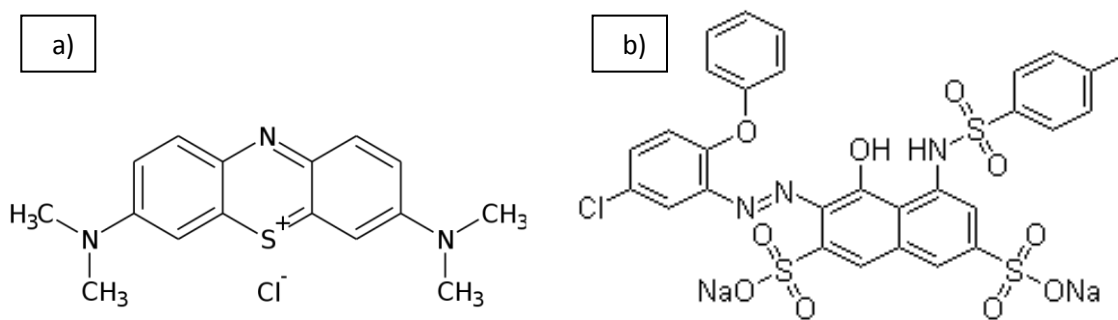

Fig 7.6 – a) Methylene Blue and b) Acid Red C.I. 249 molecular formula

In chapter 5 was described bubble column reactor and its sample ports along the reactor wall used to detect liquid samples. The highest port took number 4 and the lower number 1.

To determine the global longitudinal dispersion coefficient of the column, only the concentration values from sample 1 and 2 were considered. As shown in [3], the distance between the injection tracer point and the measuring point must be sufficiently long not to have a negative interaction with the motion created by tracer introducing. Then, the Ez average value is calculated by minimal square regression from concentration measurements by 1 and 2 sample points.

7.5.1 Longitudinal dispersion coefficient E_z - liquid batch, gas continuous

The aim of the following experiments is to define the transport mechanisms involved in bubble column in the liquid phase. Therefore, salt concentration, superficial gas velocity and tracer types are the main parameters of each study.

7.5.1.1 Effect of liquid coalescence and tracer type

As an example, in Fig 7.7 some graphs in reference to non coalescence media are reported. In each graph the experimental values and the best curve that fits the experimental data (Model) are reported. The parameter of the model is the dispersion

coefficient and it is calculated thanks to square minimum method. The model is in good agreement with the experimental point and the average error is 5%.
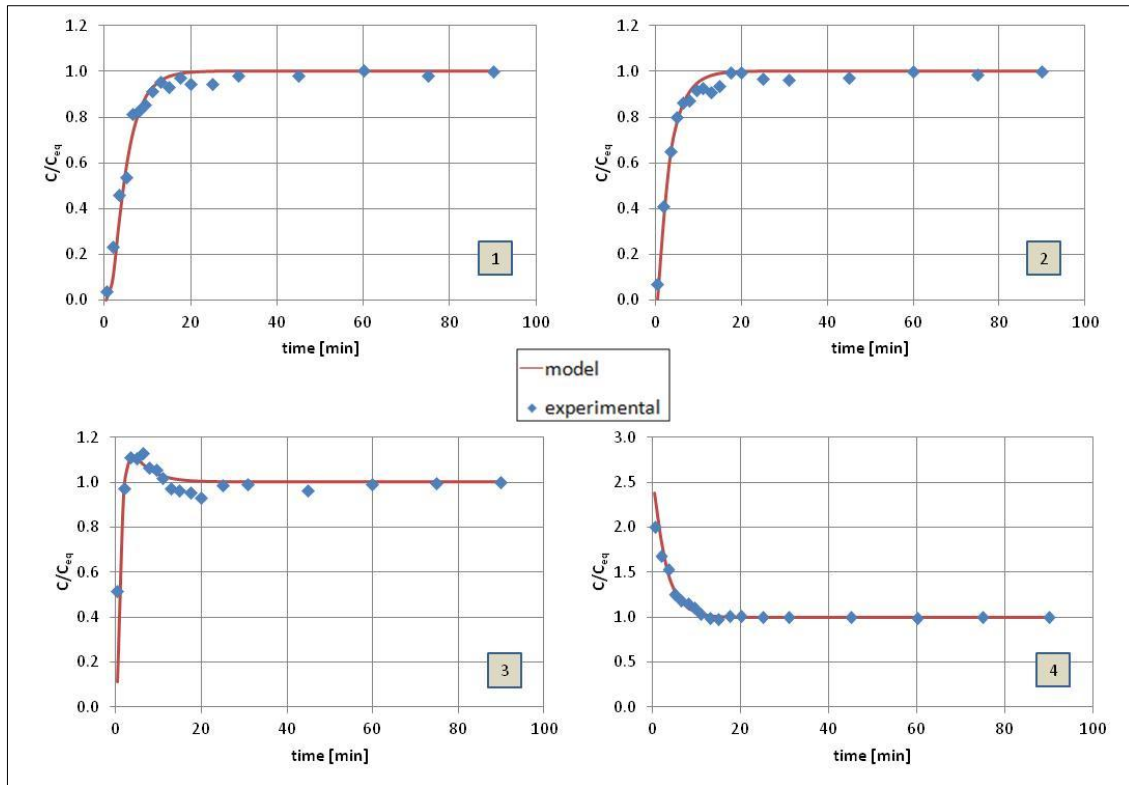
Fig 7.7 – The model line and experimental data for each sample point (no coalescent fluid)

Bubble coalescence can change, in a great way, the transport mechanism of the tracer in the reactor and consequently its fluid-dynamic. Therefore, salt is added in the solution to simulate no coalescence liquid media. In this way, bubbles coalescence probability is lower and bubbles have similar diameter along the bubble column. When only tap water is used, bubbles may increase in diameter along the column due to the coalescence phenomena.

In Fig 7.8 the concentration trends using the tracer Methylene Blue in no coalescent (a) and coalescent (b) condition are reported. No coalescence condition is guaranteed with a NaCl concentration of 10 g/L. The gas flow rate is imposed to 100 L/h, which corresponds to a mean superficial velocity of $3.54 \cdot 10^{-3}$ m/s.
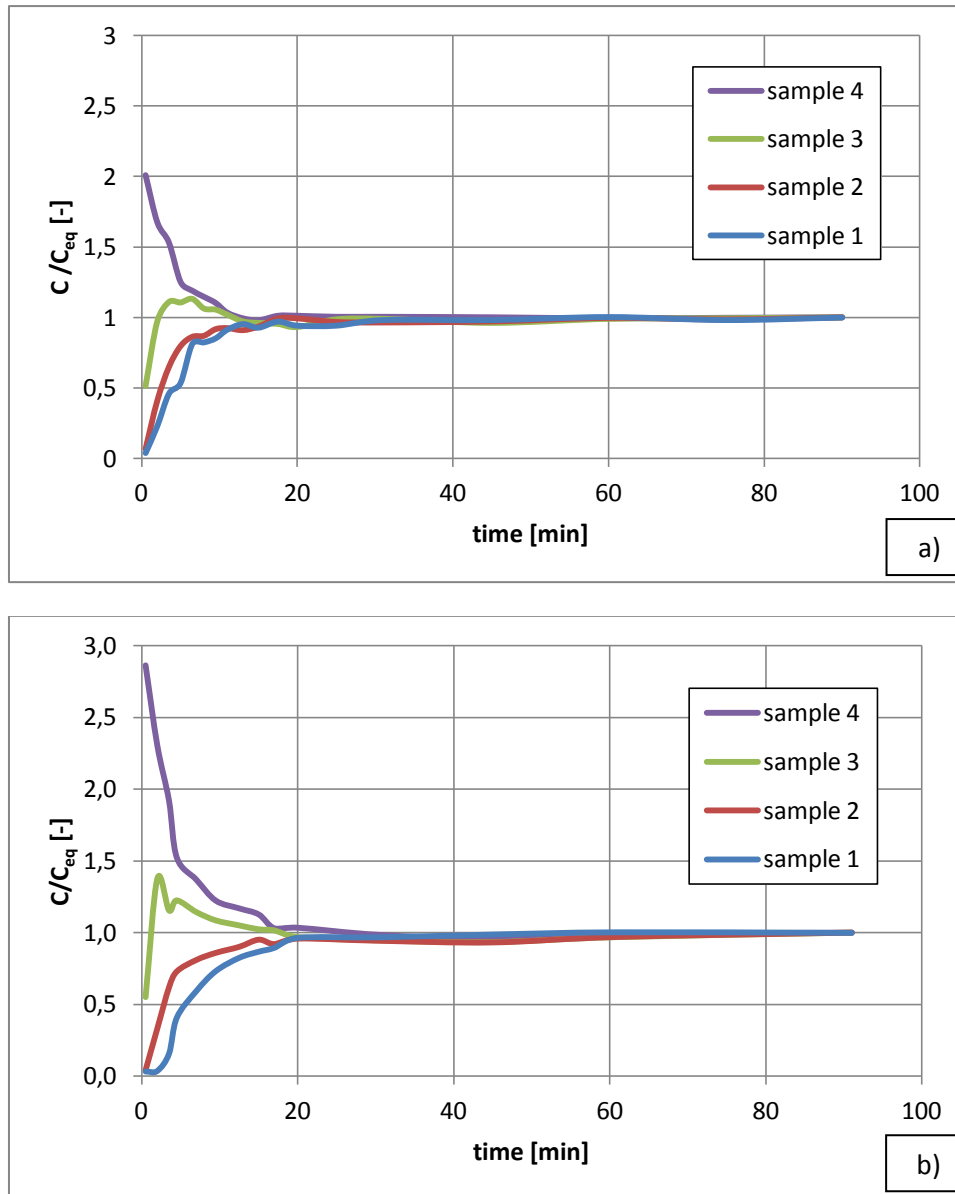
Fig 7.8 – Concentration trend Methylene Blue: a) NaCl 10 g/L b) no salt content

The column reaches the equilibrium concentration just after 15 min in no coalescence media and about 10 min after in the other case.

The calculated dispersion coefficients are listed in the following table.

Table 7.1 Dispersion coefficient

Sample point	E_Z [m^2/s] coalescence	E_Z [m^2/s] no coalescence
1	$3.49 \cdot 10^{-3}$	$5.14 \cdot 10^{-3}$
2	$4.35 \cdot 10^{-3}$	$5.40 \cdot 10^{-3}$
3	$6.93 \cdot 10^{-3}$	$4.30 \cdot 10^{-3}$
4	$8.93 \cdot 10^{-3}$	$5.88 \cdot 10^{-3}$

The average dispersion coefficient are respectively $3.72 \cdot 10^{-3}$ and $5.16 \cdot 10^{-3}$ m^2/s in the case of coalescence and no coalescence liquid media. These values are calculated with the contribution of the dispersion coefficients of sample 1 and 2. The other samples are too close to injection point.

These experiments show that the main dispersion mechanism is due to convective motion caused by bubbles. The smaller are the bubbles, more intense are the convective bubbles motion and consequently tracer dispersion. No foam is formed on the top of bubble column in consequence of pure dye tracer.

Changing the tracer type and maintaining the same gas flow rate, the transport mechanism is not so easy to describe because lots of phenomena occur. Using Acid Red as tracer, Fig 7.9 describes the trend of its concentration, again in the case of coalescence or no coalescence condition.

In coalescence condition the equilibrium concentration is reached in about 25 min. From the experimental point, it was possible to calculate longitudinal dispersion coefficient: the average value is $4.8 \cdot 10^{-3}$ m^2/s. However, the experimental line doesn't converge to the equilibrium value in a clear way, in comparison to the homologous lines in Fig 7.9 b. The reason is that no persistent foam was formed in the top column. Using an industrial tracer, dye is not pure but there are also some bulking agents. Therefore, the liquid is not able to be considered as completely coalescent but in a status between coalescence and no coalescence: it is a pseudo coalescence media. In this condition the tracer motion to the column bottom is more complicated. In other words, there are two types of foam. The first one is on the liquid surface and it segregates the tracer and the second one is the foam created by bubbles wake that hinders the transport mechanism to the column lower part. Therefore, it is possible to suppose that longitudinal dispersion coefficient decreases in favour of the radial one.

This phenomena is even more evident in the case in which salt is used to have no coalescence condition in presence of Acid Red as tracer (Fig 7.9 a). The graphs can be divided in three parts and each of them represents a particular type of tracer transport:

- *First part from 0 to 15 min*
  The tracer concentration is high and the main transport mechanism is due to longitudinal dispersion: the trace was transported from the top to the column bottom.

- *Second part from 15 to 90 min*
  In this region, the concentration decreases even under equilibrium concentration (from 15 to 60 min) and go back at the same initial level. This is due to the superficial foam. Foam segregates tracer and consequently decrease its concentration in the mean liquid phase. Tracer segregation is due to a decrease in the superficial tension in the foam and probably by the formation of dye micelle. Obviously, at the initial time, the concentration is higher at top liquid and so the foam segregates tracer. After that, probably diffusive and convective motion increases and the tracer is transported along the column.
  A simple experiment is carried out in order to verify this affirmation; the results are reported in Fig. 7.10.

Air was bubbled into a becker containing a water solution composed of NaCl (10 g/L) and Acid Red (5 g/L). The foam liquid and the solution concentration were detected during time.

After 15 min, the concentration of foam was about four times greater than the bath initial concentration.

- *Third part from 90 min to the end*

In this region, a sort of stable equilibrium is established, but the concentration is not equal on the column: lower concentration at the bottom and higher concentration at the top. Probably the bubble wake are responsible for column dye non-uniformity, because radial dispersion coefficient may be predominant on longitudinal one. This being said, this is typical for a plug flow system.
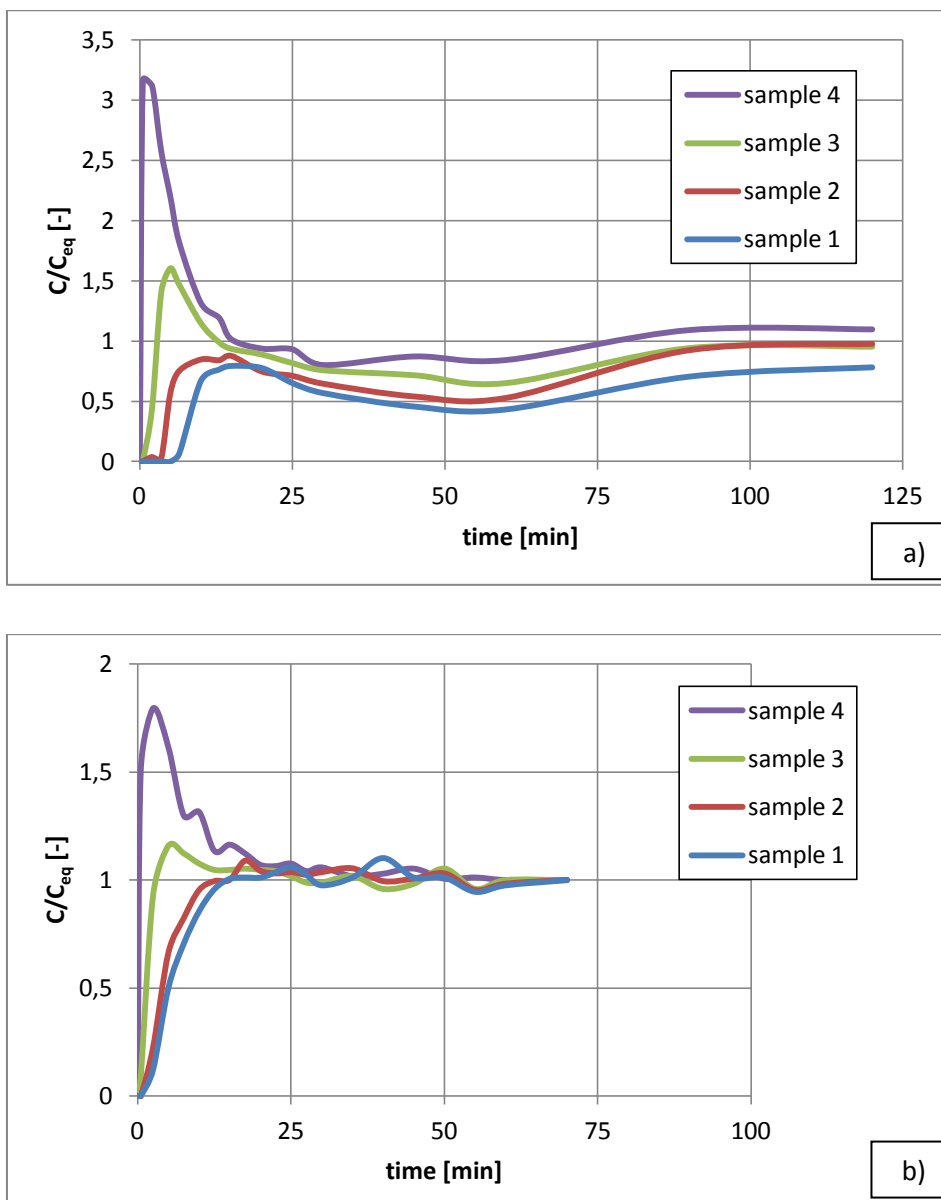
Fig 7.9 – Concentration trend Acid Red, Qg = 100 L/h: a) NaCl 10 g/L b) no salt content
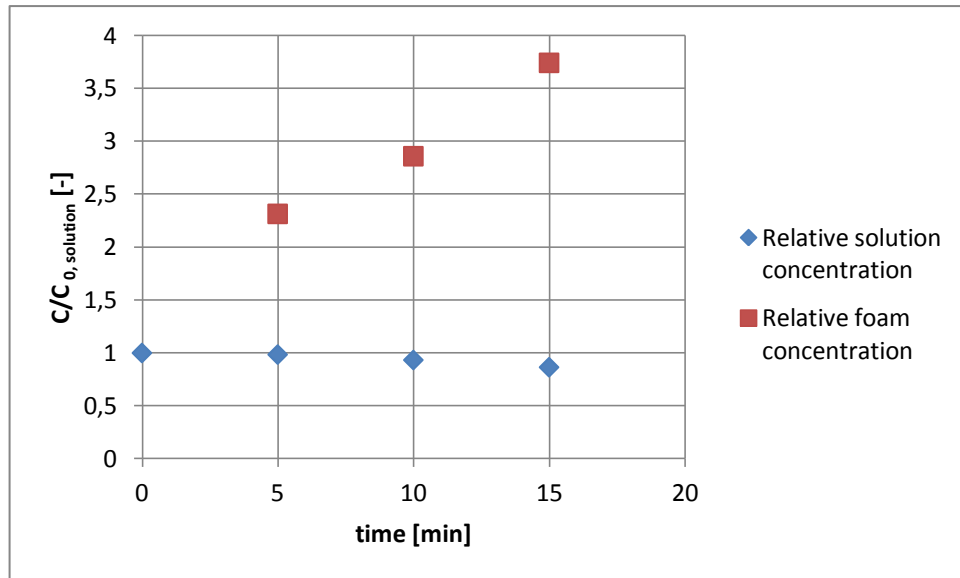
Fig 7.10 – Foam tracer segregation

7.5.1.2 Effect of gas superficial velocity

Increasing gas flow rate, column dispersion behaviour change. Considering a pseudo coalescence liquid (by adding the bulking agents of the Acid Red tracer) and gas flow rate equal to 100 and 400 L/h (respectively $u_g = 3.55 \cdot 10^{-3}$ and $1.42 \cdot 10^{-2}$ m/s) the liquid concentration samples are reported in Fig 7.11.
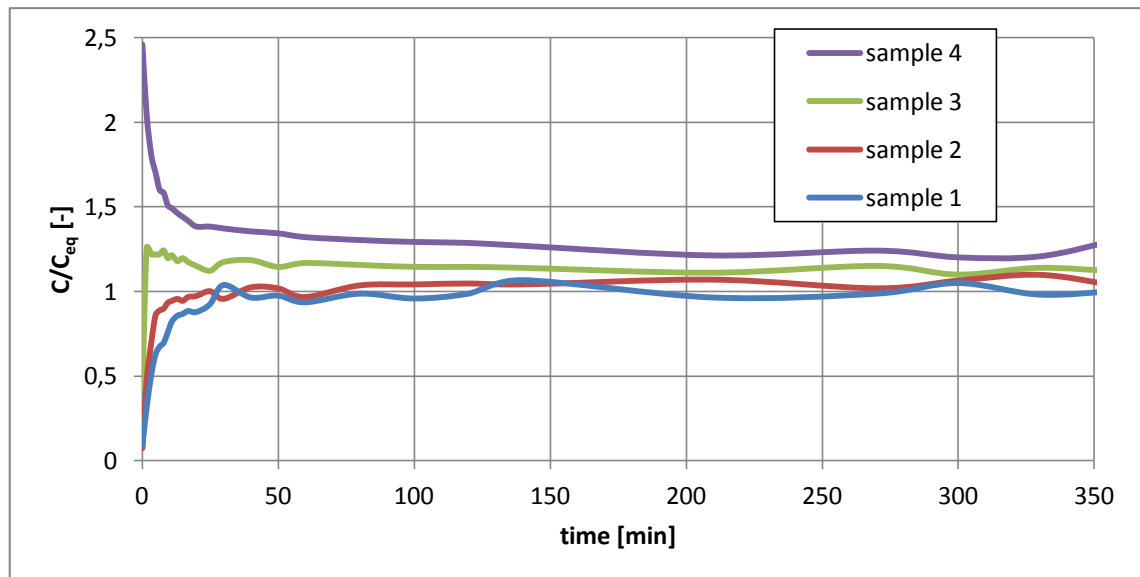
Fig 7.11 – Concentration trend Acid Red, pseudo-coalescence media, $Q_g = 400$ L/h

Comparing the trends of the experimental data of graph Figg 7.11 and 7.9b, superficial gas velocity increases of four magnitude orders. In this condition, non-persisting foam increases its action while longitudinal dispersion decreases. In this case, the foam that has greater influence is created by wake bubbles. Therefore, in this situation radial

dispersion behaviour is improved rather than longitudinal one. This is the consequence of the fact that concentration equilibrium along the column is not reached in all the height and the concentration in each section is quite constant for long time, more than 6 hours.

7.5.1.3 Effect of circulation patterns, gas diffuser

As mentioned in paragraph 7.2, lots of circulation patterns may be involved in the bubble column. Among them, the type of gas diffuser can change the mixing along the column.

The previous experiments were conducted using a sinterized gas distributor, as showed in the picture in Chapter 5. It generates bubbles with diameter approximately of 4 mm and the gas dispersion is quite uniform in the column section.

To understand what happened when bubbles are introduced in an inhomogeneous manner, another gas distributor is implemented. It consists of a single tube (ID 2 mm) positioned 40 mm distance from the symmetric axis.

Therefore, it is immediately evident that the mixing changes completely in comparison with the sintered gas diffuser.

The experiments were conducted used Acid Red as tracer.

Table 7.2 – Single tube gas diffuser

Sample point	E_Z [m^2/s] sinterized glass	E_Z [m^2/s] single tube
1	$3.49 \cdot 10^{-3}$	$7.73 \cdot 10^{-3}$
2	$4.35 \cdot 10^{-3}$	$7.83 \cdot 10^{-3}$

The dispersion coefficient values obtained using the two diffuser systems are much different: the single tube diffuser values are about twice greater than the sintered glass diffuser ones.

This is due to the liquid mixing generated by a column of bubbles, opposite to the homogeneous distribution of bubbles generated using the two gas diffusers.

Using the single tube diffuser, the gas flow generated a strong longitudinal upward liquid motion and consequently an extreme mixing condition.

7.5.1.4 E_z as a function of gas velocity and diffuser systems

The main data obtained from the above experiments are reported in Fig 7.12. The first characteristic to outline with respect to data is the dotted curve trend. Increasing gas flow rate up to 100 L/h, dispersion coefficient increase, but at 150 L/h it drops off and increases again.

This strange behaviour was caused probably by bubbles non homogeneity along the section area of the column. Strictly connected to this is the problem of bubbles coalescence and so the increase in rise velocity for particular gas flow rate.

Empirical correlations are found in literature in order to calculate longitudinal dispersion coefficient. Usually it is defined using three parameters: d (reactor diameter),

g (gravitational acceleration) and u_g (superficial gas velocity based on the reactor section). Among other Camacho Rubio [4] (Eq. 7.6) and Miyauchi [2] (Eq. 7.7) correlations [12] were found to fit the data.

$$E_Z = 0.301 \, d^{3/4} (g u_g)^{1/3} \qquad (7.6)$$
$$E_Z = 0.5 \, g^{1/4} \, d^{5/4} \, u_g^{\ 1/2} \qquad (7.7)$$

Both correlations seem to approximate only one part of the data. So this means that in the column different fluid-dynamic conditions exist, changing the gas flow rate. In other words, the empirical correlations were defined according to the experimental condition. Consequently, also in our column the changing flow rate changes the dispersion coefficient because lots of phenomena occur contemporarily.

Gas diffuser can be regarded as one of the possible causes: the fritted glass distributor spreads homogeneously only for high gas flow rate.
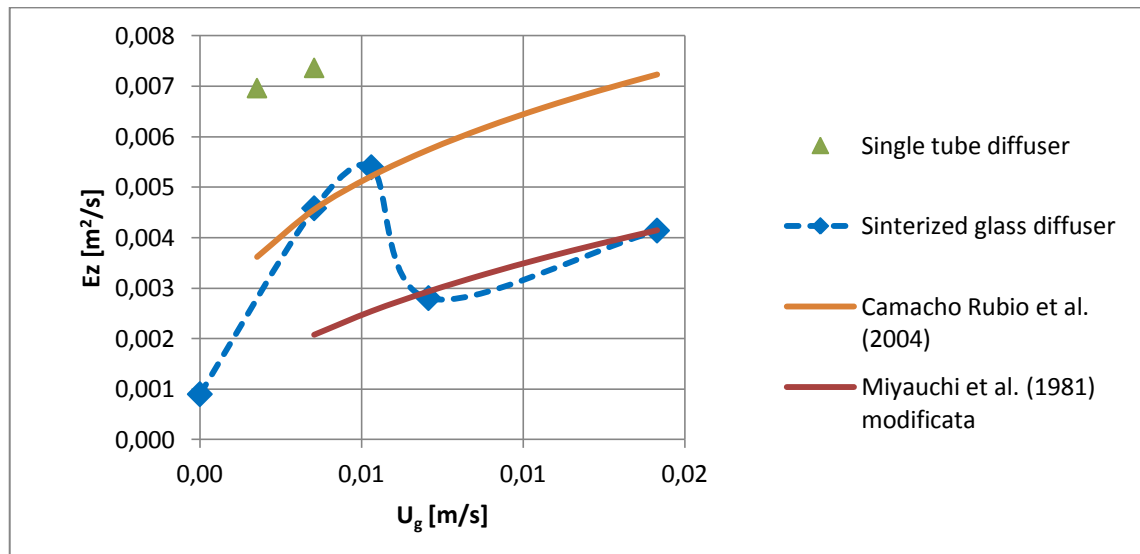
Fig 7.12 – Data summarize

The green triangular points refer to single tube gas diffuser. The dispersion coefficient values are greater than the values obtained with fritted glass diffuser: the column of bubbles come from the tube diffuser increases the mixing along the column.

7.5.2 Longitudinal dispersion coefficient E_z – continuous liquid and gas flow rates

When liquid is continuous, the model used to calculate longitudinal dispersion coefficient is given by Eq. 7.5. The equation is a function of Bodenstein number and the second moment of the residence time distribution curves is used.

Fig. 7.12 shows the variation of tracer concentration along the column (being the gas flow rate 0, 100 and 200 L/h and Q_L = 50 L/h). Also in these cases, tracer volume input is 50 ml of Acid Red dye (5 g/L).
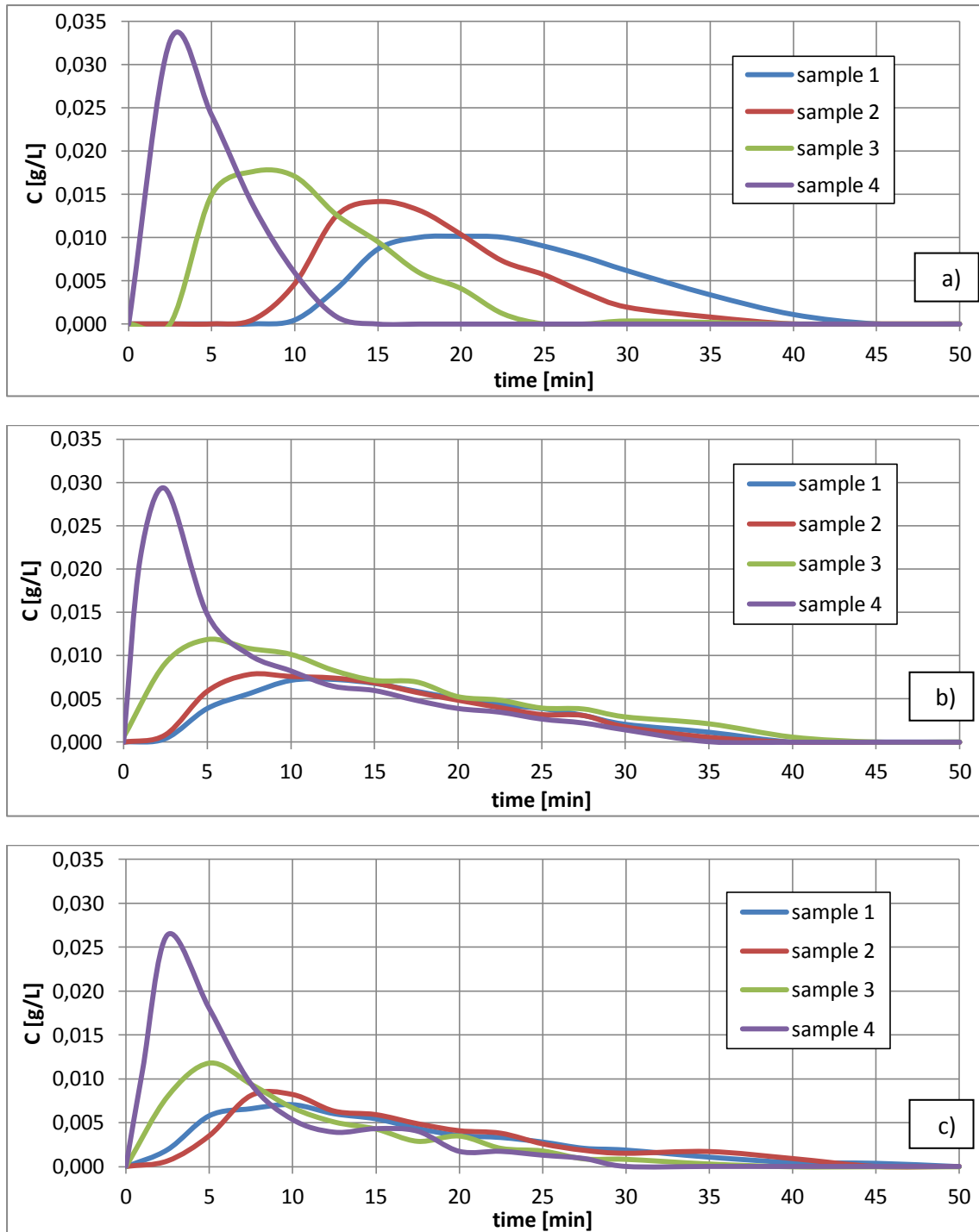
Fig 7.13 – Tracer concentration [g/L] vs time: $Q_L = 50$ L/h and a) $Q_g = 0$ L/h b) $Qg = 100$ L/h
c) $Qg = 200$ L/h

The curves in Fig 7.13 a) are more distinct than the others. The gas flow is equal to zero and hence the motion of the tracer is not influenced by the liquid flow.

As for the other curves, gas presents a remarkable influence. When there is gas flow after about 15 min, the curves are overlapping: this means that along the column the dynamic equilibrium is reached.

Table 7.3 – E_z values

Q_L [L/h]	Q_g [L/h]	u_g [m/s]	E_z [m^2/s]
	0	0	$2.17 \cdot 10^{-3}$
50	100	0.0035	$6.15 \cdot 10^{-3}$
	200	0.0071	$4.46 \cdot 10^{-3}$

The longitudinal dispersion coefficients seem to have a peak in correspondence of $Q_g =$ 100 L/h. Probably, as velocity increases, gas bubbles start to coalesce, therefore dispersion coefficient increases. In this situation, the column could be divided in segregate regions and the radial dispersion increases at the expense of the longitudinal one. Moreover, the bubbles increasing gas velocity maintain the same diameter but dispersion is not homogeneous in the section area along the column, causing different pattern configurations.

In Fig 7.14 the trends of the longitudinal dispersion coefficient changing liquid and gas flow rates are summarized.
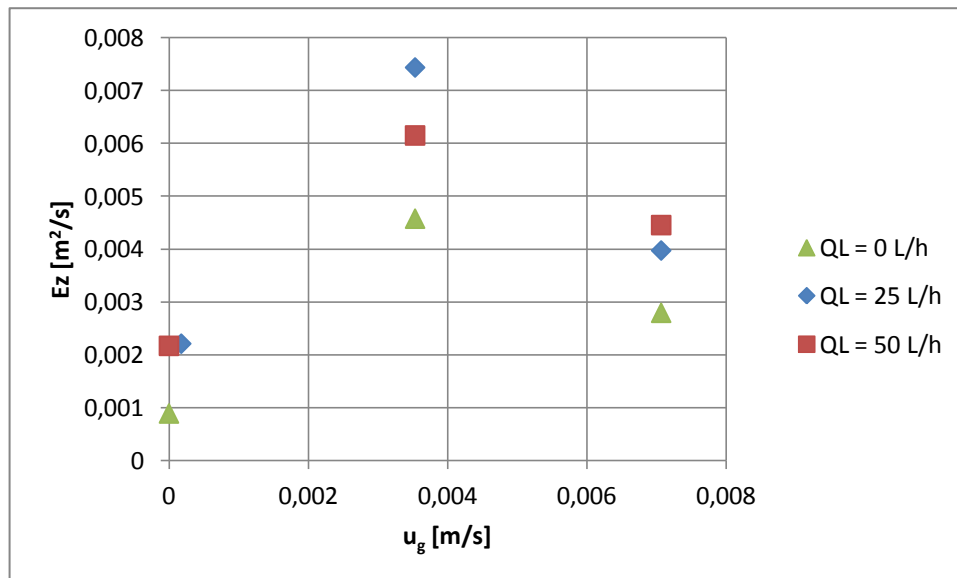

Fig 7.14 – Longitudinal dispersion coefficients at various conditions

The following conclusion can be done:
- the trends are similar;
- the coefficient values increase in presence of liquid flow rate;
- the values do not change in a consistent way in the presence of liquid flow rate, so gas flow rate is the main factor that affects dispersion.

References

[1] B.F. Alexander, Y.T. Shah, Axial dispersion coefficients in bubble columns, The Chemical Engineering Journal, 11, 1976, 153-156.

[2] F. Camacho Rubio, A. Sánchez Mirón, M.C. Cerón García, F. García Camacho, E. Molina Grima**,** Y. Chisti, Mixing in bubble columns: a new approach for characterizing dispersion coefficients, *Chemical Engineering Science*, **59**, 2004, 4369-4376.

[3] Y. Ohki, H. Inoue, Longitudinal mixing of the liquid phase in bubble columns, *Chemical Engineering Science*, **25**, 1970, 1-16.

[4] A. Sánchez Mirón, M.C. Cerón García, F. García Camacho, E. Molina Grima, Y. Chisti, Mixing in Bubble Column and Airlift Reactors, Chemical Engineering Research and Design, 82, 2004, 1367-1374.

[5] V. Pillay, Hydrodynamic study of gas-liquid co-current bubble column reactors at low superficial gas velocities, Master degree in Chemical Engineering, 2005.

[6] W.-D. Deckwer, Bubble column reactor, 119-122, *John Wiley and Soon*, 1992.

[7] K.B. van Gelder, K.R. Westerterp, Residence time distribution and hold-up in a cocurrent upflow packed bed reactor at elevated pressure, *Chemical Engineering Technology*, **13**, 1990, 27-40,.

[8] M. Millies, D. Mewes, Back-mixing of the continuous phase in bubble columns, *Chemical Engineering Science*, **50**, 1995, 2107-2115.

[9] A. Pinheiro Torres, F.A.R. Oliveira, Residence Time distribution studies in continuous thermal processing of liquid foods: a Review, *Journal of food Engineering*, **36**, 1998, 1-30.

[10] A. Rutherford, Mathematical Methods in Chemical Engineering, Vol 2 First order partial differential equation with applications, pp. 294-297, *Englewood Cliffs*, 1973.

[11] W.-D. Deckwer, R. Burckhart, G. Zoll, Mixing and mass transfer in tall bubble columns, *Chemical Engineering Science*, **29**, 1974, 2177-2188.

[12] W. Chen, W. Yang, J. Wang, Y. Jin, A. Tantsumi, Characterization of axial and radial liquid mixing in a liquid-solid circulating fluidized bed, *Industrial and Engineering Chemistry Research.*, **10**, 2001, 5431-5435.

[13] S. Gondo, S. Tanaka, K. Kazikuri, K. Kusunoki, Liquid mixing by large gas bubbles in bubble columns, *Chemical Engineering Science*, **28**, 1973, 1437-1445.

[14] S. Khang, S.P. Kothari, Experimental determination of axial dispersion coefficient in a bubble column, *Chemical Engineering Science*, **35**, 1980, 2203-2205.

Chapter 8 – Decolouration device comparison

In Chapter 5, bubble column reactor and multi-task pilot plant were described. In multi-task pilot plant ultrasound and hydrodynamic cavitation devices were implemented with the purposes of increasing gas-liquid mass transfer and similar alternative treatments to decolouration technologies. As described in Chapter 3, the reactions between ozone and dyes (or pollutants, in general terms) are limited by the difficulties to transfer ozone from gas to liquid phase; the kinetic reaction, instead, is generally fast.

In this chapter, the main object is comparing the different technologies designed and built, in order to define what is the best, at the same operational conditions.

In addition, four different dye classes were tested:

Table 8.1 – Dyestuffs used in the experimental tests

Dye class	Dye name
Reactive	Levafix Brilliant Blue E-B
Acid	Nylosan Blue E-2GL
Basic	Malachite Green
Disperse	Serilene Scarlet G-LS

Liquid samples taken from the operating pilot plants were analysed for dye concentration using the UV-visible spectrophotometer (Evolution 300, Thermo Scientific).

The decolouration percentage, therefore the quantity of colour removed from the liquid media, is expressed using the following formula

$$\Delta conc = 100 \, \frac{C_0 - C(t)}{C_0}$$

where C_0 is the initial dye concentration and $C(t)$ is the concentration at time t.

Levafix Brilliant Blue E-B
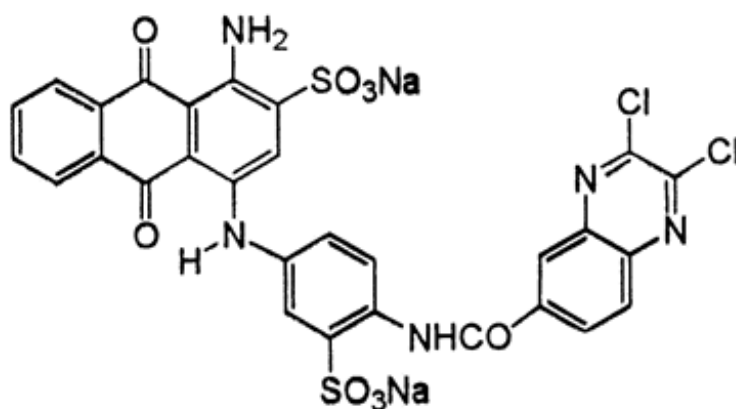
Molecular structure	Anthraquinone
Colour Index	Reactive Blue CI 29
Molecular weight [g/mol]	758.47
Max absorbance wavelength [nm]	609

Nylosan Blue E-2GL
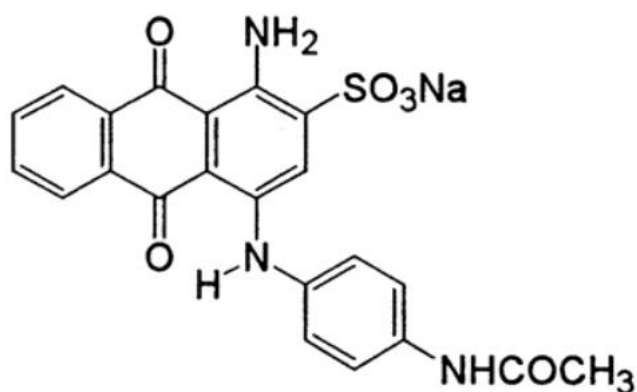
Molecular structure	Anthraquinone
Colour Index	Acid Blue CI 40
Molecular weight [g/mol]	473.43
Max absorbance wavelength [nm]	609

Malachite Green
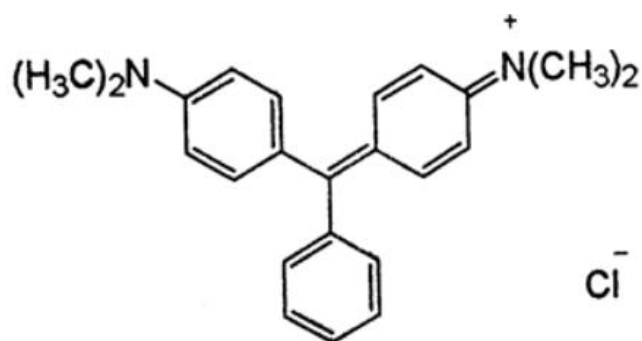
Molecular structure	Triarylmethane class
Colour Index	Basic Green CI 4
Molecular weight [g/mol]	364.91
Max absorbance wavelength [nm]	617

Serilene Scarlet G-LS
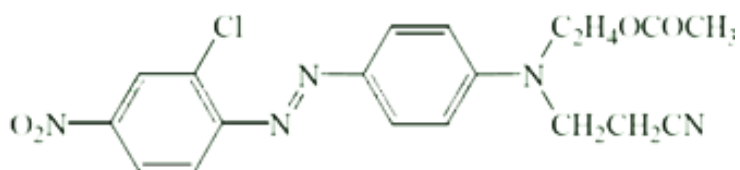
Molecular structure	Single azo
Colour Index	Disperse Red CI 54
Molecular weight [g/mol]	415.83
Max absorbance wavelength [nm]	536

8.1 Determination of reaction rate constant in semi batch process

Data taken from the semi-batch reactor (liquid batch and gas continuous) were analyzed for all the dyes to determine the reaction rate constants for the different devices. The available data were the dye concentrations measured in function of ozonation time.

The reaction between ozone and dye molecules follows a second order kinetics with respect to both ozone and dye concentrations [1, 2]. The rate law for decolouration kinetics is interpreted by the following equation:

$$-r_D = kC_{O_3,L}C_D \tag{8.1}$$

where $(-r_D)$ [mol/L/min] is the reaction rate, k [L/mol/min] is the reaction kinetic constant, $C_{O_3,L}$ [mol/L] is the ozone concentration in liquid phase and C_D [mol/L] is the dye concentration.

In a constant volume semi-batch reactor, the measure of reaction rate of dye is given by the rate of change of the dye concentration in time:

$$r_D = \frac{dC_D}{dt}$$

where t is the time [min].

The Eq. 8.1 can be simplified in the case of semi-batch reactor, considering ozone concentration in the liquid phase constant. In this way, rate law becomes pseudo-first order with respect to dye. In the semi-batch experiments, ozone concentration in the liquid media was considered as constant since the solution was ozonated to reach the equilibrium concentration of ozone. Therefore, at the uniform dissolved ozone concentration, the concentration of ozone in the aqueous phase at any time was assumed to be equal to the equilibrium concentration of ozone corresponding to the operating conditions used in the experiment.

$$C_{O_3,L} = C_{O_3,eq}$$

$$r_D = \frac{dC_D}{dt} = -kC_{O_3,L}C_D = -k'C_D \tag{8.2}$$

$$k' = kC_{O_3,eq}$$

where k' [1/min] is the pseudo-first order rate constant and $C_{O_3,eq}$ [mol/L] is the ozone equilibrium concentration in the liquid media.

The pseudo-first order rate constant (k') can be found by the integration of Equation (8.2) as follows:

$$\int_{C_0}^{C} \frac{1}{C_D} dC_D = -\int_{0}^{t} k' dt$$

$$\ln \frac{C}{C_0} = -k't$$

where, C_0 [mol/L] is the initial dye concentration and C [mol/L] is the dye concentration at time t [min].

The slope of the line $-\ln \frac{C}{C_0}$ vs t gives as result the pseudo-first order rate constant. In this study k' is used as numerical value to compare the experiments.

8.2 Semi-batch decolouration tests in different multi-task pilot plant configuration

8.2.1 Reactive dye: Levafix Brilliant Blue E-B

In the following experimental tests, the operative conditions, constant in all the trials, were initial dye concentration ($C_0 = 25$ mg/L) and gas flow rate ($Q_g = 100$ NL/h).
Decolouration kinetics was described by a pseudo-first order reaction respect to dye concentration.

8.2.1.1 Ozone mixture introduced without diffuser

The ozone was introduced in the system using a simple connection (ID 6 mm) in the pipe line. These tests were carried out like benchmarks to simulate the worst condition to mix gas and liquid phases. In this condition, it is possible to suppose that the initial bubbles diameter is in the order of 6 mm.

Different liquid recirculation flow rates were used (up to 1500 L/h) at constant initial pH and ozone dose gas mixture concentration was set to 4.4 g_{O3}/h.
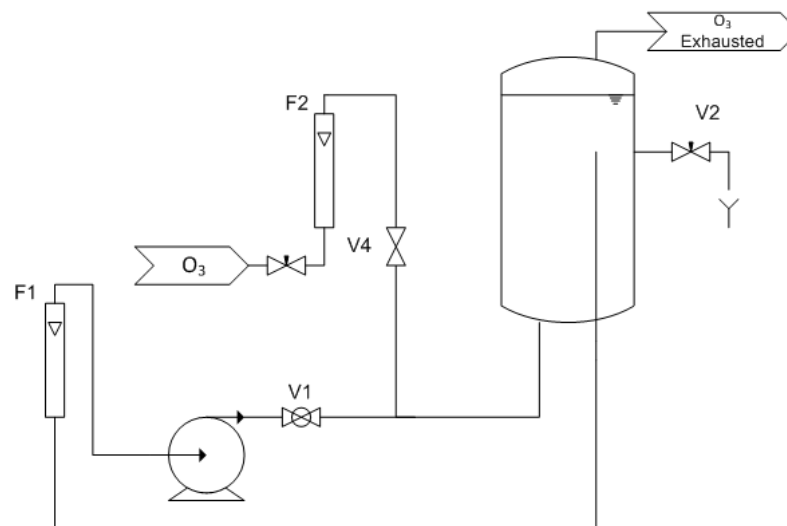

Fig 8.1 – Apparatus configuration scheme: ozone mixture introduced without diffuser

Q_L [L/h]	CT [min^{-1}]	pH (t=0)	pH (t$_f$[min])	k'	R^2	t$_{98\%}$ [min]
500	20	8.6	7.3 (45.1)	0.1331	0.9913	29.7
830	33	8.7	7.1 (45.0)	0.1409	0.9922	27.8
1300	52	8.6	7.3 (45.0)	0.1366	0.9955	28.3
1500	60	8.6	7.4 (45.0)	0.1313	0.9881	29.9

Liquid recirculation flow rate (Q_L) is closely related to the number of gas-liquid contacts in the unit of time (CT). Therefore, increasing liquid recirculation flow rate, the single portion of liquid receives fresh ozone lots of times.

The pseudo-first order kinetic constants are about constant changing liquid recirculation flow rate. Therefore, the number of contacts among fresh gas bubbles and liquid seems not to influence in the reactions: increasing the number of contacts three times, the pseudo kinetic rate remains constant and the time to reach 98% liquor decolouration is more or less the same.

8.2.1.2 Decolouration induced by ultrasound cavitation

Ultrasound device is described in Chapter 6: it is able to operate at a fixed frequency of 25 kHz and a maximum power of 1000 W (minimum power allowed by the instrument is 500 W).

The following results are obtained considering a 120 min treatment time.

Two liquid flow rates are considered in order to understand the best condition in which ultrasound work.
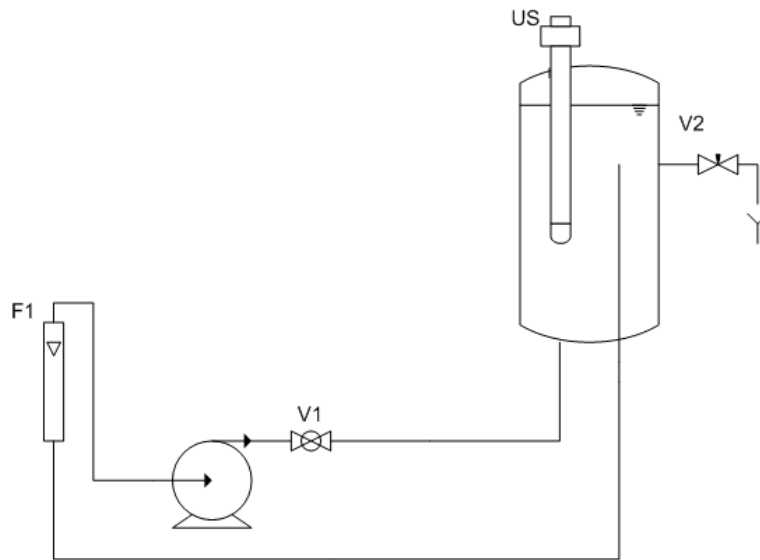

Fig 8.2 – Apparatus configuration scheme: ultrasonic decolouration

P [W]	I$_{75}$ [W/in^2]	Q_L [L/h]	Re	pH (t=0)	pH (t$_f$[min])	Δconc [%]
1000	30	500	884	8.3	7.9 (120.0)	2
500	26	500	884	8.3	8.2 (120.0)	2
500	25	500	884	5.5	5.6 (120.0)	2
500	12	830	1468	8.5	8.2 (120.0)	5

After 120 min of treatment, the maximum decolouration percentage obtained was 5% with the lower power admitted by the instrument, and Q_L = 830 L/h. Therefore the optimum cavitation power seems to be 500 W.

Using ultrasound, high power corresponds to more violent cavities implosion and more extreme conditions in terms of temperature and pressure. Formation of hydroxyl radicals is more intense and consequently reactions are faster. Unfortunately, sound waves could be affected by resonance effects by reactor wall and all the metal parts contained in the vessel. Reflection can produce a destructive sound wave and "hot spot" generation is limited.

The particular reactor geometry and the position of the transducer inside the reactor contributed in increasing kinetics at lower ultrasound potential, where resonance effects were limited.

Although the ultrasound intensity measured by Ultrasonic Energy Meter told that the cavitation is more intense for lower liquid flow rate and higher power (Chapter 6), in this experimental tests the best decolouration kinetic result was achieved at 830 L/h and 500 W. I_{75} was the ultrasound intensity measured at 75 mm distance between energy meter probe and ultrasound device. This distance corresponds to the location where intensity had the highest values. It is possible to suppose that the average ultrasound intensity field was quite different and the system hydrodynamic, in addition to resonance effects, change the ultrasound field increasing ultrasound effect at the highest flow rate and lowest power.

8.2.1.3 Decolouration induced by hydrodynamic cavitation in Herschel-type Venturi
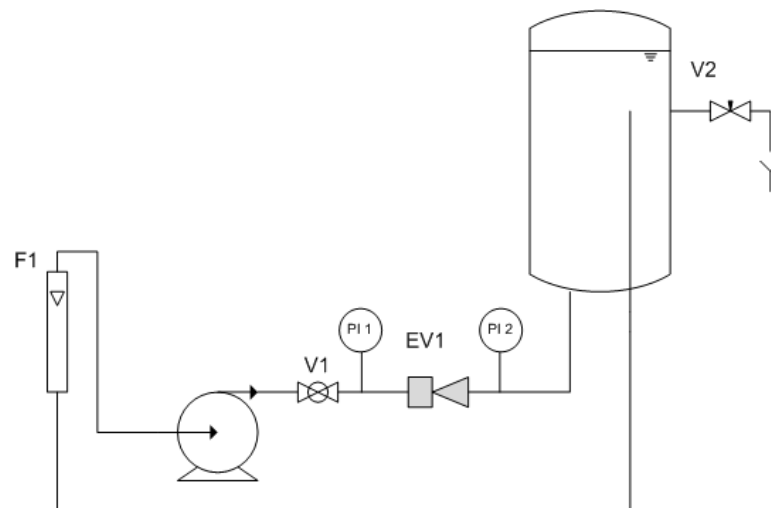

Fig 8.3 – Apparatus configuration scheme: hydrodynamic decolouration

Also in the case of hydrodynamic cavitation, the decolouration percentage was calculated after 120 min treatment. The ejector had a throat section diameter of 4 mm.

In chapter 5, one of the parameters described and used for the design of Herschel-type ejector was the inlet pressure: changing inlet pressure, the reaction efficiency change trying the optimum pressure in the range of $4 - 6$ bar. For this reason, decolouration kinetic was evaluated using the same pressure interval.

P_{in} [bar]	Q_L [L/h]	σ_c [-]	P_{TS} [mH$_2$O]	pH (t=0)	pH (t$_f$[min])	Δconc [%]
6	1350	0.22	9.8	8.3	8.2	1
5	1300	0.24	9.8	8.4	8.2	2
4	1270	0.25	9.8	8.3	7.9	2

The decolouration experiments confirmed the literature works [3, 4]: unfortunately, Δconc values obtained are low. Although the decolouration degrees achieved are very close, increasing inlet pressure (and consequently decreasing cavitation number σ_c) loads to a decrease in decolouration (as described by Saharan et al. [3]).

The cavitation events are closely related to cavitation number: when $\sigma_c < 1$ cavitation exists but changes its behaviour according to cavitation number values. When the parameters are smaller, there are lots of vapour cavities that form a cloud. The cloud adsorbs the implosion energy and so the ultrasound capacity to improve reactions decrease.

In the previous table the pressures measured in the throat section (P_{TS}) varying ejector inlet pressure are also reported: vacuum degree was the same in all the experimental tests and equal to 9.8 mH$_2$O.

8.2.1.4 Decolouration tests promoted by Mixed Venturi ejector with ozone and/or ultrasound device
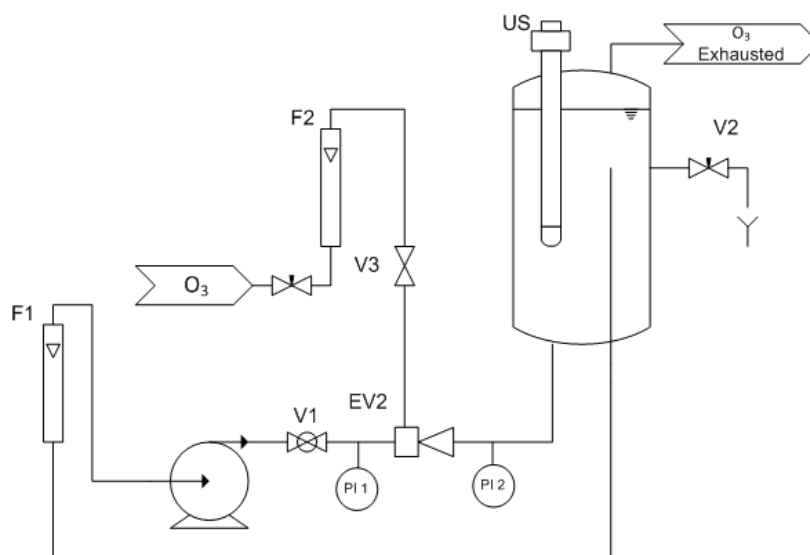

Fig 8.4 – Apparatus configuration scheme: ozonation with Mixed Venturi ejector and/or ultrasonic cavitation

Decolouration laboratory experiments were performed using two inserts corresponding to throat section diameter $d = 3$ and 4 mm. They were the best compromise to obtain eventually cavitation (without gas inlet) and lower Reynolds number to allow ultrasound cavitation in the reactor (see Chapter 6).

Effect of O_3 dosage – d = 3 mm

Flow rate was set to 830 L/h, it was the maximum flow rate imposed by the system (valve V1 completely open).

O_3 % v/v	O_3 dose [g/h]	pH (t=0)	pH (t_f[min])	k' [min^{-1}]	R^2	$t_{98\%}$ [min]
1.1	2.4	8,8	7.0 (36.1)	0.1702	0.9931	20.2
2	4.4	8,6	6.4 (20.0)	0.3289	0.9942	11.1
4.1	9	8,5	6.1 (10.3)	0.6513	0.997	7.5

Increasing ozone dose, the pseudo-first order kinetic increases in the same proportion. Ejector enhances mixing between gas and liquid phase and therefore mass transfer: $t_{98\%}$ (O_3 dose 4.4 g/h) in ejector test and with the connection directly in the pipe are 11.1 and 27.8 min, respectively. This means that to reach the same decolouration degree ejector saves much more than half time either than without it.
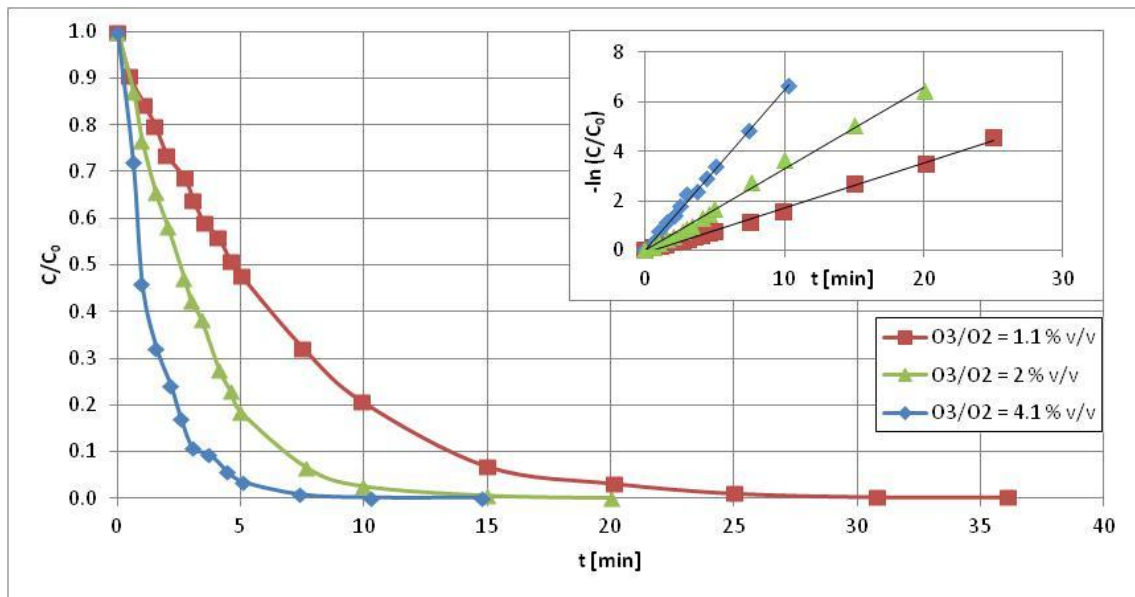

Fig 8.5 – Effect of ozone dose

Effect of pH – d = 3 mm

As mention in previous chapters, exist two reaction paths for ozone, depending on the pH solution:

- pH < 4: ozone react directly with dye molecule;
- pH > 10: ozone decompose itself in hydroxyl and other radicals in water media, and they react with dyes (the most effective is OH·);
- 4 < pH < 10: both previous reaction paths are present.

Maintaining constant ozone dose (4.4 g/h) and liquid flow rate (830 L/h), the pH influence was tested.

pH (t=0)	pH (t$_f$[min])	k' [min^{-1}]	R^2	t$_{98\%}$ [min]
10.2	8.2 (20.0)	0.3625	0.9945	9
8.6	6.6 (20.0)	0.3289	0.9942	11.1
5.7	5.0 (20.0)	0.2841	0.9882	15
4.9	4.7 (19.9)	0.2837	0.9891	15.5
3.7	3.9 (19.9)	0.2768	0.9887	16
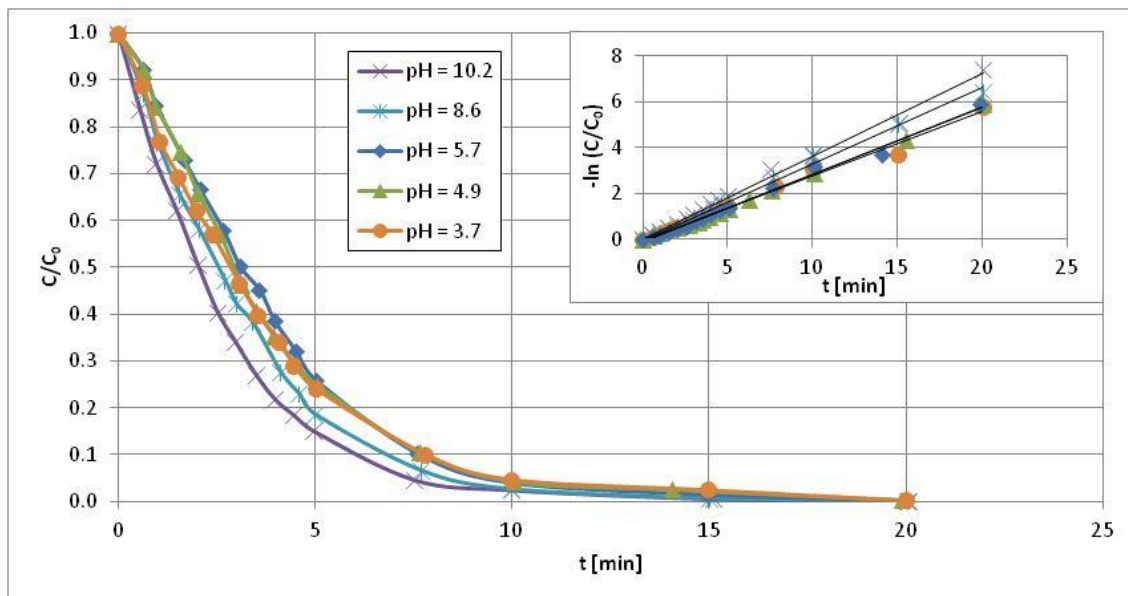
Fig 8.6 – Effect of pH

Considering t$_{98\%}$, increasing pH from acid to alkaline condition the time used to reach 98% of decolouration was decreased of about 7 min. So decolouration is more suitable in alkaline condition. It is possible to explain via the oxidation potential of the species involved in the reaction: ozone and hydroxyl radical. The first one have an oxidation potential at standard condition of 2.07 V instead the second one is greater, 2.86 V.

Effect of recirculation flow rate (Q_L) – d = 3 mm

Standard Venturi ejector was used to improve gas-liquid closing. Although the ejector is able to perform cavitation, in this case the gas phase prevents bubble implosion. Potentially, the conditions in which the liquid is forced in the ejector can generate cavity bubbles, but the gas damps down on their implosion.

Increasing flow rate increase the kinetic constant values because increases the close interaction between gas and liquid phase. In addition, the increase in kinetic reaction can also attribute to the increase in the number of contact between the liquid and fresh ozone flow.

The experimental tests were performed with the same ozone dosage, 4.4 g/h.

Q_L [L/h]	CT [min^{-1}]	pH (t=0)	pH (t_f[min])	k' [min^{-1}]	R^2	$t_{98\%}$ [min]
500	20	8.6	7.5 (20.0)	0.2881	0.9939	15.2
830	33.2	8.6	6.6 (20.0)	0.3289	0.9942	11.1
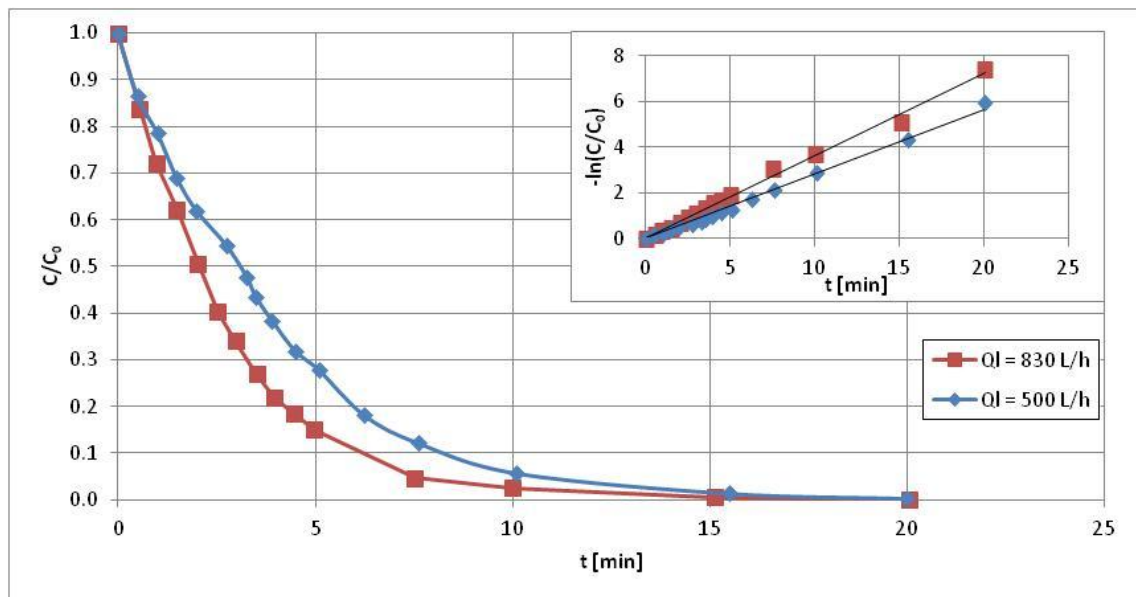
Fig 8.7 – Effect of recirculation flow rate (Q_L)

Combined effect of ultrasound cavitation and ozone – d = 3mm

In the following experimental tests, ultrasound cavitation was added to increase hydroxyl radicals production in liquid media. Ozone dosage was fixed to 4.4 g/h (2% v/v), liquid recirculation equal to 830 L/h and ultrasound frequency was 25 kHz.

P [W]	pH (t=0)	pH (t_f[min])	k' [min^{-1}]	R^2	$t_{98\%}$ [min]
0	8.6	6.6 (20.0)	0.3389	0.9942	11.1
500	8.5	6.7 (20.0)	0.3311	0.9894	14.2
1000	8.5	6.6 (20.0)	0.2687	0.9933	17.6

Ultrasound at the maximum power increase $t_{98\%}$ of about 6min. So, the global effectiveness of ozone reaction was considerably reduced. In the case of 500W ultrasound power, kinetic rate slightly increase.

Ultrasound in liquid media play a double role: on the one hand they produce hydroxyl radical and on the other they are able to decrease gas content in liquid. Probably at high ultrasound power the second effect is the predominant.

Effect of pH combining ultrasound cavitation and ozone – d = 3mm

Q_L = 830 L/h
O_3 dosage = 4.4 g/h
P_{US} = 520 W
f_{US} = 25 kHz

US	pH (t=0)	pH (tf[min])	k' [min^{-1}]	R^2	$t_{98\%}$ [min]
no	10.2	8.2 (20.0)	0.3625	0.9945	9.2
yes	9.9	7.8 (20.2)	0.3216	0.9904	10.7
no	8.6	6.6 (20.0)	0.3389	0.9942	11.1
yes	8.5	6.7 (20.3)	0.3060	0.9939	14.2
no	3.7	3.9 (19.9)	0.2768	0.9887	16
yes	3.7	3.8 (20.1)	0.2842	0.9898	15.1

As described previously, decreasing pH values in liquid media the kinetic rate decreases: ozone is less efficient than hydroxyl radical. In addition, ozone treatment combined with ultrasound cavitation show pseudo-first order kinetic lower than in the cases without ultrasound.

From the data it possible to observe that the ultrasound action maintain about constant the kinetic constant at acid condition, in the other case have a worst behaviour.

Effect of O$_3$ dose combining ultrasound cavitation and ozone – d = 3 mm

Q_L = 830 L/h
P_{US} = 520 W
f_{US} = 25 kHz

US	O$_3$ % v/v	O$_3$ dose [g/h]	pH (t=0)	pH (t$_f$[min])	k' [min^{-1}]	R^2	$t_{98\%}$ [min]
no	2	4.4	8,6	6.6 (20.0)	0.3389	0.9942	11.1
yes	2	4.4	8.5	6.7 (20.3)	0.3060	0.9939	14.2
no	4.1	9	8,5	6.4 (10.3)	0.6513	0.997	7.8
yes	4.1	9	8.9	6.7 (9.9)	0.5769	0.9893	8.5

Ultrasound cavitation combined with ozone had worst effects during decolouration kinetic.

Effect of recirculation flow rate (Q_L) combining ultrasound cavitation and ozone – d = 3 mm

O_3 dosage = 4.4 g/h
P_{US} = 520 W
f_{US} = 25 kHz

US	Q_L [L/h]	pH (t=0)	pH (t_f[min])	k' [min^{-1}]	R^2	$t_{98\%}$ [min]
no	500	8.6	7.5 (20.0)	0.2821	0.9939	14.2
yes	500	8.5	7.7 (20.0)	0.2897	0.9894	14.9
no	830	8.6	6.6 (20.0)	0.3389	0.9942	11.1
yes	830	8.5	6.7 (20.3)	0.3060	0.9939	12.2

Ultrasounds cavitation influences in a negative way decolouration kinetics, considering flow rate greater than 500 L/h. Increasing recirculation flow rate, the ultrasounds negative effect appeared.

Effect of recirculation flow rate (Q_L) on ultrasound cavitation with ozone – d = 4 mm

Using the ejector with throat section diameter 4 mm, decolouration tests were performed. In this case, recirculation flow rate was changed to test the mixing degree in the mixing chamber (ozone dose 4.4 g/h).
In addition, US cavitation with ozone was implemented.

O_3 dose = 4 g/h
P_{US} = 520 W
f_{US} = 25 kHz

US	Q_L [L/h]	pH (t=0)	pH (t_f[min])	k' [min^{-1}]	R^2	$t_{98\%}$ [min]
no	500	8.6	7.0 (20.0)	0.2917	0.9916	12.9
yes	500	8.3	7.0 (20.2)	0.2032	0.9839	17.8
no	1500	8.7	7.3 (20.0)	0.3432	0.9963	10.8
yes	1500	8.7	7.4 (20.1)	0.2923	0.9919	13.8

Increasing recirculation flow rate, and consequently the contact number (CT), the pseudo-first order kinetic constant increases.
As been described in the case of d = 3 mm, ultrasound cavitation activity has negative effect on decolouration, drop off the kinetic values.

Insert diameter mixing effect

To understand what is the best insert between throat section d = 3 and 4 mm on kinetics, decolouration curves at 500 L/h were compared.

Q_L = 500 L/h (CT = 20 min^{-1})
O_3 dose = 4 g/h

d [mm]	pH (t=0)	pH (t_f[min])	k' [min^{-1}]	R^2	$t_{98\%}$ [min]
3	8.6	7.5 (20.0)	0.2881	0.9939	13.2
4	8.6	7.0 (20.0)	0.2917	0.9916	12.9

The curves are overlapping and the kinetic constants are more or less the same. This means that the turbulence degree inside the ejector does not affect contact time values.
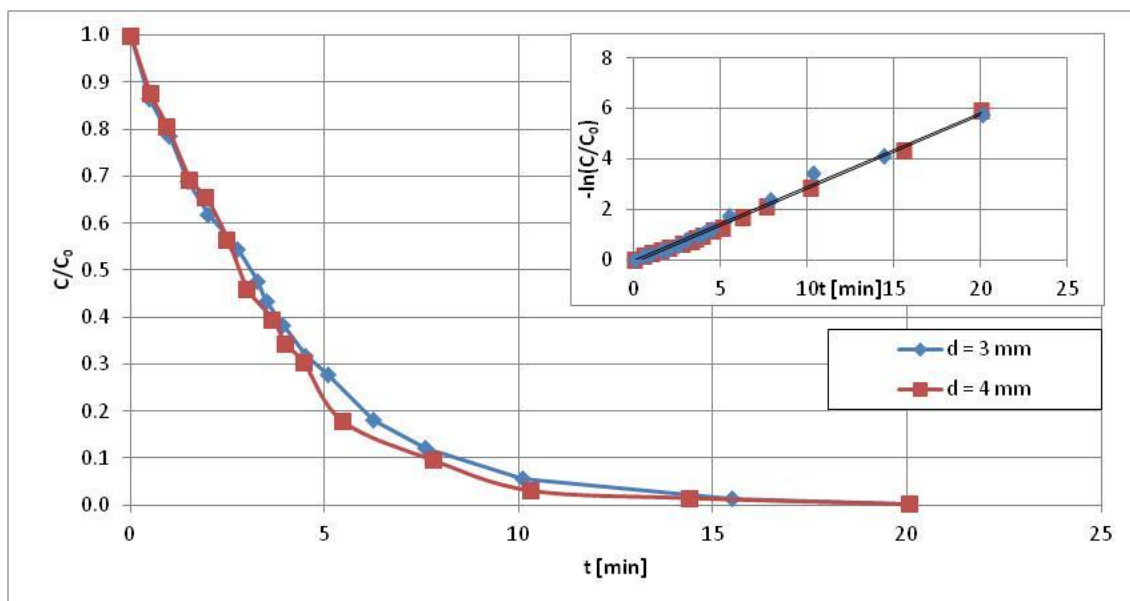

Fig 8.9 – Effect of recirculation flow rate (Q_L)

8.2.1.5 Decolouration tests promoted by Mixing and Herschel-type Venturi ejector in parallel

In the following laboratory experiments two ejector configurations in parallel were adopted:
1)   - Mixed Venturi ejector used to introduce ozone in the system;
        - Hershel-type Venturi used to improve hydrodynamic cavitation;
2)   - Mixed Venturi ejector used to improve hydrodynamic cavitation;
        - Hershel-type Venturi used to introduce ozone in the system.

To compare results, liquid recirculation flow rate, ozone dose and ultrasound power were fixed to 1500 L/h, 4.4 g/h and 520 W (25 kHz), respectively.

Liquid recirculation flow rate was chosen to guarantee cavitation in the appropriate ejector. For this reason, the phonometer was used to reach the effective noise corresponding to bubble implosion (see Chapter 6) without gas.
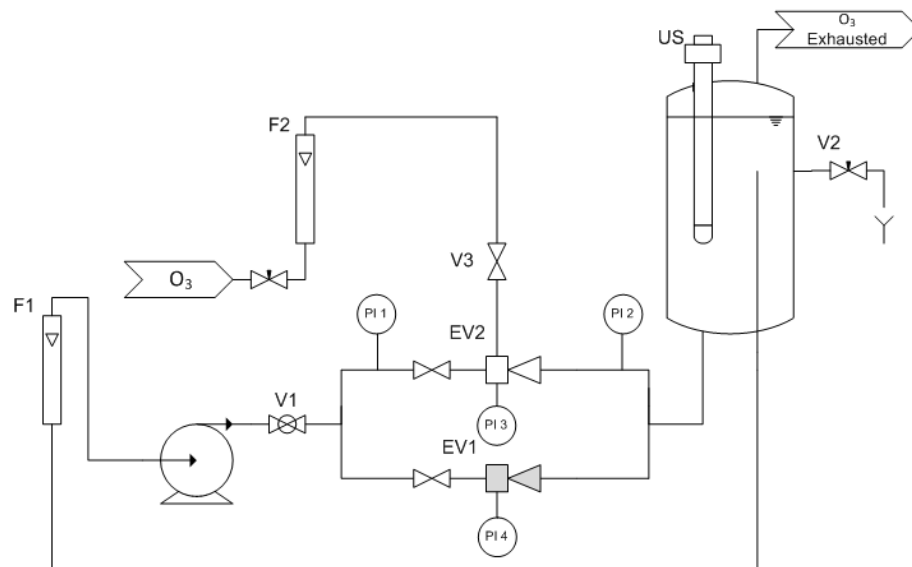

Fig 8.9 – Apparatus configuration scheme: parallel configuration EV2 – ozone inlet and EV1 – hydrodynamic cavitation

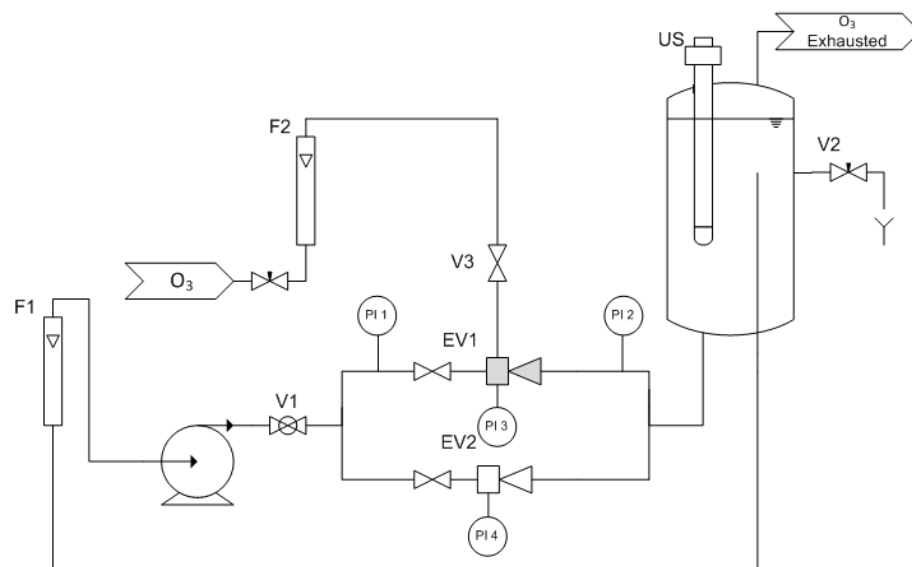| US	pH (t=0)	pH (t_f[min])	k' [min^{-1}]	R^2	p_G [mH$_2$O]	$t_{98\%}$ [min]
no	9.2	6.9 (20.0)	0.3180	0.9886	9.7	11.5
yes	8.9	6.8 (20.1)	0.3031	0.9969	9.7	12.7

Fig 8.10 – Apparatus configuration scheme: parallel configuration EV2 – hydrodynamic configuration and EV1 ozone inlet

US	pH (t=0)	pH (t_f[min])	k' [min^{-1}]	R^2	p_B [mH$_2$O]	$t_{98\%}$ [min]
no	9.2	7.4 (20.1)	0.3148	0.9862	9.2	11.5
yes	9.1	6.9 (20.1)	0.3098	0.9949	9.3	12

From kinetics evaluation, no difference was observed between the two configurations. In addition, like all the above experiments, ultrasounds decrease decolouration by ozonation.

Comparing the above results to the kinetic value measured in the case of ozone introduced by ejector EV1, they are lower. Therefore, both ultrasound and hydrodynamic cavitation showed a negative effect on decolouration.

8.2.2 Acid dye: Nylosan Blue E-2GL

In the following experimental tests, the operative conditions are initial dye concentration $C_0 = 25$ mg/L and gas flow rate $Q_g = 100$ NL/h, constant in all the trials.

Decolouration kinetics was described by a pseudo-first order reaction with respect to dye concentration.

Mixed Venturi ejector (d = 3 mm) was used in the following experimental tests (scheme Fig. 8.4). To compare the results, the following parameters were kept constant:

$Q_L = 830$ L/h
$P = 520$ W
$f = 25$ kHz

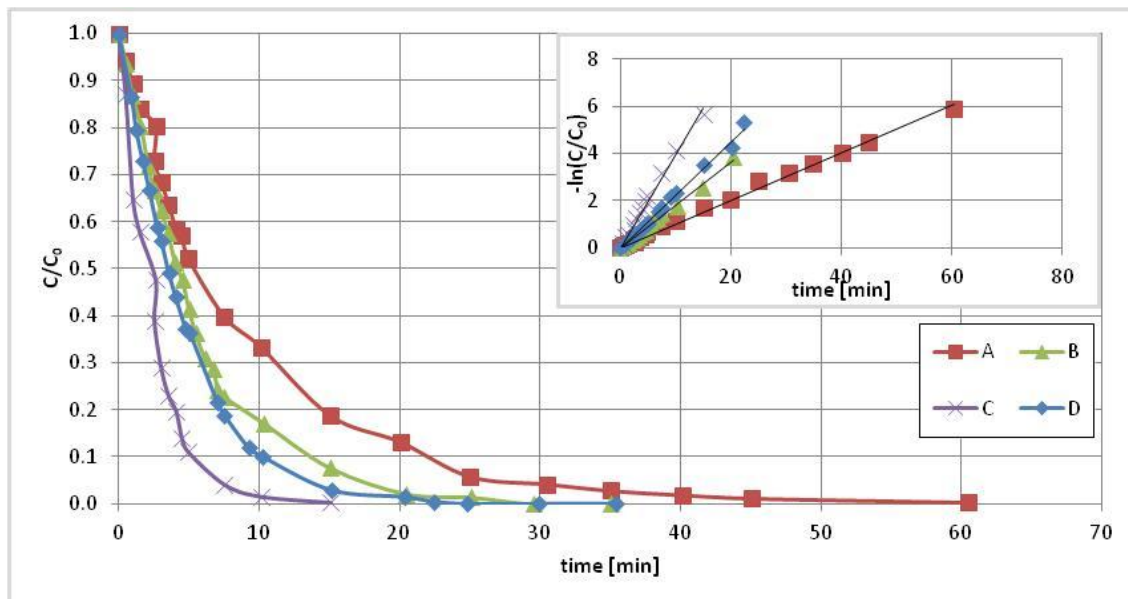| sample	O_3 dose [g/h]	US	pH (t=0)	pH (t_f[min])	k'	R^2	$t_{98\%}$ [min]
A	2.4	no	7.1	5.9 (60.5)	0.1009	0.995	39
B	4.4	no	6.9	6.1 (35.1)	0.1808	0.9919	21
C	9	no	6.9	4.5 (15.1)	0.3941	0.9899	8.9
D	4.4	yes	7.1	5.6 (35.4)	0.2234	0.9924	20

Fig 8.11 – Effect of recirculation flow rate (Q_L)

In addition, the kinetic constant and $t_{98\%}$ were evaluated in the case in which ozone mixture was introduced through the connection (samples E and F, respectively), as showed in Fig. 8.1.

sample	O₃ dose [g/h]	US	pH (t=0)	pH (t_f[min])	k'	R²	t₉₈% [min]
E	4.4	no	6.9	6.0 (72.2)	0.0701	0.9913	52.3
F	4.4	yes	7.1	6.2 (70.2)	0.0534	0.9909	69.7

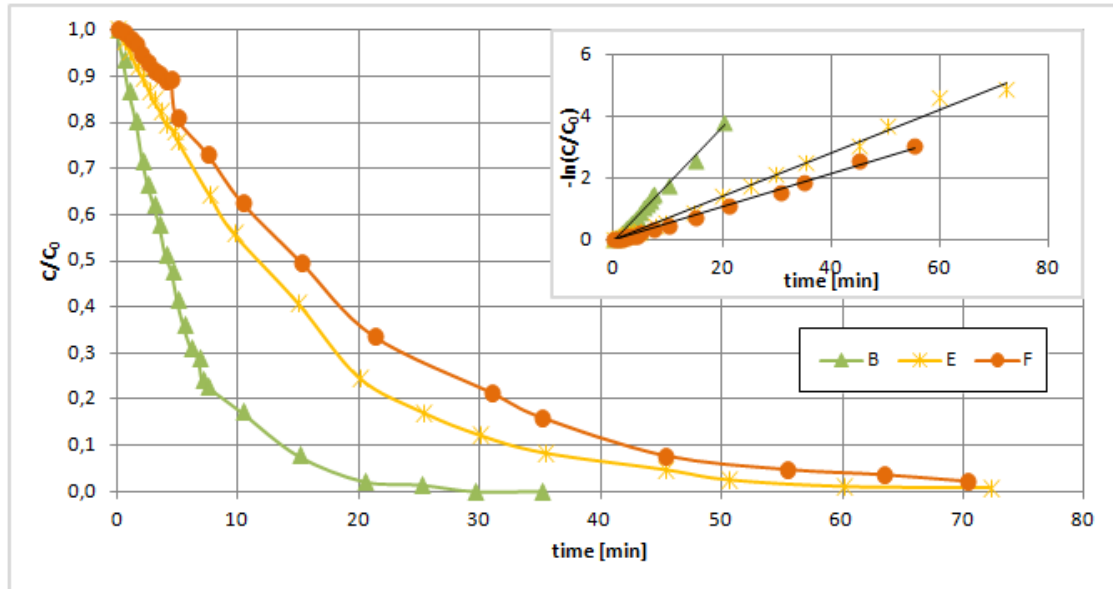| sample	O_3 dose [g/h]	US	pH (t=0)	pH (t_f[min])	k'	R^2	$t_{98\%}$ [min]
E	4.4	no	6.9	6.0 (72.2)	0.0701	0.9913	52.3
F	4.4	yes	7.1	6.2 (70.2)	0.0534	0.9909	69.7

Fig 8.12 – Improving kinetics using ejector device (B), compared to ozone mixture introduced without diffuser without (E) and with (F) US

Also in the case of acid dye, the ultrasound induced a decrease in the kinetic constant.

8.2.3 Basic dye: Malachite Green

In the following experimental tests, the operative conditions are initial dye concentration (C_0 = 25 mg/L) and gas flow rate (Q_g = 100 NL/h), constant in all the trials.

Also in this case, decolouration kinetics was described by a pseudo-first order reaction with respect to dye concentration.

Mixed Venturi ejector (d = 3mm) was used in the following experimental tests (scheme Fig. 8.4). In order to compare the results, the following parameters were kept constant:

Q_L = 830 L/h
P = 520 W
f = 25 kHz

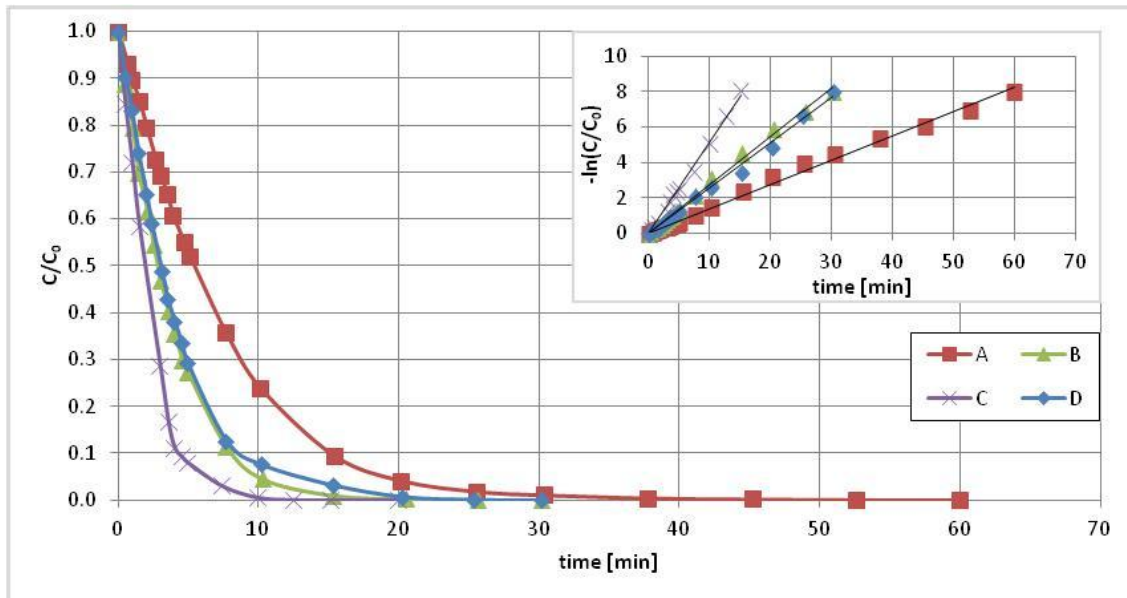| sample	O_3 dose [g/h]	US	pH (t=0)	pH (t_f[min])	k'	R^2	$t_{98\%}$ [min]
A	2.4	no	6.1	4.7 (60)	0.1376	0.9943	25
B	4.4	no	6.3	4.5 (30.3)	0.2735	0.9956	13.2
C	9	no	6.3	4.4 (15.1)	0.5185	0.9944	9.7
D	4.4	yes	6.2	4.9 (30.1)	0.2548	0.9943	17.1

Fig 8.13 –Basic dye experimental tests

Also in the case of cationic dye, ultrasound waves induced a decrease in the kinetic constant.

8.2.4 Disperse dye: Serilene Scarlet G-LS

Disperse dyes are barely soluble in water [5]. Therefore, compared to the other dye classes studied in this work, the decolouration mechanism is different.

For water soluble dyes, the decolouration reaction limiting step is only ozone mass transfer from gas to liquid phase. On the other hand, when there are disperse dyes in the liquid to treat, therefore insoluble, it is possible to observe another limiting step: dye dissolution.

Ozone is able to oxidize dye when they are dissolved in water. Usually, disperse dyes in water form micelle: as the small amount of dissolved disperse dye reacts with ozone, additional dye dispersed in solution is dissolved, until the disperse dye is nearly completely removed by liquid media.

The described mechanism has a consequence on the global treatment time. From the experiments performed, disperse dye decolouration took up to 4 times more than the decolouration time used for the other dye classes.

In the following experimental tests, the operative conditions are initial dye concentration $C_0 = 25$ mg/L and gas flow rate $Q_g = 100$ NL/h, constant in all the trials.

Mixed Venturi ejector (d = 3mm) was used in the following experimental tests (scheme in Fig. 8.x). In order to compare the results, the following parameters were kept constant:

$Q_L = 830$ L/h
$P = 520$ W
$f = 25$ kHz

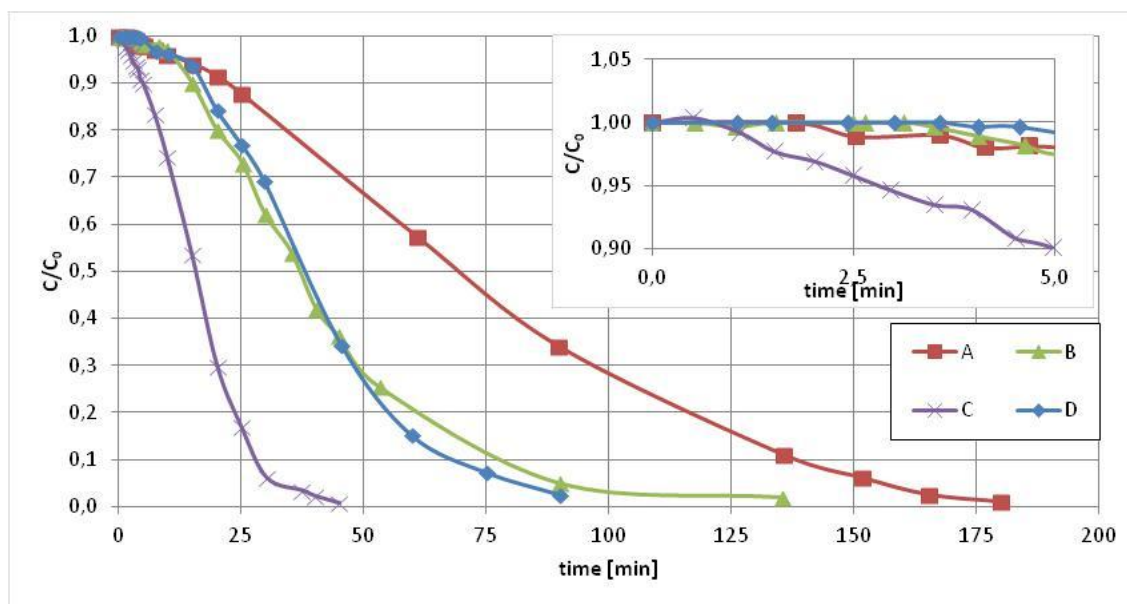| sample	O$_3$ dose [g/h]	US	pH (t=0)	pH (t$_f$[min])	t$_{98\%}$ [min]
A	2.4	no	7.1	5.5 (180)	168
B	4.4	no	6.9	4.6 (135.5)	135.5
C	9	no	7.1	4.1 (40)	40
D	4.4	yes	6.9	4.2 (90.1)	75.2

Fig 8.14 –Disperse dye experimental tests

From the graph, the dissolution step is clearly visible: in all the trials a latent period is present and it corresponds to about 2.5 min of the global decolouration reaction.

In this case, ultrasounds are used with the main scope of enhancing dye dispersion, reducing the micelle dimension. Comparing t$_{98\%}$ in the case of samples B and D (same ozone dose and with/without ultrasound work, respectively), ultrasounds reduce the treatment time of about 60 min.

8.3 Bubble column reactor and multi-task pilot plant comparison in continuous experimental tests

In the previous paragraphs experimental tests, carried out in multi-task pilot plant in semi-bath conditions, are described (liquid batch and gas continuous). In the following ones, instead, gas and liquid flow rate were imposed continuous into multi-task system and the decolouration results were compared with bubble column reactor at the same conditions. In this way, the results obtained in bubble column reactor can be used as reference to multi task reactor ones.

Taking into account the results obtained in multi-task equipment semi-batch experiments, Mixed Venturi ejector was the best device in dyestuffs decolouration reaction by ozone. Only in the case of disperse dye treatment, Standard ejector was coupled with ultrasound device to disaggregate dye micelles.

The multi-task equipment configuration and bubble column reactor used in the following experiments are reported in Fig 8.15 and 8.16, respectively.
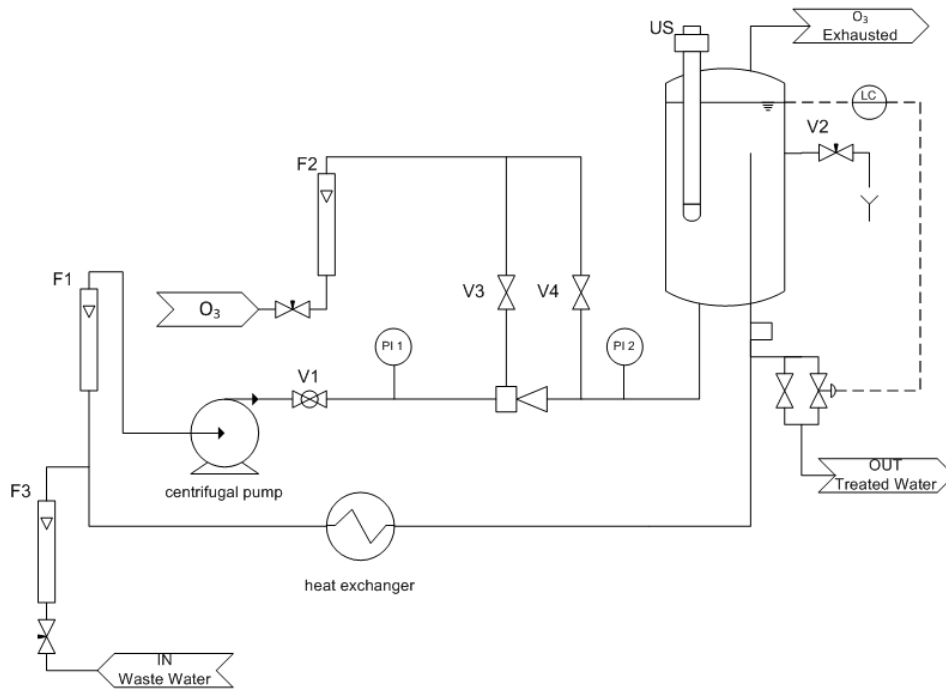
Fig 8.15 – Multi-task apparatus configuration scheme in continuous experimental tests
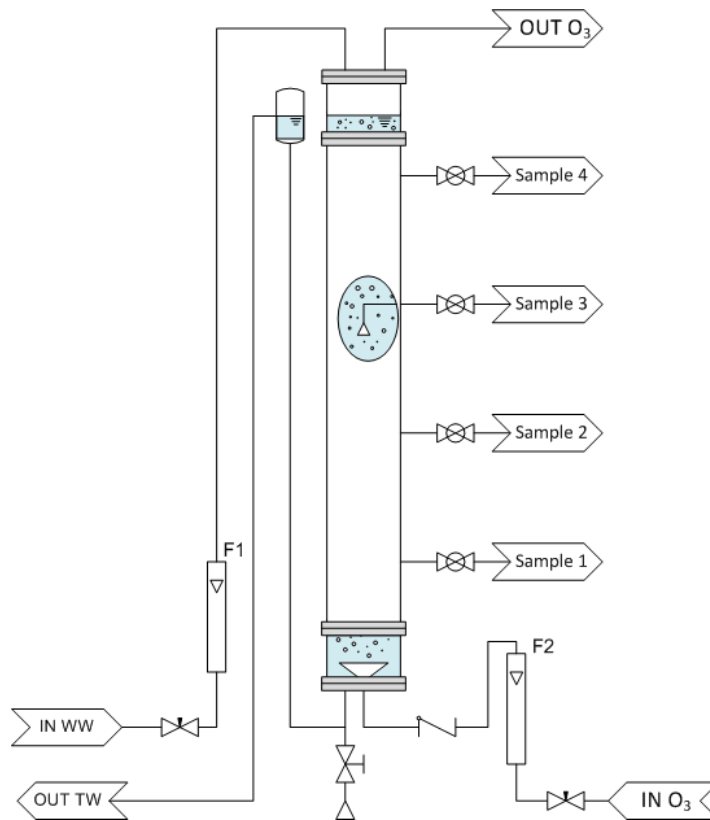

Fig 8.16 – Bubble column reactor scheme in continuous experimental tests

Generally, the two pilot plants were full of liquid containing the desired dye concentration. Subsequently, a new liquid flow rate (at the same concentration) was

imposed to the system to have the permanence time required. Finally, the ozone/oxygen mixture was introduced.

Exhaustion parameter (E%) was used to indicate the decolouration reaction efficiency. It is defined as

$$E\% = 100 - \Delta conc = \frac{C(t)}{C_0} \, 100$$

8.3.1 Reactive dye: Levafix Brilliant Blue E-B

8.3.1.1 Multi-task reactor

Some experiments were carried out with the main focus of understanding what is the best ejector, in continuous experimental tests, which guarantees the best mixing, and therefore mass transfer, from gas to liquid media. So, Mixed Venturi ejector (EV2) and Herschel-type Venturi (EV1) were compared.

The experiments were characterized by the following parameters:

- initial dye concentration $C_0 = 25$mg/L;
- gas flow rate $Q_g = 100$ NL/h;
- recirculation liquid flow rate $Q_L = 830$ L/h;
- ozone dosage 4.4 g/h (2% v/v);
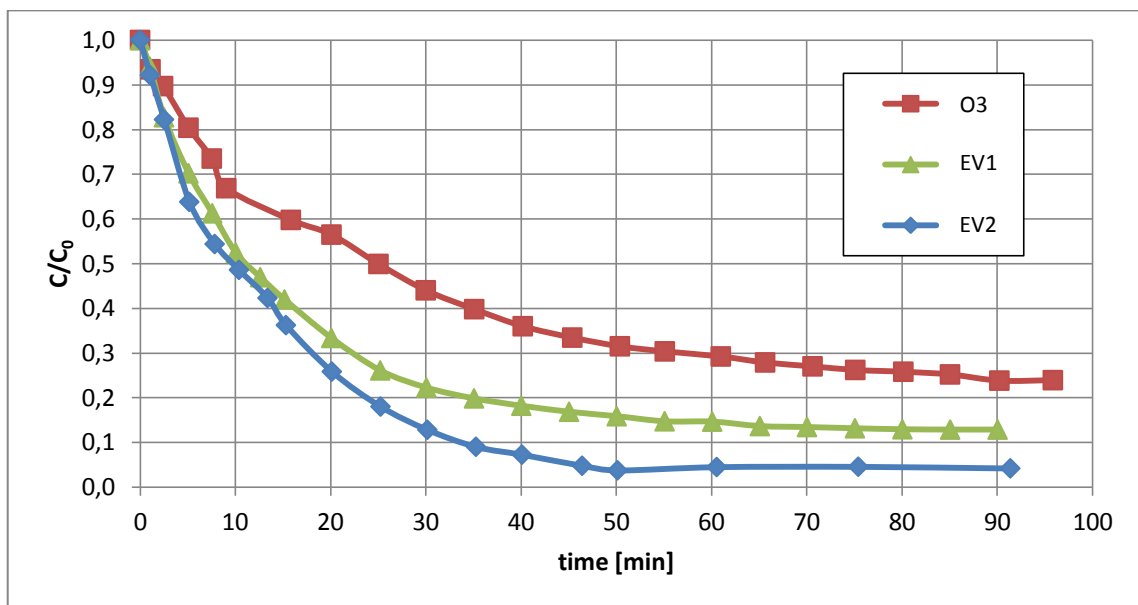- permanent time $\tau = 30$ min;
- initial pH 8.4.

Fig 8.18 – Effect of different gas diffuser types

Configuration	E%
O_3 mixture	75
EV1	86
EV2	96

Maximum exhaustion rate was reached with Mixed Venturi ejector. Probably the ejector mixing room confers a peculiar characteristic.

Using Mixed Venturi ejector, the influence of liquid permanent time (τ) was evaluated. In addition to this, one test was carried out introducing ozone in the system without ejector (through the connection in the circuit pipe) and 30 min liquid permanence time. The operative conditions were:

- initial dye concentration $C_0 = 25$ mg/L;
- gas flow rate $Q_g = 100$ NL/h;
- recirculation liquid flow rate 830 L/h;
- ozone dosage 4.4 g/h (2% v/v);
- $pH_0 = 8.4$.

τ [min]	E%
ejector EV2	
15	81
30	96
45	99
60	99
without ejector	
30	79
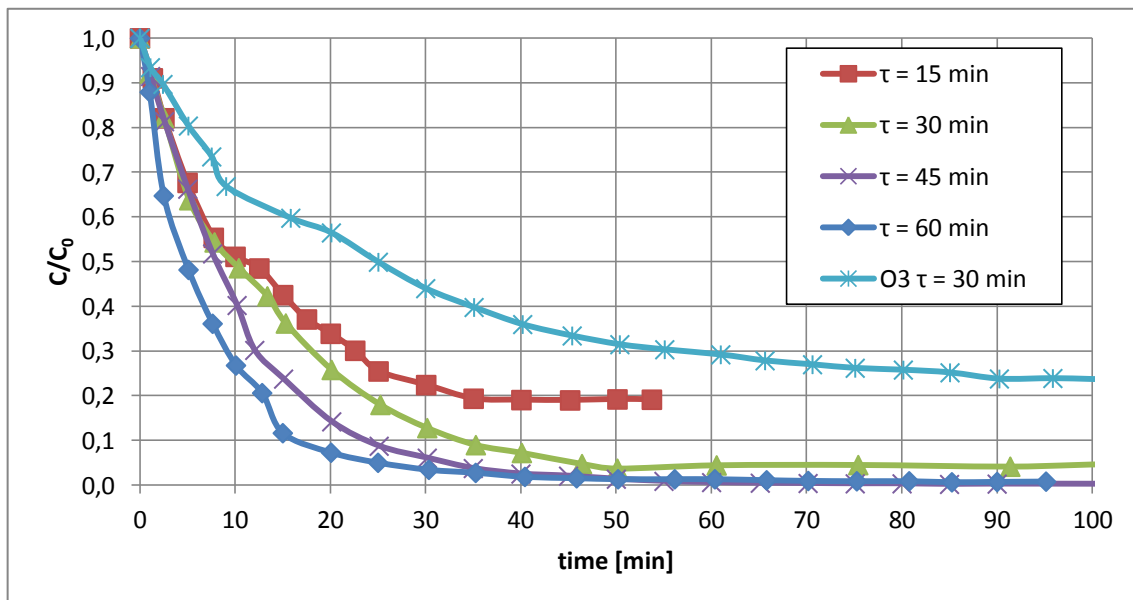
Fig 8.18 – Effect of different permanence time on decolouration kinetics

Ejector mixing degree enhances ozone transfer in the liquid media: taking into account the tests with the same permanence time, the stationary condition were reached at final exhaustion bath of 76% and 95% ($\tau = 30$ min), respectively.

Considering the operational conditions, permanence time higher than 30 min are excessive. Therefore, $\tau = 30$ min seems to be the most appropriate permanence time value.

8.3.1.2 Bubble column reactor

In order to validate the results obtained in multi-task reactor, a bubble column reactor was used with the same operational conditions.

The graph (Fig 8.19) shows the concentration trends along the bubble column at the following conditions:

- initial dye concentration $C_0 = 25$ mg/L;
- gas flow rate $Q_g = 100$ NL/h;
- recirculation liquid flow rate $Q_L = 830$ L/h;
- ozone dosage 4.4 g/h (2% v/v);
- permanence time $\tau = 30$ min;
- initial pH 8.4.
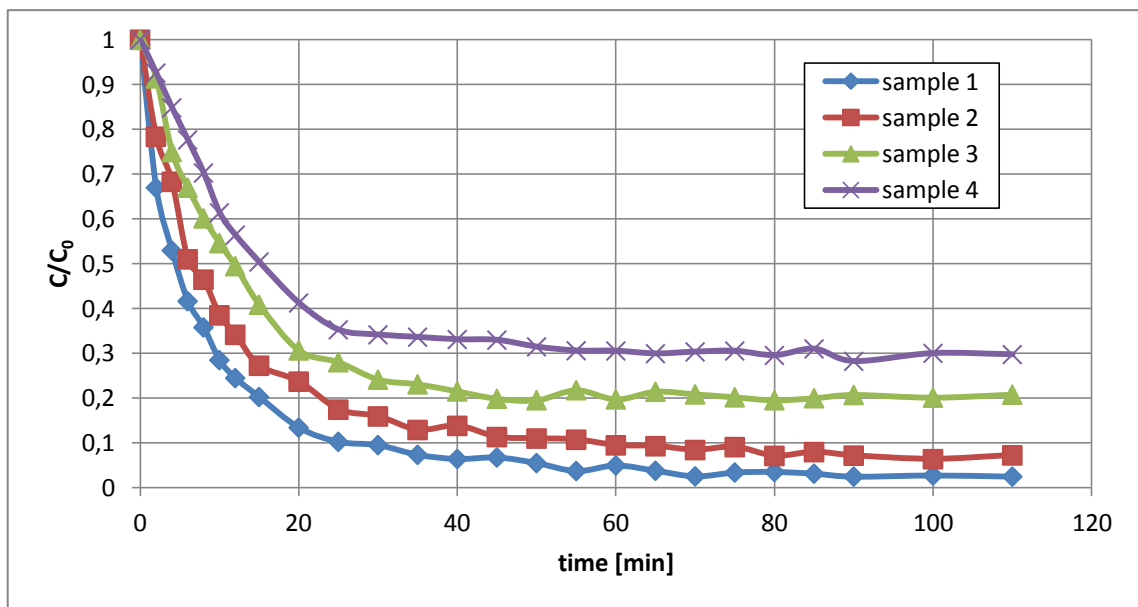
Fig 8.19 – Decolouration curves by bubble column reactor sample ports

The violet curve correspond to the samples took through sample port 4, the highest of the column.

Sample port	E %
4	70
3	79
2	93
1	98

In conclusion, it is possible to assert that the final decolouration efficiency of the two equipments is comparable: decolouration obtained with Mixed Venturi ejector reached exhaustion value of 96% and that in the bubble column of 98%.

8.3.2 Acid dye: Nylosan Blue E-2GL

Bubble column reactor and ejector performance were compared using the acid dye Nylosan Blue E-2GL. The experimental tests variables are reported above:

- initial dye concentration $C_0 = 25$ mg/L;
- gas flow rate $Q_g = 100$ NL/h;
- recirculation liquid flow rate $Q_L = 830$ L/h;
- ozone dosage 4.4 g/h (2% v/v);
- permanence time $\tau = 30$ min;
- initial pH 6.7.

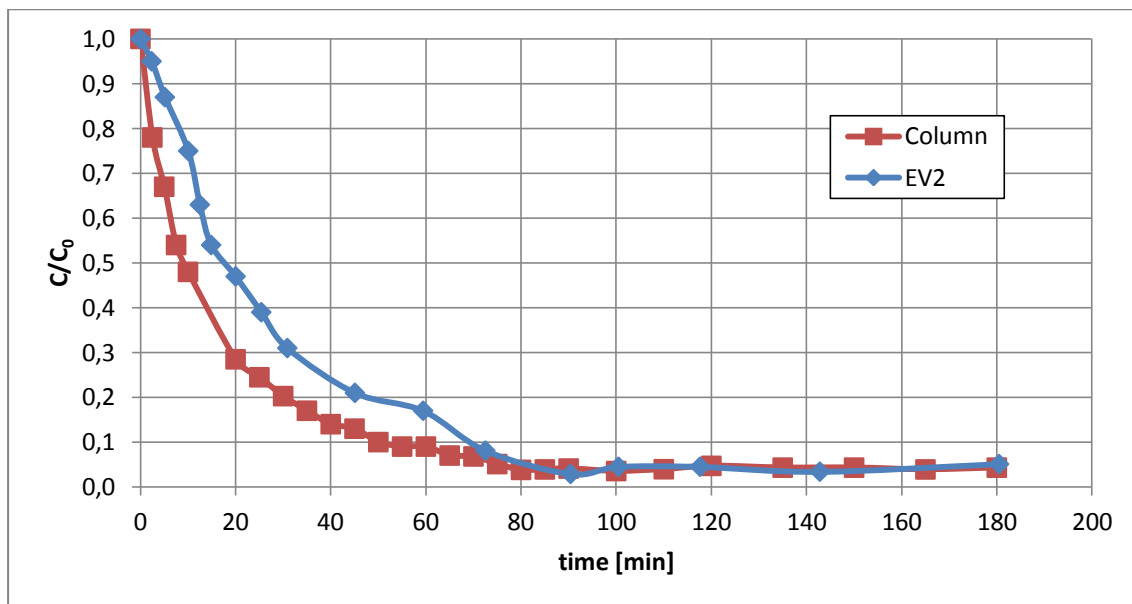Fig 8.20 – Comparison between bubble column (sample port 1) and Mixed Venturi ejector (d = 3mm), acid dye

The two devices reached the stationary conditions at the same decolouration degree: the colour exhaustion was about 95%. As happened in the batch tests, acid dye took more time to reach the maximum exhaustion percentage than the reactive dye used in the previous tests. This fact is independent from the molecular weight of the dyes; in fact, reactive dye molecular weight is about double that that acid dye one.

Although the final exhaustion degree is the same, the decolouration pathways are quite different comparing the results from the equipments: therefore, with the same reaction time, bubble column reached a colour exhaustion greater than ejector dynamic.

8.3.3 Cationic dye: Malachite Green

Bubble column reactor and Mixed Venturi ejector devices experimental tests are listed:

- initial dye concentration $C_0 = 25$ mg/L;
- gas flow rate $Q_g = 100$ NL/h;
- recirculation liquid flow rate $Q_L = 830$ L/h;
- ozone dosage 4.4 g/h (2% v/v);
- permanence time $\tau = 30$ min;
- initial pH 6.4.

Fig 8.21 – Comparison between bubble column (sample port 1) and Mixed Venturi ejector (d = 3mm), cationic dye

Acid and basic dyes seem to have the same behaviour in decolouration by ozone. Basic dye reached a little further of 95% decolouration degree in stationary conditions.

8.3.4 Disperse dye: Serilene Scarlet G-LS

Ultrasound cavitation was used to improve the dissolution of disperse dye in water. Namely, the ultrasounds aim was to reduce the dye micelle dimension.

Laboratory experimental tests had the following variables:

- initial dye concentration C_0 = 25mg/L;
- gas flow rate Q_g = 100NL/h;
- recirculation liquid flow rate Q_L = 830L/h;
- ozone dosage 4.4 g/h (2% v/v);
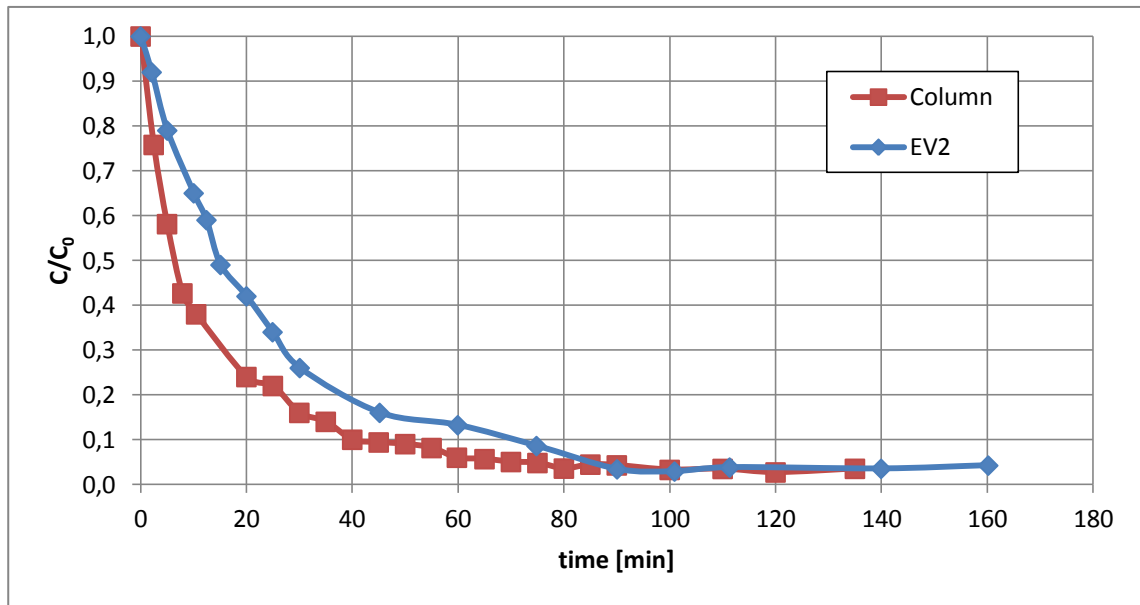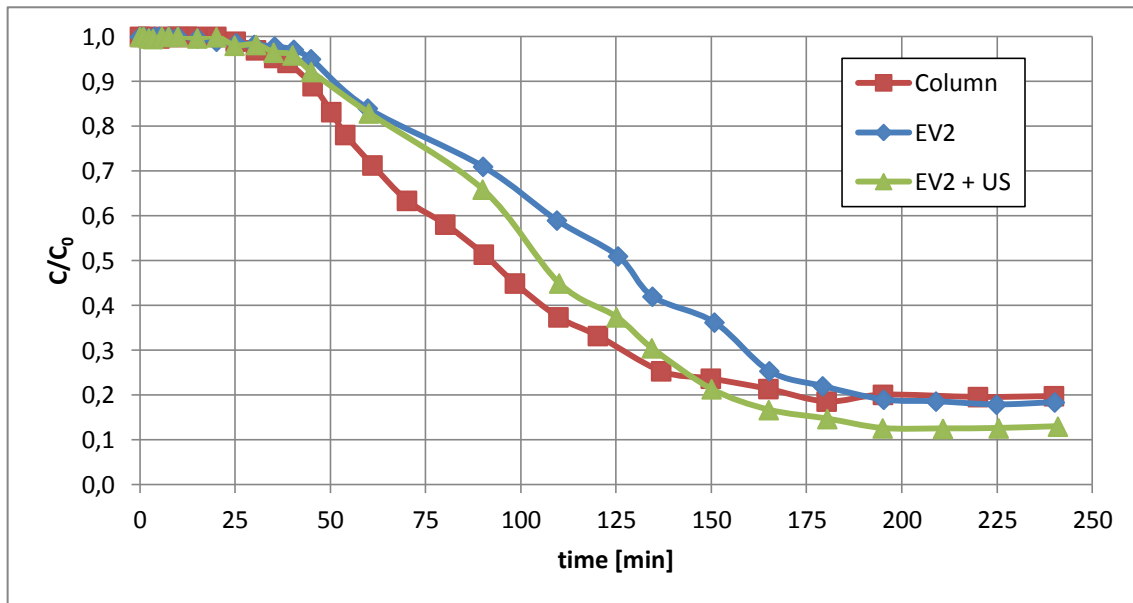- permanence time τ = 30min;
- initial pH 7.0.

Fig 8.22 – Comparison between bubble column (sample port 1) and MixedVenturi ejector (d = 3mm), disperse dye

From the curves, ultrasound cavitation seems to affect the final exhaustion degree: at the stationary conditions, decolouration reached about 88%; instead, the same test in multi-task equipment, without ultrasound decolouration, is five percentage points lower (same result as in bubble column).

Taking into account the results of the experimental tests carried out with ultrasound cavitation, it is possible to assume that ultrasounds operate only on solid phase rather than on the liquid one: ultrasounds are able to break up the disperse dye micelle and, consequently, increase the dissolution velocity in water.

Therefore, ultrasounds seem to operate only by mechanical effects. Certainly, ultrasounds cavitation exists in the reactor vessel but the effects are negligible: hydroxyl radicals by cavitation are present for a short time period, has a limited action volume and negative resonance effects could be the cause of the cavitation inefficiency.

8.4 Bubble column reaction rate interpretation

In Chapter 7, dispersion coefficient in bubble column was discussed. Moreover, the methodology used to calculated axial dispersion coefficients was described. Consequently, axial dispersion model was adopted to model the concentration values along the column height in the particular case of Reactive Blue decolouration. Moreover, from the conclusion of chapter 7, we want to underline possible differences between axial dispersion model and ideal plug flow model in data analysis.

8.4.1 Axial dispersion and ideal plug flow model

The following assumptions were considered in order to define the models:

- mass transfer resistance in the gas and liquid film are considered negligible, consequently the reaction is written as the ozone used in the reaction was just in liquid phase;

- steady-state condition;
- superficial gas and liquid velocities are constant along the *z*-direction of the column;
- the reaction between by-products and ozone is not included in the liquid phase equation.
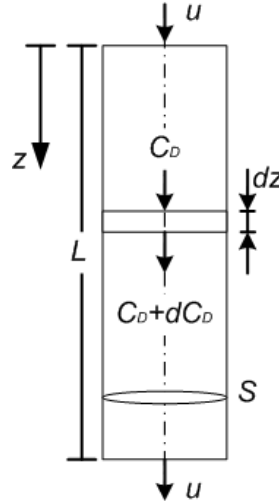
Fig 8.23 – Control volume control for continuity equation for reactor model

In the case in which bubble column reactor is modelled using axial dispersion coefficient, the material balance for the dye (D) around the differential control volume shown in Fig 8.23, can be written:

$$uSC_D - E_zS\frac{dC_D}{dz} - uS\left(C_D + \frac{dC_D}{dz}dz\right) + E_zS\left[\frac{dC_D}{dz} + \frac{d}{dz}\left(\frac{dC_D}{dz}\right)dz\right] + \\ + S(+r_D)dz = 0 \tag{8.1}$$

where S is the column superficial area, u is the superficial liquid velocity, C_D is the dye concentration, E_L is the axial dispersion coefficient and r_D is the reaction term. In our case, the kinetic reaction is pseudo-first order to dye concentration, from the batch experimental tests. Therefore $r_D = -k'C_D$ where $k' = kC_{O_3}$.

The above Eq. 8.1 can be simplified to

$$E_z\frac{d^2C_D}{dz^2} - u\frac{dC_D}{dz} - k'C_D = 0$$

In partial non-dimensional form with $x = z/L$, $Bo_L = uL/E_z$ and $C = C_D/C_{D,0}$, the equation becomes

$$\frac{d^2C}{dx^2} - Bo_L\frac{dC}{dx} - Bo_L\tau k'C = 0$$

- 143 -

where τ is the permanence time of the single fluid portion in the reactor.

For this equation, an analytical solution is available for closed-closed vessel boundary conditions.

The result is

$$C = \frac{C_D}{C_{D,0}} = \frac{4\beta exp\left(\frac{Bo_L}{2}\right)}{(1+\beta)^2 exp\left(\beta\frac{Bo_L}{2}\right) - (1-\beta)^2 exp\left(-\beta\frac{Bo_L}{2}\right)} \quad (8.2)$$

where

$$\beta = \sqrt{1 + \frac{4k'\tau}{Bo_L}}$$

and C_D is the dye concentration at the steady-state and $C_{D,0}$ is the initial dye concentration.

By trial and error method, k' was evaluated considering the measured values $\frac{C_D}{C_{D,0}}$ and τ.

In addition, the longitudinal dispersion coefficient (E_z) was calculated by the methodology described in Chapter 7 for Reactive Blue CI 29.

In the case in which bubble column reactor is modelled as an ideal reactor (plug flow reactor), the material balance for the dye (D) around the reactor can be written as follows, at steady-state condition

$$uSc_D - uS\left(C_D + \frac{dC_D}{dz}dz\right) + S(r_D)dz = 0$$

Considering pseudo-first order kinetics and simplifying the equation is as follows

$$udC_D = -k'C_D dz$$

Integrating the equation, the equation becomes

$$k' = -\frac{1}{\tau}ln\frac{C_D}{C_{D,0}}$$

where τ is the permanence time defined as follows

$$\tau = \frac{L}{u}$$

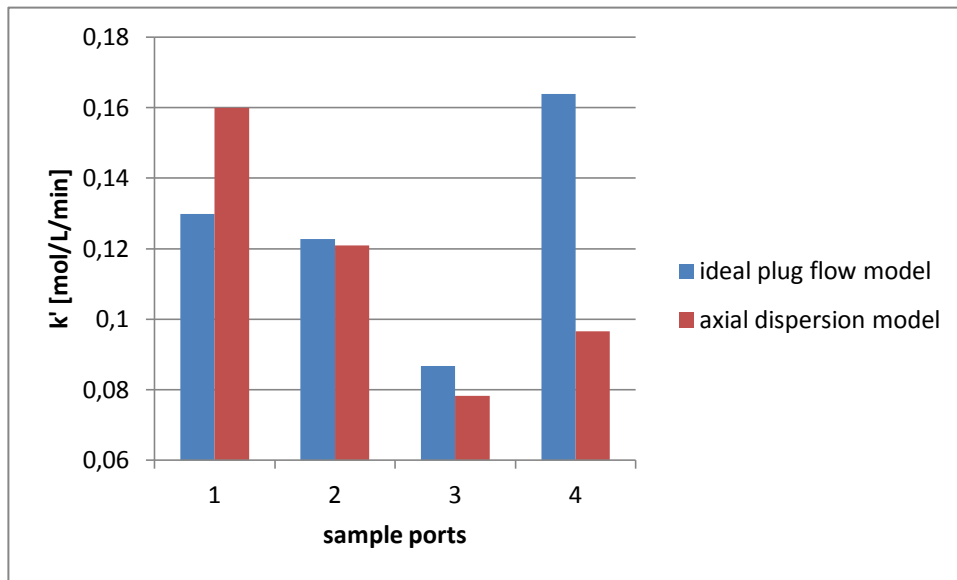## 8.4.2 Bubble column reaction rate interpretation

Fig 8.24 – Pseudo-first order kinetic constant: ideal plug flow and axial dispersion model; bottom position sample port 1

Fig 8.24 shows the kinetic rate values, calculated considering the two previous models and taking into account each sample port along the reactor and the corresponding dispersion coefficient. The values reported can be compared only at the same sample port, since k' is the product between the real kinetic constant and the mean ozone liquid phase concentration corresponding to the volume control taken into account.

Values calculated in sample points 1 and 4 are not comparable: dispersion coefficient has a greater influence corresponding the gas and liquid inlet, respectively. The variation is much more evident in sample port 4 due to liquid inlet: the liquid is introduced punctually in the reactor creating a strong mixing. On the other hand, gas flow is introduced by sintered gas diffuser in a homogeneous way and the mixing is less pronounced.

Considering the sample ports 2 and 3, input flow (liquid or gas) are quite distant from the sampling points, therefore the kinetic constants assume quite the same values.

Using the mean kinetic values and the mean dispersion coefficients calculated in sample ports 2 and 3, the theoretical curves based on the models are reported in the Fig 8.25 (abscissa equal to 0 m corresponds to the bubble column top).

Both the model curves are quite similar and they fit the experimental data obtained in sample ports number 1, 2 and 3. The last value is quite distant: the pseudo-first order kinetics in correspondence of sample port number 4 is wrong. At the top of the bubble column, the ozone liquid concentration can reach low values due to ozone consumption along the column. On the other hand, liquid has the maximum concentration. In this conditions, the assumption of pseudo-first order kinetics decays.

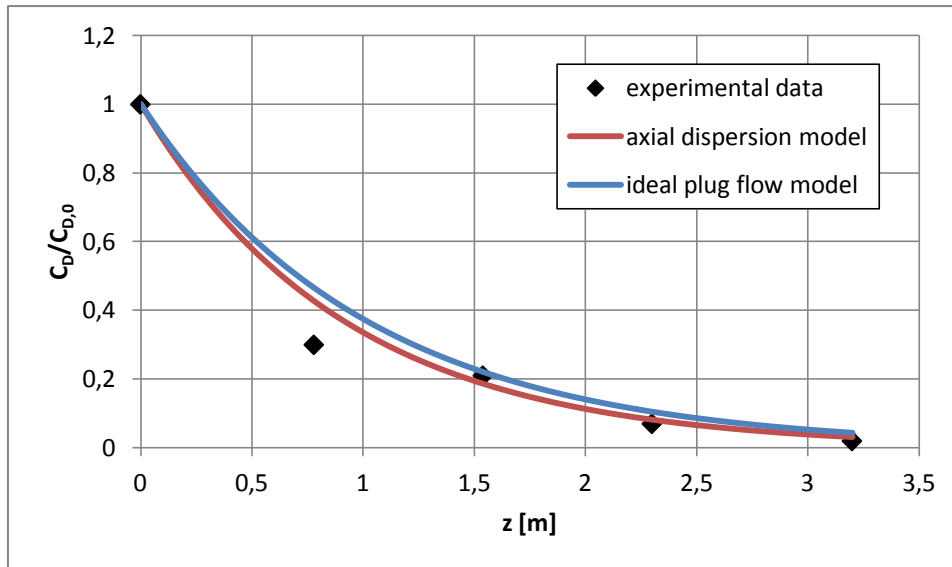Fig 8.25 – Experimental data, axial dispersion and ideal plug flow models trends

Thanks to this result, preliminary conclusions can be done:

- axial dispersion and ideal plug flow models can be used to predict bubble column concentration profile only for the middle-bottom column section;
- the assumption of pseudo-first order kinetics is wrong considering top-middle column section, at the operational conditions used in this work.

References

[1] F. Saunders, J.P. Gould, C.R. Southerland, The effect of solute competition on ozonolysis of industrial dyes, *Water Resource,* **17**, 1983, 1407-1419.

[2] M. Matheswaran, I.S. Moon, Influence parameters in the ozonation of phenol wastewater treatment using bubble column reactor under continuous circulation, *Journal of industrial and engineering chemistry*, **15**, 2009, 278-292.

[3] V.K. Saharan, M.P. Badve, A.B. Pandit, Degradation of reactive red 120 dye using hydrodynamic cavitation, *Chemical Engineering Journal*, **178**, 2011, 100-107.

[4] P.R. Gogate, G.S. Bhosale, Comparison of effectiveness of acoustic and hydrodynamic cavitation in combined treatment schemes for degradation of dye wastewater, *Chemical Engineering and Processing*, **71**, 2013, 59-69.

[5] H.L. Needles, Textile fibers, dyes, finishes, and processes, *Noyes Publications*, 1986.

Chapter 9 – Decolourised water dyeing

As mentioned in the first chapter of this work, two are the wastewater treatment purposes: the first was to give to treated water the minimal characteristics to drain into superficial water and the second to optimize some parameters (such as COD, colour, salt content, etc.) to recycle treated water in the same process. The last was the focal point of this research.

The following experiments are focused on colour problem. In detail, we tried to understand what is the optimum decolouration degree, and therefore the minimum dye concentration, to have a good fibre dyeing, in terms of colour, compared to fibre dyeing with pure water.

As for the colour, what is the minimum dye concentration needed to maintain the same quality colour of the dyeing process with natural water? This is a difficult question, and the only answer is performing tests able to give useful indications for industrial reuse of decolourised water. To reach this scope the pilot and laboratory apparatus of the LATT (Laboratory of Advanced Textile Technology) laboratories in Biella were used.

9.1 Pilot plant, machinery and instruments of LATT laboratory used

9.1.1 API/O OBEM

API/O is an industrial dyeing device built by Obem S.p.A. The apparatus is composed from a minimum of 12 to a maximum of 24 horizontal tubes (autoclaves) which contain the textile material to dye. Textile material is in yarn package conformation. Each autoclave is able to take up to 12 bobbins, with a weight of about 2 kg, placed on a special perforated barrel.

The autoclaves are connected with a series of heat exchangers, in order to heat the fluid. The fluid motion is guaranteed by a centrifugal pump that enables a circular radial dye bath through the bobbins. In addition, a four way diverter is used to change fluid direction, in order to increase textile material colour homogeneity.

An expansion vessel is used to circulate the dye bath, thanks to a static pressure pump which allows to maintain the apparatus at a pressure sufficiently high for the dyeing cycle to be performed.

The maximum dyeing temperature is 100 °C and the liquor ratio can be reached with a very low value from 1:4 to 1:6, that allows to obtain sensible savings of thermal energy, water and chemical products.

In our laboratory, an API/O device is present, but it is adapted for dyeing laboratory tests. Of course, it is built with only one autoclave (Fig 9.1). The other parts of the apparatus are the same of the industrial one, obviously designed to dye a lower quantity of textile material.
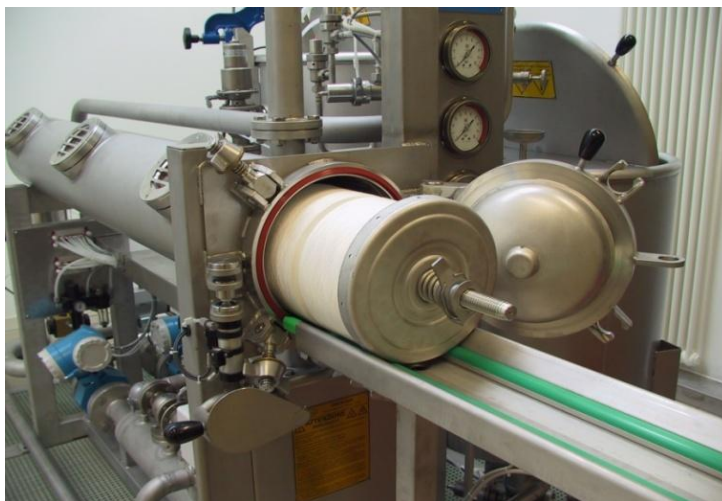

Fig 9.1 – API/O device

9.1.2 Teintolab

Teintolab [2] is a diagnostic laboratory-scale dyeing machinery that allows the interpretation of the ongoing process in terms of exhaustion and diffusion of the dyes and optimal temperature profiles. Although in small scale, Teintolab is also used in the industrial field because it is able to simulate a proper industrial dyeing process.

It is interfaced with a computer provided with a control application, so it is possible to instantly check the values of dye-bath exhaustion, pH and temperature. These information, provided continuously from the equipment, are a great innovation for the development and the optimization of the dyeing processes.

On the main circuit there is the tank where the dyeing takes place: its liquid maximum volume capacity is 1 L.

Teintolab analysis system uses the Lambert – Beer law: it relates the attenuation of light to the properties of the liquid through which the light is travelling.

A light beam, from a halogen lamp, passes through the bath and, after that, it is analyzed by four different wavelength phototubes. The data obtained are in terms of transmittance, and the software transforms them in dyebath exhaustion percentage. Consequently, it is possible to evaluate the dye kinetic behaviour directly from the exhaustion curves in function of temperature, pH and other chemicals used in the dyeing process studied.
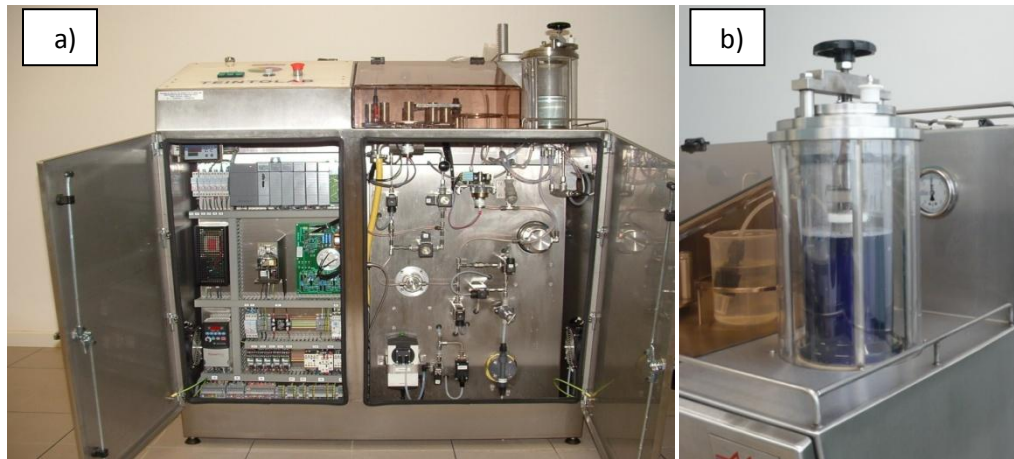
Fig 9.2 – Teintolab: a) device structure and b) dyeing tank

9.1.3 Colour space and Datacolor device

Datacolor device is the instrument used in this work to compare colour among samples. Taking into account a standard yarn dyeing, the other dye yarns are compared to it. Datacolor gives, as a result, a numerical value that means how much the colour is different. Before discussing about Datacolor, it is important to understand what is colour and its representation.

The CIE 1976 L*a*b colour space system (CIELAB) [3], is one of the most used method for measuring and ordering colour. CIELAB was created to describe the visible colours detected by the human eye and as a device-independent model to be used in order to define the difference between two apparently equivalent objects.

It is normally used in textile, ink, paint, paper, printed materials and other industrial painted objects.

CIELAB is the evolution of the 1931 CIE system. The fundamental principle governing the two methods is given by the definition of colour: colour is a subjective sensation defined by the combination of light, object and observer.

The *light* has an important role in the determination of the colour. Light can be artificial (it is generated, for example, by heating a metal filament, or exciting atoms or molecule by an electric arc) or natural (sun). Sun is the most important light source and it is influenced by different parameters such as latitude (affecting the incident angle between sunlight and the Earth), season, meteorological condition, time, air pollution and so on. Usually, colour is characterized by the colour temperature. Colour temperature of one light source is defined as the equivalent temperature of one black body whose aspect is similar to the original light source. It is measured in Kelvin degree. For this reason, standard light needs to have a comparable colorimetric measure.

The *object* modifies the direction of the light. The incident light hit the object and only the emitting light source is captured by the observer. The energy corresponding to the incident light can be divided in two categories: diffusion energy and specular energy. The first one is responsible of object colour and it is an intrinsic characteristic of the material. On the other side, the second one gives shine or opacity to the object. When

the emitting energy is completely classified as diffused energy, the human eyes perceives white colour, contrarily black is the dominant colour.

The last element used to define colour is the *observer*, especially the interpretation of the brain to the light stimulus coming from the transmitting object. The light signal is captured by particular organs receptors in the retina, called cones and rods. They transform the signal into three neural signals, which are passed along the nerve fibres. Cones are sensible to the colour (responsible for the daylight vision) while rods are organs specialized in night vision. Study conducted in the 19th and 20th centuries demonstrated that the retina has three different receptors that capture the light (namely for blue, green and red light). These signals are converted between the eye and optical nerve in other three series of signals called opponent or antagonist couples. They are white - black, red - green and yellow - blue couples (Hering theory -1878- confirmed by Muller -1930-). Consequently, the main concept of opponent couples is that a colour cannot be at the same time red and green, yellow and blue or black and white.

The luminosity represents another parameter that influences the observer's colour perception. Rezold-Bruke effect is a condition in which, if the observer is dazzled, his colour perception will be different. In other words, the increase of brightness corresponds in the shifting of the reds and greens to yellows and the violets and blue-greens to blue: in this way, brightness transforms a tri-chromatic vision in a bi-chromatic one.

The main advantage of CIELAB is the organization of colours where visual perception of colour is well correlated with numerical values. Thanks to this, CIELAB gives the possibility to compare objects with different colour using numerical evaluations.

The CIELAB space can be described in Cartesian coordinates corresponding to:

- L*: lightness (L* > 0 to white, L* < 0 to black);
- a*: red/green coordinate (a* > 0 to red, a* < 0 to green);
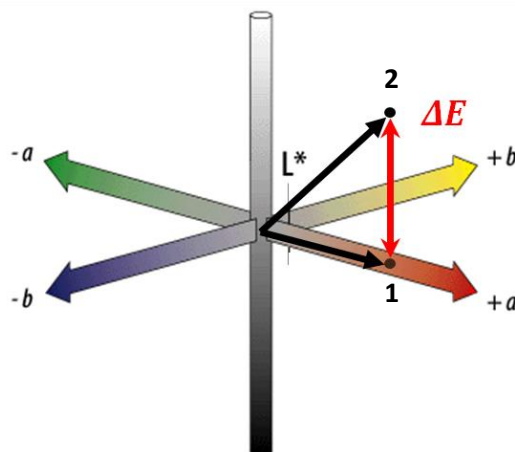- b*: yellow/blue coordinate (b* > 0 to yellow, b* < 0 to blue).

Fig. 9.3 – CIELAB space and example of ΔE: point 1-standard, and 2-sample

If the three coordinates are defined, the colour will be well known and located in the space.

Thanks to this representation, it is possible to define colour difference between different objects that apparently seem of the same colour. The colour difference of two objects is simply defined as the space distance between the two colour locations in the CIELAB space, ΔE.

Generally, a standard coloured object is defined as the benchmark (L*$_b$, a*$_b$, b*$_b$) and from its colour characteristics is defined the distance ΔE of the second studied object, characterized by its own L*, a* and b* parameters.

ΔE expression is written below:

$$\Delta E = \sqrt{\Delta L^{*2} + \Delta a^{*2} + \Delta b^{*2}}$$

where

-   $\Delta L^* = L^* - L_b^*$: lightness difference;
-   $\Delta a^* = a^* - a_b^*$: red/green difference;
-   $\Delta b^* = b^* - b_b^*$: yellow/blue difference.

In textile dyeing, the limit ΔE under which two colours are considered without difference is 1.

Fig 9.4 – Datacolor 3890

In this work, the instrument used to locate colour in the CIELAB space is the spectrophotometer Datacolor 3890. This instrument is able to detect colour from solid matters. Its mode of operation is based on reflection spectrophotometry, i.e. the instrument receives the portion of light reflected by the solid surface when it is hit by visible light.

It is important to remember that a white light source can be decomposed in its chromatic components if it passes through a glass prism. When the incident light waves hit a solid surface, some waves will be absorbed by the solid and the others will be reflected. The reflected waves give the colour sensation to the observer and the others are classified as the complementary waves.

Reflectance $R(\lambda)$ is defined as the ratio between the radiation flux (I_r) reflected by the surface and the total radiation given by the light source (I_0).

$$R(\lambda) = \frac{I_r}{I_0}$$

It is a dimensionless value and depends on the wavelength (λ).
The light is generated from the Ulbricht sphere: it consists of a hollow sphere with the inner walls perfectly diffusing; thanks to this, it is possible the total reflection of light.
As mentioned before, light is one of the three parameters that characterize colour. In our case, the light chosen for the analysis is light D65, that means average daytime light of the central Europe latitudes.

9.2 Dyeing results using wastewater treated with ozone

The experimental part was organized according to the following steps.

9.2.1 API/O industrial dyeing

The wool bobbins were dyed by using the API/O device as an industrial process and collect the wastewater. Wool dyeing characteristic are reported in Table 9.1.

Table 9.1 – API/O dyeing characteristics (owf: on weight fibre)

Dye	Red Kemanol FGN		2 g/L
	Indigol IW/C	dispersing agent	5.0 % owf
Chemicals	Cerriopal WM	levelling agent	0.2 % owf
	Lanasan PW	wool protecting agent	0.8 % owf
Salt	Sodium sulphate		2.5 % owf
Acetic acid		pH = 5	5.0 % owf
Liquor ratio		1:25	

9.2.2 Wastewater ozonation

The volume of wastewater to treat with ozone is the sum of the exhaust dye-bath after dyeing treatment and the washing water. Usually, in the dyeing plant three washing cycles are done. Therefore, a large volume of water was available to be treated with ozone in the pilot plant.
For our purpose, it is important to know the dye bath concentration, before treating it with ozone. After API/O dyeing, the exhaustion bath is attested to 95% of the initial dye concentration. After the dilution with water comes from washing processes, the final dye concentration is about 50 mg/L (defined by spectrophotometrical analysis).
During ozonation treatment, about 1 L of treated water was taken at different times that correspond to different decolouration degree (respectively 53, 76, 89, 96, 98, 99 and 100%). The colour and the corresponding percentage are reported in Fig 9.5.
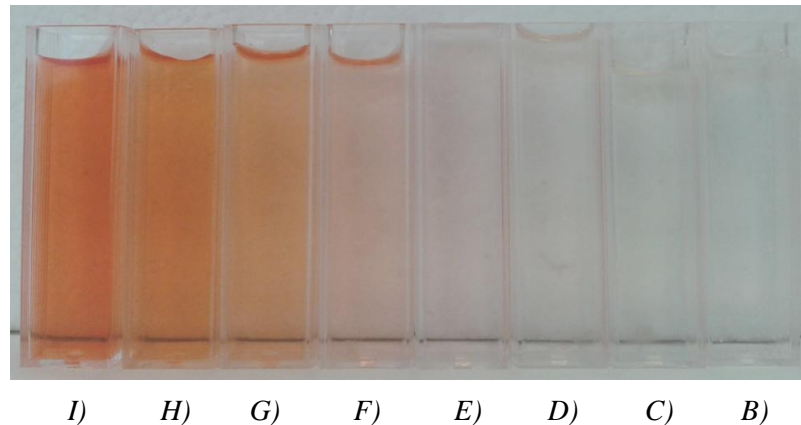
Fig 9.5 – Decolouration degree: form left to right exhausted bath from API/O dyeing with dilution and 53, 76, 89, 96, 98, 99, 100 % decolouration by ozone process

9.2.3 Teintolab dyeing with ozonated wastewater

The liquid obtained after the ozone treatment was used as the water for dyeing wool with Teintolab (same type as used in point 2) with Blue Nylosan E-2GL (Acid Blue CI 40) according to the dyeing characteristics showed in Table 9.2. Blue dyestuff is used to underline the difference, in terms of colour, of the final fibre colour.

Table 9.2 – Teintolab dyeing characteristics (owf: on weight fibre)

Dye	Blue Nylosan E-2GL		0.3 g/L
	Indigol IW/C	dispersing agent	5.0 % owf
Chemicals	Cerriopal WM	levelling agent	0.2 % owf
	Lanasan PW	wool protecting agent	0.8 % owf
Salt	Sodium sulphate		2.5 % owf
Acetic acid		pH = 5	5.0 % owf
Liquor ratio		1:25	

In Fig 9.6 are presented the wool dyeing results obtained. The correspondence between the wool samples in Fig 9.6 and the water used for dyeing this samples (Fig 9.5) is that for sample *b* was used water *B*, for sample *c* water *C*, and so on.

Sample *a* in Fig 9.6 refers to wool dyeing with pure water. It is clear that the worse is the water used for dyeing from *I* to *B* and the worse is also the wool results from *i* to *b* due to the residual red dye after ozonation presents in the water used for dyeing process. In Fig 9.6 *l* represents the wool dyed by red using the API/O semi-industrial machinery (point 1).
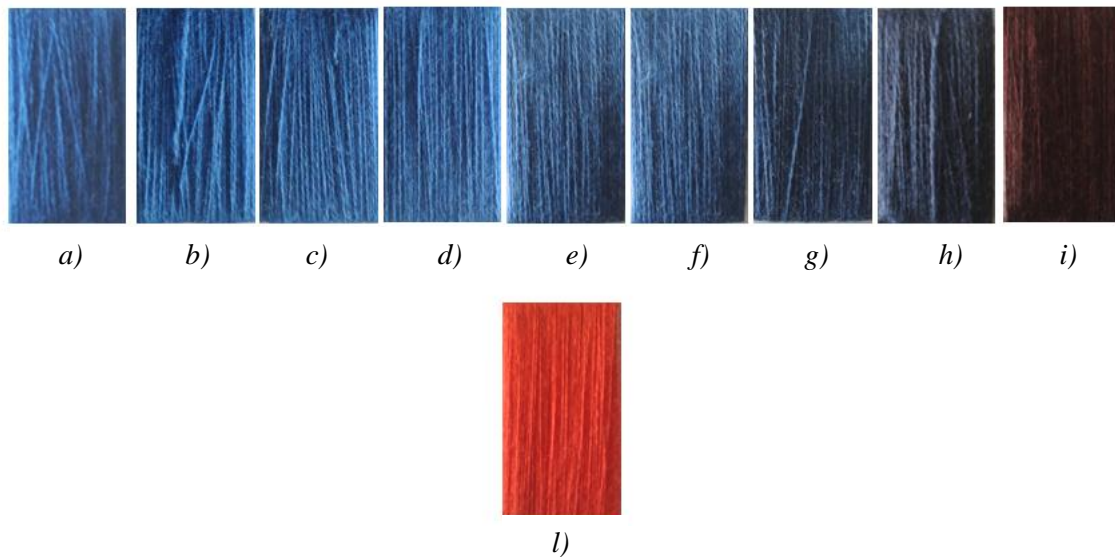
Fig 9.6 – Wool dyeing results

Table 9.3 – Samples characteristics

Sample	Dyeing device	Bath decolouration degree E [%]	Other
a		-	Benchmark
b		100	-
c		99	-
d		98	-
e	Teintolab	96	-
f		88	-
g		76	-
h		53	-
i		-	Exhausted dye bath
l	API/O	-	-

9.2.4 Quantitative examination of the wool dyed with the waste liquid treats with ozone

The wool dyed with the liquid from *B* to *I* of Fig 9.5 are detected by Datacolor instrument and the results are reported in Table 9.4, in terms of ΔE.

Every sample (from *b* to *h*) was compared with sample *a* dyed with pure water. Generally, two dyed fibres are considered in agreement when the ΔE variation with the reference (sample *a*) is less than 1. As can be seen in Table 9.4, ΔE < 1 only for the samples *b* and *c* that is 0.68 and 0.82, respectively.

Consequently, the samples dyed with decolourised water up to 98% are not acceptable (ΔE > 1).

Table 9.4 – *ΔE* results

Sample	L*		a*		b*			
a	*44,14*		*-10,55*		*-28,16*			
b	43,74		-11,02		-27,90			
c	43,30		-10,83		-27,72			
d	43,24		-10,80		-27,65			
e	41,51		-9,09		-23,43			
f	39,65		-6,44		-20,21			
g	37,34		-2,58		-16,33			
h	33.87		-2,86		-12.48			
	*ΔL**		*Δa**		*Δb**		*ΔE*	
b	-0,40	to black	-0,47	to green	0,26	to yellow	0,68	+
c	-0,84	to black	-0,28	to green	0,44	to yellow	0,82	+
d	-0,91	to black	-0,25	to green	0,51	to yellow	1,07	+/-
e	-2,63	to black	1,46	to red	4,73	to yellow	5,61	-
f	-4,50	to black	4,11	to red	7,95	to yellow	10,02	-
g	-6,80	to black	7,97	to red	11,83	to yellow	15,80	-
h	-10.27	to black	7.69	to red	23.37	to yellow	26.66	-

In conclusion, if the decolouration degree is equal or greater than 98%, treated water will be reused in another dyeing cycle. This means that the wastewater dye concentration after ozonation (Red Kemanol FGN) must be lower than 1 mg/L to be recycled.

References

[1] F. Corbani, Nobilitazione dei tessili, *Centro Tessile Cotoniero*, 1990.

[2] Teintolab: Operating instructions, Coumereg.

[3] A. Chrisment, Colore e colorimetria, *Datacolor International*, 1998.

[4] M. Muthukumar, D. Sargunamani, M. Senthilkumar, N. Selvakumar, Studies on decolouration, toxicity and the possibility for recycling of acid dye effluents using ozone treatment, *Dye and Pigments*, **64**, 2005, 39-44.

Chapter 10 – Conclusions

The degradation of dyes with ozone is a typical gas-liquid two-phase oxidation where an effective transfer of ozone to liquid is the critical point of view. The kinetics of decolouration is generally fast, though, the mass transfer representing the rate limiting step.

In this work, hydrodynamic and ultrasonic cavitation were studied with the main purpose of enhancing ozone mass transfer. In order to verify mass transfer efficiency, decolouration experimental tests were performed. In addition, decolouration kinetics was also studied both for hydrodynamic and ultrasonic cavitation without ozone, thanks to their ability to produce hydroxyl radical during vapour cavity collapse.

Hydrodynamic cavitation effect was produced by two ejector devices having different geometry (Herschel-type Venturi -EV1- and Mixed Venturi -EV2-) and ultrasonic cavitation was generated by a cylindrical device (up to 1000W, 25 kHz).

Four different dyestuffs were used to give general considerations: Reactive Blue CI 29 , Acid Blue CI 40, Basic Green CI 4 and Disperse Red CI 54.

The first part of the present work was focused on the experimental equipments, particularly on their hydrodynamics. Two pilot equipments were designed and built: a bubble column reactor (characterized by plug flow hydrodynamic) and a recirculation multi-task reactor (characterised by well mixing hydrodynamic). The bubble column reactor was built as a benchmark process for continuous tests, because it represents the most common reactor used in oxidation wastewater treatment. In addition, hydrodynamic characterization was done, in order to calculate commercial dye disperse coefficients the column. The recirculation multi-task equipment was designed in order to accommodate ultrasonic and hydrodynamic devices.

Before decolouration experimental tests, each ejector performance was evaluated. Particularly, experimental tests were done changing operative conditions (liquid flow rate – inlet pressure) and geometry (throat section diameter) in order to define:
-   cavitation number (σ_c);
-   vacuum pressure degree;

- sucked air flow rate.

The following conclusions were drawn according to the results obtained in the previous described tests:
- in Hershel-type Venturi, minimum cavitation number to have effective cavity implosion was 0.2. For lower σ_c values, cavities implosion efficiency decreased because a cavitation cloud formed (the cloud was made of high numbers of very small bubbles). Cushioning effect prevails and the implosion of bubbles was not able to create "hot spot";
- 12 dB relative noise, with respect to room noise, corresponds to cavitation inception;
- vacuum pressure in the throat section tends to absolute vacuum, increasing liquid kinetic energy through the ejector device (maximum vacuum degree equal to 9.8 mH_2O);
- ejectors capacity to suck air is quite different, due to their geometry. Ejector EV2 was designed with convergent and divergent sections connected by a small diameter channel, instead ejector EV1 middle section had a "mixing room". Air flow rate evaluation showed that at the same diameter (e.g. 4 mm) Herschel-type Venturi ejector was able to suck air about three times more than standard Venturi one;
- hydrodynamic cavitation was ineffective when gas was sucked in the ejectors throat section. The bubbles implosion effect was softened by compressed air.

Preliminary ultrasound evaluation tests were performed in the reactor, using an instrument able to detect ultrasound cavitation intensity. The main validation results are described below:
- cavitation intensity in the liquid medium varies from the US surface with a sinusoidal trend, the maximum intensity value was obtained at a distance of 75 mm;
- gas flow rate influences the ultrasound cavitation fields: generally, increasing gas flow rate, ultrasound intensity decreases;
- cavitation intensity was closely related to the power generated by ultrasound transducer. Generally, halving the power, the cavitation intensity reduced of about three times.

Fluid dynamic behaviour results in the bubble column led to the following conclusions:
- dispersion coefficient was evaluated in bubble column as semi-bath reactor (liquid flow rate absent) and continuous reactor;
- in accordance with literature, dyes were used to define the dispersion coefficient. Methylen Blue and Acid Red CI 249 were used.
- three dye transport mechanisms were found and demonstrated;
- dye transport mechanisms along the column were influenced by coalescent liquid behaviour (in term of salt concentration) and gas flow rate;
- bubble column reactor fluid-dynamic involved as a plug flow reactor.

The second part of the present work aimed to investigate the equipments ability to improve ozone transfer in liquid medium. Ultrasound and hydrodynamic cavitation were performed also without ozone to test their ability to decolourise dyestuff, thanks to hydroxyl radical generation. First of all, decolouration experiments were performed in a multi-task equipment in semi-batch conditions. After that, continuous tests were carried out and the results were compared with bubble column decolouration experiments at the same operational conditions (liquid residence time, gas flow rate, ozone dose, dyestuffs and its concentration).

Below, the main results obtained in the recirculation reactor in semi-batch conditions are reported:

- decolouration by ultrasound cavitation without ozone is not much effective: maximum decolouration degree obtained was 5% after 120 min treatment;
- also decolouration via hydrodynamic cavitation brings to the previous conclusion but only 2% decolouration was reached with the same treatment time;
- ozone is a powerful oxidizing agent and it reaches, alone, a reasonable decolouration kinetics. Increasing gas-liquid mixing, e.g. in ejector, decolouration kinetics enhances;
- reaction kinetics can be ascribed to a pseudo-first order with respect to dye concentration;
- colour degradation was influenced by pH, recirculation liquid flow rate, ozone dose and ejector geometry;
- ultrasounds have worst effects on decolouration kinetics, combined with ozone. In order to reach the same decolouration level, much more time was necessary. Ultrasounds increase degassing velocity, decreasing contact time between ozone and dye.
- acid, basic and reactive dyes were easier to decolourise than disperse dye: interaction between ozone and dye is much more efficient if dyes are well solubilised in water.
- disperse dye is the most difficult class of dye to decolourise, due to their low solubility in water. Mechanical ultrasound effect enhances disperse dye decolouration by increasing dye dissolution in water.

In continuous decolouration tests, the following conclusions can be done:

- ejectors geometry influenced final decolouration efficiency. Strictly connected with it is the mixing degree and therefore the capacity to improve ozone transfer in the liquid wastewater, at the same operating conditions. For example, considering Reactive Blue CI 29 dye, Standard Venturi ejector reached 96% of decolouration against 86% of Herschel-type Venturi one, with the same treatment time.
- removal efficiency of bubble column reactor and Mixing Venturi ejector were quite close for reactive, acid and basic dye classes.
- recirculation reactor, with ozone supplied through Mixing Venturi ejector combined with ultrasonic mechanical effect activity, may be the best technology to remove disperse dye. Ultrasound are able to break up the dyestuff micelle and therefore improve dye dissolution in water.

In conclusion, comparing the experimental decolouration results obtained with the mentioned technologies, bubble reactor seems to be the best technology for oxidizing treatment.

Notwithstanding, technological aspects assume great importance with respect to bubble column:

- to generate high gas-liquid mixing by ejector, liquid must be pumped through restricted sections to have high kinetic energy. Therefore a specific pump is necessary in the reacting loop. In addition, more gas-liquid contacts are needed to have decolouration;

- hydrodynamic cavitation could be performed through ejector devices and perforated plates, which have small diameters in the magnitude of few millimetres. In order to prevent obstructions, a washing system and at the same time parallel loops are needed to maintain the water treatment continuous. Consequently, higher investments cost than bubble column are needed.

Finally, dyeing test were performed using ozonated wastewater. Wastewater originated from an industrial wool dyeing process was ozonated at different treatment time to obtain different decolouration degree. After that, treated water was reused to dye wool.

The benchmark wool dyed with fresh water and wool dyed using ozonated wastewater were compared using a reflection spectrophotometry. In conclusion, the minimum dye-bath exhaustion to obtain the same colour is about 98-99%.